METEOROLOGY AND AIR QUALITY

WINTER FIELD STUDY

IN THE AOSERP STUDY AREA

MARCH 1976

compiled by

F. FANAKI

Atmospheric Environment Service

4905 Dufferin Street

Downsview, Ontario

for

ALBERTA OIL SANDS ENVIRONMENTAL RESEARCH PROGRAM

Project ME 1.5.1

May 1978

TABLE OF CONTENTS

TABLE OF CONTENTS (CONCLUDED)

LIST OF TABLES

LIST OF FIGURES

LIST OF FIGURES (CONTINUED)

LIST OF FIGURES (CONTINUED)

LIST OF FIGURES (CONTINUED)

LIST OF FIGURES (CONCLUDED)

ABSTRACT

In March 1976, the first in a series of intensive field studies was carried out in the Alberta Oil Sands Environmental Research Program study area in northeastern Alberta to examine the fine structure of the atmosphere and dispersion characteristics under winter conditions. The study comprised several co-ordinated sets of measurements over a two week period. These included: minisonde flights, tethersonde vertical profiles, acoustic sounder and delta-T sonde profiles, correlation spectrometer and ground level sulphur dioxide measurements, plume rise photography and background air and precipitation chemistry.

Plume dispersion measurements made by aircraft were co-ordinated with the study and are reported in a separate publication. All measurements, except those for background air chemistry, were made within 20 km of Mildred Lake taking in the present oil sands processing facility of Great Canadian Oil Sands Ltd. and the future production site of Syncrude Canada Ltd.

The study was successful in identifying unique features of the winter environment of the area such as diurnal formation and breakup of inversion layers, the effects of the river valley on circulation patterns, plume characteristics, pollutant deposition patterns in the snowpack and background levels of gases and particulates.

1. INTRODUCTION

The first Meteorology and Air Quality winter field study was held in March 1976. This was to be a study of winter conditions and March was chosen for the following reasons:

- climatological records indicated that winter conditions should prevail for the period of the study;
- a variety of atmospheric stability transition situations would be experienced; and
- longer days--12 hours of daylight versus 8 in January--would allow more operational hours.

The study had three objectives: (1) to obtain information on the rise and dispersal of the Great Canadian Oil Sands Ltd. (GCOS) plume as a function of meteorological conditions, (2) to investigate air quality and pollutant deposition and, (3) to provide meteorological support to other facets of the total program.

The field measurements consisted of time lapse photography of the GCOS plume, measurements of SO_2 concentration at the ground using mobile gas monitor, plume SO_2 dispersion using the Barringer Correlation Spectrometer and the measurements of concentration of sulphur in the atmosphere and the snow.

Most of the scientific activities of the field study took place either at the Lower Syncrude site or on the roads in the vicinity of the GCOS plant (Figure 1.1) in the Alberta Oil Sands Environmental Research Program (AOSERP) study area (Figure 1.2). A summary of these experiments is described in the "Weather and Activities Summary" (see Section 8.1).

Minisonde flights provided a basic framework for the other experiments. Times of flights were scheduled well in advance of the field study and only rarely were scheduled releases cancelled. Additional flights were added to the basic schedule on a number of occasions depending on the weather and/or the operational requirements of other experiments.

Whenever possible, and on request, the tethersonde was operated in support of the aircraft measurement experiment (Intera)

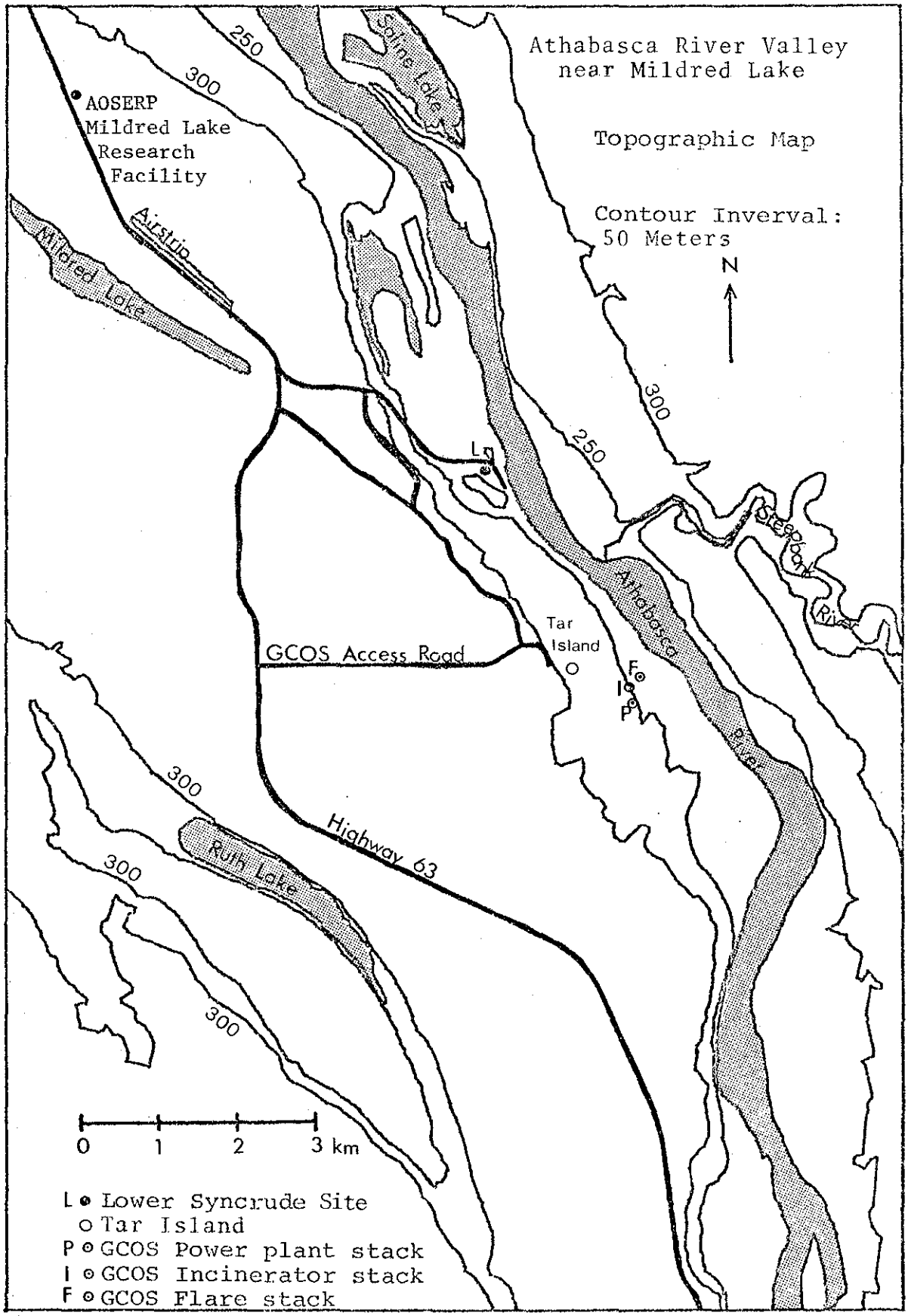

Figure 1.1. Map of the Athabasca Oil Sands Area showing the locations of the GCOS plant and the Lower Syncrude Site.

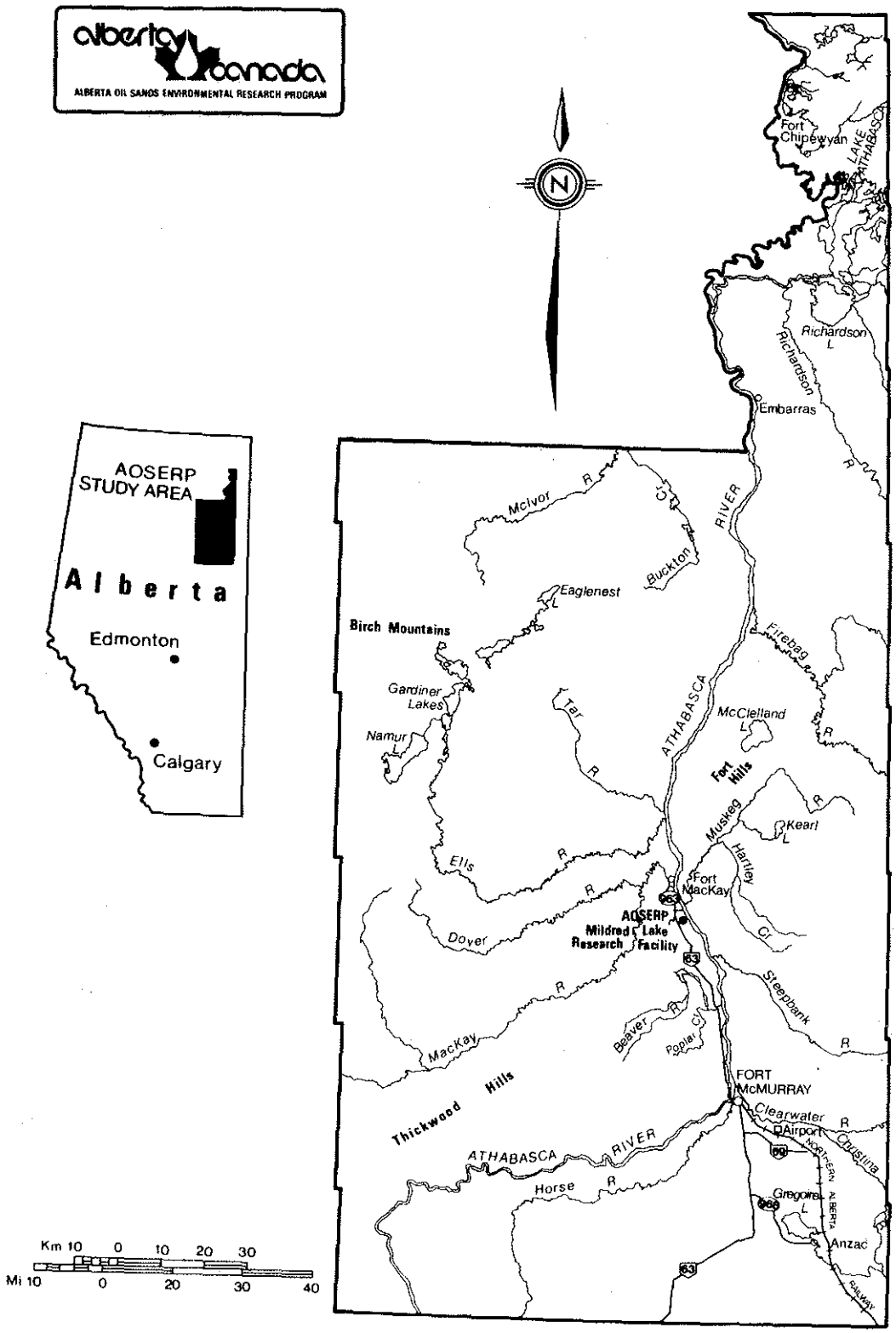

Figure 1.2. The Alberta Oil Sands Environmental Research Program study area.

by taking data at fixed levels (plume height) during the aircraft's plume runs and in the profile mode during a portion of the turbulence runs.

The sections which follow contain reports on the individual experiments. In general, where appropriate, the reports include the objectives of the experiment, a description of the field operation, a description of the instrumentation, a sample of the analyzed data, recommendations regarding logistics, instrumentation and experimental procedures and conclusions that can be made based on experience during the study or in preliminary analysis of the data.

A list of the participants together with the experiments comprising the field study is contained in Section 8.2.

2. MINISONDE

by J. L. Walmsley, A. J. Arnold, and G. G. Vickers

The minisonde program provided the basic framework of wind and temperature data for the lower atmosphere in the study areas. Two teams had a fixed schedule of four releases daily. Extra flights could be called for. During the study period 128 minisonde flights were made.

2.1 DESCRIPTION OF DATA

A preliminary quality control was performed during the field study on all observational data. Graphs of wind speed, wind direction, and temperature were plotted against height. A sample of the output for a flight at the Lower Syncrude complex at 0540 MST, 11 March 1976 is shown in Figure 2.1. In some cases the data will require smoothing to reduce or remove observational error (Figure 2.2).

In addition, calculations of the vertical gradient of potential temperature have been performed as calculated with the formula:

$$\frac{\partial \Theta}{\partial z} = \frac{\partial T}{\partial z} + \gamma_d \approx \frac{\Delta T}{\Delta z} + \gamma_d$$

where γ_d = the dry adiabatic lapse rate = 9.8 $K^{o} \cdot km^{-1}$. A sample of these results is also included (Table 2.1). Due to large errors associated with computing the difference in temperature and/or height between two levels that may be only 30 m apart, the results must be treated with caution. Smoothing is one possible method of dealing with the problem. Another is to compute gradients over somewhat thicker layers: a surface mixed layer, an inversion layer, and an upper layer. This analysis seemed to give reasonable results.

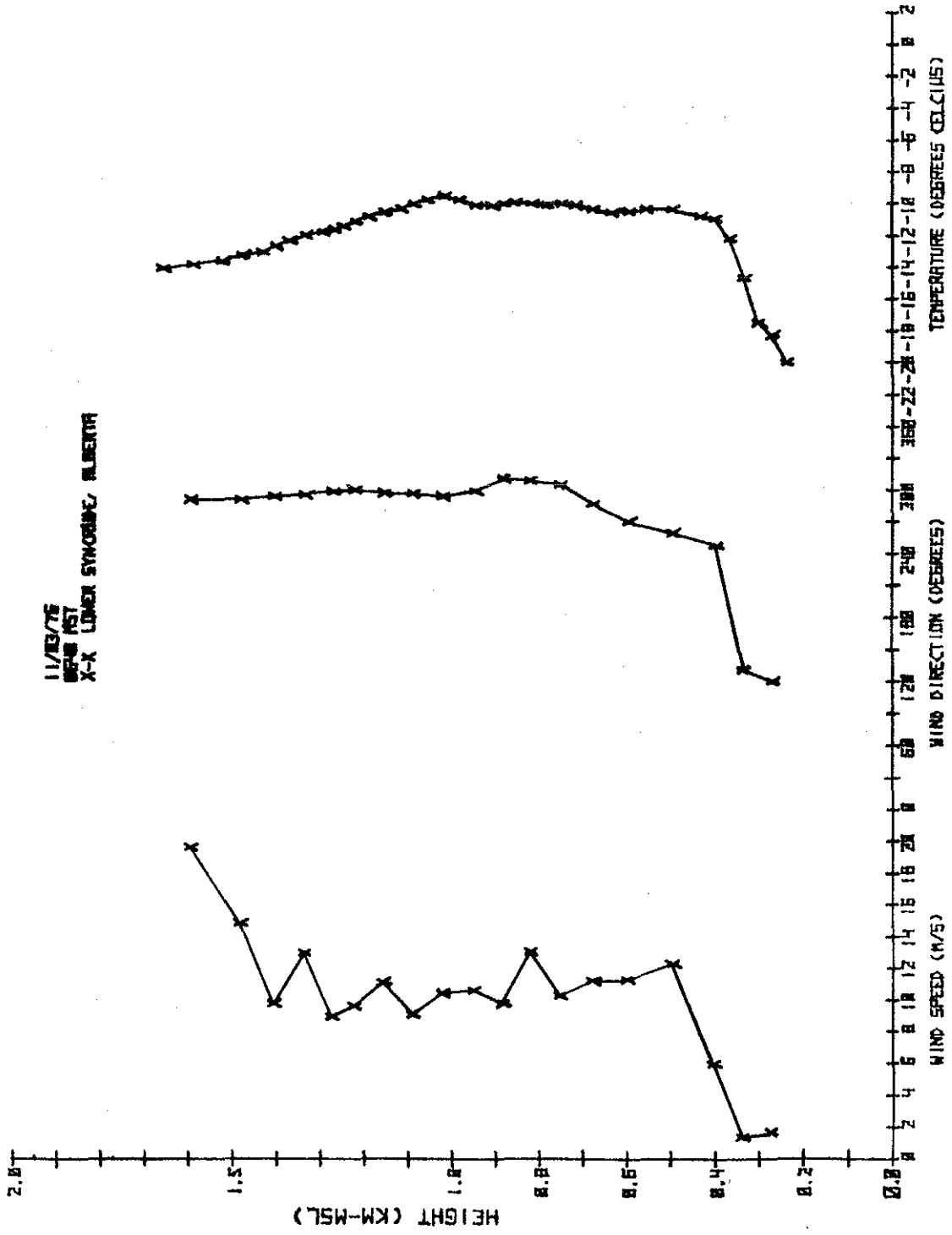

Figure 2.1. Sample unsmoothed minisonde profiles, Lower Syncrude site, 11 March 1976.

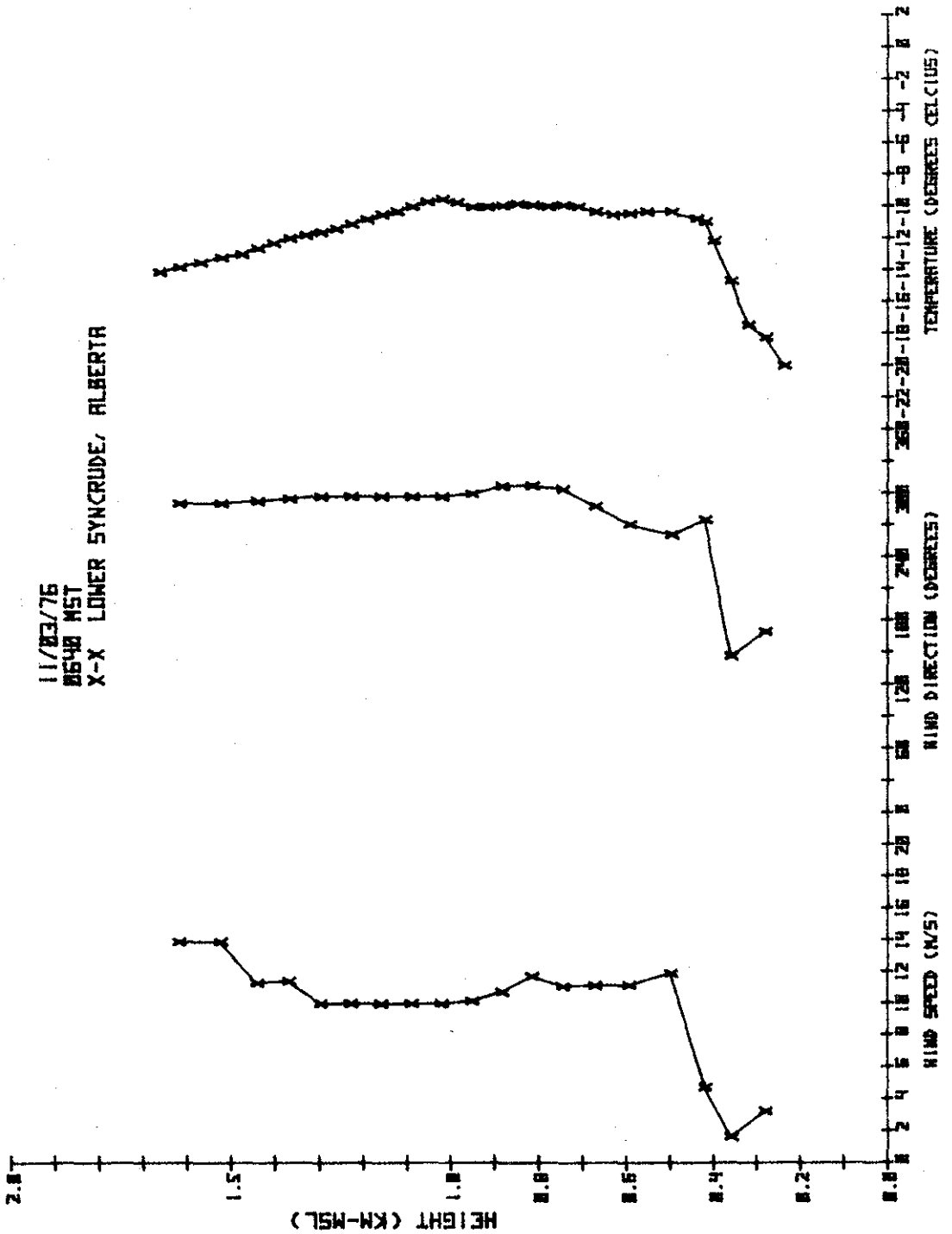

Figure 2.2. Sample smoothed minisonde profiles, Lower Syncrude site, 11 March 1976.

Table 2.1. Vertical gradient of potential temperature at different heights.

Level	Ht(m)	$\partial\theta/\partial z$(K°/km)	Level	Ht(m)	$\partial\theta/\partial z$(K°/km)
1	254.8	60.31	31	1316.8	4.82
2	288.0	34.28	32	1357.0	2.33
3	320.6	95.48	33	1391.6	-0.51
4	353.3	86.30	34	1420.8	-3.94
5	386.0	46.52	35	1458.2	5.42
6	418.7	15.92	36	1503.9	3.24
7	466.2	16.21	37	1561.2	5.45
8	528.7	9.80	38	1630.1	5.45
9	579.1	7.20	39	1699.0	5.45
10	617.6	7.20	40	1767.9	5.45
11	657.8	14.56	41	1822.2	2.27
12	699.8	16.94	42	1862.1	2.27
13	736.5	13.00	43	1915.0	6.77
14	767.8	6.60	44	1980.9	5.25
15	802.0	12.49	45	2034.0	4.84
16	839.3	12.49	46	2074.4	4.84
17	870.9	5.96	47	2114.7	4.84
18	897.0	5.96	48	2155.1	4.84
19	929.0	9.80	49	2195.4	4.84
20	966.9	17.72	50	2235.7	2.36
21	1004.1	15.29	51	2276.1	7.32
22	1040.5	4.31	52	2316.4	4.84
23	1073.9	-0.11	53	2356.7	-0.12
24	1104.1	-0.11	54	2397.1	4.84
25	1137.9	4.42	55	2437.4	2.36
26	1175.0	1.73	56	2477.8	2.36
27	1207.7	-0.90	57	2518.1	2.36
28	1235.7	-0.90	58	2558.4	2.36
29	1261.5	1.29	59	2598.8	2.36
30	1285.0	1.29	60	2639.1	2.36

2.2 DATA AVAILABILITY

The data from the field study minisonde program are available as graphs of smoothed results for each flight and as cassette tapes produced by HP-9830 containing height, wind speed, wind direction, and temperature for each flight.

2.3 DISCUSSION AND CONCLUSIONS

In addition to the primary purpose of data gathering, the minisonde program served to familiarize the staff of the Western Region Atmospheric Environment Service (AES) and AOSERP staff with the operation and with data processing.

Due to the fact that the AES tethersonde was in operation during the field study, the minisonde program served primarily as a benchmark operation in support of the other experiments. This was perhaps the first field study in which minisonde flights were not necessarily regarded as the principal means of sounding the lower atmosphere. Hence, for the most part, flights were spaced about 1.5 h apart between 0700 and 1500 MST. On most days, three flights (0930, 1100, 1300) were made at two locations simultaneously in an effort to obtain information on horizontal inhomogeneities (particularly between the river valley itself and the broader-scale valley flats). It is felt that this spatial and time resolution was about right for the purposes of this study, considering the fact that the tethersonde, delta-T sonde, and acoustic sounder were taking fairly continuous data, finely resolved in time and/or the vertical dimension.

The procedure of data processing as soon as possible after the flight had several advantages. It saved time at the end of the study. It gave the scientists working on other experiments an idea of the basic structure of the planetary boundary layer, thus assisting their planning, and, later, their analysis of data. It also provided feedback to the observers on the accuracy of their observations. In a double theodolite program, even small errors show up glaringly in the graphical output.

It was unfortunate that the data smoothing routine was not quite ready in time for the field study. In future studies it should be possible to produce final graphical output in more-or-less real time (e.g., within about 24 h).

Despite the limited resolution of the Askania theodolite (0.1^{o} in both elevation and azimuth angle), the instrument offers several advantages over Warren-Knight or digital theodolites (the only alternatives for AES at present). The Askania is relatively portable and relatively simple to operate. It has the ability to read high elevation angles and has no power requirements. Furthermore, the computer smoothing program partially compensates for inaccuracies caused by the limited resolution of the readings.

In summary, if the same project were to be undertaken again, no major changes are recommended except for more complete data processing (including final graphs) in real time.

3. TETHERSONDE

by R. E. Mickle, L. Guise-Bagley and W. F. Kobelka

During the AOSERP Winter Field Study of 1-19 March 1976, a tethersonde (T/S) was flown at the Lower Syncrude complex to make a more detailed study than was possible using minisondes both spatially and temporally of the layer to effective stack height. A more specific objective was to study the breakup of the early morning inversion and the effect, if any, on the windfield. Topographical effects (the Athabasca River basin) were also of interest. In support of dispersion measurements and to study the variability of the winds, fixed level mean/variance measurements were made of the windfield. Both profile and fixed level data had been requested by Intera Environmental Consultants Ltd. prior to the field study to complement their aircraft measurement program.

3.1 INSTRUMENT DESCRIPTION

The T/S flown during the field study (Mickle and Davison 1974) (Figure 3.1) was a modification of an original design by Klein and Bourke (1967). The instrument had been extensively flown during Global Atmospheric Tropical Experiment (GATE) (1974); analysis of these data had confirmed its reliability during warm-weather operation. The harsh, cold environment of the March study initially presented instrumental problems, which were eventually overcome after a day's delay.

The T/S package weighing 2 kg was carried aloft to heights of 500 m on the tethering cable of a 17-m^3 balloon (Figure 3.2). The instrument package was free to rotate around the tethering cable and was aligned into the wind by a vane above and behind the main meteorological package. Temperature, measured by a pair of rod thermistors (coated white to minimize radiational effect, time constant $\sim$ 10 s and accuracy $\pm.1^{\circ}C$) mounted on the forward arm of the package; relative humdity, measured by a 2% Premium Hygristor with an accuracy ±2%; and pressure, measured by modified Feuss barometer, were sequentially sampled at a rate of 1 channel/5 s. The wind speed information

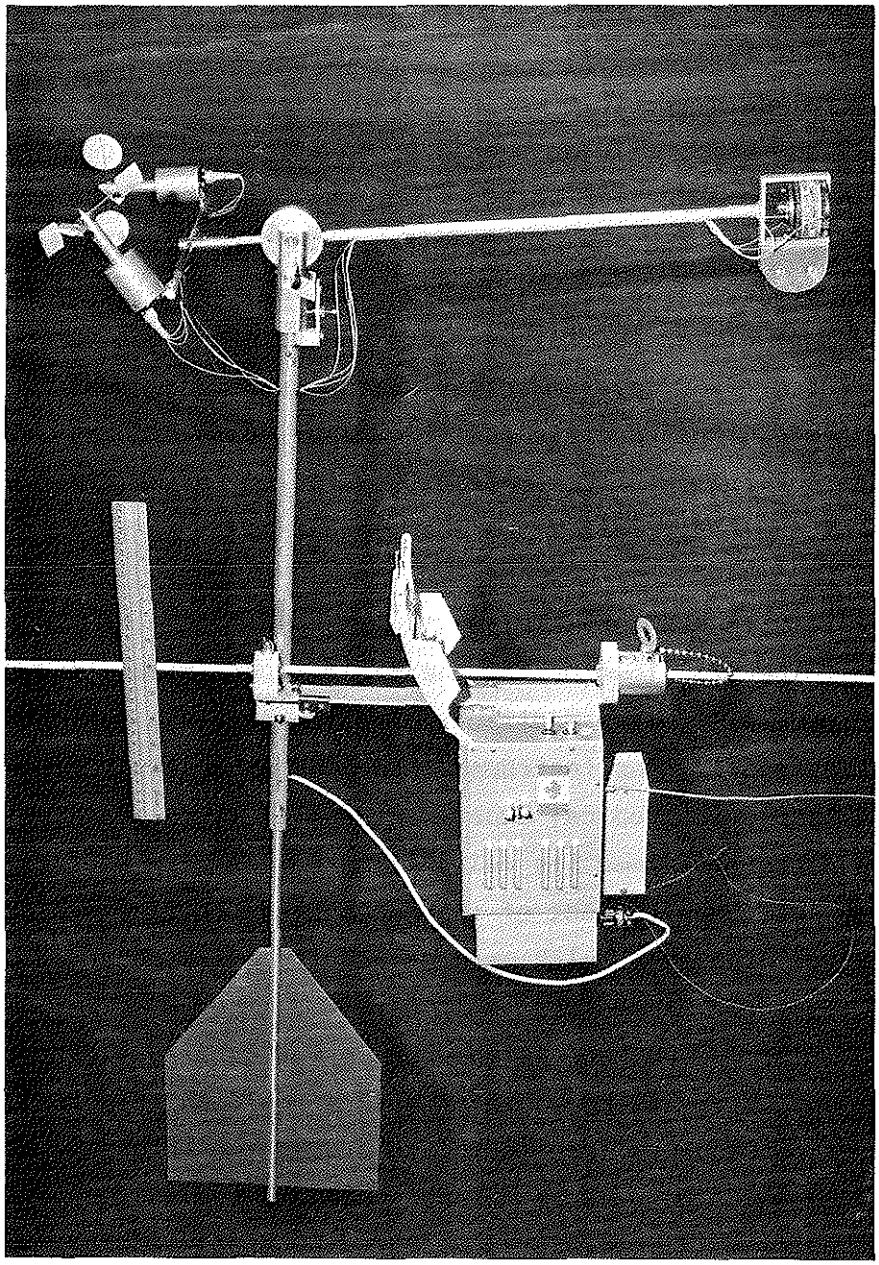

Figure 3.1. T/S flown at Lower Syncrude site during intensive field study, 1-19 March 1976.

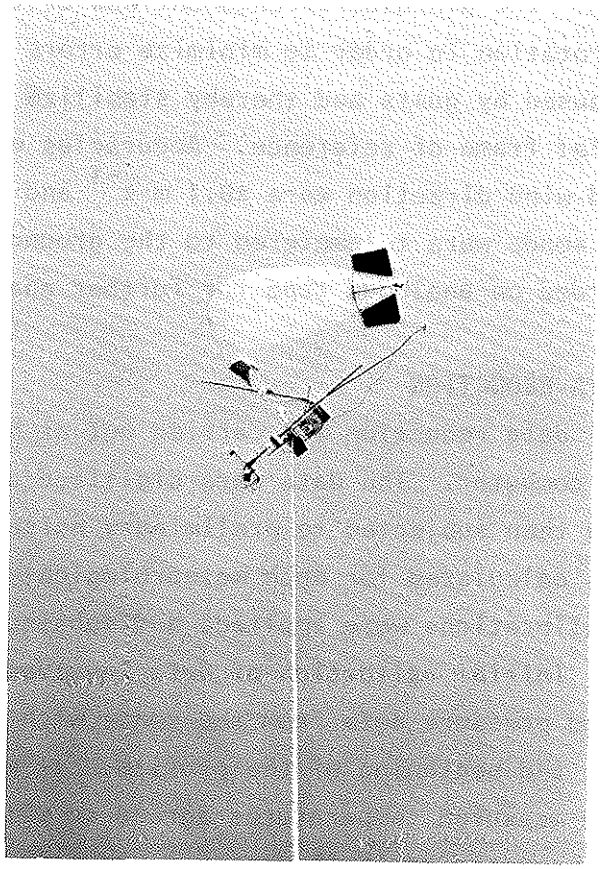

Figure 3.2. Balloon and sonde assembly for T/S operations.

was obtained from the miniature blade and cup anemometers situated on a pendulum at the front of the vane. The cosine response combination of the two anemometers permitted the extraction of both vertical and horizontal winds. At the base of the pendulum was a clamping compass from which wind direction was obtained. The directions presented in this report are referenced to magnetic north and have not had the appropriate 25^{o} correction applied for the true north. The pendulum arrangement was critically damped in both axes of rotation in order to minimize errors due to oscillations of the line caused by gusts and thereby stabilize the pendulum in the geopotential frame of reference. Accuracies of measurements of wind speed and wind direction were ± 0.1 m·s^{-1} and $\pm 3^{o}$ respectively. Data from the sonde were telemetered to the ground in the 89-105 MHz band and recorded on analogue tape for further analysis.

3.2 DATA REDUCTION

All data reduction was carried out at headquarters on a PDP 11/20 minicomputer. The data were digitized at 20 Hz (real time) and were then subjected to preliminary noise removal. A mean (5 s) was calculated for each meteorological channel of data, appropriate calibrations were applied, and subsequent profile data were plotted. Initial validation of data involved comparision of temperature and pressure data from the sonde with surface measurements taken at the beginning of the profile. It was found generally that the sonde-measured temperatures agreed to within 0.25^{o}C absolute with psychrometer dry bulb measurements, and so no correction was necessary. Pressure changes in the sonde barometer tracked the surface pressure changes sufficiently closely not to warrant correction. Wind speed and direction data were compared for a couple of cases to minisonde data (direction corrected to magnetic north) taken during lapse conditions.

3.3 EXPERIMENTAL PROCEDURE

The T/S experiment was conducted solely at the Lower Syncrude complex. The time/height status for the sonde is given in Figure 3.3 for the experimental period from 6-16 March. During the morning, the T/S was flown in a profiling mode in order to study the lifting and breakup of existing inversion layers and any related changes in the windfield. A profiling rate of 0.3 $m \cdot s^{-1}$ was used to give a mean temperature every 3 m and relative humidity and pressure every 10 m. Around noon, the T/S was left at a fixed level of 300-500 m in order to obtain turbulence statistics (variances) characteristic of that particular level.

3.4 DISCUSSION OF PROFILE DATA

The profile data for 6-16 March can be found in Section 8.3. Each set of profiles (T, R_H, U, D) has been identified by the date and time when the sonde was at the surface either prior to a profile up or after a profile down. Temperature (T) as well as the potential temperature (V) are plotted to the nearest 0.25^{o}C as a function of height. The relative humidity (H) to the nearest 2% R_H is plotted to the right. The wind speed and direction data for this particular profile are presented in the following pair of graphs. Wind speed (U) has been plotted to the nearest 1/6 $m \cdot s^{-1}$. Direction (D) has been plotted to the nearest 1/8 radian and is referenced to magnetic north. The bars at approximately 2.125 and 5.25 radians represent the direction for flow up the valley (north winds) and down the valley from GCOS to the Lower Syncrude site. The representative valley direction at the Lower Syncrude complex was chosen to be 0.977 radians (56^{o}) west of magnetic north. Due to cold weather, wind data were not obtained until the late afternoon of 7 March.

Interpretation of the profile data has been grouped according to stability categories, namely stable conditions characteristic of early morning profiles and neutral to slightly unstable conditions characteristic of mid-afternoon profiles. No effort has

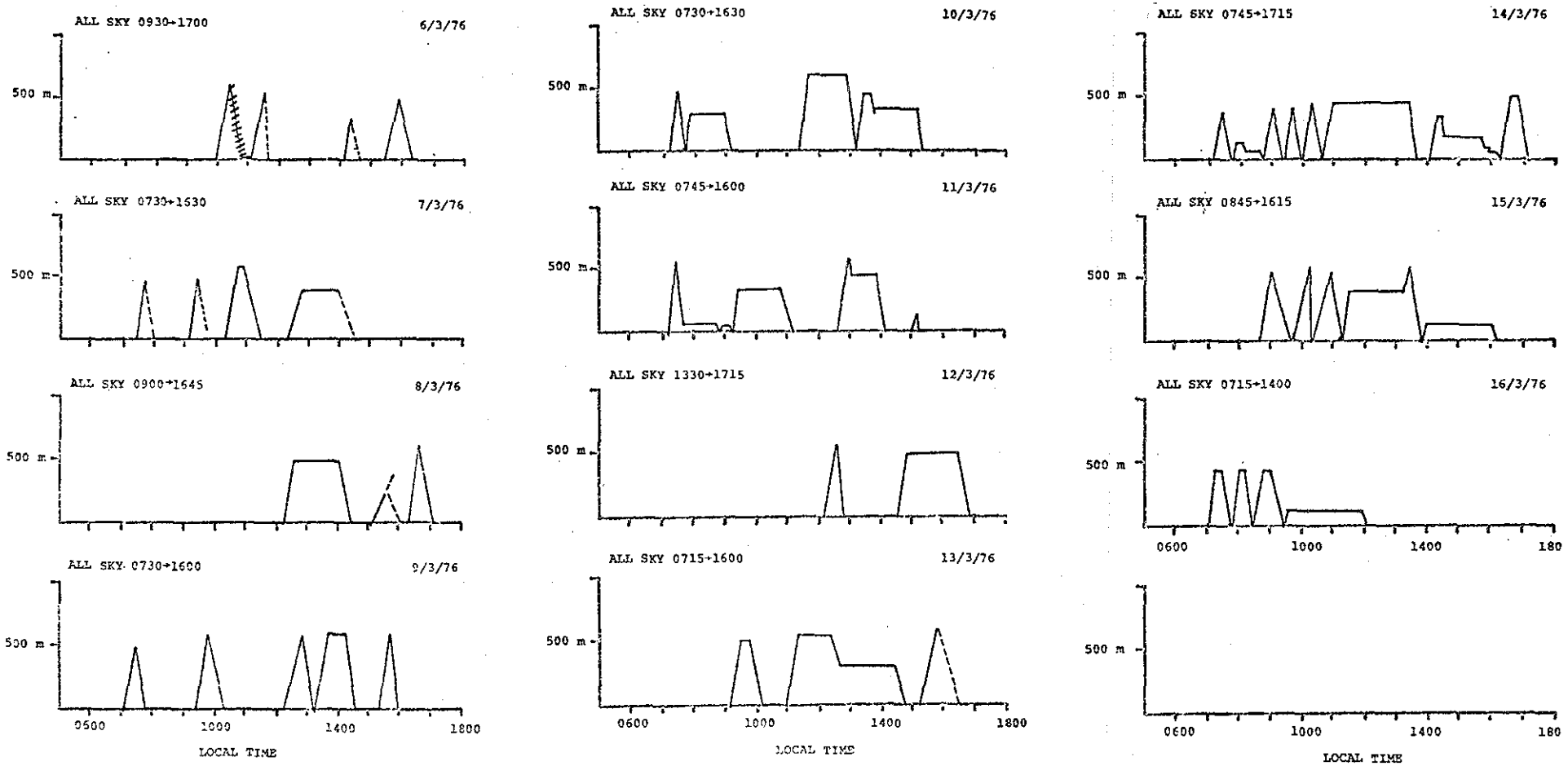

Figure 3.3. Time/height record of tethersonde

been made, however, to study the detailed changes in the profile structure during the transition from the stable to neutral states.

3.4.1 Stable conditions

During early-morning stable conditions, the layer from the valley basin to 400 m was generally characterized by three stable layers that will be referred to as:

1. The basin-related inversion layer;
2. The intermediate or veer layer; and
3. The upper inversion layer.

3.4.1.1 Basin-related inversion layer. In general, early morning profiles in the valley were characterized by a surface inversion to 80 m, probably related to cold air drainage into the valley during the night. From T/S flights on 14 March, it was found that this surface inversion was well formed by 2300 and proceeded to deepen over the subsequent hour of observation. On several occasions, the relative humidity within the valley was found to be significantly higher than at heights above 100 m (9 March, 0700, 10 March, 0719, 11 March, 0716, 14 March, 0703, 16 March, 0702). This is probably due to the open ponds around GCOS. Those mornings when R_H was greater than 90% were associated with a southerly valley flow from GCOS to the Lower Syncrude complex. The top of this layer was usually associated with the top of the intermediate inversion around 150-200 m. On 10 March, high humidity and low temperature ($-29^{\circ}C$) led to ice fog in the valley and consequent riming of the instruments.

Winds in the valley during these stable conditions were generally light and decoupled from winds aloft. The flow showed a consistent up- and down-valley character to the height of the westerly valley wall.

3.4.1.2 Intermediate inversion layer. Above the valley wall to heights of 300-400 m, there was a layer in which a second inversion or isothermal layer existed (7, 9, 10, 11, 14, 15, 16 March). The data from 14-16 March especially show an intermediate inversion existing at 100-200 m. Associated with the base of this inversion was a local maximum in wind speed. This jet was found to lock onto the base of the inversion, especially apparant on 15 March, when the base of the inversion/jet initially descended from 0851 to 0947 and rose again between 0947 and 1033. Through this layer from the base of the intermediate inversion to the base of the upper inversion, the winds veered from the lower valley flow to the upper flow reasonably approximated the wind direction at the upper inversion. Large veers in wind direction over relatively narrow depths were found to exist under stable conditions (10 March, 0743 showing a veer of 3.2 radians over 50 m, and 14 March, 1031 showing three distinct layers of wind direction).

3.4.1.3 The upper inversion layer. For many of the profiles, only the base of the upper inversion was reached. However, from these data, a local maximum in the winds was found to be locked onto the base of this inversion (15 March, 0851- → 1125 where the upper inversion descended from 310 m to 270 m with an associated lowering of the wind maximum).

Generally it was found in this set of data under stable conditions that there was a layering effect in the temperature and wind structure of the profiles. In the valley, the flow was along the valley itself. Above, the wind veered from the valley direction to the upper flow direction approximated by the winds at the base of the upper inversion. Associated with the base of the two upper inversions were local wind maxima (jets). Each jet was found to have a distinct wind direction; maximum wind veer associated with the wind speed minima between jets (viz. 10 March 0743, 14 March 0703). It must be emphasized at this point, however, that these observations do not necessarily characterize the flow above the

plain. Because of the locking of flow within the valley and predominant westerly flow aloft for these data, the observations made in the intermediate region may in fact be only the result of the adjustment of the winds to the imposed upper and lower conditions. Only by studying the flow above the plain well removed from the valley can this question be answered.

3.4.2 Neutral conditions

During neutral conditions, the decoupling of the valley flow from winds aloft is no longer apparent (11 March, 1242, 12 March, 1431, 13 March, 1007, 14 March, 1618). For these particular sets of data, the wind veer (dD/dz) is effectively a constant with height, the flow in the valley no longer aligning with the valley topography (12 March 1431). The wind speed over the profile layer was found to be effectively a constant (u(z)=const.).

3.5 DISCUSSION OF FIXED-LEVEL DATA

The fixed-level mean/standard deviation data are presented in Table 3.1. The mean has been taken over 10 min. The standard deviation for wind speed was calculated in the normal fashion, while that for direction was calculated using the trig function:

$$(\theta_i - \theta_m) = \text{atan}\left(\frac{\tan\theta_i - \tan\theta_m}{1 + \tan\theta_i \tan\theta_m}\right)$$

where θ_m is the average direction. In this way, π discrepancies were avoided.

In general, the 10-min means of wind speed were found to vary up to factors of two over periods of 1 h (11 March, 0746, 0946, 12 March, 1451). These fixed-level data were obtained in both stable and neutral conditions with similar results. It is apparent, therefore, that the extraction of wind information from profile data at hourly intervals and the application of these data for intermediate times may at best be no better than a factor of two. Over the 10-min

Table 3.1. Fixed-level statistics for wind data, 9-16 March 1976.

Date	Time	Height M	U M/S	SD	Dir Rad	SD
9 March	13:32	331.	2.07	0.65	3.75	0.29
	13:42	355.	2.45	0.27	3.87	0.20
	13:52	354.	4.13	1.14	3.99	0.16
	14: 2	360.	3.29	1.44	4.06	0.97
	14:12	365.	2.70	0.23	4.18	0.13
10 March	11:46	355.	1.50	0.16	-0.19	0.15
	11:56	361.	1.18	0.15	0.01	0.16
	12: 6	357.	0.93	0.06	-0.05	0.17
	12:16	361.	0.92	0.17	0.07	0.08
	12:26	369.	1.01	0.26	-0.25	0.13
	13:56	230.	1.49	0.25	3.68	0.27
	14: 6	243.	1.28	0.37	3.98	0.60
	14:16	235.	1.08	0.22	3.66	0.15
	14:26	237.	1.10	0.22	3.98	0.21
	14:36	240.	1.24	0.20	3.28	0.34
11 March	7:46	95.	2.82	0.46	0.00	0.00
	7:56	91.	3.83	0.45	0.00	0.00
	8: 6	84.	3.19	0.24	0.00	0.00
	8:16	90.	2.47	0.53	0.00	0.00
	8:26	91.	1.00	0.34	0.00	0.00
	8:36	91.	1.76	0.25	0.00	0.00
	8:46	93.	2.60	0.48	0.00	0.00
	9:46	311.	5.41	0.35	0.00	0.00
	9:56	329.	4.49	0.46	0.00	0.00
	10: 6	344.	3.80	0.24	0.00	0.00
	10:16	362.	2.82	0.31	0.00	0.00
	10:26	385.	2.41	0.19	0.00	0.00
	10:36	379.	2.15	0.24	0.00	0.00
	10:45	343.	2.32	0.38	0.00	0.00
12 March	13:14	451.	2.62	0.37	3.95	0.16
	13:24	446.	3.07	0.27	4.13	0 12
	13:34	447.	3.02	0.78	4.09	0.09
	13:44	459.	3.28	1.12	4.15	0.09
	14:51	443.	3.48	0.51	-1.57	0.33
	15: 1	442.	3.46	0.42	-1.50	0.40
	15:11	465.	3.10	0.25	-0.99	0.41
	15:21	442.	2.73	0.71	-0.76	0.30
	15:31	449.	2.34	0.29	-1.12	0.48
	15:41	444.	2.35	0.29	4.47	0.18
	15:51	455.	1.71	0.43	-1.37	0.48
	16: 1	435.	1.89	0.58	-1.15	0.44
	16:11	440.	2.01	0.83	-1.02	0.40
13 March	11:15	511.	2.86	0.40	0.55	0.17
	11:25	511.	3.39	0.61	0.57	0.06
	11:35	492.	3.17	0.48	0.64	0.07
	11:45	502.	3.44	0.36	0.76	0.14
	11:55	503.	4.55	1.26	1.02	0.12

Date	Time	height M	U M/S	SD	Dir Rad	SD
	12: 5	519.	2.86	0.30	1.36	0.17
	12:41	274.	2.40	0.48	1.23	0.16
	12:51	277.	2.31	0.19	1.06	0.19
	13: 1	270.	2.40	0.41	1.08	0.16
	13:11	274.	1.95	0.18	1.28	0.14
	13:21	274.	2.22	0.53	1.24	0.15
	13:31	271.	2.17	0.10	1.44	0.09
	13:41	274.	1.74	0.40	1.50	0.13
	13:51	276.	2.01	0.27	1.42	0.13
	14: 1	273.	2.36	0.24	1.40	0.07
	14:11	271.	2.74	0.80	1.62	0.09
	14:21	279.	2.08	0.39	1.65	0.18
14 March	10:50	322.	2.09	0.20	-0.08	0.06
	11: 0	323.	1.67	0.07	-0.04	0.05
	11:10	327.	1.44	0.12	-0.18	0.06
	11:20	322.	1.34	0.09	-0.34	0.06
	11:30	314.	1.81	0.20	-0.32	0.04
	11:40	317.	1.57	0.30	-0.30	0.05
	11:50	319.	0.76	0.14	0.42	0.09
	12: 0	323.	0.76	0.07	0.35	0.17
	12:10	325.	0.86	0.12	0.34	0.08
	12:20	328.	0.65	0.07	0.46	0.07
	12:30	325.	0.64	0.04	0.36	0.04
	12:40	324.	0.00	0.00	0.00	0.00
	14:30	142.	1.97	0.38	-0.28	0.19
	14:40	138.	2.36	0.19	-0.39	0.14
	14:50	140.	2.54	0.42	-0.24	0.32
	15: 0	137.	2.57	0.62	-0.32	0.27
	15:10	124.	3.58	0.38	-0.26	0.05
	15:20	122.	4.12	0.39	-0.11	0.12
	15:30	124.	3.93	0.68	0.09	0.13
15 March	11:37	283.	0.75	0.10	-0.34	0.19
	11:47	283.	0.78	0.06	-0.22	0.13
	11:57	284.	0.57	0.00	-0.94	0.24
	12: 7	284.	0.38	0.16	3.95	0.10
	12:17	283.	1.27	0.26	3.44	0.35
	12:27	282.	1.35	0.20	3.62	0.13
	12:37	284.	1.12	0.19	3.94	0.13
	12:47	288.	0.68	0.13	1.66	0.80
	12:57	287.	0.72	0.04	0.90	0.03
	13: 7	287.	0.65	0.04	0.79	0.21
	14: 7	97.	0.91	0.18	2.36	0.23
	14:17	100.	0.74	0.09	1.89	0.19
	14:27	98.	0.62	0.12	1.86	0.05
	14:37	99.	0.91	0.10	2.48	0.24
	14:47	100.	0.94	0.15	2.13	0.20
	14:57	101.	0.81	0.08	2.31	0.26
	15: 7	105.	0.89	0.11	2.67	0.11
	15:17	106.	0.79	0.12	2.74	0.15
	15:27	111.	1.04	0.10	2.86	0.11

Date	Time	Height M	U M/S	SD	Dir Rad	SD
	15:37	112.	1.12	0.21	2.46	0.15
	15:47	112.	1.22	0.15	2.33	0.18
	15:57	111.	1.33	0.22	2.68	0.16
16 March	9:38	121.	1.74	0.23	2.60	0.19
	9:48	120.	1.65	0.22	2.44	0.12
	9:58	123.	1.94	0.10	2.51	0.06
	10: 8	121.	1.95	0.09	2.51	0.13
	10:18	124.	1.74	0.15	2.43	0.15
	10:28	126.	1.91	0.25	2.31	0.06
	10:38	124.	1.83	0.14	2.37	0.15
	10:48	126.	1.81	0.24	2.31	0.11
	10:58	129.	1.90	0.11	1.95	0.12
	11: 8	129.	1.38	0.22	1.94	0.19
	11:48	349.	3.78	0.15	3.40	0.03
	11:58	384.	3.47	0.24	3.44	0.04
	12: 8	346.	4.27	0.35	3.51	0.03
	12:18	341.	4.36	0.22	3.54	0.03
	12:28	342.	4.13	0.16	3.56	0.02
	12:38	351.	4.32	0.08	3.58	0.03
	12:48	353.	4.18	0.14	3.55	0.03
	12:58	355.	4.04	0.09	3.57	0.02
	13: 8	359.	4.07	0.24	3.60	0.02
	13:18	353.	3.43	0.29	3.60	0.05

periods, the standard deviation of wind speed on the average was found to be 0.1 of mean; however, there were times at which the standard deviation/mean ratio was substantially greater (9 March, 1332, 11 March, 1314). Under these conditions, winds estimated from profile data (i.e. a quick sample through a given level) may give erroneous results if interpreted as representative of the mean wind at that particular level. Both of the above variations would lead to errors in mass flux calculations if the wind speed information was obtained from profile data. Hence, good fixed level data at plume height are necessary in order to obtain meaningful mass fluxes.

3.6 REFERENCES CITED

Klein, G. L., and R. S. Bourke. 1967. An audio modulated tethersonde package for detailed micrometeorological sounding. Journal of Applied Meteorology 6:707-716.

Mickle, R. E., and D. S. Davison. 1974. Results from sea trials of a new boundary layer tethersonde package. Paper presented at the 8th Annual Congress of the Canadian Meteorological Society. York University, Toronto.

4. AN APPLICATION OF ACOUSTIC SOUNDING TO THE ESTIMATION OF MIXING DEPTH AND VERTICAL PLUME SPREAD IN THE ALBERTA OIL SANDS AREA

by B. R. Kerman and H. E. Turner

The theoretical treatment of wave propagation in the atmosphere indicates that acoustic backscatter should be proportional to the intensity of thermal turbulence of scale of the order of the acoustic wavelength (Tatarskii 1961). Acoustic echo sounding, therefore, can portray details of large-scale features of the planetary boundary layer when there are adequate small-scale fluctuations in temperature to provide the tracer. These fluctuations usually arise when turbulence occurs within a region with a gradient in potential temperature associated, for example, with temperature inversion layers or convection regions produced by strong surface heating. As a consequence, acoustic sounder records have been used to infer the stability of the boundary layer in terms of the existence of stable (predominantly horizontal structure in the acoustic sounder record), unstable (predominantly vertical structure) and neutral (absence of structure) atmospheric regions.

The application of the acoustic sounder to air pollution dispersion studies seems obvious, particularly for the demarcation of atmospheric mixing depths as indicated by the heights of stable layers that inhibit pollutant dispersion (see for example Beran and Hall 1974). Such measurements are important for the Alberta oil sands region where atmospheric stability can be extremely strong and where the potential for multiple layering is significant. Unfortunately, however, such a straightforward analysis of acoustic sounder records is often hampered by the extreme complexity of the data and by a frequent lack of direct correlation between the acoustic returns and simultaneously measured atmospheric stability inferred from simultaneously measured vertical wind and temperature profiles (Wyckoff et al. 1973).

This problem of record interpretation is related to a lack of knowledge about thermal turbulence in the atmosphere particularly when it is stably stratified. The relationship between turbulence

properties and fluctuating acoustic echoes and between thermal turbulence structure and the concurrent temperature profile is a subject of current research. In addition, it is probable that the latter relationship is site-specific, so that it remains to link these variables together. This study was an initial attempt to assess the potential of the acoustic sounder as a monitor of mixing depth for the oil sands area. For this purpose, a sounder was operated during the AOSERP Meteorology and Air Quality Field Study near Mildred Lake, Alberta, 1-19 March 1976. Acoustic returns within the height-range of the equipment were then correlated with simultaneous measurements of atmospheric stability (tethersonde and minisonde) and thermal turbulence structure (delta-T sonde). In addition, the feasibility of using acoustic data to quantitatively indicate vertical dispersion coefficients in the atmosphere was tested through comparison with photographs of actual pollutant plume growth.

This report discusses the acoustic sounder study and presents a case study that compares the acoustic sounder output with atmospheric profiles of wind, temperature, and thermal turbulence.

4.1 INSTRUMENTATION

4.1.1 The acoustic sounder

The general construction and theory of operation of monostatic acoustic sounders is well described elsewhere (e.g., Little 1969). A functional diagram of the AES version is given in Kerman (1976c). Once every 10 s an acoustic pulse is transmitted vertically upward from an antenna which consists of a six-fold manifold in an inverted hyperbolic dish with a conical horn. The acoustic echoes are received by the same antenna, preamplified, band-pass filtered, logarithmically amplified, and then digitized for later analysis as well as displayed on a chart recorder as a function of range and tone. The maximum range recorded is 1000 m; this display may be expanded to examine only the first 500 m. Figure 4.1 contains photographs of the acoustic sounder horn, electronics, and recorder unit.

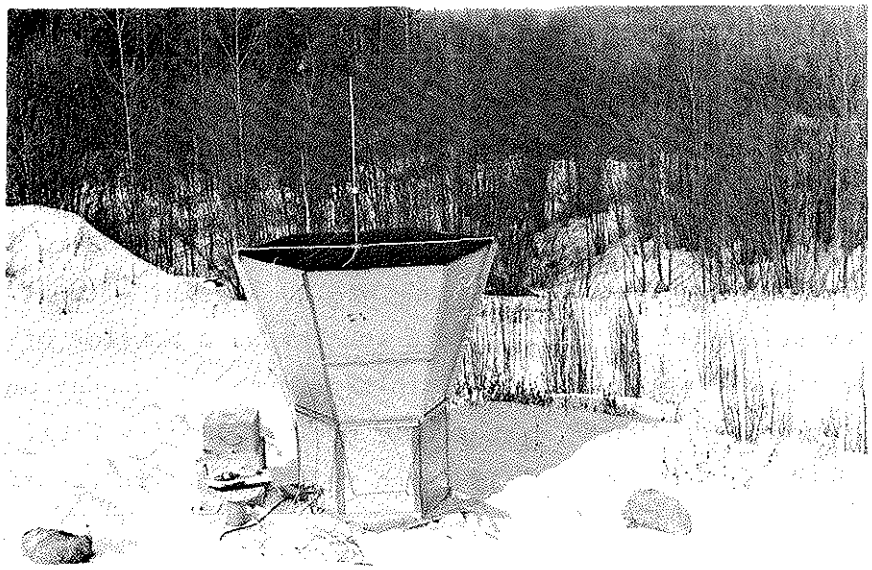

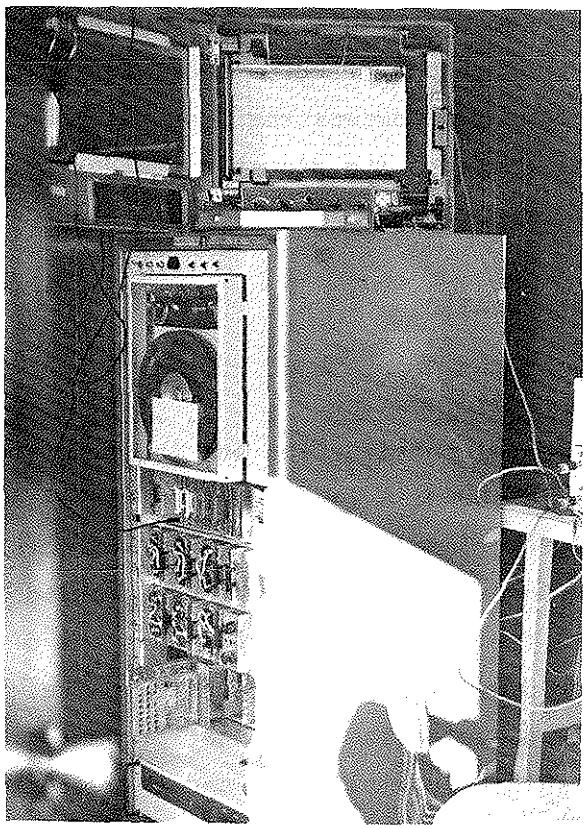

Figure 4.1. The acoustic sounder horn (above) and electronics as installed during the study, March 1976.

The system specifications for the AES acoustic sounder are given in Table 4.1.

According to theory, the acoustic energy backscattered from a region of the atmosphere is proportional to the local "temperature structure parameter", C_T^2, which may be defined as:

$$C_T^2 = \overline{(T_1 - T_2)^2} \; / \; r^{2/3}$$

where r is the distance separating two points where the temperature T_1 and T_2 are measured and is of the order of the acoustic wavelength (the overbar indicates a time-mean value). In this study, the sounder was calibrated (Kerman 1976c) and corrections were calculated for acoustic power loss due to atmospheric attenuation (derivable from concurrent temperature and humidity profiles) in order that the data could be tabulated in terms of C_T^2.

4.1.2 The Delta-T Sonde

For comparison with the acoustic sounder output, vertical profiles of C_T^2 were measured directly with the delta-T sonde. With this devise, $(T_1 - T_2)$ was measured continuously while the sonde was carried aloft on the flying line of a tethered balloon. The temperature difference data were then used to derive incremental spatial averages of C_T^2 as a function of height. The variation of $(T_1 - T_2)$ was also recorded for long periods at fixed heights where the acoustic sounder indicated strong echo returns.

The delta-T consists of two identical fine-wire thermopiles referred to one another and held apart by a rigid 1-m rod. Their output signal, which corresponds to the temperature difference $(T_1 - T_2)$ for temperature fluctuations up to several hundred hertz, is used to drive a voltage-controlled oscillator. The oscillator, in turn, is used to modulate a 403 MHz telemetry transmitter.

On the ground, a UHF receiver recovers the modulation and feeds the variable frequency information to the recording head of an instrumentation tape recorder. At the same time, the playback head

Table 4.1. Parameters of the AES acoustic sounder.

Parameter	Specification
Frequency	1470 Hz
Wavelength	0.22 m (T= 263^{o}K)
Peak Power Output	130 dB_A
Effective Power Output	126 dB_A
Pulse Duration	0.1 s
Pulse Repetition Rate	10 s
Aperture Area	2.2 m^2
Effective Aperture Area	0.627 m^2

relays the signal to a frequency meter where it is converted back to a dc signal proportional to $(T_1 - T_2)$ for visual inspection on the chart recorder. The tape recorder was included in the ground equipment chain in order to permit the subsequent computer reduction of the data and to allow the eventual analysis of much higher frequency turbulence than the chart recorder is capable of responding to.

The delta-T sonde is shown in the upper half of the photograph in Figure 4.2. It is mounted on a vane that is free to pivot about the flying line and thus it always faces into the instantaneous wind. The 1-m rod that supports the thermopiles is shown mounted vertically on the front of the frame while the package containing the amplifier and modulator is fastened near the frame's center. In order to avoid unwanted coupling with the amplifier, the transmitter package hangs about 2 m below the frame.

Values of C_T^2 were calculated over 10-s intervals (the acoustic pulse repetition frequency) with an upper frequency limit of 10 Hz. Since the average rise-rate of the tethered balloon was about 0.5 $m \cdot s^{-1}$, the C_T^2 profile data corresponded approximately to a 5-m spatial average.

4.2 EXPERIMENTAL DATA

The acoustic sounder was installed at the Lower Syncrude complex from 4 March, 1700 LST to 16 March, 0830 LST, with minor interruptions due to power failure and system testing. The facsimile (chart) record was surveyed for various meteorological events signifying various different regimes. A descriptive data catalogue, Table 4.2, is attached describing the backscatter regime during various time periods, usually closely related to periods of digital tape recording. In general, the equipment detected most of the common phenomena seen elsewhere by acoustic sounding, for example, the convective pluming, inversion rise, and the presence of nocturnal inversions and their breakup (Figure 4.3).

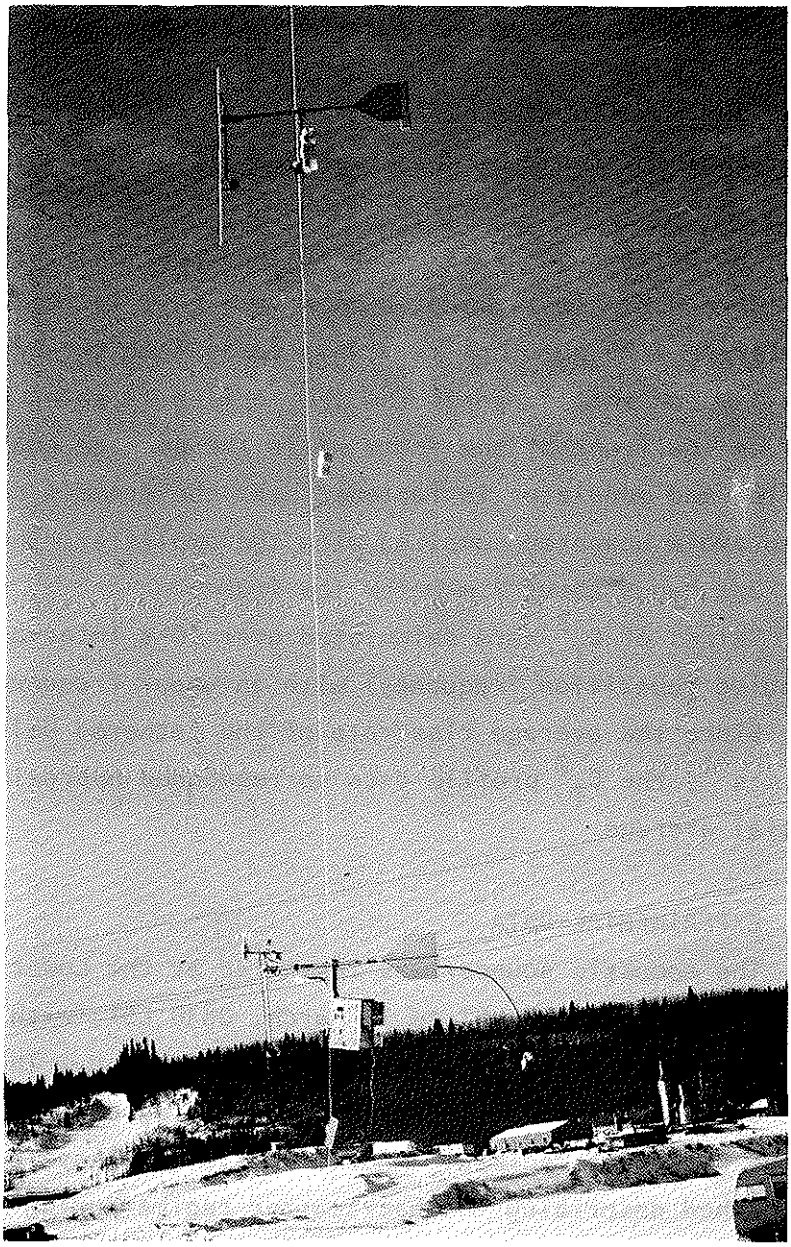

Figure 4.2. Delta-T sonde (upper instrument).

Table 4.2 Acoustic sounder descriptive data catalogue.

Day	Hour	
4	2150 to 0620 5	Low level nocturnal inversion to 250 m--thinning after 0430 --definite intermittency to returns--no waves apparent.
5	2240 to 0800 6	Low level layering to 250 m--some wave structure of lowest layer about 0600.
6	0945 to 1620 6	Convective plumes, steady penetration to 150 m from 1000 to 1230 with slight decrease in activity to 1600.
6	2300 to 1500 7	Multiple layering to 200 m--upper echo rising after 0800 to 300 m and dissipating at 0900 with increased insolation--other echo remaining steady as penetrative convection to 170 m until 1130, then apparently decreasing somewhat.
7	2220 to 0000 8	Weak echoes--possible layering--decreasing in intensity with snowfall.
8	1030 to 1700 8	Very steady, multiple echoes at 60 and 20 m, may be instrumental, balloon detected overhead from 1245 to 1330, with undulations ~10 m and frequency of 15 min--plumes to >100 m during afternoon.
8	2220 to 1500 9	Very distinct, multiple waves up to 200 m--upper echo at 150 m with ± 50 m excursions, steady throughout the night, sudden rise to upper echo at 0640, rises linearly to 400 m at 0920 (~1.5 m/min)--inversion associated with sharp humidity gradient--then linear decrease to background noise level by 1200--decrease corresponded to freshening wind.
9	2100 to 1600 10	Strong, low inversion <100 m--some layering apparent--rising after 0720, layers remain distinct to 0950, then collapse and convective plumes through afternoon.
10	1700 to 0520 11	Undulating inversion about 100 m deep, from 1900 thickening by 0500 to 200 m.
11	0715 to 1430 11	Continuation of 180 m-deep layer--very intense cover with very rapid/fall behavior at about 0830--layer dissipates to weak convective plumes and eventually no echoes.
11	1620 to 1600 12	Building inversion to 150 m during night and most of morning --pluming after 1230 to 200 m then decreasing after 1510.
13	1000 to 1600 13	Pluming to 150 m during day--some reduction in intensity about midday, increasing in windiness about 1600 corresponded to collapse of echoes.
13	1930 to 1600 14	Very intense ground inversion echo, multiple layers 2200-2300, more diffuse top after 0010, lifted upper layer to 300 m by daylight, present through morning, indication of Kelvin-Helmholtz instability about 1100-1200--may be low level ~100 m pluming in late afternoon.
14	1900 to 1400 15	Building inversion to 2230, loses diffuseness for stronger lower layer which builds after 2300 to 300 m at 0330, descends in multiple layers to 200 m at 0800--layers persist to 1200 then dissipate with some pluming apparent to 1400.
15	1900 to 0900 16	Inversion building to 300 m by 2300, decreasing to 15 m by 0400, then a split layer to 0700 and gradual lowering of echo top.

4.3 CASE STUDY

4.3.1 Description of observed structure

The situation of 9 March from 0600 to 1100 LST, was selected for representative analysis. Originally, it was chosen in the belief that, of all the data, it would most likely prove to contain a free convective regime under the echo layer (Figure 4.3) seen by the acoustic sounder. As will become apparent, the case study contained a wealth of detail on boundary level development.

The nighttime situation existing before 0700 was fairly typical of the experiment: a pronounced nocturnal inversion rising on occasion to 150 m, topped by an oscillating echo layer of about 30 m depth with a mean base of about 100 m. This base level is comparable to the depth of the Athabasca River valley below essentially the surrounding plain. At 0640-0650 there was a sudden change in the height of the echoes, the maximum jumping to 225 m from 140 m. Over the next hour the principal echo layer slowly descended at a rate of about 1.4 $cm \cdot s^{-1}$, with evidence of another weak and intermittent layer between 0720 and 0740 at 250 m. Again at 0750 there was resurgence of the echoing up to 270 m and continual ascent of one echo layer to 300 m, but descent of another layer rather rapidly (-1.3 $m \cdot s^{-1}$ between 0815 and 0830). The upper echo layer equilibrated at 300 m from 0820 to about 0900, with four regular upwardly directed spikes appearing. Then followed a period of extensive background noise during which time the upper layer moved to about 375 m; again there was evidence of a very thin but discernible echo layer descending rapidly to the surface. After what appeared to be several rapid oscillations of amplitude in excess of 25 m, the upper layer as the last vestige of mixing seemed to blend with the lower underlying regions and descend at about 3.1 $cm \cdot s^{-1}$. After 1130 there was essentially no discernible structure to the echoing above the intermittent spikes of the acoustic noise emanating from industrial equipment upwind about a kilometre.

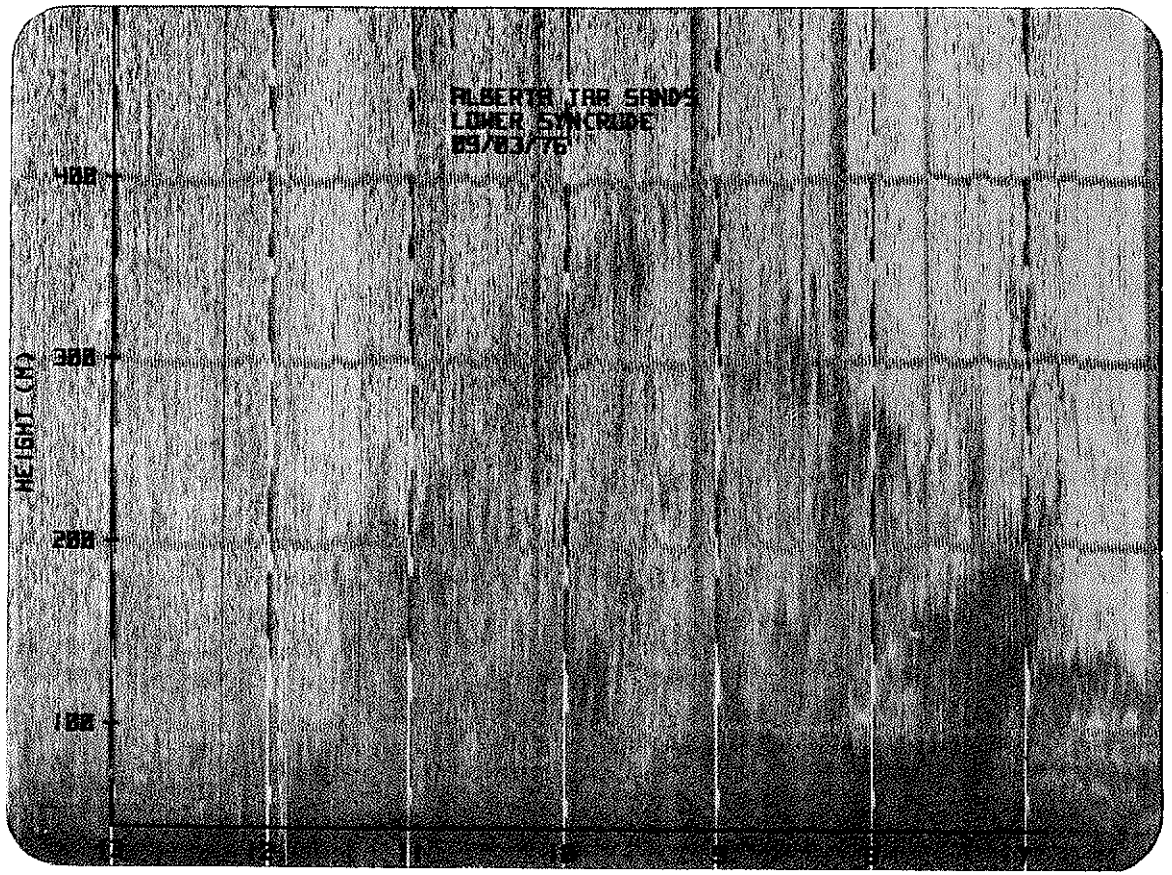

Figure 4.3. Acoustic sounder record for 9 March 1976. Time increases from right to left; height increments are 100 m.

The outstanding point of interest in this record is the splitting of the layering, one layer ascending a discrete increment, and another layer descending continuously towards the ground. Further visual consideration of the initial events at 0650 and even 0715 indicates that the pulse splitting may have existed then also. The accompanying tethersonde and minisonde data are not adequate in their time resolution to capture the comparison structure in the wind, temperature, and humidity fields. Several tethersonde profiling runs were made during the course of the "pyramid inversion" from 0700 to 1100, namely at 0700 to 0720, 0722 to 0737, and 0920 to 0944, as well as a flight from 1300 to 1320. Minisondes were flown from two sites, one in the valley near the sounder, the other upwind up on the plain with releases at approximately 0700, 0830, 0930, 1030, 1100, and 1300. Figures 4.4 and 4.5 are the tethersonde profiles of potential temperature, relative humidity, and wind speed and direction for the times mentioned. Several features are apparent. On the 0700-0720 profile there is essentially a constant potential temperature gradient to 230 m ($3.94\ 10^{-2}\ ^{\circ}C \cdot m^{-1}$), a constant wind shear up to a local maximum ("jet") at 180 m from 100 m ($5.5\ 10^{-2}\ \cdot s^{-1}$), and a distinct humidity gradient beginning about 180 m. In the next 20 min, when the only distinct acoustic echoes are descending, there is cooling in the region of the jet and a destabilization of the potential temperature gradient, up to 270 m. The jet core itself is rising slightly and intensifying. There is a noticeable acceleration also in the region of the echoes. Presumably after destabilization has proceeded far enough, the jet either totally collapses at the local level or jumps to the region of the new maximum. In any case, the echoes consistently track the maximum shear layer.

The building of the echo layer is in essence different from the classical situation of erosion of the local stable layer at the base of an inversion by the penetration of buoyant plumes. Here the vertical growth will proceed as long as there is a reservoir of cold air that can be progressively advected horizontally to override the current boundary layer cap. This is not to say that there was no

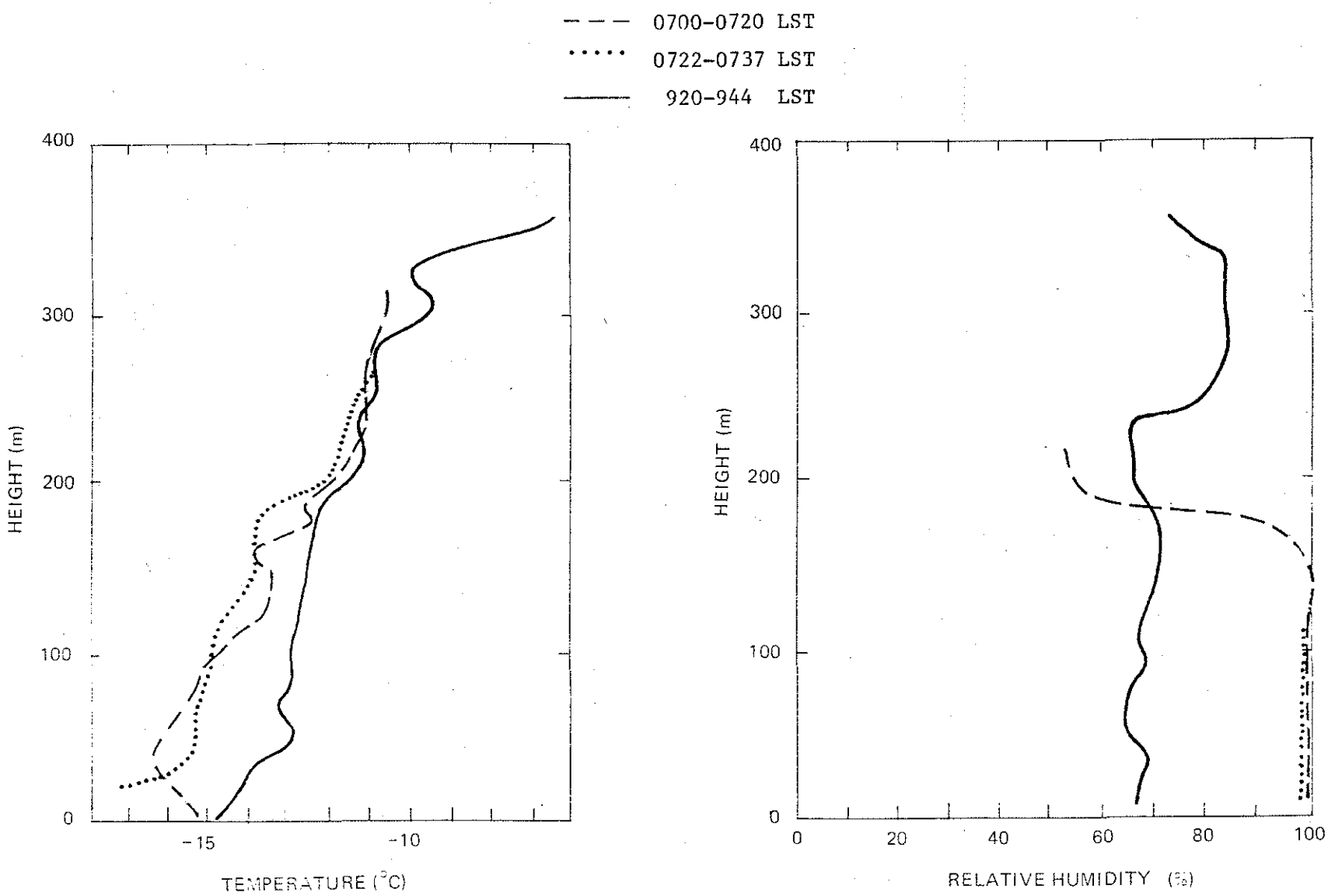

Figure 4.4. Potential temperature and relative humidity profiles with height, derived from tethersonde data for several different times on 9 March 1976.

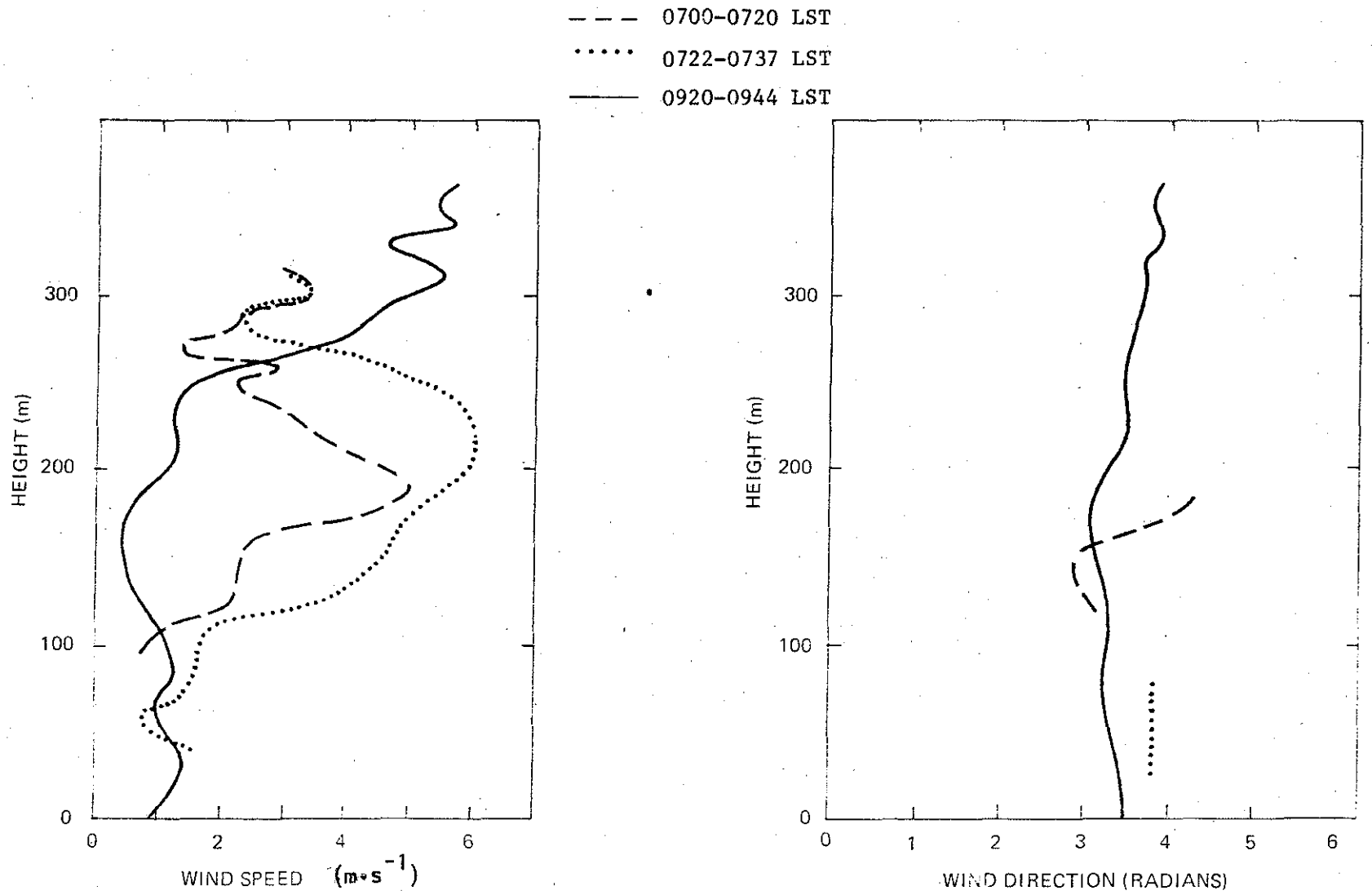

Figure 4.5. Wind speed and direction profiles with height, derived from tethersonde data for several different times on 9 March 1976.

causal effect from surface heating in excess of 12°C from sunrise to midafternoon. Up until 0930 the entire depth to the height of the echoes remained stable, with the possibility of imbedded adiabatic layers. After 0930 there is no further tethersonde data until 1300, only minisonde data. Figure 4.6 describes the time development of temperature at the Lower Syncrude site. From a very deep noctural inversion at 0650, surface heating progresses to a depth of about 180 m by 0930, with a capping inversion fixed at about 300 m. By 1030, further erosion has lifted beyond the sounder's range. This lifting after 0930 corresponds to the arrival of the lifting layer as seen by the sounder. There is significant cooling in the region above 100 m before 0830 as the layer assumes a quasi-isothermal structure to 300 m by 0930. There continues to be cooling above the 0930 and 1030 profiles.

Clearly, within the resolution of the minisonde, the growth of the boundary layer appears to be surface-controlled. However, such considerations could not explain the descending layer after 0930, which is coupled to a secondary inversion as seen on the 1100 Lower Syncrude minisonde flight at about 150 m. The downward growth of the echo layer and the inversion apparently are associated with more warming aloft than at the surface. It would seem reasonable to assume that this heating comes from advection from the plain over the valley. However, the upwind minisonde station is consistently colder with height rather than warmer. This may be due to a calibration error in one station against another. Additionally, we observed that the descending echo layer after 0930 was the last of a series of convulsive changes that accompanies the growth of inversion. Downward propagating layers, somewhat thinner, had been observed between 0700 and 0930 with similar preliminary behavior. No explanation is offered for the behavior of the step changes in the inversion and the descending layers at this time.

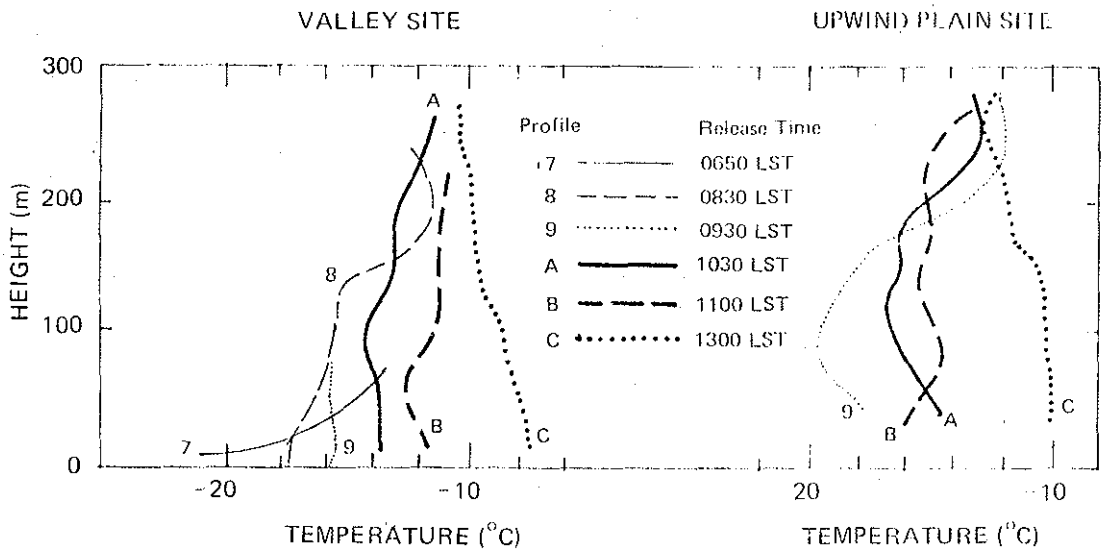

Figure 4.6. Temperature profiles with height, derived from minisonde data for several different times on 9 March 1976.

4.3.2 Scattering structure

The results of 20-min averaged profiles of $\log_{10} C_T^2$ for times corresponding to delta-T sonde soundings are displayed in Figures 4.7 to 4.9. The first case, 0700-0720, shows excellent agreement with the delta-T sonde in the region of 70 to 140 m, with distinct differences above 150 m and below 60 m. The extremely large values of C_T^2 nearest the ground are probably contaminated by acoustic ringing of the radiating horn and echoing from nearby trees. Comparison with the accompanying tethersonde profile of potential temperature indicates that the acoustic sounder "saw" the two nearly adiabatic or unstable layers between 110 and 150 m and between 175 and 190 m. On the other hand, the delta-T sonde captured the lower C_T^2 maximum and an indication of a thin upper maximum about 200 m. The acoustic sounder indicates a smaller background of C_T^2 than the delta-T sonde. It is suspected that this arises from the treatment of the noise in the acoustic derivations.

The delta-T sonde was colocated with the acoustic sounder at the Lower Syncrude complex; data were gathered over 11 days. These data were comprised of 71 profiles, of which 47 were useful, and 14 fixed-level measurements, of which 11 were of value. Table 4.3 lists the useful data.

A second profile for which there is supporting delta-T sonde and tethersonde data, 0722-0737 (Figure 4.8), again shows similarity of structure but with the acoustic sounder exceeding the delta-T sonde up to 180 m. It is not known which profile is correct; both have possible sources of error that must be further investigated. Nevertheless, both display a generally decreasing structure of $\log_{10} C_T^2$ with superimposed maxima in the vicinity of 70, 150, and 240 m. The upper maxima compare closely with the location of the maxima in shear as seen by the tethersonde. It is also worth mentioning that there was significant shear 20 min earlier in two layers about 40 m higher. Apparently the layering has distinctly split and settled. The upper maxima may herald the arrival of a new state in the convulsive inversion growth.

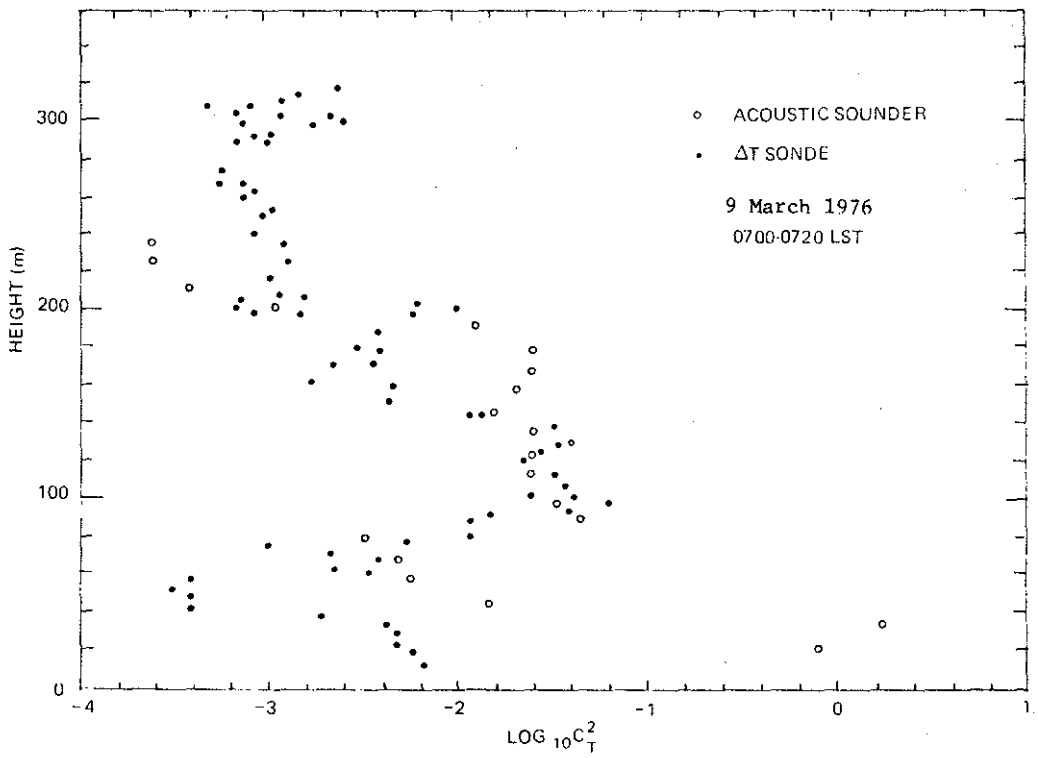

Figure 4.7. Comparison of C_T^2 estimates derived from acoustic sounder and delta-T sonde, 0700-0720, 9 March 1976.

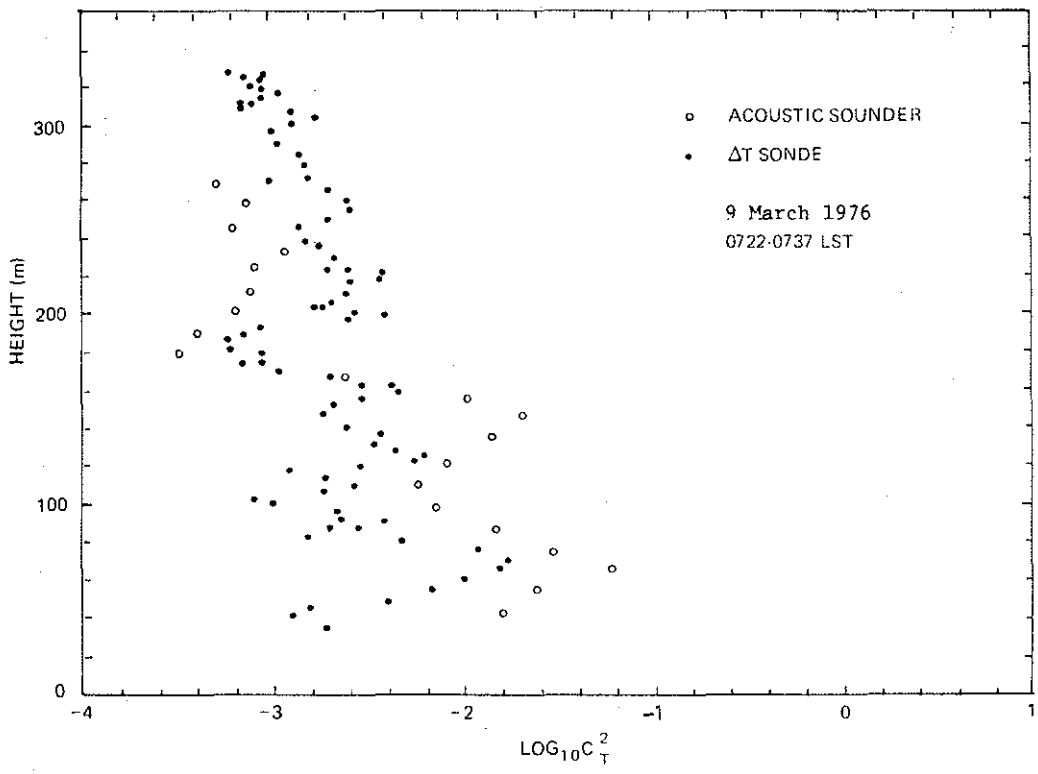

Figure 4.8. Comparison of C_T^2 estimates derived from an acoustic sounder and delta-T sonde, 0722-0737, 9 March 1976.

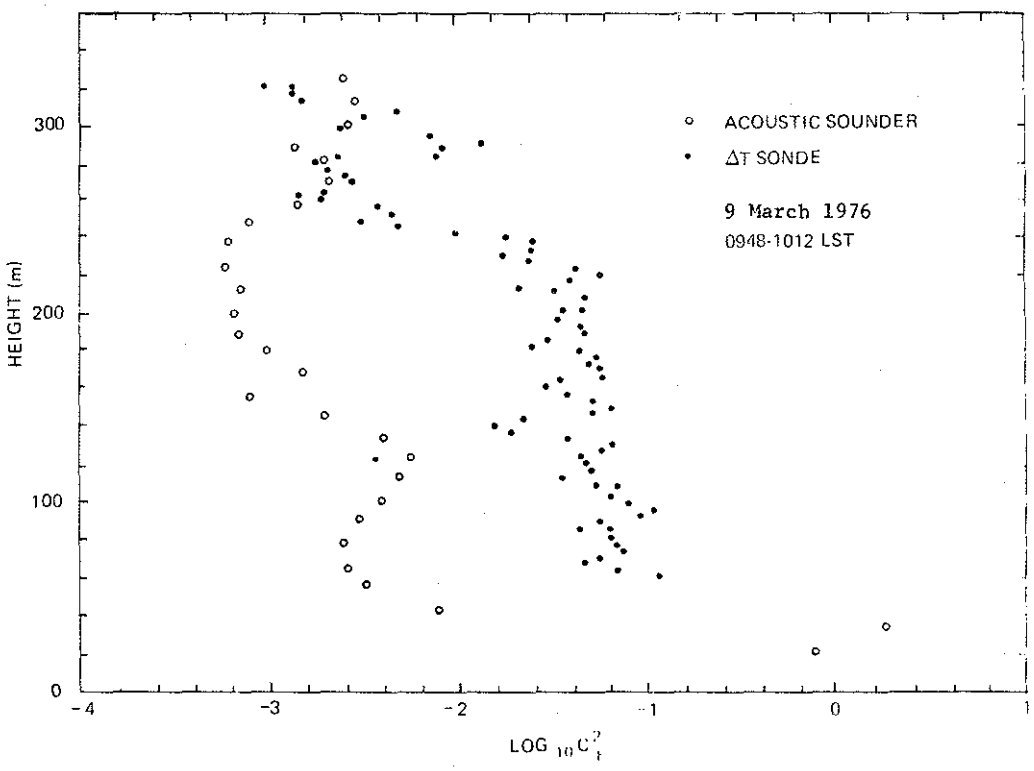

Figure 4.9. Comparison of C_T^2 estimates derived from an acoustic sounder and delta-T sonde, 0948-1012, 9 March 1976.

Table 4.3. Delta-T sonde data catalogue, March 1976.

Day	Hour	Measurement
7	0704-0731	Profile
	0740-0750	Profile
	1100-1130	Profile
	1447-1457	Fixed Height
	1511-1520	Fixed Height
8	1400-1408	Profile
	1505-1516	Profile
	1615-1648	Profile
9	0710-0743	Profile
	0919-1012	Profile
	1038-1053	Fixed Height
	1100-1109	Fixed Height
	1125-1141	Profile
10	0710-0740	Profile
	0855-0905	Profile
	0953-1026	Profile
11	0716-0747	Profile
	0748-0807	Fixed Height
	0835-0845	Fixed Height
	0853-0900	Profile
	0905-0913	Fixed Height
	0914-0937	Profile
12	1958-2013	Profile
14	0705-0740	Profile
	0742-0758	Profile
	0800-0835	Fixed Height
	0841-0920	Profile
	0921-0952	Profile
	0955-1032	Profile
	1034-1048	Profile
	1429-1442	Fixed Height
	2252-2344	Profile
	2352-0030	Fixed Height
15	0852-0914	Profile
	0916-0939	Profile
	0944-1004	Profile
	1009-1032	Profile
	1059-1121	Profile
	1330-1346	Profile
	1350-1615	Fixed Height
16	0656-0740	Profile
	0926-0951	Fixed Height
	1114-1120	Profile
	1320-1346	Profile

The comparison between the Delta-T sonde and acoustic sounder for the 0948-1012 period (Figure 4.9) is rather puzzling. Although the instruments had agreed well in a qualitative sense in most aspects, there is essentially no agreement in Figure 4.9. The delta-T sonde indicates that the scattering had increased by over an order of magnitude, since 0740 up to 200 m. The acoustic sounder indicates a general decrease in C_T^2 after 0740 near the ground. The decrease in the lower maximum near 120 m is of the order of four. No explanation of this disparity has been found to this time.

4.3.3 Estimation of turbulent diffusion parameters

Plume dispersion coefficients (σ) may be characterized under rather idealized conditions by empirical relationships of the form:

$$\sigma = V_c t \; F \; (\hat{z}_s, \hat{x}, \hat{z}, \mu)$$

where $\hat{z}_s$, $\hat{x}$, $\hat{z}$, and μ are normalized source height, downwind distance, height, stability and t is the travel time from the source. V_c is a characteristic velocity commensurate with the normalization of lengths and stability. For example, for a freely convective boundary layer the characteristic length is z_i, the inversion height, and the normalizing velocity is given by Kerman (1976b):

$$V_c = (\varepsilon_c \, z_i)^{1/3}$$

where ε_c is the characteristically constant dissipation rate in the upper reaches of the convective boundary layer, $z \simeq z_i$.

A recently proposed method (Kerman 1976a) utilizes C_T^2 estimates from an acoustic sounder and wind shear estimates from an acoustic sounder or by an alternative method to infer the value of the characteristics applied to the data from 0700 to 0720 period of 9 March. The region between 200 and 280 m was of particular interest because a plume from Stack A of the GCOS plant was confined there (see Section 5). In this region, according to the delta-T sonde,

C_T^2 is essentially constant at about $10^{-3}{}^{o}C^2 \cdot m^{-2/3}$. The acoustic sounder indicates the value of C_T^2 is about $2.5\ 10^{-4}{}^{o}C^2 \cdot m^{-2/3}$. This latter estimate is probably too low because of the elimination of valid signals in the treatment of the noise spikes. A similar disparity between the estimates of C_T^2 arises in the 0722 to 0737 data period in the 200- to 300-m interval (Figure 4.8). It was therefore assumed that the delta-T sonde produced the more reliable estimate of C_T^2. The shear in the region of 190-270 m was estimated from the tethersonde data to be 3.75 $m \cdot s^{-1}$, and the average potential temperature gradient to be $3 \cdot 10^{-2}\ {}^{o}C \cdot m^{-1}$.

The stability parameter (Kerman 1976a) was computed for the 200- to 280-m layer according to the formula:

$$\zeta = \frac{g}{\bar{\theta}} \frac{C_T}{\beta^{1/2} (\kappa \Delta z)^{2/3}} \left[\frac{\partial \bar{U}}{\partial z}\right]^{-2}$$

where Δz is the layer depth, g is the acceleration due to gravity, $\bar{\theta}$ is the mean potential temperature, β is the constant ($\sim$3.2), κ is von Karman's constant ($\sim$0.4), $\bar{U}$ is the mean wind velocity. The use of a layer depth seems more appropriate than height in view of the vertical layering and the constancy of the C_T^2 and $\bar{U}/\partial z$ in these layers.

For the 200- to 280-m layer $\zeta \sim 0.047$. Following the method, this value of ζ implies certain values of the "universal" similarity functions of shear, dissipation variance, etc., that allows for computation of the turbulence parameters. From published graphs and supporting data drawn from the Kansas experiment (Izumi 1972) we compute for $\zeta = 0.047$, $V_c = 0.8\ m \cdot s^{-1}$. This value seems reasonable when compared to surface-based experimental results, but somewhat large for an elevated layer. It is emphasized that it is probably reliable to no better than a factor of two considering the variability of the mean and turbulent flow during the time, the approximation from height to layer depth, and the insensitivity of the method in a stable regime.

As a last step in applying the method, the vertical plume spreading (σ_z) was estimated and compared to Fankai's visual estimate. From theoretical arguments and experimental validation:

$$\sigma_z \sim 0.4\ V_c t$$

in a neutral surface boundary layer if the source is ground-based and

$$\sigma_z \sim 1.2\ V_c t$$

for an elevated source. It would appear from Fanaki's published plume height values, reproduced in Table 4.4, that the plume used up its superbuoyancy on reaching the 200-m level and was effectively "ground based" to the 200- to 280-m layer. Accordingly, the vertical spreading is more likely to be approximated with the 0.4 coefficient.

Fanaki's estimate of vertical spread (σ_z = 96 m) was made at the point of maximum plume rise or at 1000 m. The depth averaged wind from the tethersonde was 3 $m \cdot s^{-1}$ at this time. Accordingly, the estimate of the vertical standard deviation is:

$$\sigma_z = 0.4\ (0.8)\ (1000/3)$$
$$= 106 \text{ m.}$$

It must be emphasized that uncertainty in the factors listed above as well as the 0.4 coefficient preclude having much confidence in this estimate, although the estimate is certainly not unreasonable, in fact, surprisingly good. More cases need to be analyzed before assessing the accuracy of the method.

Table 4.4 Summary of Fanaki's plume rise measurements (Section 5) for 0700 on 9 March 1976 from the GCOS plant.

Distance Downwind (m)	0	200	400	600	800	1000
Plume Height (m)	196	266	274	286	286	281

4.4 SUMMARY AND CONCLUSIONS

An acoustic sounder, delta-T sonde, and tethersonde were combined in a study of atmospheric mixing structure in the AOSERP Study Area. Problems associated with cold-weather operation of the equipment were overcome and a reasonable data set was obtained.

An overview of the acoustic data has indicated some rather complex and unsuspected atmospheric structure, especially under stable, light-wind conditions in the Athabasca River valley. In particular, these include the convulsive growth and layer splitting of the local boundary layer and the appearance of shear-dominated layers of constant C_T^2. The origin of these and other features as well as their impact upon plume dispersion require further study.

The complex nature of many of the acoustic records has indicated that the acoustic sounder still requires additional supporting data if it is to act as an effective indicator of mixing structure from the air pollution point of view. The rich diversity of the boundary layer structure still provides a challenge in interpreting the records and making meaningful estimates of mixing. The observed discrepancies between acoustic returns and in situ turbulence characteristics need further study before a proper picture of the mixing phenomena can be developed. On the other hand, the results of the initial attempt to estimate the vertical plume dispersion coefficient from calibrated acoustic data appears promising. However, this area requires additional in-depth study into the characteristics of diffusion in a stable boundary layer before it can be properly utilized.

Even at the current state-of-the-art, an acoustic sounder is a valuable adjunct to the more classical approach to empirical air pollutant dispersion studies. The methodology is ground-based, can be automated, and therefore, is relatively inexpensive. It can perform as a high-resolution indicator of atmospheric inhomogeneities that might be missed by standard sensors and will permit both temporal and spatial interpolation of atmospheric structure between conventional soundings. Also, its sensing of atmospheric turbulence parameters directly assists in the application to estimating diffusion (Kerman 1976b).

4.5 REFERENCES CITED

Beran, D.W. and F.F. Hall Jr. 1974. Remote sensing for air pollution meteorology. Bull. Am. Meteorol. Soc. 55: 1097-1105.

Izumi, Y. 1972. Kansas 1968 field program data report. Air Force Cambridge Research Laboratories (U.S.A.), Report AFCRL-72-0041. Environmental Research Paper 379. 80 pp.

Kerman, B.R. 1976a. A note on the interpretation of acoustic sounder returns. Boundary-Layer Meteorol. 10: 303-310.

_____ 1976b. Application of acoustic sounding to estimating diffusion in an atmospheric boundary layer. Presented to the 92nd meeting of the Acoustical Society of America, San Diego, Nov. 1976. (Abstr. in J. Acoust. Soc. Am. 60, Suppl. 1: 532).

_____ 1976c. An application of acoustic sounding to the estimation of turbulence and vertical plume spread in a stable boundary layer. Report /ARQL-76/1, Air Quality and Inter-Environmental Research Branch, Atmospheric Environment Service Environment Canada: Downsview, Canada. 30 pp.

Little, C.G. 1969. Acoustic methods for the remote probing of the lower atmosphere. Proc. IEEE 57: 571-578.

Tatarski, V.I. 1961. Wave propagation in a turbulent medium, McGraw-Hill. 89 pp.

Wycliff, R.J., D.W. Beran and F.F. Hall Jr. 1973. A comparision of the low-level radiosonde and the acoustic echo sounder for monitoring atmospheric stability. J. Appl. Meteorol: 1196-1204.

5. PLUME RISE

by F. Fanaki, J. Kovalick and R. Froude

There is a tendency for industrial complexes to use stacks to discharge their waste into the atmosphere in order to elevate the exhaust fumes above the ground. This reduces the magnitude of the pollution problem.

Other factors of equal importance such as wind speed, wind direction, topography of the area, and thermal stability of the atmosphere influence the rise of the industrial plume. These may combine to bring the plume to ground level a short distance from the plant. They may also produce an inversion layer which, in a limited region, would prevent the plume from rising and dispersing the pollutants. Such a "lid" on the plume rise increases the concentration of pollutants. Thus, in order to plan some controls of the air quality for an area, one needs to have data available concerning the rise and behaviour of industrial plumes as a function of all these factors. The following report is directed towards this end.

Field observations of the rise and behavior of the plumes emitted from the GCOS plant at Tar Island were made as part of the Meteorology and Air Quality Winter Field Study from 4 to 16 March 1976. The study also included measurements of SO_2 ground concentrations. This report presents the analysis of the observations in table form for duplication and distribution as required. It also includes a comparison of the observations with predictions calculated on the basis of concurrent meteorological measurements. This information will be useful in the stack design of other plants in the area.

5.1 SOURCE DESCRIPTION

The GCOS plant is located 40 km north of Fort McMurray, Alberta, on the west bank of the Athabasca River (Figure 5.1). The elevation of the area ranges from 250 m along the Athabasca River to over 300 m MSL above the river valley. The land slopes gently upwards to the northeast. The topography around the river is slightly variable, ranging from undulating to rolling.

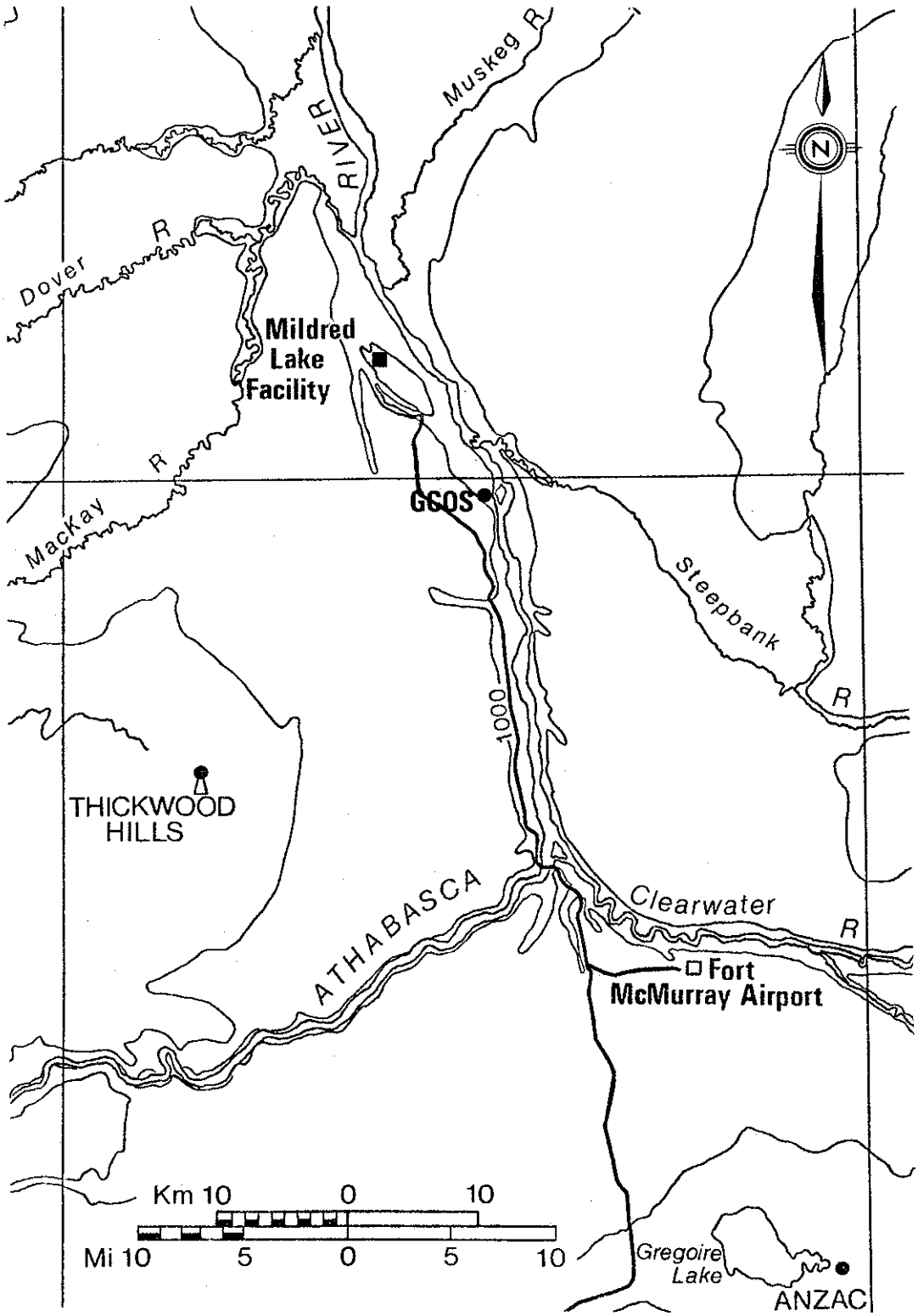

Figure 5.1. Map of the Tar Island Area.

The major emission sources in the GCOS plant are three stacks: the power plant stack (A), the refinery flare stack (B), and the incinerator stack (C). They discharge SO_2-bearing gases into the atmosphere. Figure 5.2 shows the GCOS plant in operation. Locations of the stacks are shown in Figure 5.3. Only the plume rises from stacks A and B were measured. Physical characteristics of the stacks are given in Table 5.1; emission parameters of stack A during the study period are in Table 5.2.

5.2 PLUME RISE MEASUREMENT

There are three basic techniques available for measuring the rise of the plume:

1. plume sampling by an aircraft,
2. traversing the plume by a remote sensor, and
3. photographing the plume.

The latter is the method used in this study. This technique is the simplest, is economical, and provides a permanent record at any given instant of the shape of the plume (Fanaki and Lessins 1975). To provide a method of levelling the camera and to ensure that the film plane would lie along the vertical, the camera used in this study was mounted on a theodolite (Figure 5.4). Before each experiment the wind direction was determined and the theodolite optical axis was set parallel to the wind direction. The theodolite, together with the camera, was rotated by 90° from this bearing towards the smoke.

Location of the photographing site (Figure 5.5) was chosen before the measurements were made. Due to the uncertainty of the azimuthal position of the plume at any instant and the randomness of the plume height, many photographs were required in order to average out deviations from the mean. The plume of the GCOS plant was photographed every 15 s over a period of about 10 min. By superimposing several photographs and tracing the plume outlines, or by using time-average photographs of the plume (Figure 5.6), a time-mean path of the plume was obtained. A sample of an experimental result is shown in the form of a plume trace (Figure 5.7). Table 5.3 shows the mean plume rise above the stack top as a function of the downwind distance

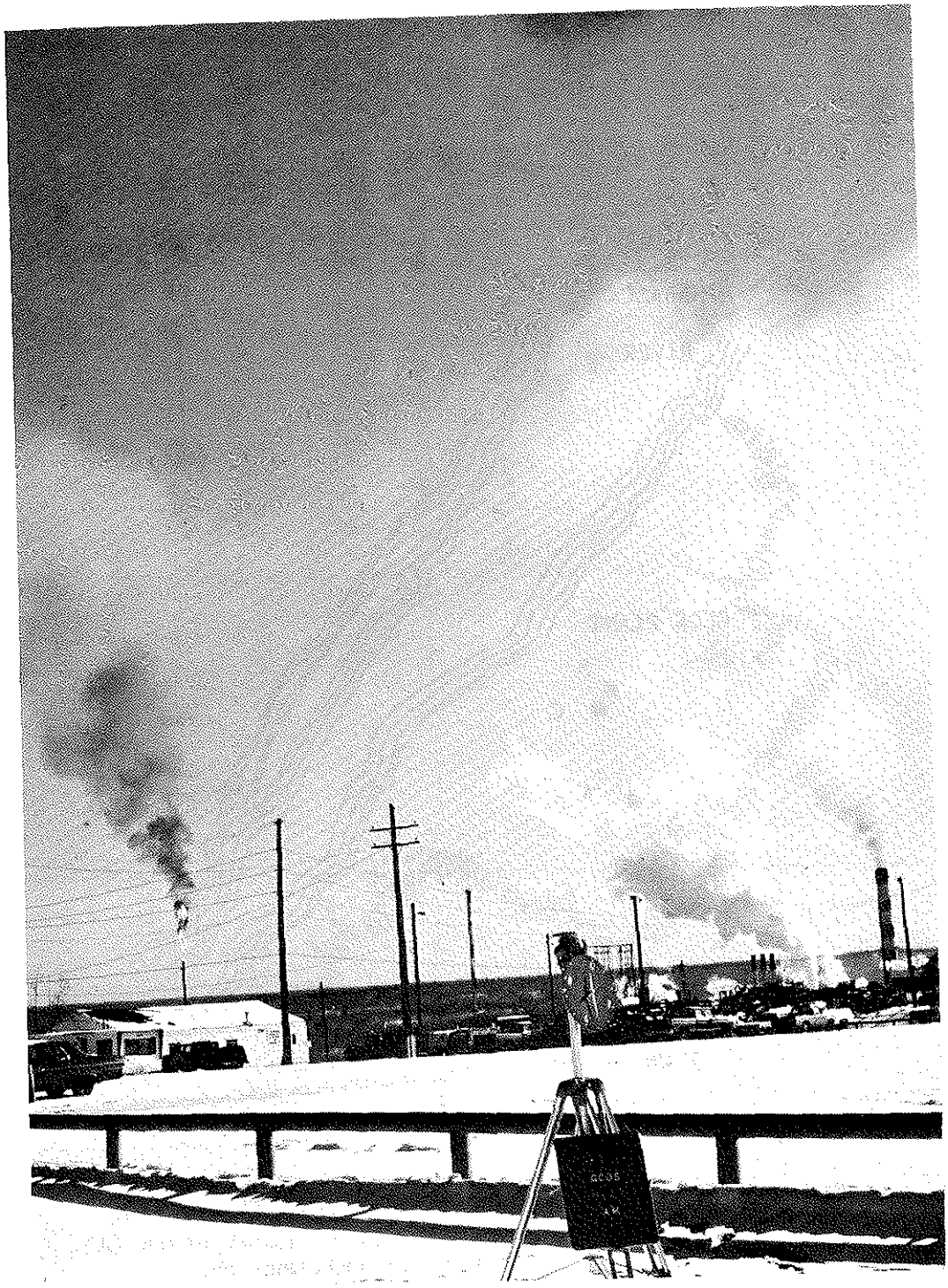

Figure 5.2. The GCOS plant in operation.

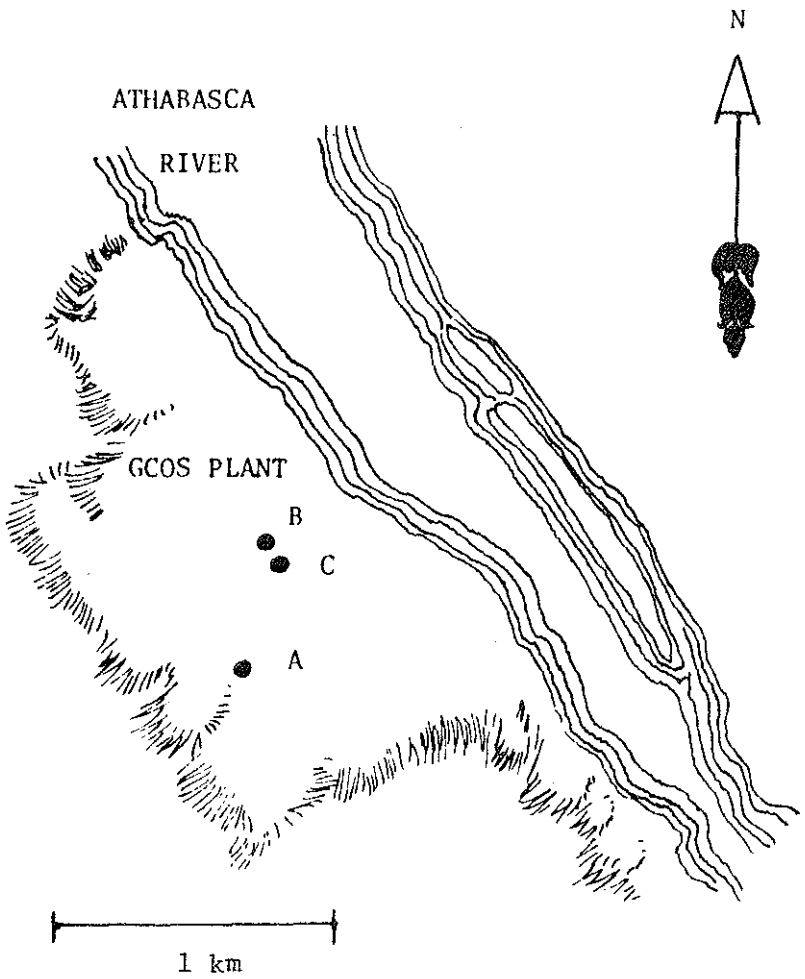

Figure 5.3. Map of the GCOS plant area illustrating the location of the power plant stack (A), refinery flare stack (B), and the incinerator stack (C).

Table 5.1 Physical characteristics of the GCOS stacks.

Parameter	Magnitude		
	Stack A	Stack B	Stack C
Height above ground (m)	106	99	107
Inside Diameter (m)	5.89	1.1	1.8

Table 5.2. Emission parameters of stack A*.

Date	Effluent Rate $m^3 \cdot s^{-1}$	Gas Temp C^o	Gas Velocity $m \cdot s^{-1}$	Heat Flux k cal sec^{-1}	SO_2 in Stack Gas ppm
Mar 4	470	280	17	17978	4300
Mar 5	437	263	16	15676	3169
Mar 6	437	265	16	16085	4035
Mar 7	462	276	17	17639	3915
Mar 8	457	258	17	16966	4061
Mar 9	485	279	18	18655	3812
Mar 10	520	289	19	19721	3718
Mar 11	539	283	20	20093	3718
Mar 13	425	253	16	15836	3293
Mar 14	522	273	19	19510	3661
Mar 16	450	265	17	17152	4020

* Data from which the calculations are made were obtained from Mr. W.L. Cary, GCOS, Ltd.

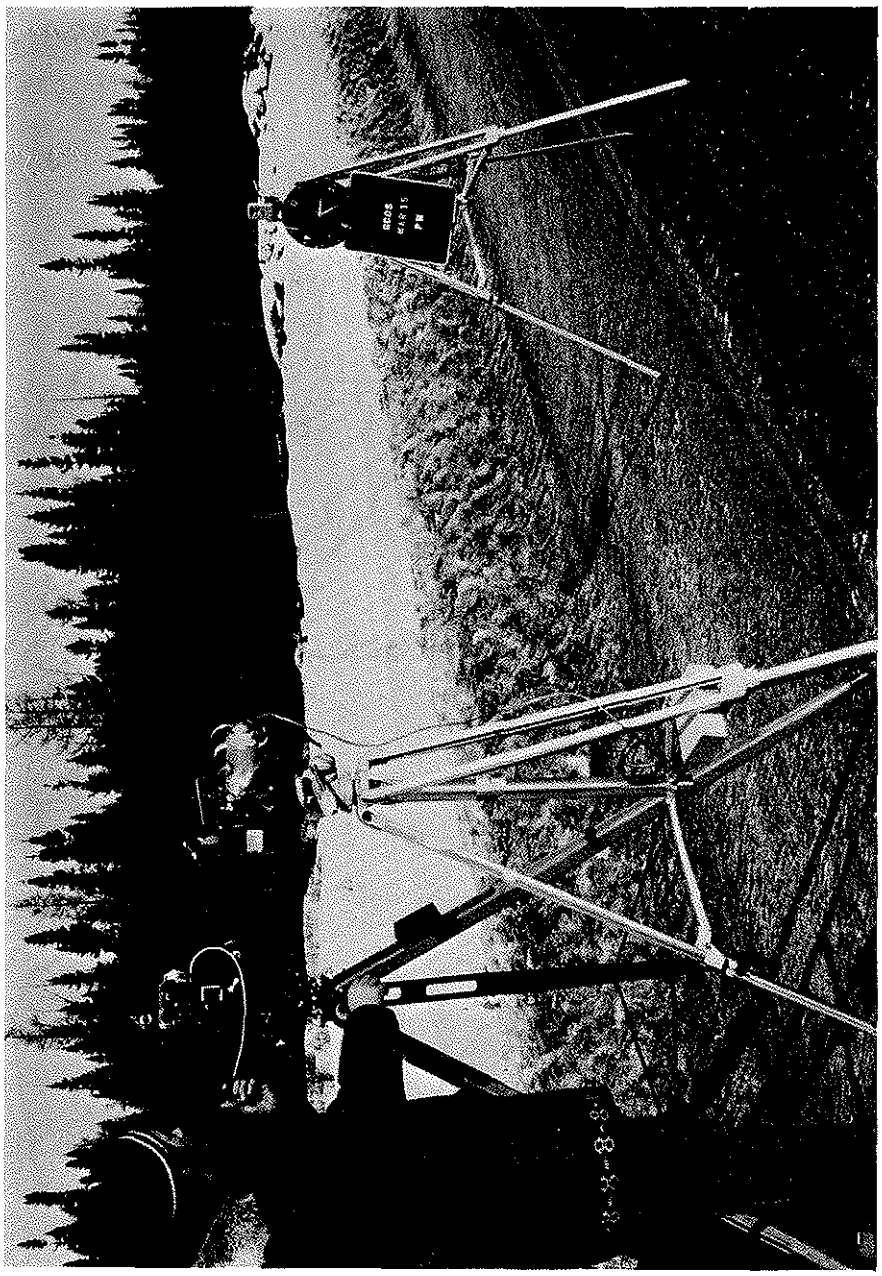

Figure 5.4. Camera setup and associated equipment.

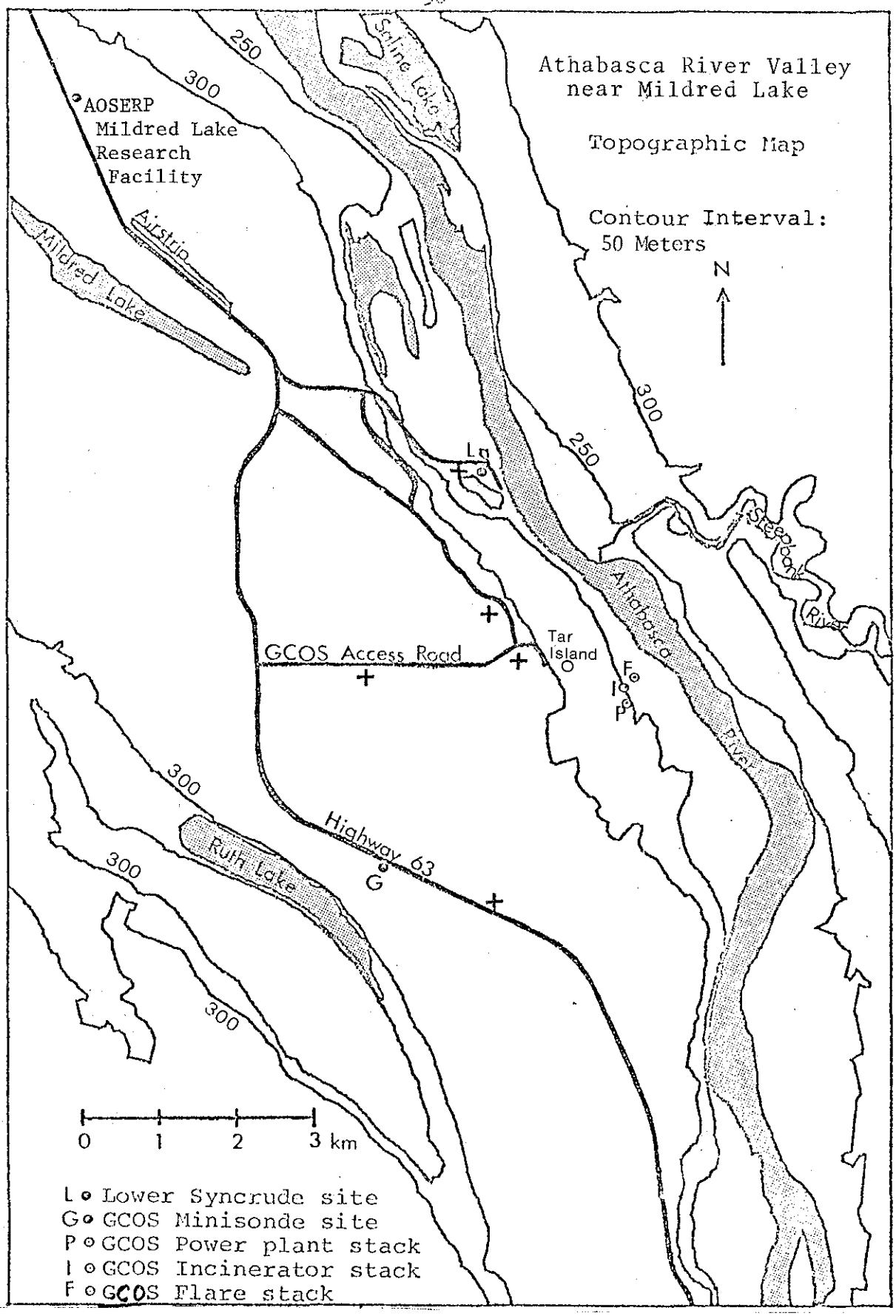

Figure 5.5. Map of the Athabasca River valley near Mildred Lake, showing the location of the plume photography (+ + +) March 1976 Winter Field Study.

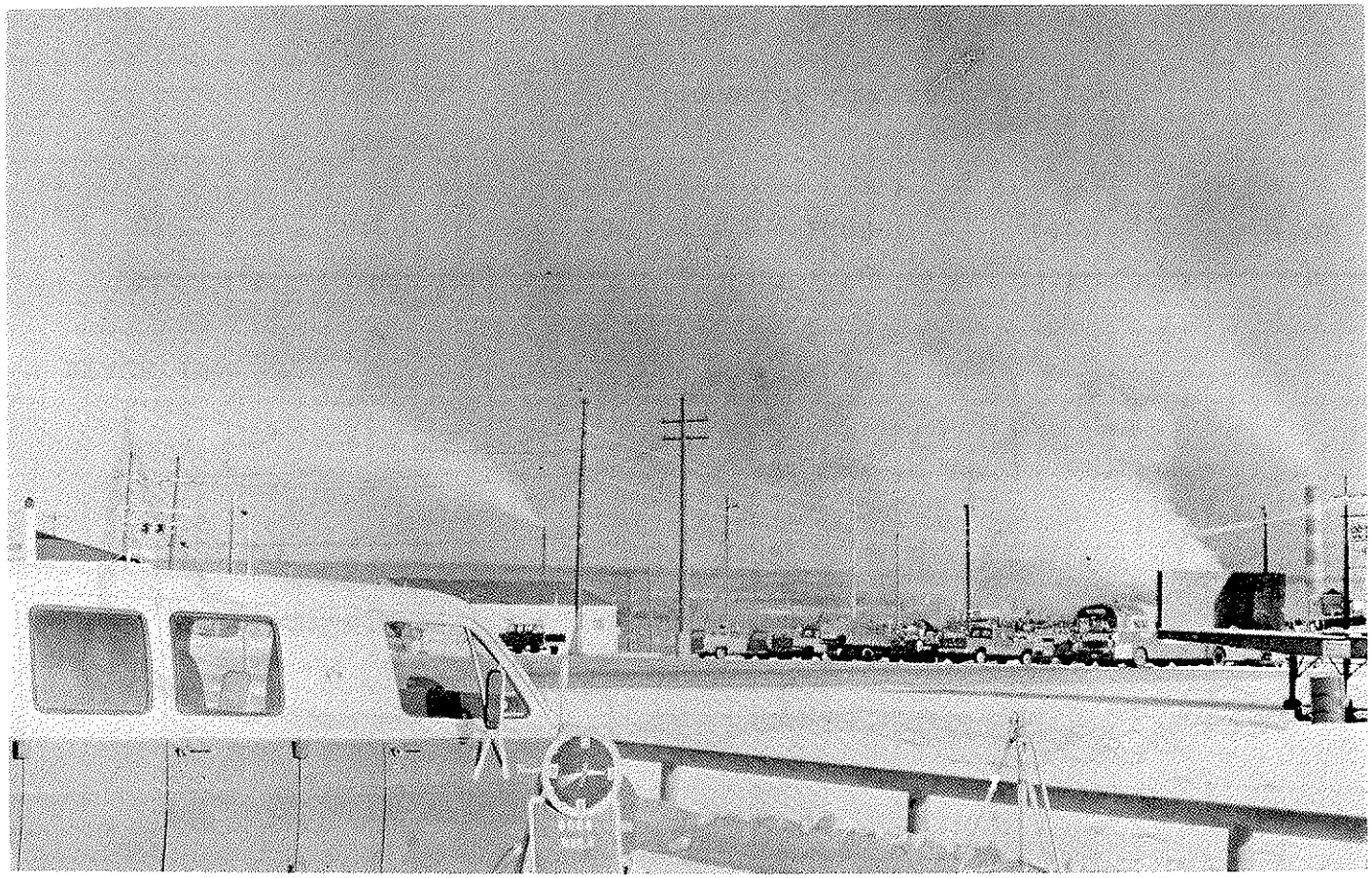

Figure 5.6. Time-average photograph of the power plant and the flare plumes of the GCOS plant.

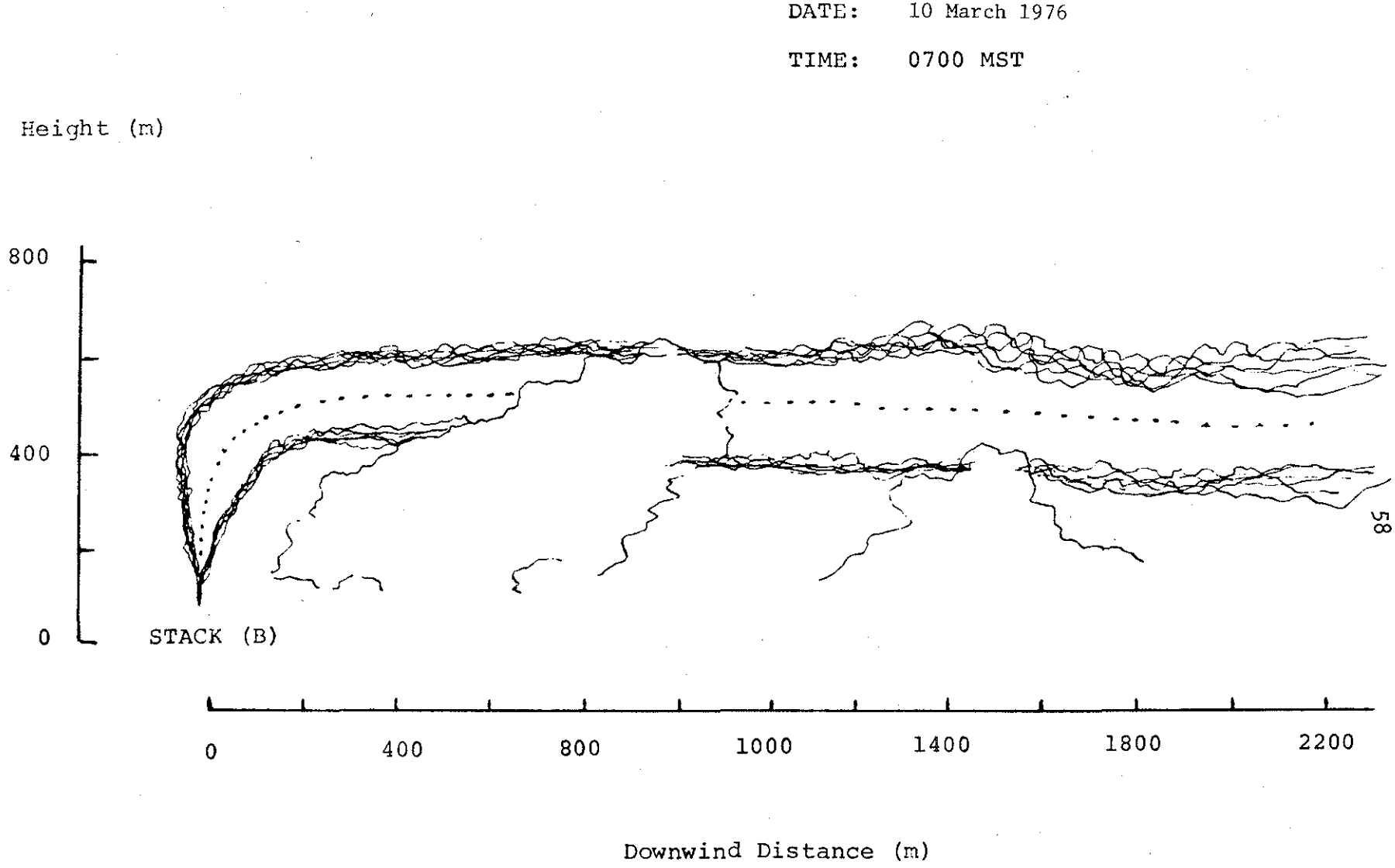

Figure 5.7. Trace of the refinery flare plume (stack B) as a function of height and horizontal distance.

Table 5.3. Plume rise above stack top as a function of downwind distance.

Date	Time	Stack	Downwind Distance (m)								
			0	200	400	600	800	1000	1200	1400	1600
4 March	0845	A	0	135	225	75	287	87			
	0845	B	0	88	112	125	125	125			
	0920	A	0	81	109	110	110	114			
	0920	B	0	36	45	45	39	40			
	1405	A	0	120	170	178	180	180			
	1407	A	0	126	166	180	181	180			
	1410	B	0	69	95	100	101	100			
	1415	B	0	7	84	96	100	100			
	1418	B	0	60	91	97	100	101			
	1530	A	0	145	180	181	181				
	1530	B	0	86	90	95	96	96			
	1545	A	0	150	205	204	205	205			
	1545	B	0	43	80	81	81				
	1620	A	0	136	192	264	320	320	328	344	341
	1620	B	0	72	72	56	80	80			
	1620	A	0	140	191	259	310	321	330	345	346
	1620	B	0	69	70	79	80	81			
5 March	0645	A	0	85	128	157	185				
		B	0	142	185	187	185				
	0810	A	0	58	70	75	83	83	83	83	
	0815	A	0	52	66	75	83	83	86	83	
	0820	A	0	46	60	70	78	79	85	83	
	0825	A	0	43	64	72	75	79	84	84	
	0830	A	0	44	70	79	80	81	84	83	
		B	0	50	56	70	70				
	1500	A	0	33	77	88	78	65	78	99	97
	1505	A	0	44	78	44	44	60	79	90	98
	1510	A	0	60	80	59	78	78	90	90	
	1540	A	0	80	80	90	110	143	142	140	
	1545	A	0	71	90	91	100	129	140	141	
6 March	0700	A	0	123	169	170	171	170			
		B	0	46	79	80	79	80			
		A	0	126	157	189	180	179			
		B	0	50	79	91	81	81			
		A	0	130	168	179	180	180			
		B	0	35	71	94	71	60			
	1045	A	300	363	363						
	1600	A	0	71	100	129	130	131			
7 March	0645	A	0	146	180	186	186				
	0645	A	0	140	173	186	185				

continued...

Table 5.3. Continued.

Date	Time	Stack	Downwind Distance (m)								
			0	200	400	600	800	1000	1200	1400	1600
8 March	0950	A	0	360	480	570	610	610	610	590	580
	0950	A	0	346	425	530	538	613	610	580	580
	1015	A	0	256	344	400	424	416	400	400	410
	1015	A	0	350	360	430	460	410	400	410	400
	1350	A	0	425	537	587	587	587	589	588	
	1355	A	0	437	537	575	588	588	588	588	
	1400	A	0	384	492	530	561	561	561	561	
	1400	A	0	400	470	550	570	560	560	570	
9 March	0720	A	90	160	168	180	180	175			
	0750	A	89	163	168	182	180	178			
	0805	A	80	166	162	172	181	179			
	0810	A	79	168	162	173	179	180			
	0820	A	80	172	181	179	180	180			
	0845	A	133	240	233	220					
	0845	A	146	220	227	227					
	1730	A	120	610	750	820	830	830			
	1730		110	630	760	860	800	800			
10 March	0655	A	300								
	0700	B	125	412	425	412	400	389	387	382	382
	0715	B	0	357	371	385	400	385	385	385	380
	1125	A	0	470	460	450	430	440	440		
	1135	A	0	480	410	410	400	400	410		
	1540	A	64	791	773	764	718	700	691		
	1540	A	109	782	755	709	691	682	682	682	
11 March	1110	A	150	425	450	437	412	387	362	312	312
	1120	A	175	430	412	375	350	359	360	290	290
		A	150	400	430	390	330	290	250	250	280
	1125	A	187	450	450	437	400	362	362	350	337
	1505	A	0	142	192	200	200	205			
	1520	A	0	121	171	200	207	200			
	1525	A	0	140	160	192	207	206			
13 March	0645	A	0	120	130	130					
		A	0	106	130	130	133				
		A	0	99	128	133	130				
	1040	A	0	200	290	380	440	475	480	476	474
14 March	0915	A	0	142	150	142	150	157	157		
	1035	A	0	157	160	158	164	150	158		
	1105	A	554								
15 March	1210	A	466	600	580	589	580				

continued...

Table 5.3. Concluded.

Date	Time	Stack	Downwind Distance								
			0	200	400	600	800	1000	1200	1400	1600
16 March	0700	A	0	172	200	218	218	200	200	200	200
	1105	A	125	350	351	356	350				
	1115	A	150	349	348	350					
	1120	A	160	340	350	350					
	1135	A	57	300	320	330					
	1505	A	0	191	208	216	216				

from stacks A and B. Since the plume never levels off, its final rise was assumed to be reached when its rate of rise was minimum (Montgomery et al. 1971).

In applying this technique there are some sources of error due to fluctuations in wind direction, distortion and visibility of the plume image, camera orientation, and data reduction.

The inconsistency of wind direction produces the largest error of concern. The direction of the wind depends on many meteorological factors and on the topography of the area. The theory used in calculating the plume rise in this work incorporates changes in the wind direction, which requires measurements of the direction of the wind. Data on the wind direction were obtained from the minisonde observations at the Lower Syncrude complex. The measurements, however, may be uncertain by approximately 5^{o}. Errors arising from such uncertainty introduce an error of about 9% in the estimation of the rise of the plume.

One other error which may arise in the course of applying this technique is due to human misjudgment and the use of less accurate measuring equipment. To minimize errors of this type, care must be taken in measuring distances and angles from the print and in the field. An aerial photograph of the site is most useful. The contribution to the error in estimating the plume rise is of the order of 3%.

When the plume image is projected for analysis, distortion is created by the camera and projector lens system. The largest error of this type is due to the pincushion effect, which varies from one lens system to another. This effect was held to a minimum by keeping the plume in the center of the view field of the camera and is ignored in this study.

The total error arising from applying this technique is estimated to be about 10%.

5.3 APPLICATION OF PLUME RISE FORMULAS

There are numerous formulas for modeling the rise of a buoyant plume (Briggs 1969). In order to model the rise of a buoyant stack plumes in the Tar Island area, these widely used formulas require

re-evaluation. In this study the most commonly used formulas, namely Briggs (1969, 1971, 1972), TVA 1971 and 1972 (Montgomery et al. 1971, 1972), Holland (1953), CONCAWE (Brummage 1968) and Moses and Carson (1967) were selected to examine their predictive capability in determining the rise of the GCOS from Stack A plume. This was done by comparing the observed plume rise with the predictive value; the results are shown in Figures 5.8-5.13. Mean wind speed between the stack top and the top of the plume was used in the comparison. Values of the wind speed were obtained from the minisonde observations that were made at the Lower Syncrude complex. It can be seen by the scatter of the points in the figures that none of the models is a good predictor for the measured values. Briggs, TVA 1972, and Moses and Carson's formulas underpredict the rise of the plume, which will lead to overestimation of the maximum ground-level pollutant concentration. The reverse is true with the remaining formulas.

The predictive capability of the formulas depends on the wind speed. Table 5.4 shows the mean values of the ratio of the observed plume rise to the predicted value of the plume rise for different ranges of wind speed. With all the formulas except Briggs's, the fit becomes steadily worse with increase in the wind speed. By comparison, Holland's model appears to perform best, but the correlation is still low when one considers the strong dependence of predicted concentrations upon assumed plume rise.

In addition to the determination of the plume rise, some interesting observations on the behavior of the plume are recorded. These were made using still and movie cameras (Figure 5.4) on the ground and from the air in a helicopter.

A sample of these salient features is shown in the next few figures (Figures 5.14-5.21). On some occasions during the morning, the plumes from the GCOS plant were trapped under an inversion layer and fanned. This limited their rise to the inversion base height, and the plume outlines appeared as a thin ribbon. On other occasions, some of the plumes were able to penetrate the inversion layer and continue to rise till they lost their buoyancy and momentum.

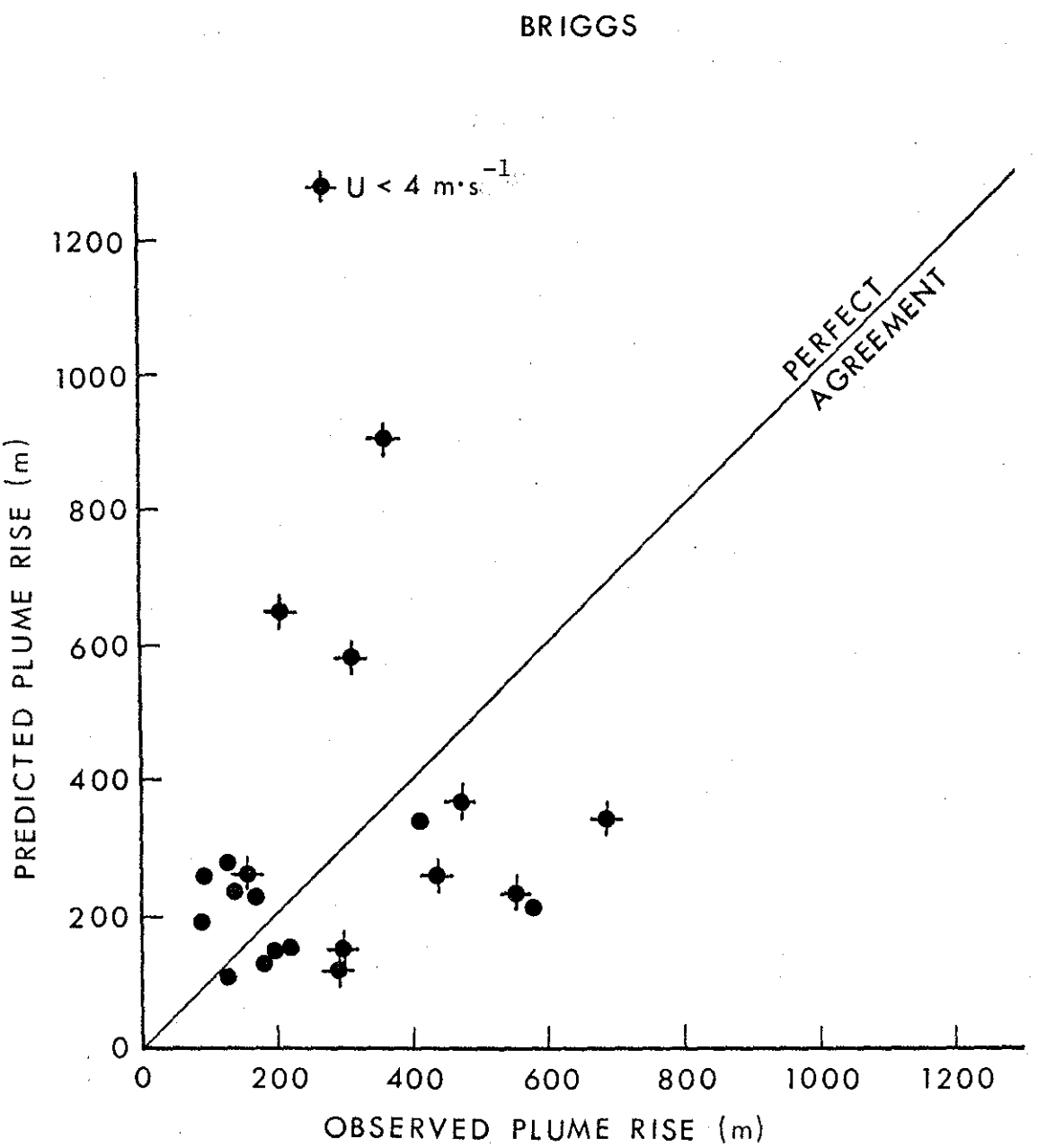

Figure 5.8. Comparison of predicted versus observed plume rise using Briggs's model.

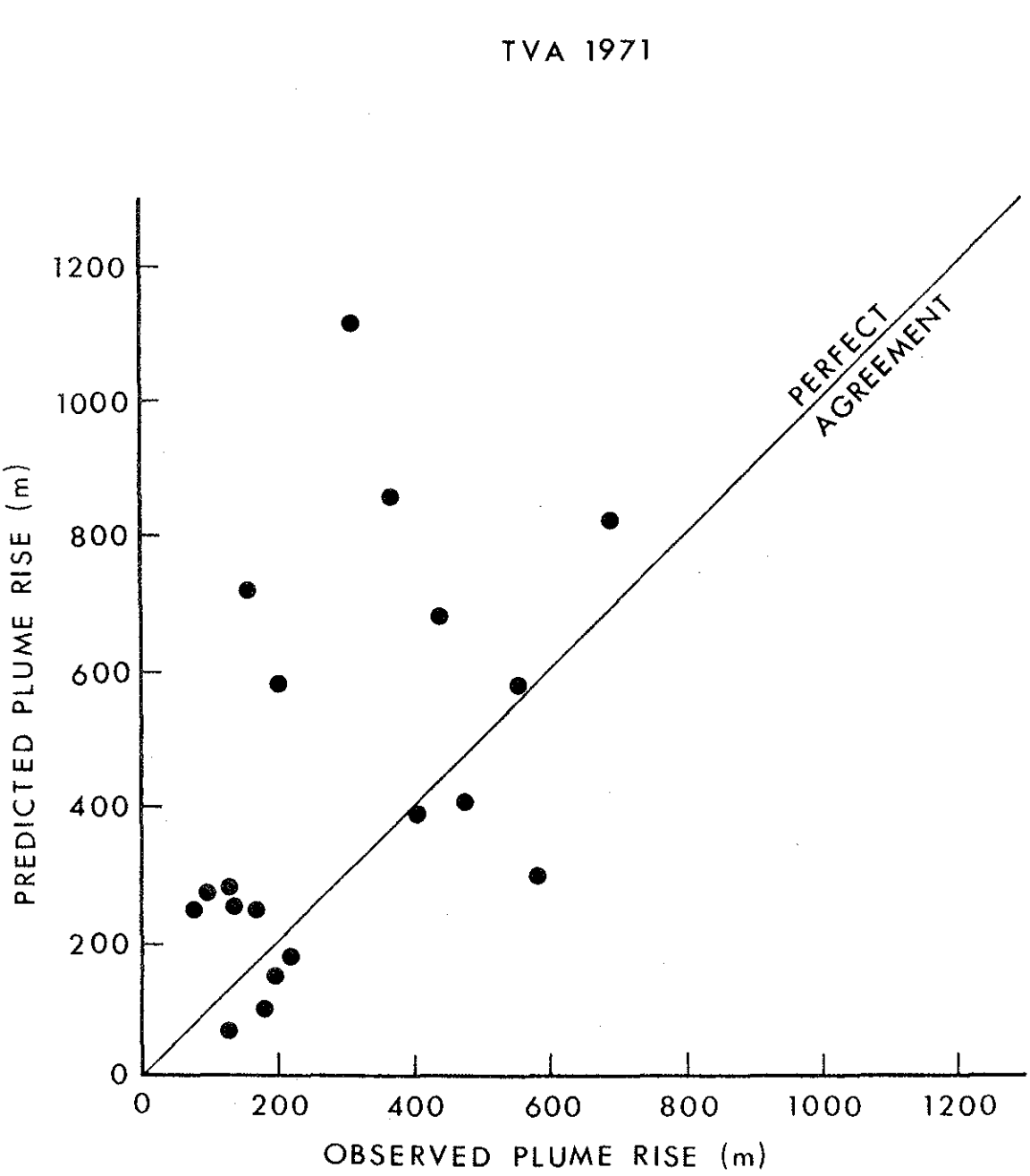

Figure 5.9. Comparison of predicted versus observed plume rise using TVA (1971) model.

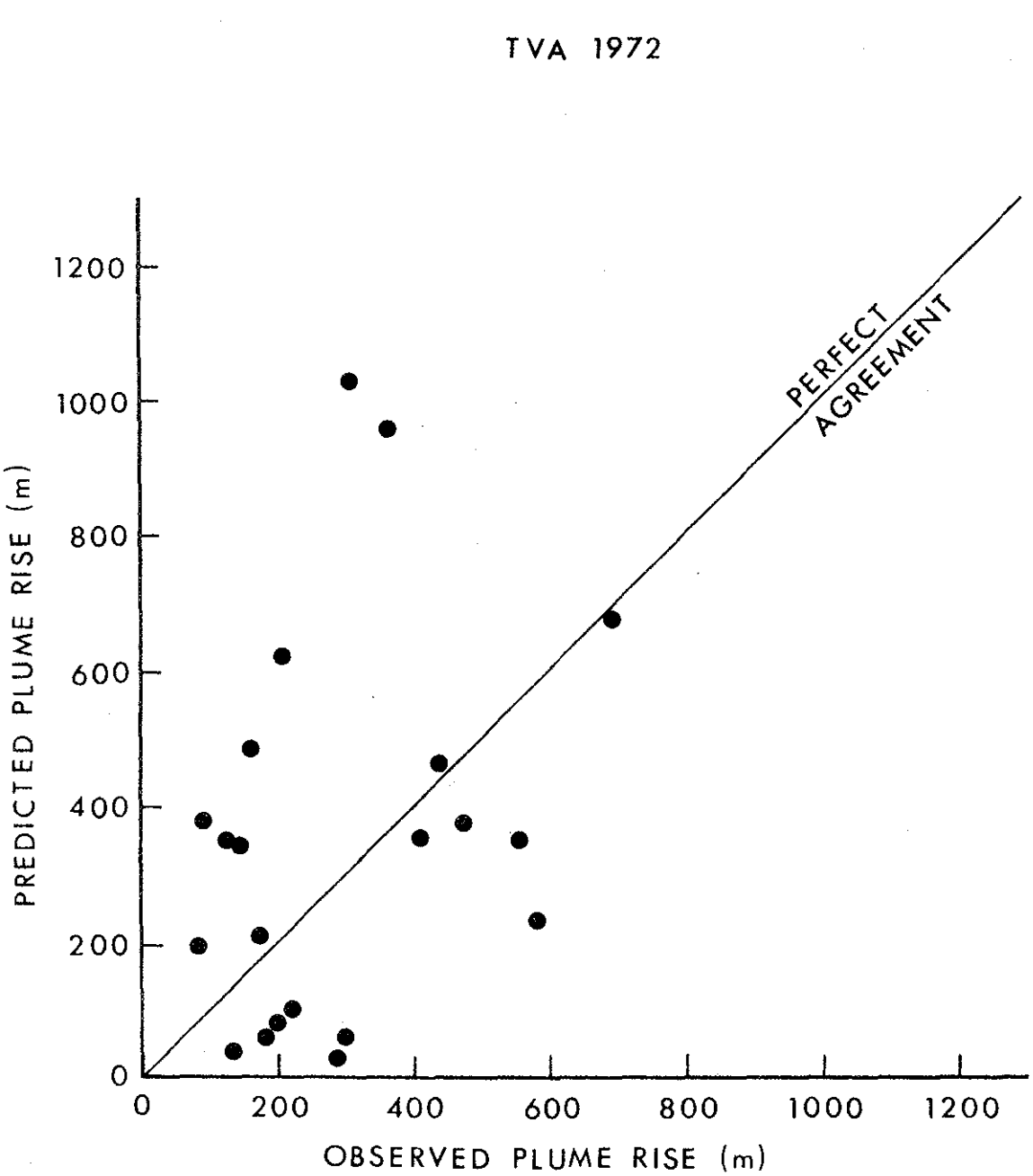

Figure 5.10. Comparison of predicted versus observed plume rise using TVA (1972) model.

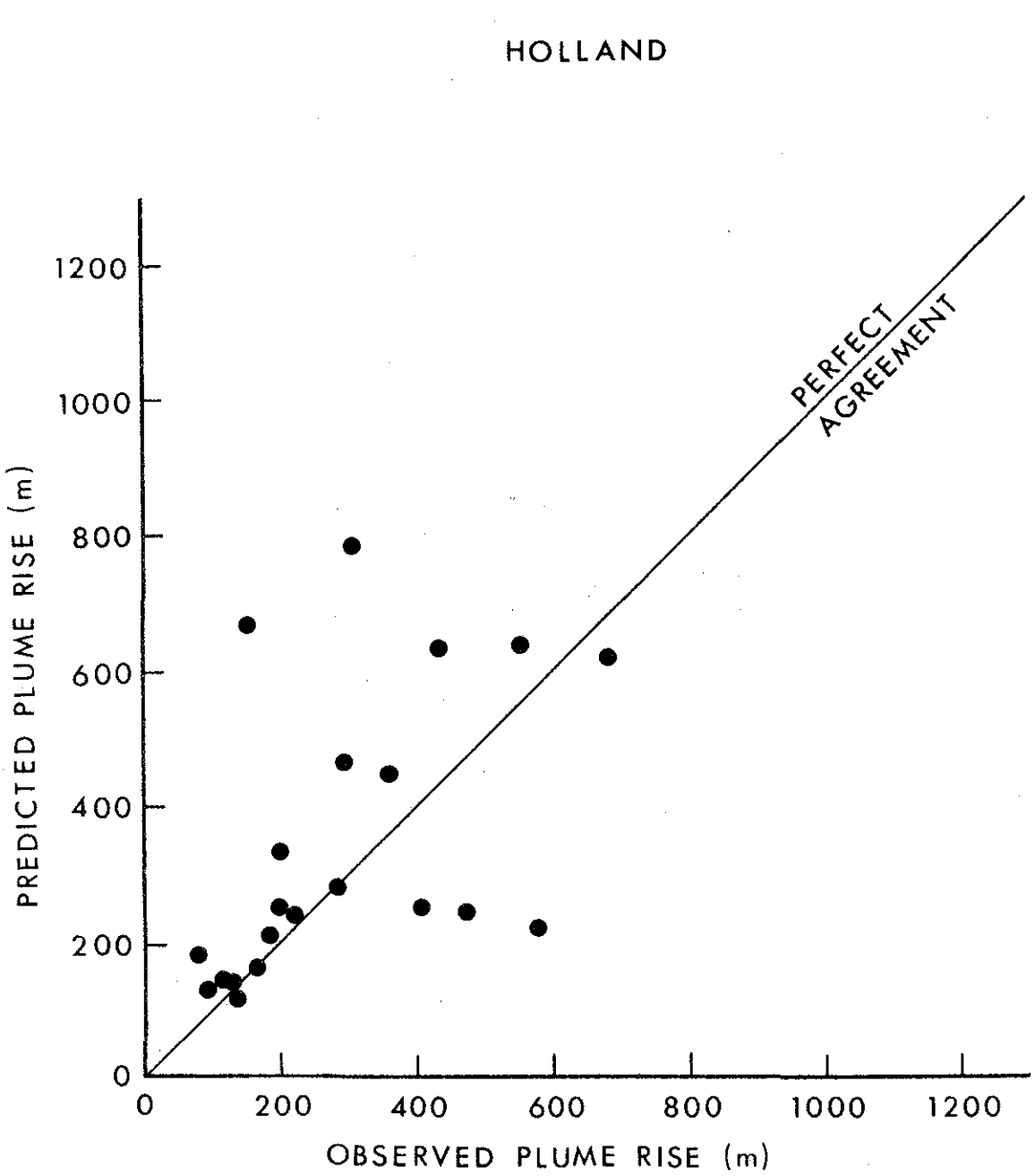

Figure 5.11. Comparison of predicted versus observed plume rise using Holland's (1953) model.

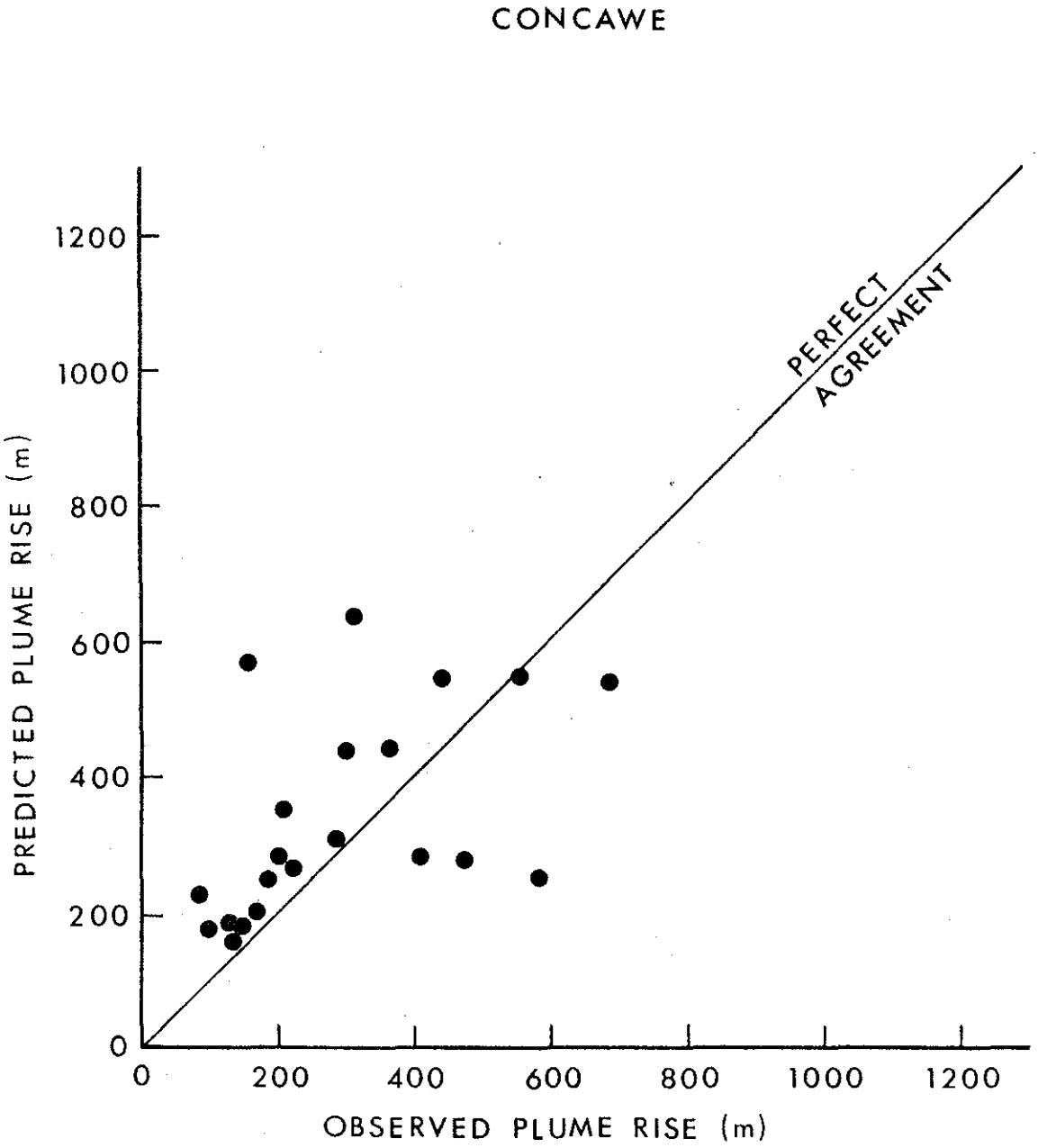

Figure 5.12. Comparison of predicted versus observed plume rise using Concawe's (1968) model.

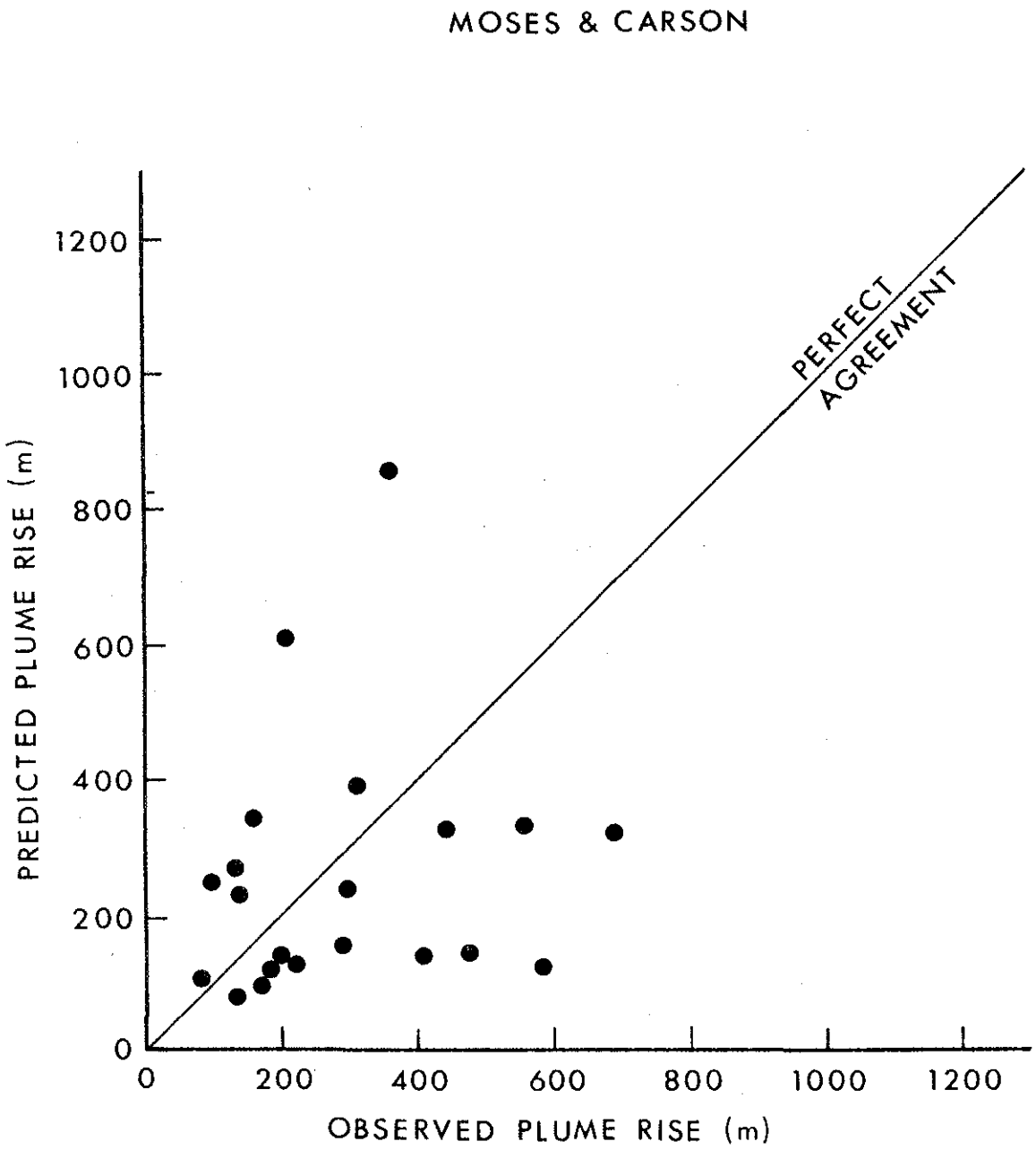

Figure 5.13. Comparison of predicted versus observed plume rise using Moses and Carson's (1967) model.

TABLE 5.4. Ratios of observed to predicted plume rise for different wind speed ranges.

Wind Speed Range ($m \cdot s^{-1}$)	Ratios of Observed to Predicted Plume Rise					
	Briggs	TVA 1971	TVA 1972	Holland	Concawe	Moses & Carson
$U<2$	1.46	0.59	1.8	0.66	0.77	1.28
$2 \leq U<3$	1.19	0.43	1.42	0.73	0.76	0.83
$3 \leq U<4$	1.33	0.74	1.09	1.09	0.98	1.74
$4 \leq U<6$	1.15	1.01	1.14	1.15	0.97	2.03
$6 \leq U$	1.3	0.82	2.36	0.95	0.71	0.78

Figure 5.14. Pond fog and the penetration of the inversion layer by the GCOS plume.

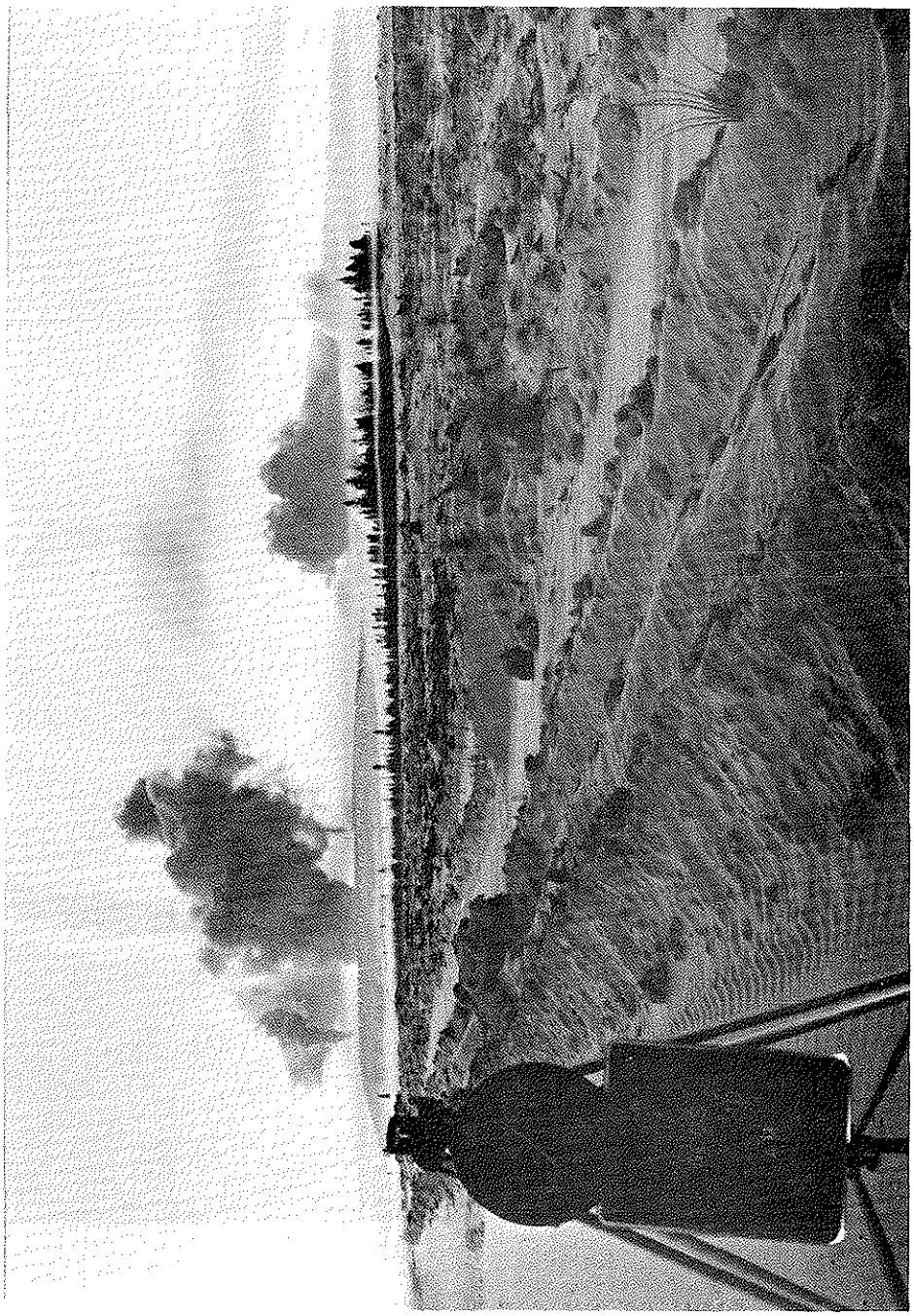

Figure 5.15. Fanning plume under morning inversion layer.

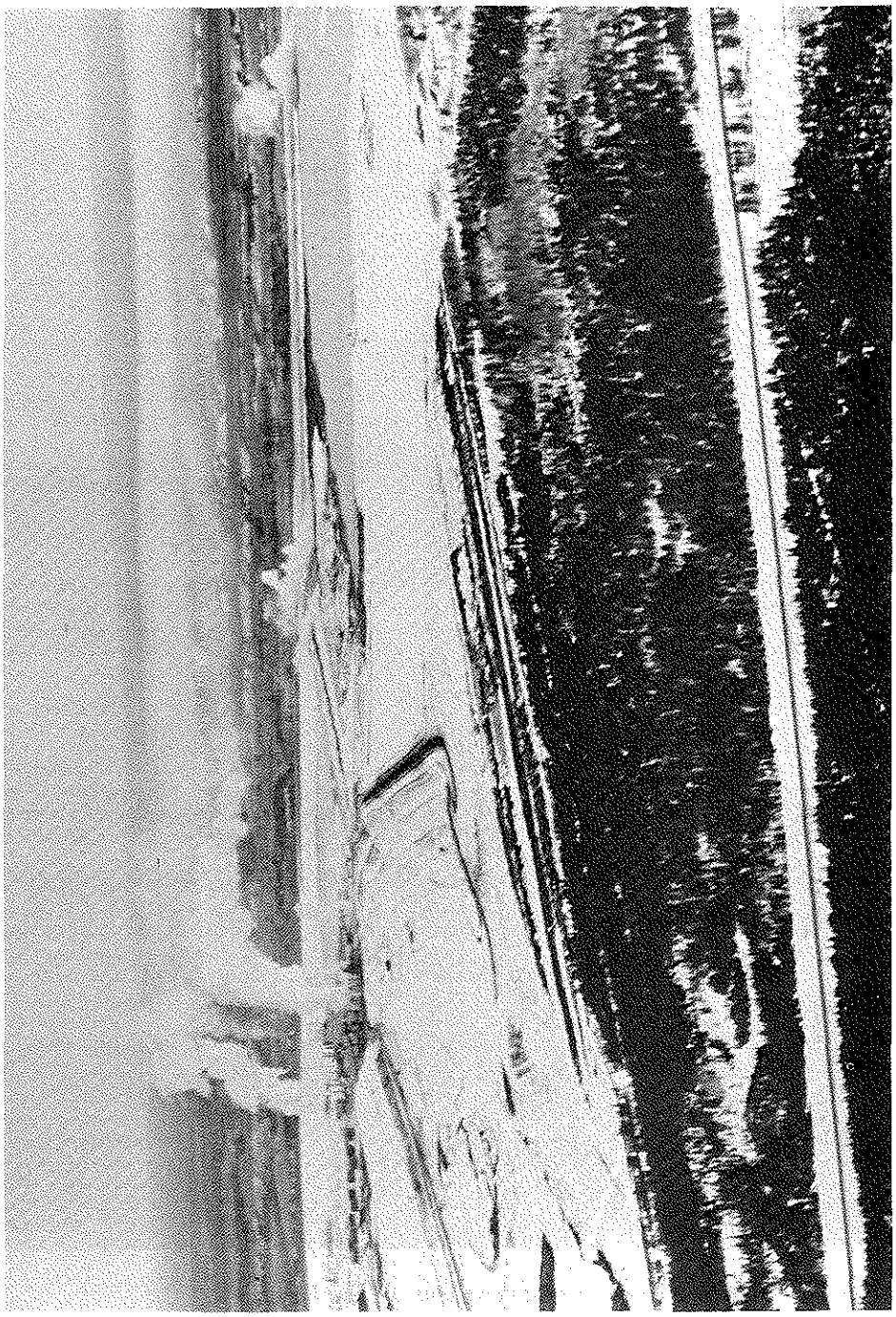

Figure 5.16. Fanning plume under an inversion layer during the daytime.

Figure 5.17. GCOS plumes penetrating a series of inversion layers.

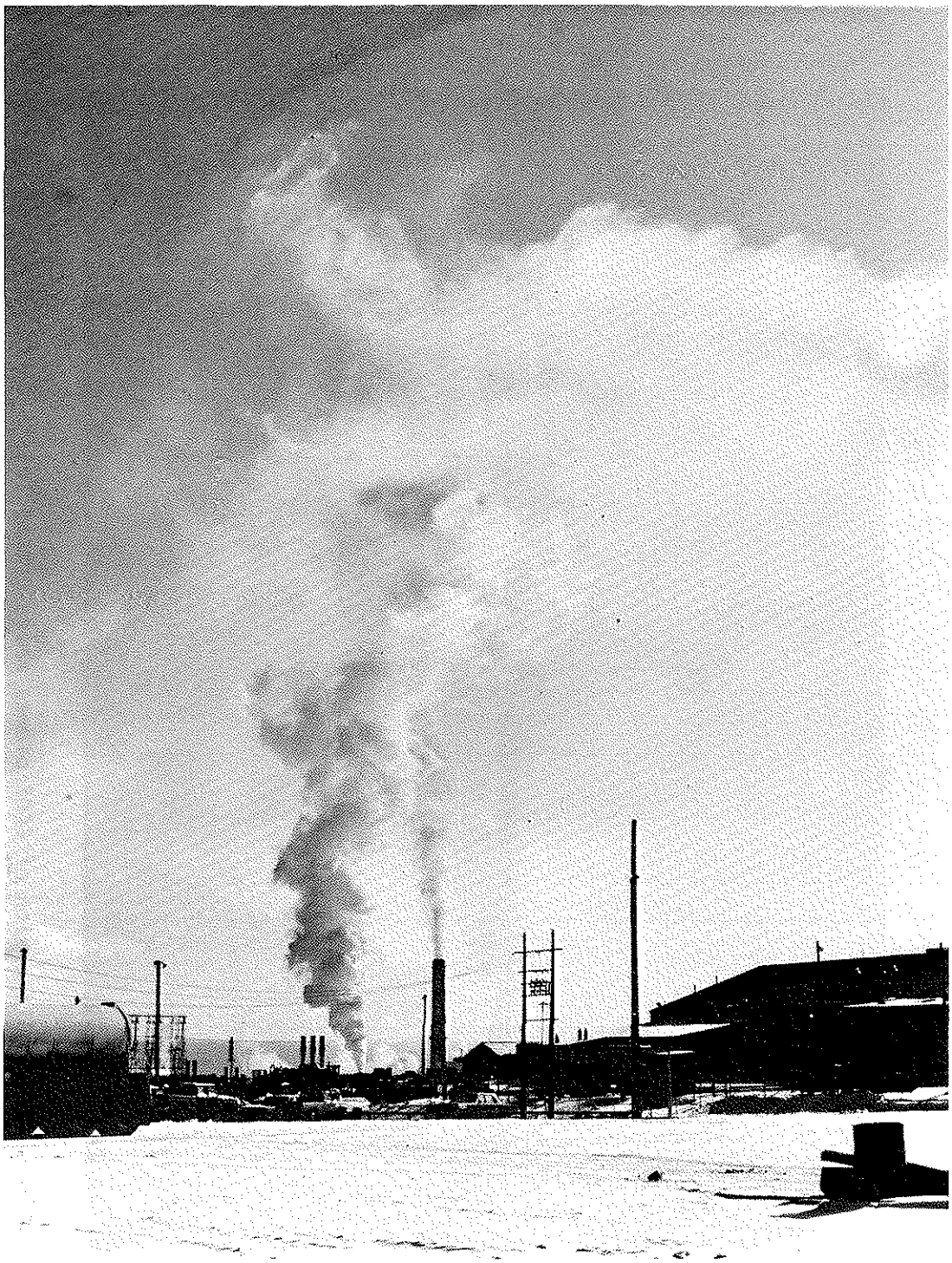

Figure 5.18. Dispersion of the GCOS plumes in a limited mixing layer at the plant.

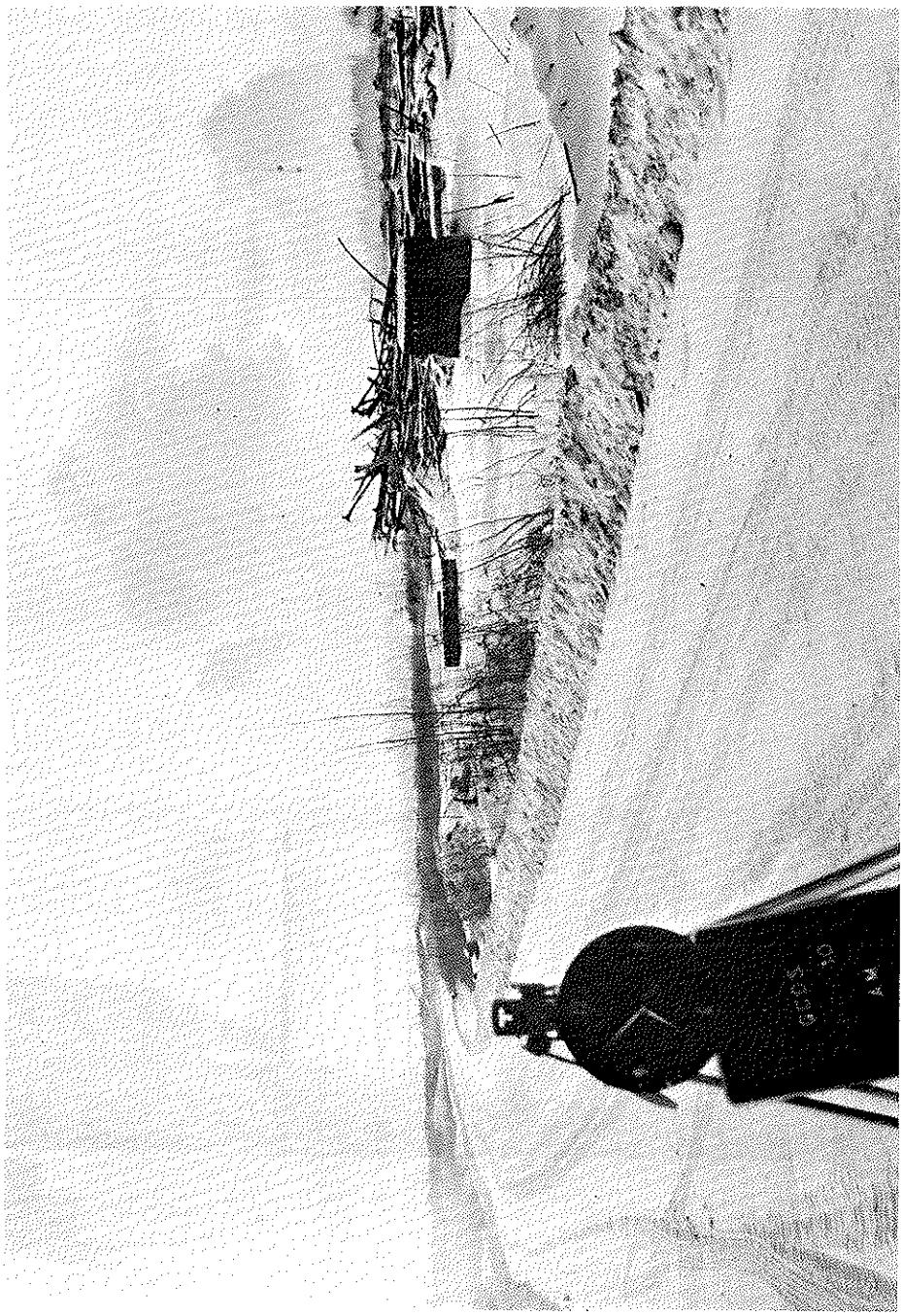

Figure 5.19. Dispersion of GCOS plumes above ground fog.

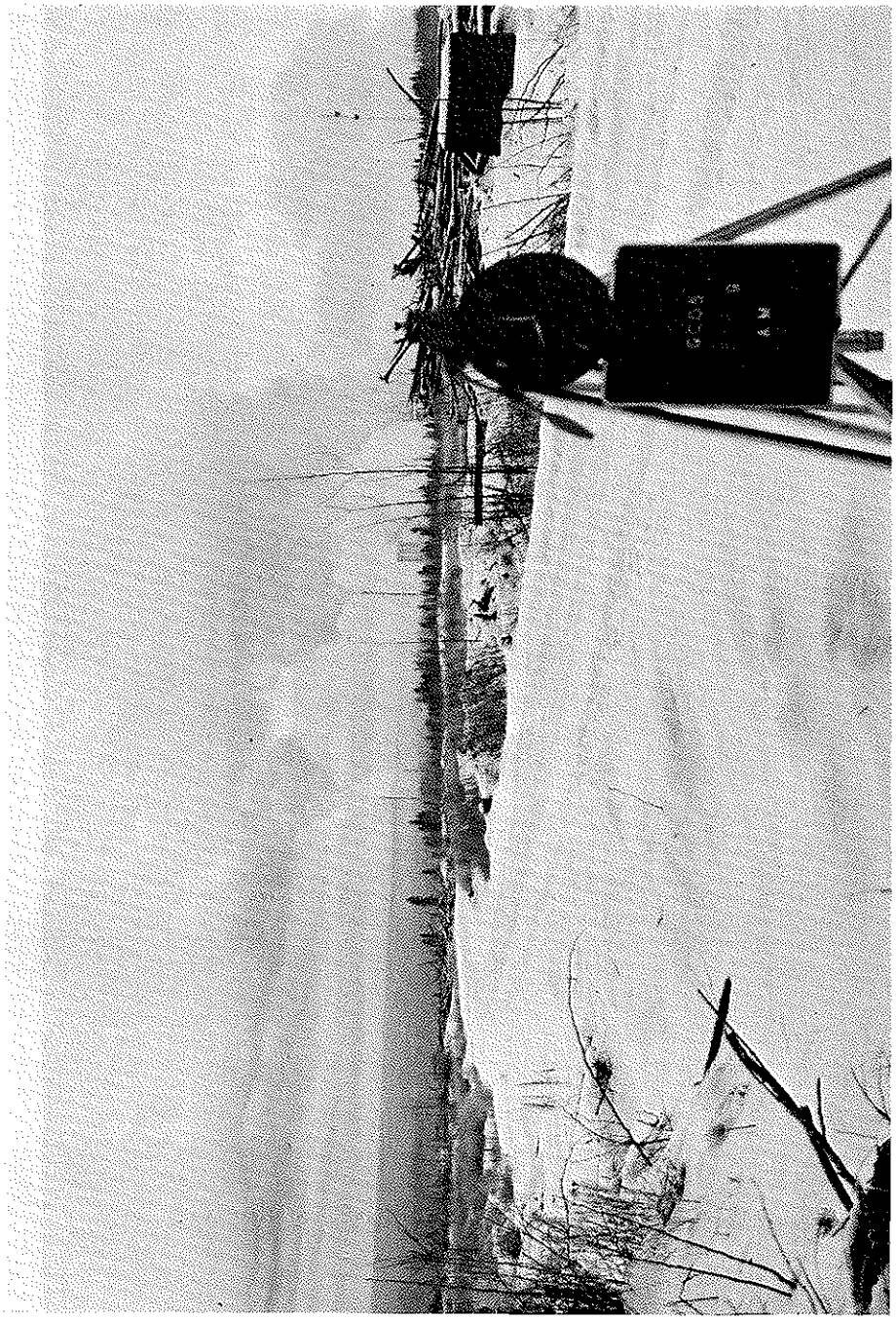

Figure 5.20. Dispersion of the GCOS plumes under high level fog.

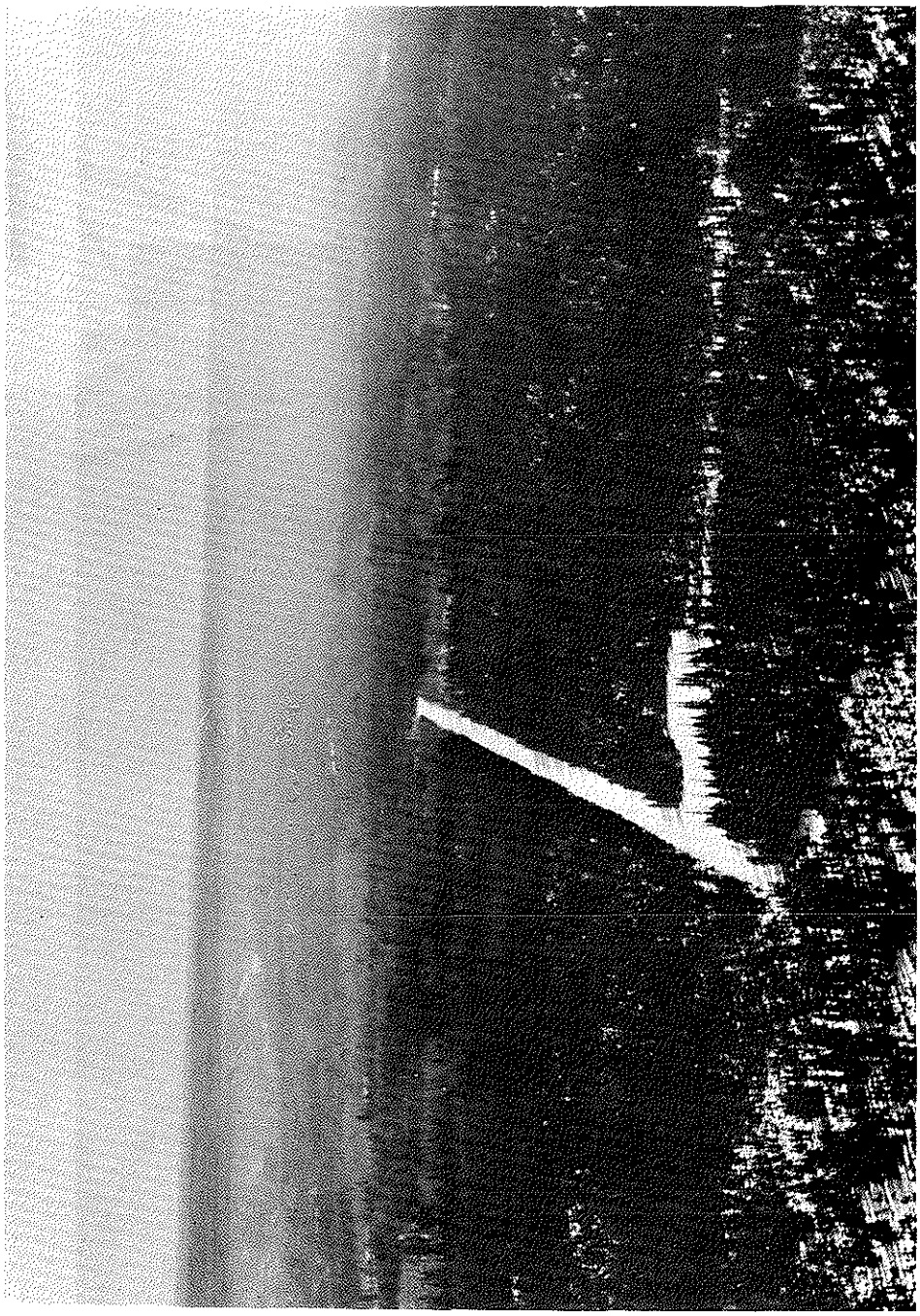

Figure 5.21. GCOS Plume during fumigation.

An attempt was made to determine the vertical dispersion coefficient (σ_z) of the plume from Stack A using the relation:

$$\sigma_z = \frac{D_z}{4.3}$$

where D_z is the plume width averaged over 5 min. In this case the plume is assumed Gaussian. It is also assumed that the concentration at the edge of the plume is equal to one-tenth that of the plume centerline. The measured D_z and the estimated σ_z are displayed in Table 5.5.

The estimated values of σ_z were grouped according to stability categories determined by applying the algorithm of Turner (1964) to the hourly observation from Fort McMurray Airport. A comparison between the estimated σ_z is made with calculations based on Pasquill-Gifford dispersion parameters as given by Turner (1967) (Figure 5.22). The values of the estimated σ_z are slightly larger and mostly compare with Pasquill-Gifford values for unstable and neutral conditions. There is no apparent relationship between the observed and the predicted values of σ_z. During stable conditions the measured σ_z tends to lie at the middle of the scattered points. However, the neutral condition cases tend to spread across the whole stability range. This disagreement may be attributed to the plume buoyancy, which tends to make the σ_z larger than that estimated.

Cramer (1957) derived a relationship between σ_z and the downwind distance from the source x in a power law form as:

$$\sigma_z = ax^b$$

where a and b are constants.

Since a power law is suspected to fit the observation, the variables were plotted logarithmically (Figure 5.23). The data were grouped according to the three different wind speed ranges at the plume level, $U<2.4$, $2.5<U<5$, and $U>5$ $m \cdot s^{-1}$ obtained from the mini-sonde observations at the Lower Syncrude complex. The least square

Table 5.5. Width of Plume along the vertical D_z and plume standard deviation σ_z.

DATE	TIME	STACK	D_z(m)	σ_z
March 4	0845	A	150	35
	0845	B	100	23
	0920	A	100	23
	0920	B	63	15
	1405	A	148	34
	1410	A	150	35
	1410	B	95	22
	1415	B	100	23
	1420	B	95	22
	1530	A	154	36
	1530	B	95	22
	1545	A	160	37
	1545	B	85	20
	1620	A	280	65
	1620	B	200	47
	1620	A	300	70
	1620	B	180	42
March 5	0645	A	228	53
	0645	B	171	40
	0810	A	137	32
	0815	A	133	31
	0820	A	136	32
	0825	A	128	30
	0830	A	138	32
	0830	B	130	30
	1500	A	66	15
	1505	A	70	16
	1510	A	80	19
	1540	A	95	22
	1545	A	90	21
March 6	0700	A	130	30
	0700	B	46	11
	0710	A	129	30
	0710	B	80	19
	0715	A	140	33
	0715	B	89	21
	1600	A	114	27

Table 5.5. Continued.

DATE	TIME	STACK	D_z(m)	σ_z
March 7	0645	A	93	22
	0650	A	100	23
March 8	0950	A	423	98
	0955	A	650	151
	1015	A	680	158
	1020	A	560	130
	1350	A	337	78
	1355	A	337	78
	1400	A	450	105
	1405	A	338	79
March 9	0720	A	210	49
	0750	A	193	45
	0805	A	187	43
	0810	A	200	47
	0820	A	200	47
	0845	A	200	47
	0850	A	210	49
	1730	A	220	51
	1735	A	165	38
March 10	0700	B	250	58
	0715	B	230	53
	1125	A	250	58
	1135	A	300	70
	1138	A	263	61
	1142	A	272	63
	1540	A	345	80
	1545	A	318	74
March 11	1110	A	250	58
	1120	A	262	61
	1125	A	250	58
	1125	A	262	61
	1505	A	214	50
	1520	A	214	50
	1525	A	214	50
March 13	0645	A	270	63
	0650	A	239	56
	0655		266	62
	1040	A	180	42
March 14	1035	A	164	38

Table 5.5. Concluded.

DATE	TIME	STACK	D_z	σ_z
March 15	1210	A	300	70
March 16	0700	A	136	32
	1105	A	237	55
	1110	A	130	30
	1115	A	132	31
	1135	A	157	36
	1505	A	158	36

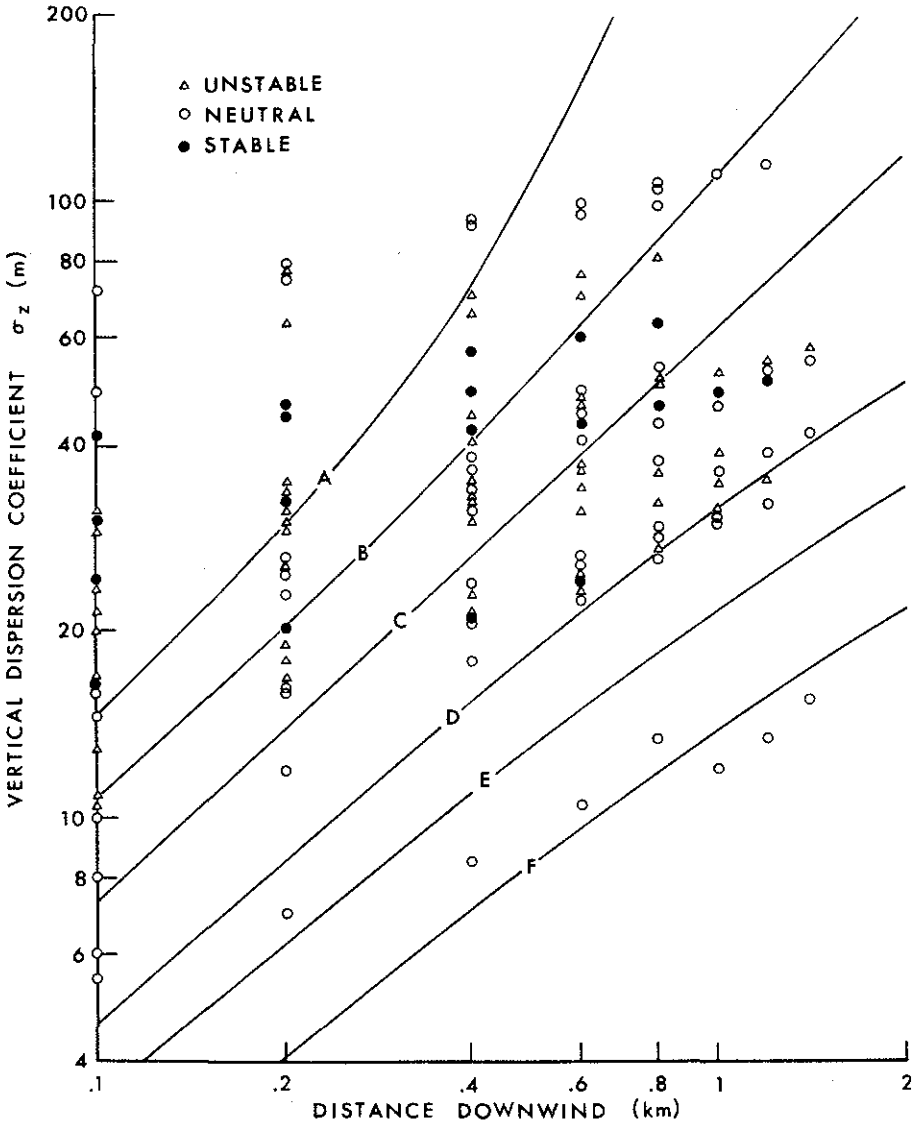

Figure 5.22. Comparison of observed vertical dispersion coefficient with Pasquill-Gifford predictions.

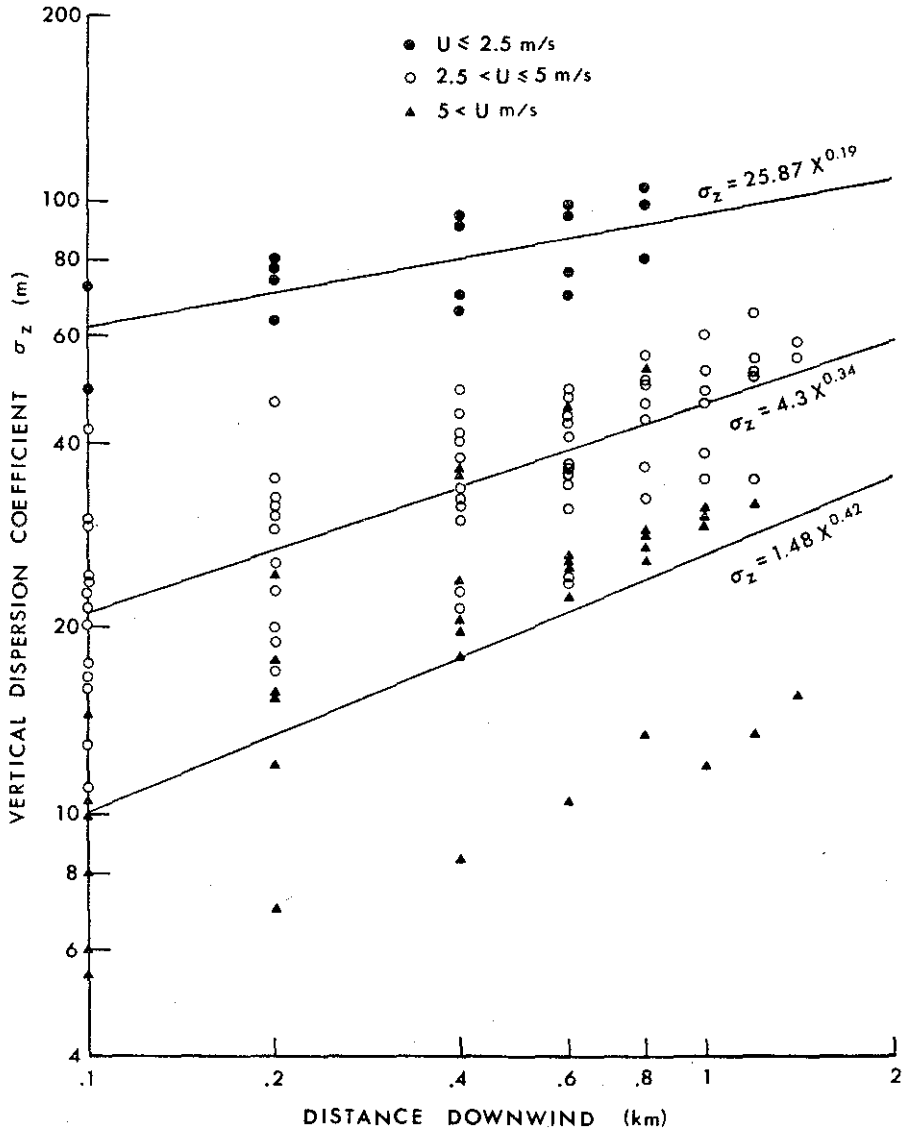

Figure 5.23. Vertical dispersion coefficient of the GCOS plume as a function of downwind distance from the source (Stack A). The solid line represents the best fit for each wind speed group.

method was applied to fit a straight line to each group. The power law appears to hold for each velocity group, each with different values of a and b. Value a decreases with increasing wind speed and b increases with increasing wind speed.

5.4 MEASUREMENTS OF SO_2 GROUND CONCENTRATIONS

The objective of this study was to gather information on the ground level concentrations of SO_2 as related to the rise of the GCOS plant plumes. Local meteorological conditions change as the earth's surface warms up or cools during the day. These changes may bring all or part of the plumes to the ground. Also, an inversion layer may prevent the plumes from rising and dispersing the pollutants, Such a lid on the plume increases the ground level concentrations of SO_2.

Ground concentration of SO_2 was measured using a Sign-X mounted in a vehicle. The intake of the Sign-X was located about 2 m above the ground, fastened to the car antenna. As the vehicle drove along the road under the plume at low speed (25 $km \cdot h^{-1}$), measurements of SO_2 concentration were made. The road was divided into seven stations (Figure 5.24) starting from Mildred Lake Research Facility to the limits of the town of Fort McMurray. By repeating the traverse several times, the location of a maximum ground SO_2 concentration was determined; measurements of SO_2 concentration were made at that location for a period of about 30 min. The data obtained were analyzed and displayed in two sets of figures. Figure 5.25 displays the variation of SO_2 ground concentration at different locations in the Tar Island area. On 15 March between 1113 and 1130 MST the concentration of SO_2 peaked to about 0.7 ppm close to location D. At a later time the concentration varied between 0.4 and 0.6 ppm.

Figure 5.26 describes the variation of SO_2 ground level concentration as a function of time. These measurements were made while the SO_2 sensor was stationed at the location of maximum concentration. On 15 March at about 1500, SO_2 concentration reached a value of about 0.28 ppm averaged over a period of 31 min. On that day and on 8 March, Barrie and Whelpdale (Section 7) reported that

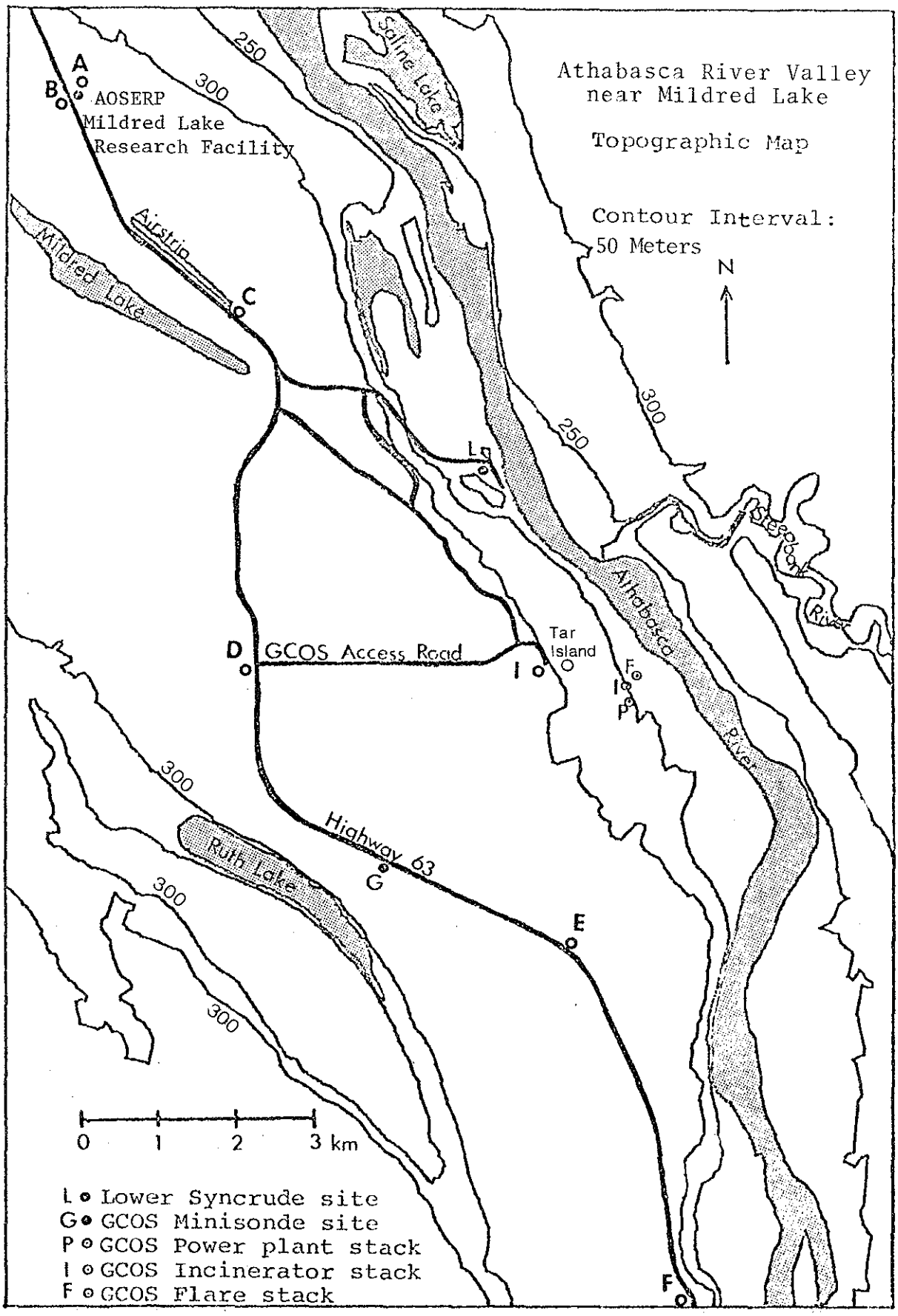

Figure 5.24. SO_2 ground concentration station location (A-I).

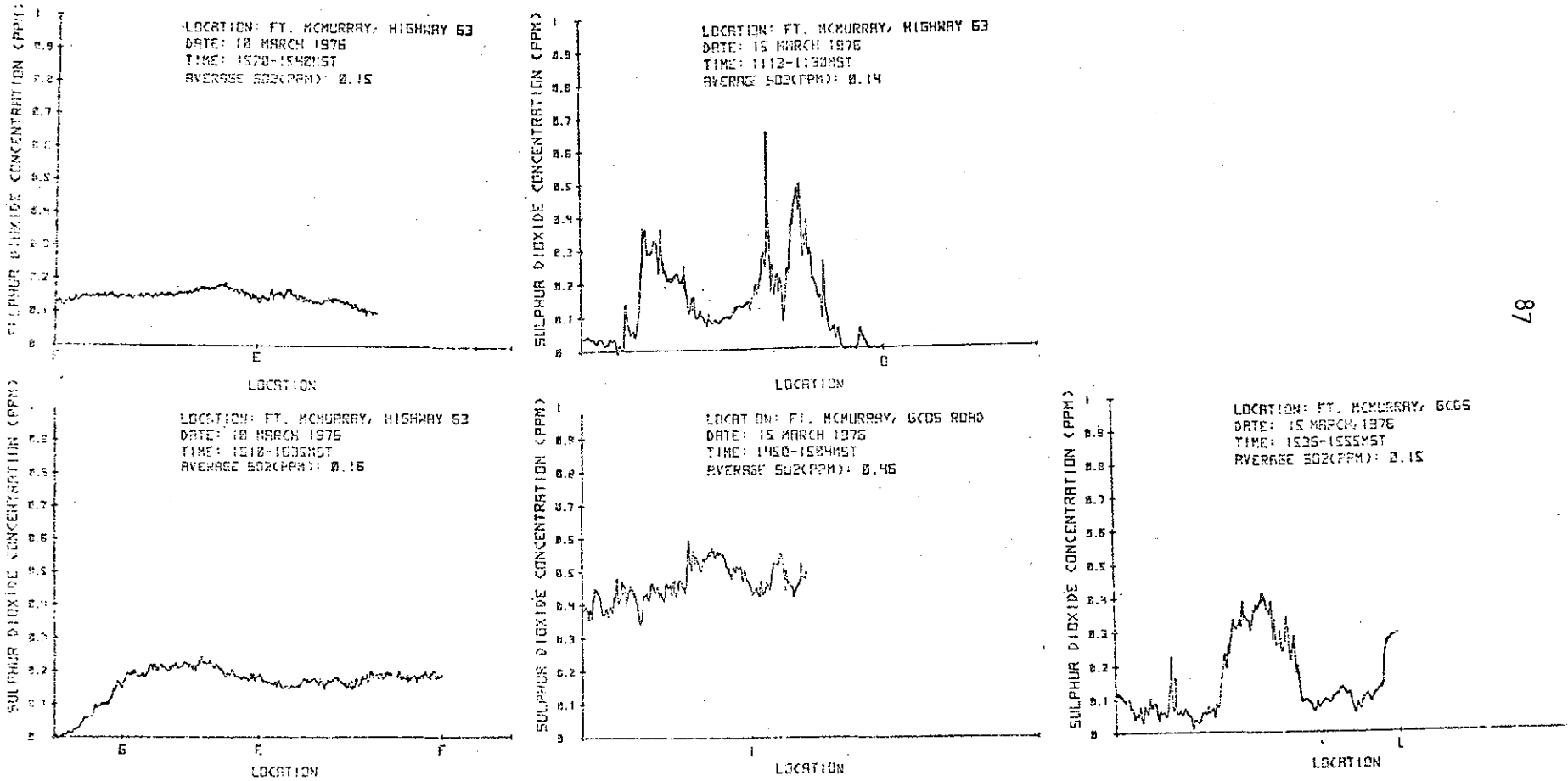

Figure 5.25. SO_2 ground concentration at different locations in the Tar Island.

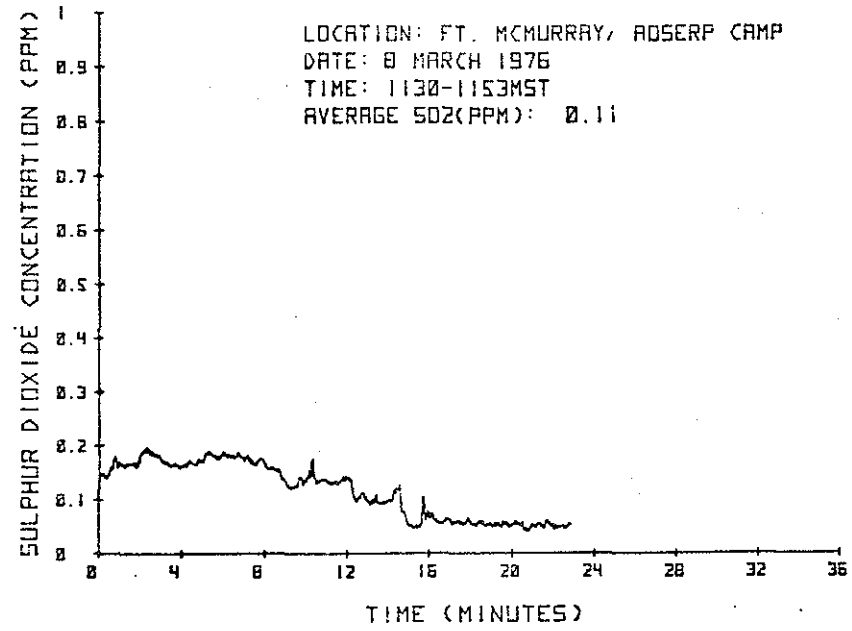

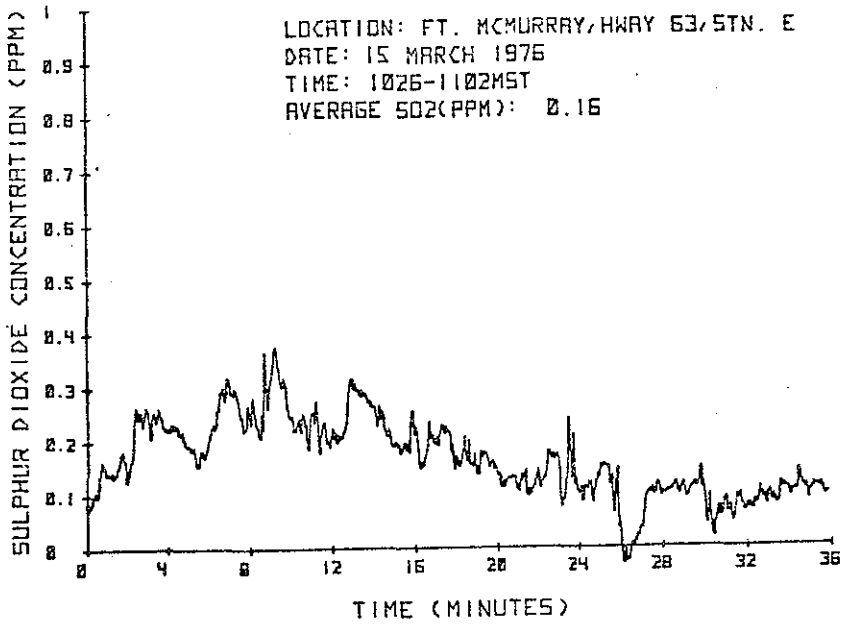

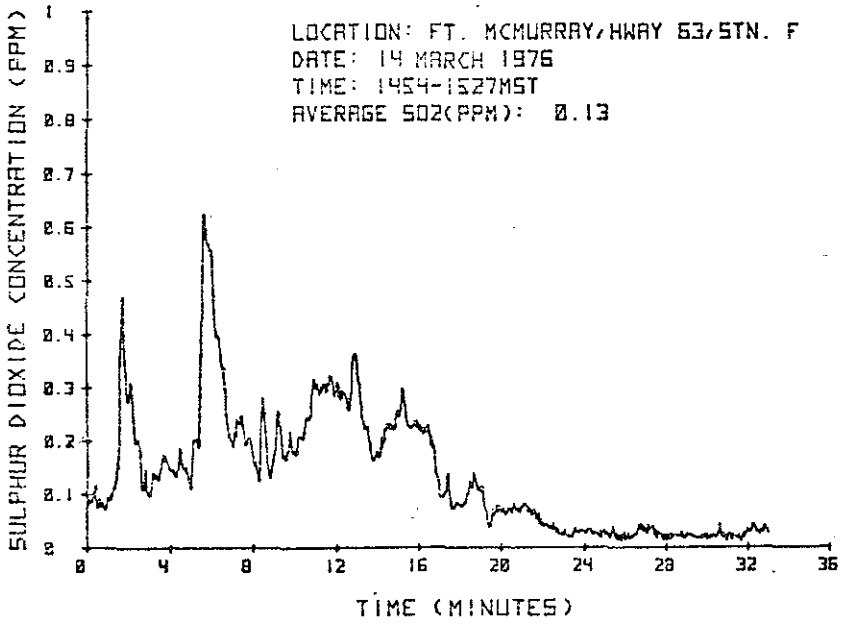

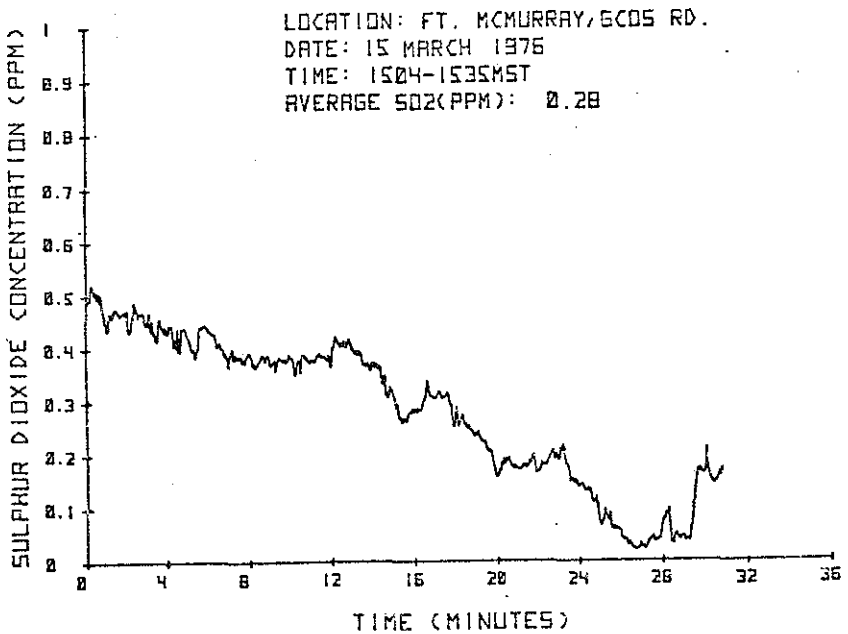

Figure 5.26. SO_2 ground concentration as a function of time.

the ground level SO_2 concentrations rose from 1 g $S \cdot m^{-3}$ to between 30 and 50 g $S \cdot m^{-3}$ at the campsite.

5.5 CONCLUSIONS

It is apparent from the observations presented in this report that the rise of the plume from the GCOS plant is not well predicted by the formulas tested. The rise of the plume is complicated by the frequent occurrence of inversion layers in the morning.

Holland's (1953) and Briggs's (1969, 1971, 1972) formulas appear to predict the rise of the plume better than the others reported in this study. The correlation, however, between the observed and predicted values is low. The model proposed by Briggs for windy conditions does not predict well the final rise of the plume for wind speeds less than 4 $m \cdot s^{-1}$. An attempt will be made later to apply Briggs's model for zero wind to predict the rise of the plume for calm conditions ($u<4$ $m \cdot s^{-1}$).

The most prominent feature of this study is the establishment of a relationship between the vertical spread of the plume (σ_z) and the downwind distance x from the source.

The lack of agreement between the observed and the predicted σ_z may be due to the unrepresentativeness of the Fort McMurray Airport data to the area around GCOS. Some of the scatter may be also due to the fact that Turner's algorithm may not apply for snow covered surfaces.

We feel there is a need to obtain more information on the value and the behaviour of σ_z and σ_y as a function of meteorological conditions and downwind distance. This should be conducted at the Syncrude site.

5.6 REFERENCES CITED

Briggs, G.A. 1969. Plume rise. AEC Critical Review Series TID-25075, National Technical Information Service. 81 pp.

Briggs, G.A. 1971. Some recent analyses of plume rise observations. Pages 1029-1032 in Proceedings, Second International Clean Air Congress. Academic Press.

Briggs, G.A. 1972. Discussion on chimney plumes in neutral and stable surroundings. Atmos. Environ. 6: 507-510.

Brummage, K.G. 1968. The calculation of atmospheric dispersion from a stack. Atmos. Environ. 2: 197.

Cramer, H.E. 1957. A practical method for estimating the dispersal of atmospheric contaminants. Proceedings of the Conference on Applied Meteorology. American Meteorological Society.

Fanaki, F.H. and G. Lesins. 1975. Photographic measurement of smoke plume heights from industrial stacks. SMPTE 84: 77-81.

Holland, J.Z. 1953. A meteorological survey of the Oak Ridge area. U.S. Atomic Energy Commission Report ORO - 99, 554.

Montgomery, T.L., S.B. Carpenter, W.C. Colbaugh, and F.W. Thomas. 1971. Fullscale study of plume rise at large electric generating stations - Bull Run supplement. Air Quality Branch, Tennessee Valley Authority. Muscle Shoals, Ala. 58 pp.

Montgomery, T.L., S.B. Carpenter, W.C. Colbaugh, and F.W. Thomas. 1972. Results of recent TVA investigations of plume rise. J. Air Pollu. Control Assoc. 22: 779-784.

Moses, H. and J.E. Carson. 1967. Stack design parameters influencing plume rise. Paper presented at the 60th Annual Meeting of the Air Pollution Control Association, Cleveland, Ohio. Paper 67-84.

Turner, D.B. 1964. A diffusion model for an urban area. J. Appl. Meteorol. 3: 83-91.

Turner, D.B. 1967. Workbook of atmospheric dispersion estimates. Public Health Service Publication 999-AP-26, U.S. Department of Health, Education and Welfare. 84 pp.

5.7 ACKNOWLEDGEMENTS

The authors gratefully acknowledge the interest in and support of this work by Mr. A.W. Smith in setting up the necessary photographic equipment and printing the photographs presented in this report. We wish to thank Mr. W.L. Cary, Great Canadian Oil Sands Ltd., for providing us with the shelter and for the use of the meteorological tower at Mildred Lake. We are greatly indebted to Dr. R. Mickel for his frequent advice during the field study and in computing the micrometeorological observations. Special thanks are

due to Mr. R. Angle, Alberta Environment for his comments on our preliminary report. Sincere appreciation is also expressed to the AOSERP staff, especially Mr. Av Mann and the Chef, Mildred Lake Research Facility, who made our stay warm, comfortable and pleasant.

6. CORRELATION SPECTROMETER

by R.M. Hoff, M.M. Millan and A.J. Gallant

As part of the Plume Dispersion program of the March 1976 AOSERP Winter Field Study, the Barringer Correlation Spectrometer (COSPEC) was proposed as the method of obtaining vertically integrated SO_2 profiles from ground based traverses.

6.1 OBJECTIVES

Three objectives were identified at the onset of this program:

1. to determine the applicability of the COSPEC to plume measurements in the Alberta oil sands area in winter conditions (low sun elevation and low temperature);
2. to investigate the logistics of plumes traversing in the area; and
3. to investigate the behaviour of very stable plumes.

Once the objectives were established, it could be determined whether or not the existing COSPEC methodology (Millan et al. 1976) was applicable to the study of dispersing plume behavior and calculation of mass fluxes under northern conditions in the area of interest.

6.2 INSTRUMENTAL TECHNIQUE

COSPEC is a passive remote sensor that can measure SO_2 (or NO_2) using ultraviolet (or blue visible) radiation. The radiation source is usually the zenith sky, and the instrument is used pointing vertically upwards.

In the near-ultraviolet waveband, 300 to 316 nm, there is a region of strong absorption bands of SO_2. Radiation at those wavelengths from the zenith sky will be selectively absorbed in the SO_2 band system as soon as this gas is present in the field of view of the instrument.

The COSPEC instrument examines the spectrum of the incoming radiation through four sets of seven narrow slits (masks) engraved on a rotating disc, which allows them to be sequentially placed to coincide with the peaks and troughs of the SO_2 absorption bands. In the presence of SO_2, the difference in signals seen by the photodetector

behind the disc is electronically processed to yield an output that is a function of the concentration times the pathlengths of the SO_2 overhead, and to a large extent is independent of background light fluctuations. Another way of viewing this result is that the same vertically integrated signal would be obtained if all the gas were compressed into a 1-m layer of SO_2 concentration equal to the signal in parts per million.

For ground-based traverses under a plume, the instrument views the zenith sky by means of 45° mirror that extends off the viewing telescope. The field of view of the instrument is very narrow so that the accepted light is quite specific to the absorption of the gas that is directly overhead.

As a passive instrument, it has been optimized to be minimally influenced by background changes. However, some factors do affect its performance. The most important is lack of light. In the SO_2 absorption region, the main reasons for the extinction of solar radiation is ozone absorption in the upper atmosphere and molecular (air) scattering. At high latitudes the low solar elevation during the day implies a long path of the radiation through the atmosphere, which in turn diminishes the available background ultraviolet radiation. A procedure has been devised by the authors that optimizes operating parameters for any background condition, including those of very low ultraviolet radiation levels. Application of this procedure to one of the AES COSPECS allowed its usage with sun elevation angles greater than 8°, vs. the $25\text{-}30^{\circ}$ lower limit of the commercial instrument. This optimization procedure, developed at AES headquarters prior to the intensive study, was mainly responsible for an instrumental operation range of more than 8 h daily centered around solar midday.

For the dates of the study (1-9 March 1976), the COSPEC was scheduled for operation 8 h/day from 3 March to 16 March. Of that total time (104.0 h) data were taken for 58.8 h (56.5%). It should be noted that the instrument itself was operational for 100% of the assigned hours and that the times when no data or uninteresting data were taken were caused by the logistics of ground traversing in the area.

The original conception of ground traversing called for the use of the four-wheel drive vehicle over roads in the area and the use of an all-terrain vehicle for cutlines on the east side of the Athabasca River. Difficulties with starting and equipping the all-terrain vehicles were alleviated by the fact that the major cutlines on the east side of the river had been plowed prior to 3 March and were easily passable with the four-wheel drive. Operation of an all-terrain vehicle on an unsounded river traverse was considered too dangerous, so it was elected to employ the four-wheel drive entirely. This gave the operators access to traverses in the northwest, southwest and northeast quadrants as seen from the GCOS power plant stack (Figure 6.1). The southeast quadrant from the stack was thus completely unavailable for ground traversing.

THE COSPEC was mounted in an Alberta Department of Environment-AOSERP Chevrolet Suburban, four-wheel drive vehicle (Figure 6.2). The power was provided by a 12-V DC to 115-V AC converter (TOPAZ, Inc.) and the data were recorded on a strip-chart recorder. Ground position was simultaneously recorded on the chart record by use of a Hartwig Survey meter attached to the speedometer of the vehicle.

The daily log of operations is given in Section 8.1. The days that proved to be of greatest interest were 7, 13, 14 and 15 March. The data of 7 March, while quite good qualitatively, are of suspicious quantitative value, since many of the profiles were obtained in blowing snow and low cloud. The data for 14 March were taken in the afternoon after the inversion had lifted and for that reason are slightly less interesting than the remaining two days. The authors have chosen to analyze the data of 13 and 15 March for several reasons. Thirteen March contained no morning ground-level inversion, even at 0630. A higher inversion at 1 km MSL changed to lapse very early in the morning. For this reason the data of 13 March serve as an interesting comparison to the 15th, which had an early morning inversion of 15^{o}C.

Another factor entering into this choice was that on 13 March plume height information was being obtained concurrently by F. Fanaki and on 15 March simultaneous Sign-X measurements were being made by F. Fanaki and F. Froude.

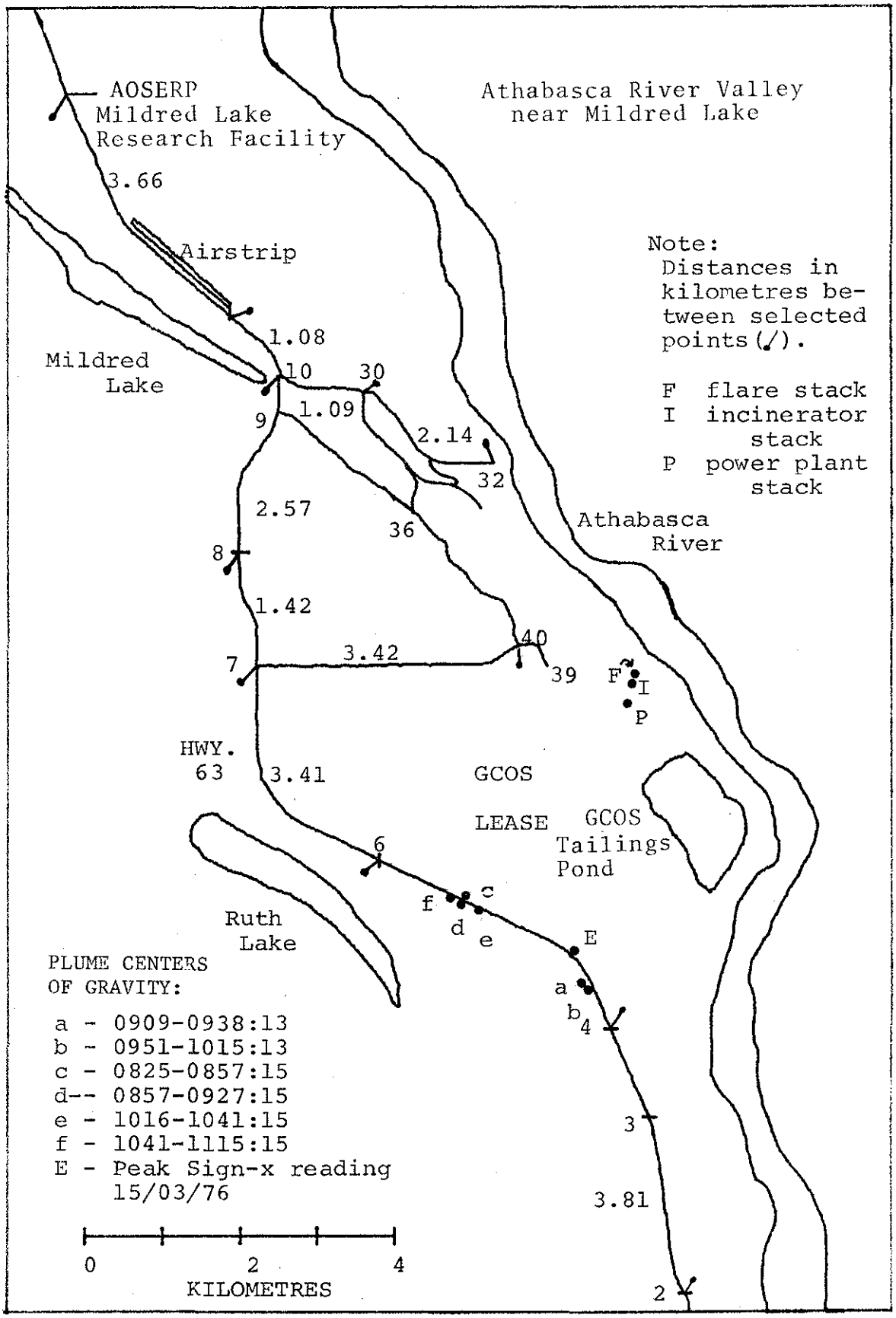

Figure 6.1. Athabasca River valley near Mildred Lake.

Figure 6.2. The COSPEC traversing vehicle showing the viewing telescope pointing vertically upwards.

6.3 DATA HANDLING AND ANALYSIS

The chart records of the COSPEC transects contain well over 100 individual profiles. Of these, a significant number contain nil, or incomplete SO_2 information. The charts were preselected to include 82 profiles for digitization.

These profiles were digitized on a Hewlett Packard Model 9864A Digitizer and stored on cassette tape. A list of the stored transects is given in Table 6.1. Hard copy plots of the profiles as well as the processed data (see below) may be obtained in a separate COSPEC Program Data Package from the AOSERP Program Management Office.

These individual road profiles were subjected to averaging. We have chosen to serially average plume profiles on a 0.5-h time base. These ground average profiles are stored on Hewlett Packard tape.

The average profile is analyzed to find the center-of-gravity (COG) (Csandy 1973) of the profile and then all subsequent data were reduced relative to this point. The plane defined by the perpendicular to the line from the stack of the COG is called the "effective plane of transect." All profiles were then projected onto this plane and were restored on magnetic tape. Two types of averaging were done:

1. Eulerian--averaging with respect to the real space COG in the effective plane; and
2. pseudo-Lagrangian--averaging with respect to superimposed individual COG's.

For each individual and each average profile that was 0.5-h averaged, the following statistical data are available about the distributions (profiles):

1. the second, third, and fourth moments:

$$\mu_n = \frac{\Sigma_i \, S_i \, (Y_i - Y_{cog})^n}{\Sigma_i S_i}$$

where S_i = signal strength at point i and Y_i are distances in effective plane.

Table 6.1. List of digitized COSPEC transects with cassette file locations.

TAPE #	FILE #	DATE AND TIME	TRANSECT
1	0	0857:04/03/76	03-05
1	1	0902:04/03/76	03-05
1	2	0910:04/03/76	03-05
1	3	0918:04/03/76	03-05
1	4	0924:04/03/76	03-05
1	5	0927:04/03/76	03-05
1	6	0843:07/03/76	04-6A
1	7	0903:07/03/76	04-07
1	8	0909:07/03/76	05-07
1	9	0922:07/03/76	05-07
1	10	0938:07/03/76	05-08
1	11	0940:07/03/76	06-08
1	12	0947:07/03/76	06-08
1	13	0954:07/03/76	06-08
1	14	1000:07/03/76	06-08
1	15	1005:07/03/76	06-08
1	16	1036:07/03/76	06-10
1	17	1045:07/03/76	06-10
1	18	1054:07/03/76	06-10
1	19	1104:07/03/76	06-10
1	20	1115:07/03/76	06-10

TAPE #	FILE #	DATE AND TIME	TRANSECT
2	0	1122:07/03/76	06-10
2	1	1135:07/03/76	06-10
2	2	1305:07/03/76	5-10A
2	3	1316:07/03/76	05-08
2	4	1325:07/03/76	4A-08
2	5	1335:07/03/76	04-08
2	6	1346:07/03/76	04-08
2	7	1400:07/03/76	4A-10
2	8	1418:07/03/76	05-08
2	9	1424:07/03/76	05-08
2	10	1433:07/03/76	06-08
2	11	1454/07/03/76	06/10
2	12	1503:07/03/76	05-08
2	13	1552/07/03/76	06/10
2	14	1601/07/03/76	06/10
2	15	1120/08/03/76	X/32
2	16	1153/08/03/76	7/12A-.266
2	17	0850:13/03/76	02-05
2	18	0900:13/03/76	02-06
2	19	0909/13/03/76	03/06
2	20	0920/13/03/76	03/06

Continued ...

Table 6.1. Continued.

TAPE #	FILE #	DATE AND TIME	TRANSECT
3	0	0929:13/03/76	03-06
3	1	0938:13/03/76	03-06
3	2	0951:13/03/76	03-06
3	3	0957:13/03/76	03-06
3	4	1008:13/03/76	03-06
3	5	1015:13/03/76	03-06
3	6	1026:13/03/76	02-06
3	7	1036:13/03/76	02-05
3	8	1053:13/03/76	2A-06
3	9	1102:13/03/76	2A-06
3	10	1301:14/03/76	4A-07
3	11	EMPTY	
3	12	EMPTY	
3	13	EMPTY	
3	14	EMPTY	
3	15	1441:14/03/76	02-05
3	16	1452:14/03/76	02-06
3	17	1503:14/03/76	4A-06
3	18	1513:14/03/76	03-06
3	19	1518:14/03/76	02-06
3	20	1529:14/03/76	02-06

TAPE #	FILE #	DATE AND TIME	TRANSECT
4	0	1539:14/03/76	02-06
4	1	1551:14/03/76	02-06
4	2	0825:15/03/76	04-07
4	3	0834:15/03/76	04-07
4	4	0844:15/03/76	04-07
4	5	0857:15/03/76	04-07
4	6	0907:15/03/76	04-07
4	7	0916:15/03/76	04-07
4	8	0927:15/03/76	04-07
4	9	1011:15/03/76	4A-04
4	10	1016:15/03/76	04-07
4	11	1024:15/03/76	04-07
4	12	1035:15/03/76	04-07
4	13	1041:15/03/76	04-07
4	14	1052:15/03/76	04-07
4	15	1103:15/03/76	04-07
4	16	1115:15/03/76	04-07

Continued ...

Table 6.1. Continued.

PROCESSED PROFILES:

TAPE #	FILE #	DATE AND TIME	FILE TYPE
5	0	0951-1015:13	GROUND POSITION AVERAGE
5	1	0951-1015:13	EULERIAN AVERAGE PROFILE
5	2	0951:13/03/76	PROJECTED INDIVIDUAL PROFILE
5	3	0957:13/03/76	PROJECTED INDIVIDUAL PROFILE
5	4	1008:13/03/76	PROJECTED INDIVIDUAL PROFILE
5	5	1015:13/03/76	PROJECTED INDIVIDUAL PROFILE
5	6	0951-1015:13	LAGRANGIAN AVERAGE PROFILE
5	7	0825-0857:15	GROUND POSITION AVERAGE
5	8	0825-0857:15	EULERIAN AVERAGE PROFILE
5	9	0825:15/03/76	PROJECTED INDIVIDUAL PROFILE
5	10	0834:15/03/76	PROJECTED INDIVIDUAL PROFILE
5	11	0844:15/03/76	PROJECTED INDIVIDUAL PROFILE
5	12	0857:15/03/76	PROJECTED INDIVIDUAL PROFILE
5	13	0825-0857:15	LAGRANGIAN AVERAGE PROFILE
5	14	1016-1041:15	GROUND POSITION AVERAGE
5	15	1016-1041:15	EULERIAN AVERAGE PROFILE
5	16	1016:15/03/76	PROJECTED INDIVIDUAL PROFILE
5	17	1024:15/03/76	PROJECTED INDIVIDUAL PROFILE
5	18	1035:15/03/76	PROJECTED INDIVIDUAL PROFILE
5	19	1041:15/03/76	PROJECTED INDIVIDUAL PROFILE
5	20	1016-1041:15	LAGRANGIAN AVERAGE PROFILE

TAPE #	FILE #	DATE AND TIME	FILE TYPE
6	0	0857-0927:15	GROUND POSITION AVERAGE
6	1	0857-0927:15	EULERIAN AVERAGE PROFILE
6	2	0857:15/03/76	PROJECTED INDIVIDUAL PROFILE
6	3	0907:15/03/76	PROJECTED INDIVIDUAL PROFILE
6	4	0916:15/03/76	PROJECTED INDIVIDUAL PROFILE
6	5	0927:15/03/76	PROJECTED INDIVIDUAL PROFILE
6	6	0857-0927:15	LAGRANGIAN AVERAGE PROFILE
6	7	1041-1115:15	GROUND POSITION AVERAGE
6	8	1041-1115:15	EULERIAN AVERAGE PROFILE
6	9	1041:15/03/76	PROJECTED INDIVIDUAL PROFILE
6	10	1052:15/03/76	PROJECTED INDIVIDUAL PROFILE
6	11	1103:15/03/76	PROJECTED INDIVIDUAL PROFILE
6	12	1115:15/03/76	PROJECTED INDIVIDUAL PROFILE
6	13	1041-1115:15	LAGRANGIAN AVERAGE PROFILE
6	14	0825-0927:15	GROUND POSITION AVERAGE
6	15	0825-0927:15	EULERIAN AVERAGE PROFILE
6	16	0825:15/03/76	PROJECTED INDIVIDUAL PROFILE
6	17	0834:15/03/76	PROJECTED INDIVIDUAL PROFILE
6	18	0844:15/03/76	PROJECTED INDIVIDUAL PROFILE
6	19	0857:15/03/76	PROJECTED INDIVIDUAL PROFILE
6	20	0907:15/03/76	PROJECTED INDIVIDUAL PROFILE

Continued ...

Table 6.1. Concluded.

TAPE #	FILE #	DATE AND TIME	FILE TYPE
7	0	0916:15/03/76	PROJECTED INDIVIDUAL PROFILE
7	1	0927:15/03/76	PROJECTED INDIVIDUAL PROFILE
7	2	0825-0927:15	LAGRANGIAN AVERAGE PROFILE
7	3	0909-0938:13	GROUND POSITION AVERAGE
7	4	0909-0938:13	EULERIAN AVERAGE PROFILE
7	5	0909/13/03/76	PROJECTED INDIVIDUAL PROFILE
7	6	0920/13/03/76	PROJECTED INDIVIDUAL PROFILE
7	7	0929:13/03/76	PROJECTED INDIVIDUAL PROFILE
7	8	0938:13/03/76	PROJECTED INDIVIDUAL PROFILE
7	9	0909-0938:13	LAGRANGIAN AVERAGE PROFILE

2. related parameters:

$$\sigma_y = \sqrt{\mu_2}$$

$$\text{skewness} = \mu_3/\sigma_y^3$$

$$\text{kurtosis} = \mu_4/\sigma_y^4$$

Sigma-y (σ_y) is the standard deviation of the distribution (horizontal dispersion coefficient), the skewness measures the asymmetry of the profile (symmetric would be zero), and the kurtosis measures the flatness or peakedness of the distribution (Gaussian would be 3.0).

3. Area under the distribution in ppm-m^2:

$$\text{Area} = \int_{-\infty}^{\infty} S(y)dy \simeq \Sigma_i S_i \cdot \Delta_y,$$

where Δ_y = digitization interval = 11.9 m.

6.4 EXPERIMENTAL RESULTS

As mentioned earlier, 13 and 15 March provide interesting comparisons for similar days with and without a surface-based inversion. On 13 March, plume rise photography was being conducted by F. Fanaki at the time the COSPEC was traversing. This provides plume height information as well as visual σ_z of the plume. On 15 March, concurrent Sign-X measurements were being made that indicated that a strong directional shear in the plume was present.

6.4.1 13 March 1976

The morning of 13 March was characterized by -11°C surface temperature and broken clouds. Snow began to fall later in the morning at approximately 1100. There was no inversion and the lapse rate was slight ($\simeq$ 4°C/1000 m) giving rise to a coning plume.

During the monitoring a total of 14 profiles were obtained. The most significant were 8 runs around midmorning; two 0.5-h averages 0909-0938 and 0951-1015 have been processed and are shown in Figures 6.3 and 6.4 in two groups of diagrams per 0.5-h average. The first

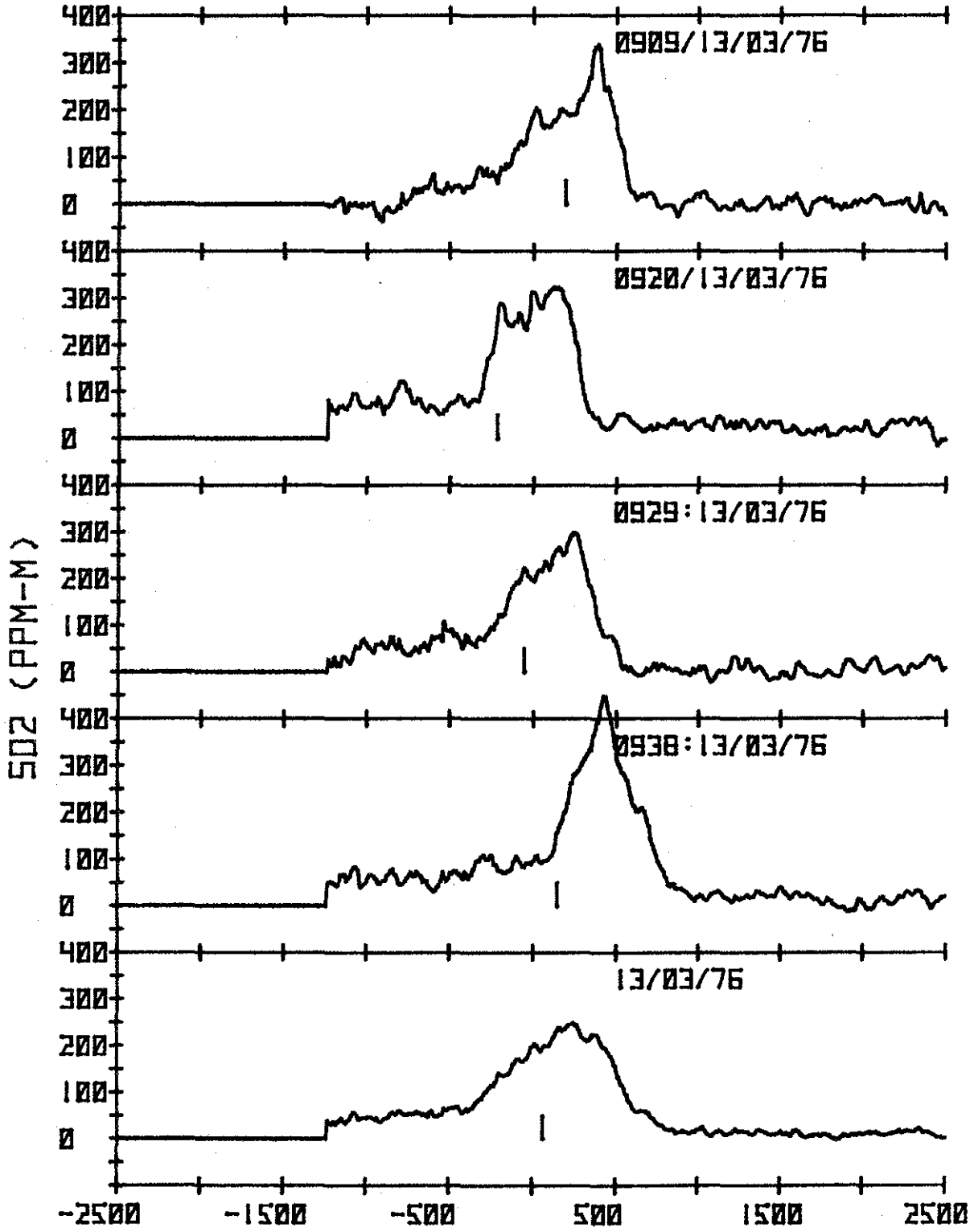

Figure 6.3a. Eulerian Average 0909-0938, 13 March 1976.

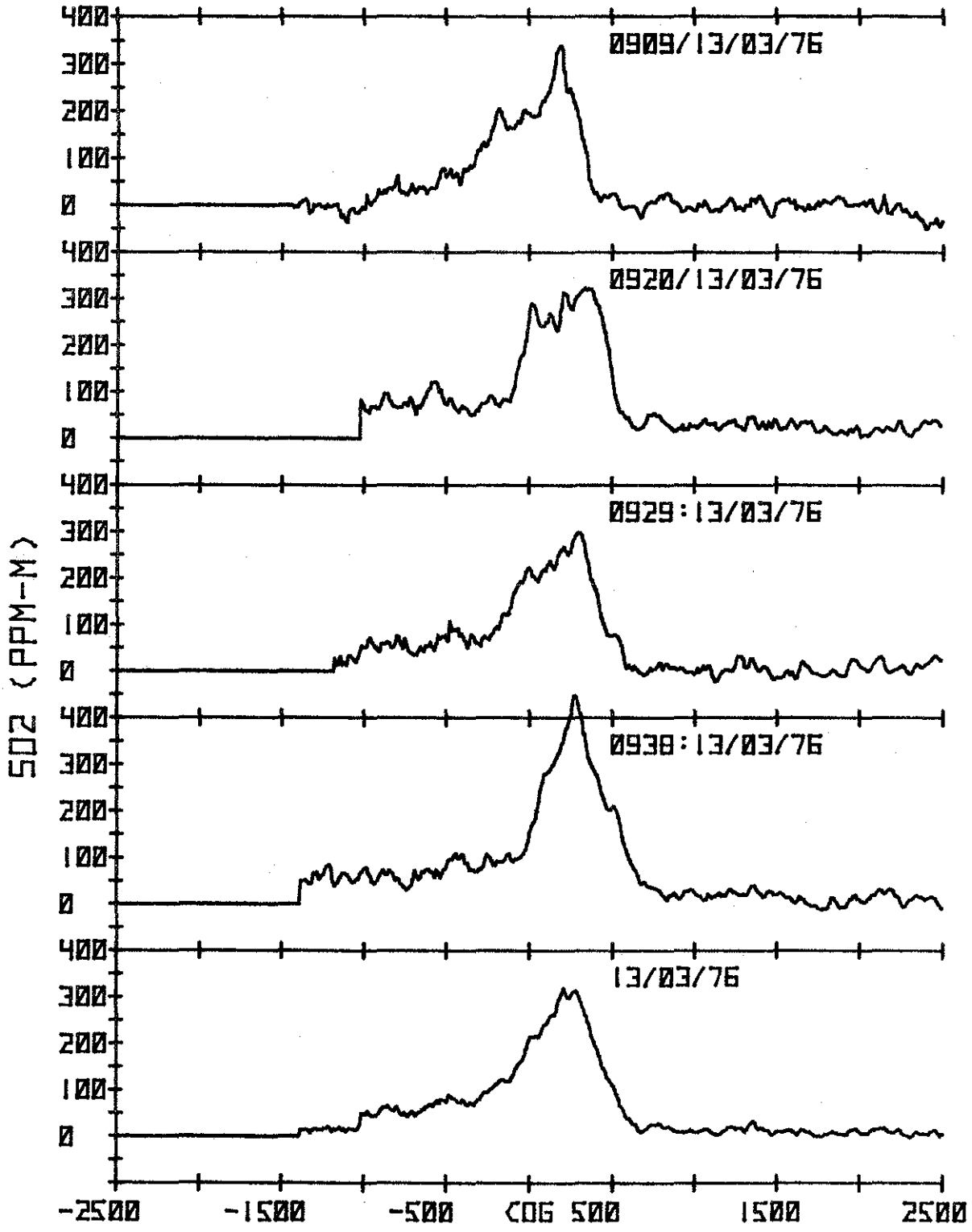

Figure 6.3b. Lagrangian Average 0909-0938, 13 March 1976.

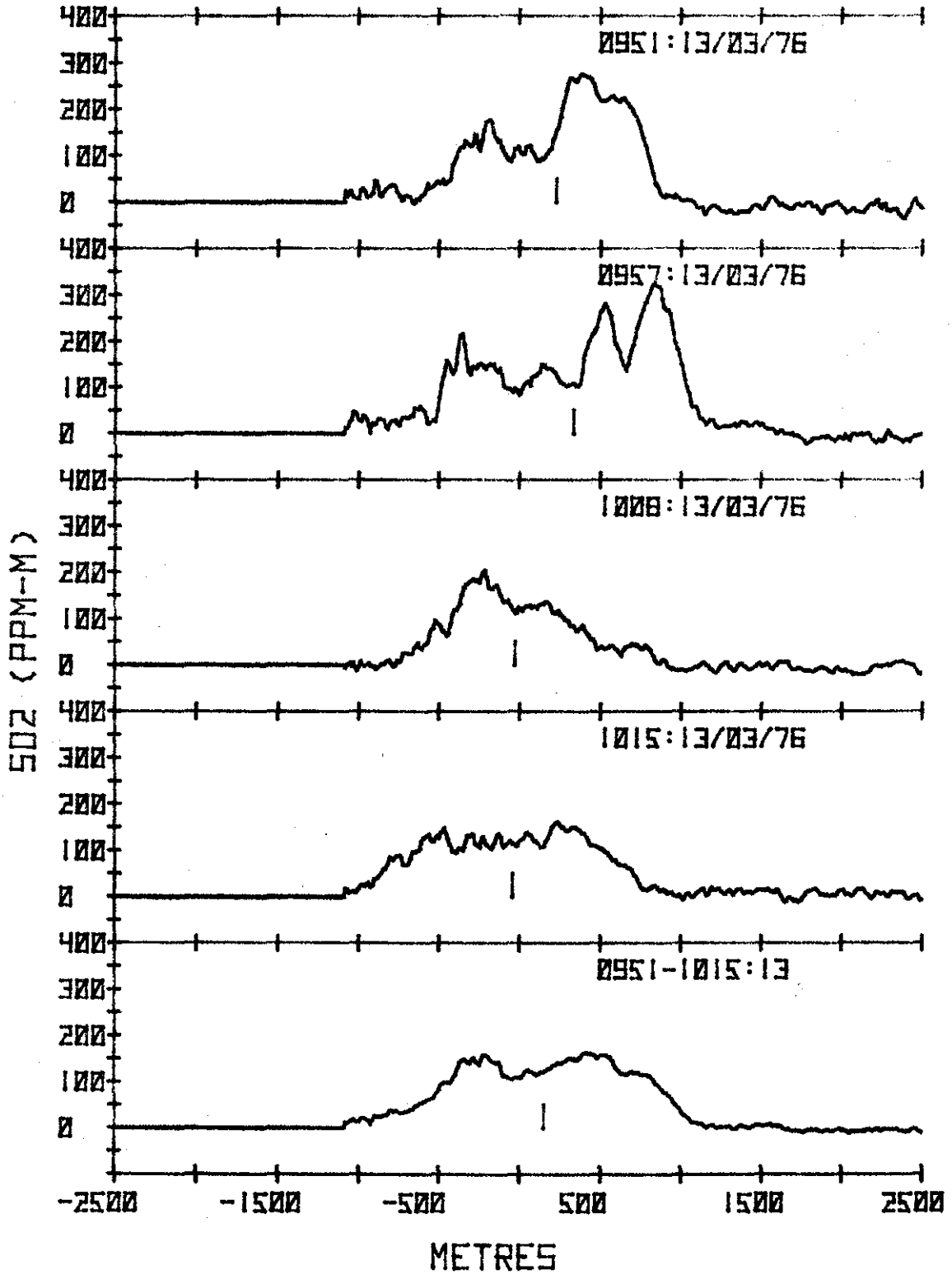

Figure 6.4a. Eulerian Average 0951-1015, 13 March 1976.

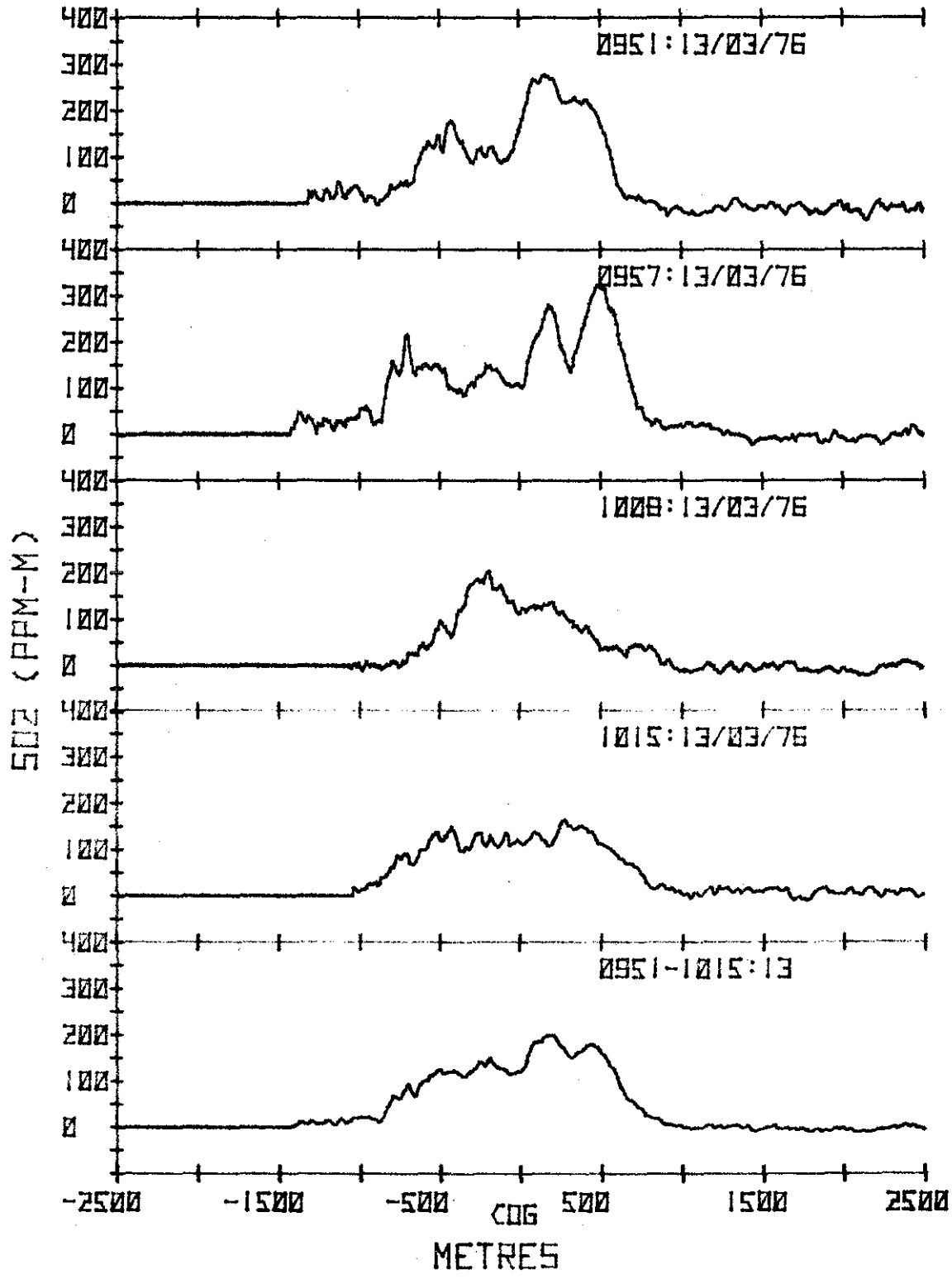

Figure 6.4b. Lagrangian Average 0951-1015, 13 March 1976.

figure of each set (a) shows the profiles relative to the true ground COG of the plume (the origin) in the "effective plane of transect." The COG's of each profile have been calculated using all data above 20 ppm·m^{-1} (a necessity to remove background noise) and are indicated by a vertical line under the profile. The last of the (a) group is the Eulerian average profile.

The second figure of each set represents the profiles as seen with superimposed COG's and their average, the pseudo-Lagrangian, is shown at the bottom. In an unstable plume these two ways of displaying the plumes will be quite dissimilar. The statistical data for these profiles are given in Table 6.2. The bearing of the plume COG is given for each plume and the two types of averages (the bearing of the Lagrangian is meaningless). Also given are the horizontal dispersion coefficient σ_y, the skewness, the kurtosis, and the integrated area (in 10^5 ppm·m^2) under the profiles.

6.4.2 15 March 1976

The morning of 15 March was clear with a strong early-morning inversion of 15°C. The upper level flow was north-northwesterly nearly all day. The plumes were trapped under or at the inversion until approximately 1300 MST when the inversion turned over to isothermal and later lapse. After 1200 MST the plume turned to follow the upper level flow.

At 0830 the plume appeared nearly ribbonlike from the side (Figures 6.5, 6.6) and was found crossing Highway 63 to the southwest of the GCOS plant. The horizontal extent of the plume proved to be far larger than the vertical, indicating fanning beneath the inversion. In fact, striations in the plume crosswind direction were seen on the south side of the plume, possibly due to the upper levels of the plume penetrating into the northerly flow.

A total of 15 runs was taken during the morning, 14 of which have been analyzed. The runs have been broken into four 0.5-h averages, 0825-0857, 0857-0927, 1016-1041, and 1041-1115. The 0.5-h sets of profiles are shown in Figures 6.7 - 6.10. The statistical data on the profiles are given in Table 6.2 as well.

Table 6.2. COSPEC transect results 0.5-h averaging.

TRANSECT (TIME)	BEARING (T.N.) OF COG (DEGREES)	SIGMA-Y (METRES)	SKEW-NESS	KURT-OSIS	AREA (10^5 PPM-M^2)
0909 - 13/03/76	193.1	240	-0.66	2.91	1.52
0920 "	186.8	420	-0.79	2.61	2.32
0929 "	189.3	374	-0.96	3.18	1.88
0938 "	192.4	489	-1.12	3.38	2.61
EULERIAN	191.1	376	-0.77	3.21	2.01
LAGRANGIAN	-	351	-0.59	2.73	2.00
0951 "	192.0	405	-0.71	2.92	2.20
0957 "	193.6	533	-0.45	2.27	2.90
1008 "	188.1	345	0.41	2.56	1.45
1015 "	187.9	503	1.14	8.34	1.85
EULERIAN	190.9	469	-0.15	2.09	2.08
LAGRANGIAN	-	422	-0.19	2.09	2.05
0825 - 15/03/76	212.7	1087	0.44	4.4	6.90
0834 "	231.5	1453	0.84	2.9	3.85
0844 "	214.7	1244	0.01	2.4	7.48
0857 "	226.8	1383	1.17	3.8	4.80
EULERIAN	218.1	1276	0.70	4.3	5.61
LAGRANGIAN	-	1165	0.35	3.1	5.56
0857 "	227.1	1391	1.17	3.8	4.80
0907 "	215.5	1048	0.55	4.5	5.48
0916 "	220.7	1350	1.53	5.1	5.12
0927 "	214.9	807	0.39	5.7	4.04
EULERIAN	218.9	1188	1.36	5.9	4.81
LAGRANGIAN	-	1049	0.83	5.4	N/A
1016 "	218.4	947	-0.22	3.6	5.04
1024 "	215.2	754	-0.95	3.2	6.04
1035 "	218.6	785	-0.72	2.8	5.18
1041 "	218.5	940	-0.46	2.3	5.33
EULERIAN	217.0	837	-0.68	2.9	5.35
LAGRANGIAN	-	833	-0.80	3.0	5.34
1041 "	218.4	932	-0.47	2.3	5.25
1052 "	224.0	1146	-0.40	2.5	8.82
1103 "	224.1	1157	-0.27	2.3	8.81
1115 "	220.8	1155	-0.21	2.3	8.63
EULERIAN	222.0	1115	-0.31	2.4	7.84
LAGRANGIAN	-	1107	-0.39	2.4	7.83

Figure 6.5. GCOS plumes at 0830, 15 March 1976. Darker plumes are low level sources, while power plant plume levels off under the inversion at a distance of a few hundred metres from the stack (Photograph courtesy of F. Fanaki).

Figure 6.6. GCOS plumes at 0810, 15 March 1976. Photograph taken from Highway 63 between points 6 and 7 (see Figure 6.1).

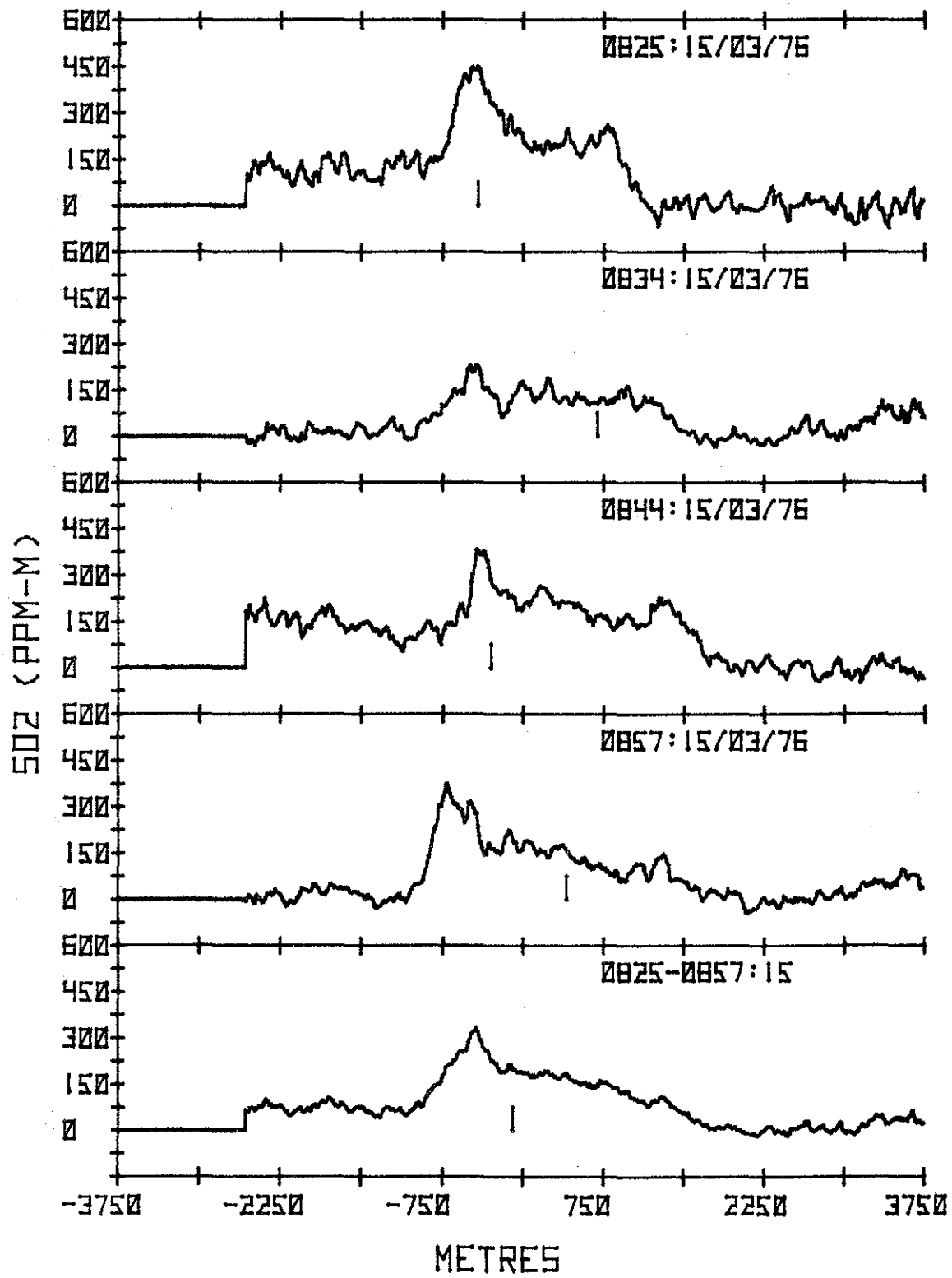

Figure 6.7a. Eulerian Average 0825-0857, 15 March 1976.

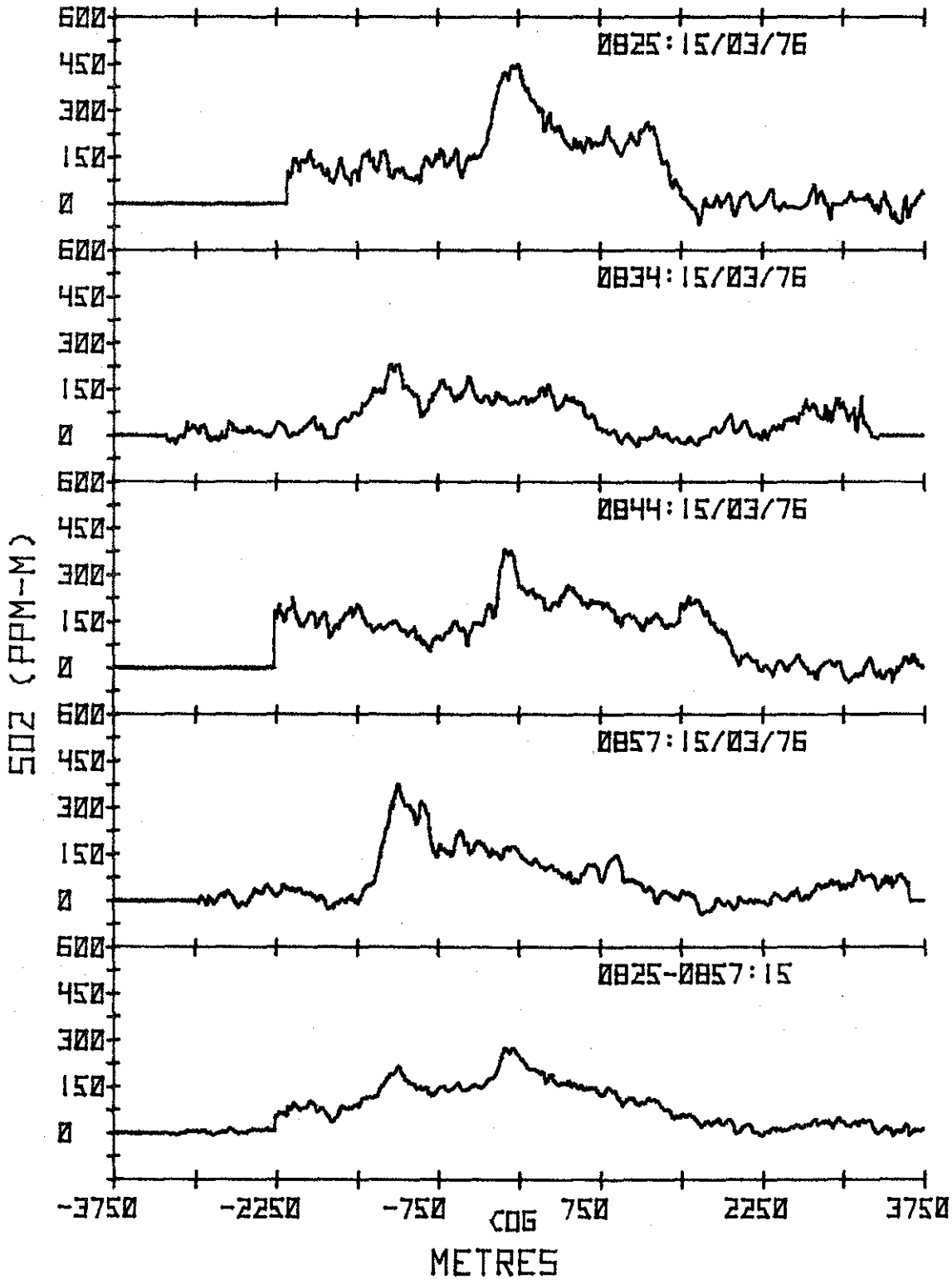

Figure 6.7b. Lagrangian Average 0825-0857, 15 March 1976.

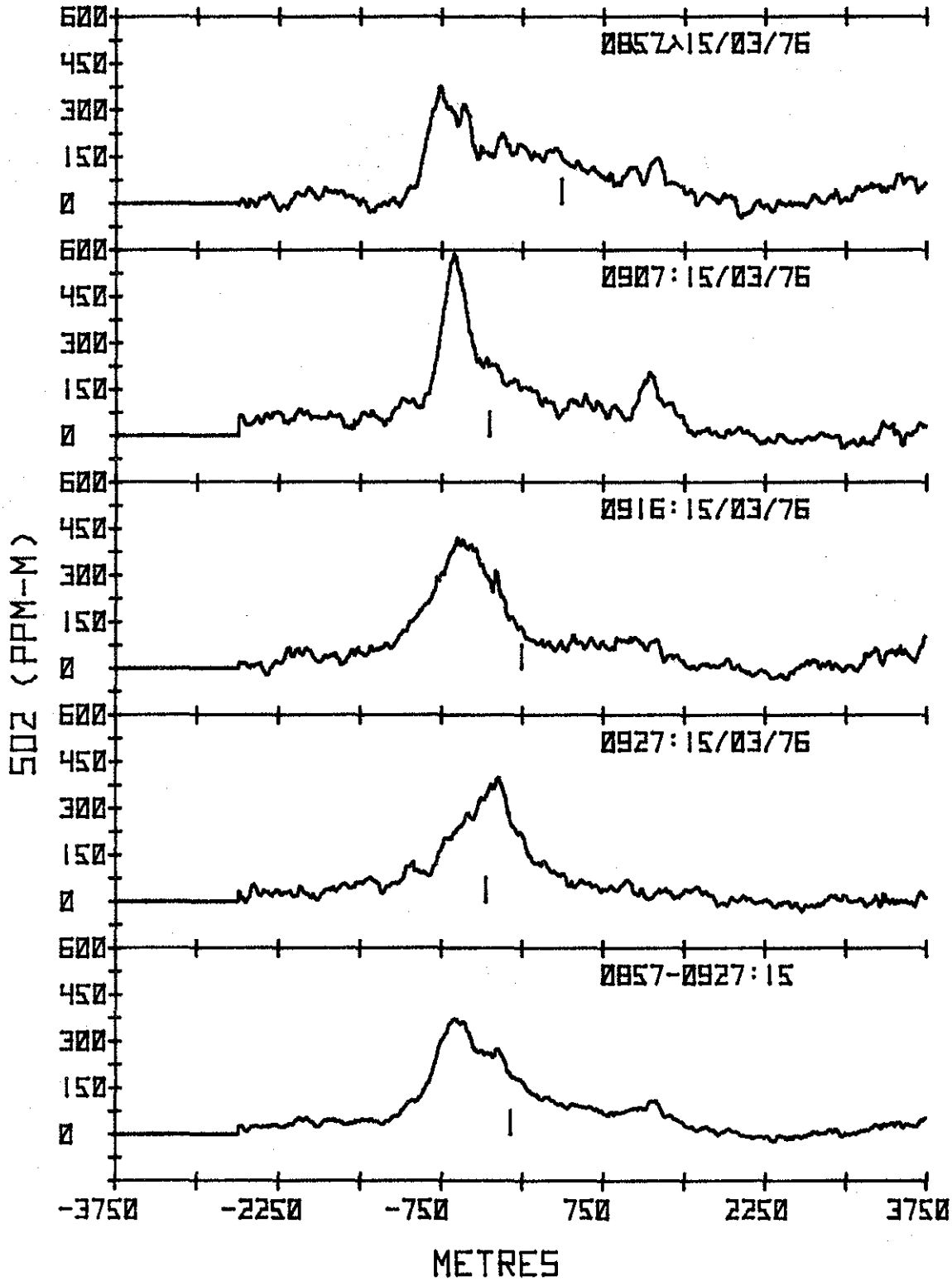

Figure 6.8a. Eulerian Average 0857-0927, 15 March 1976.

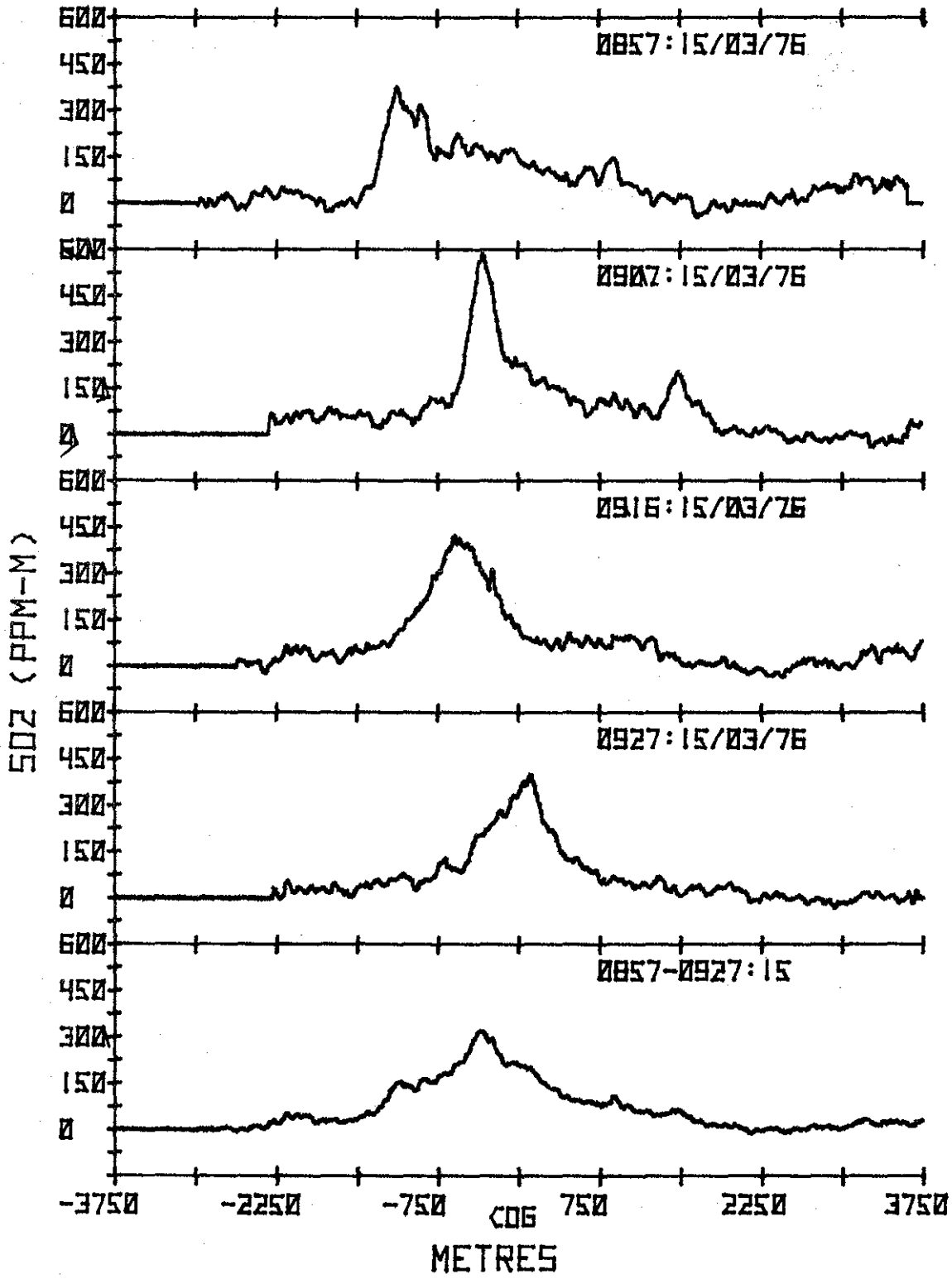

Figure 6.8b. Lagrangian Average 0857-0927, 15 March 1976.

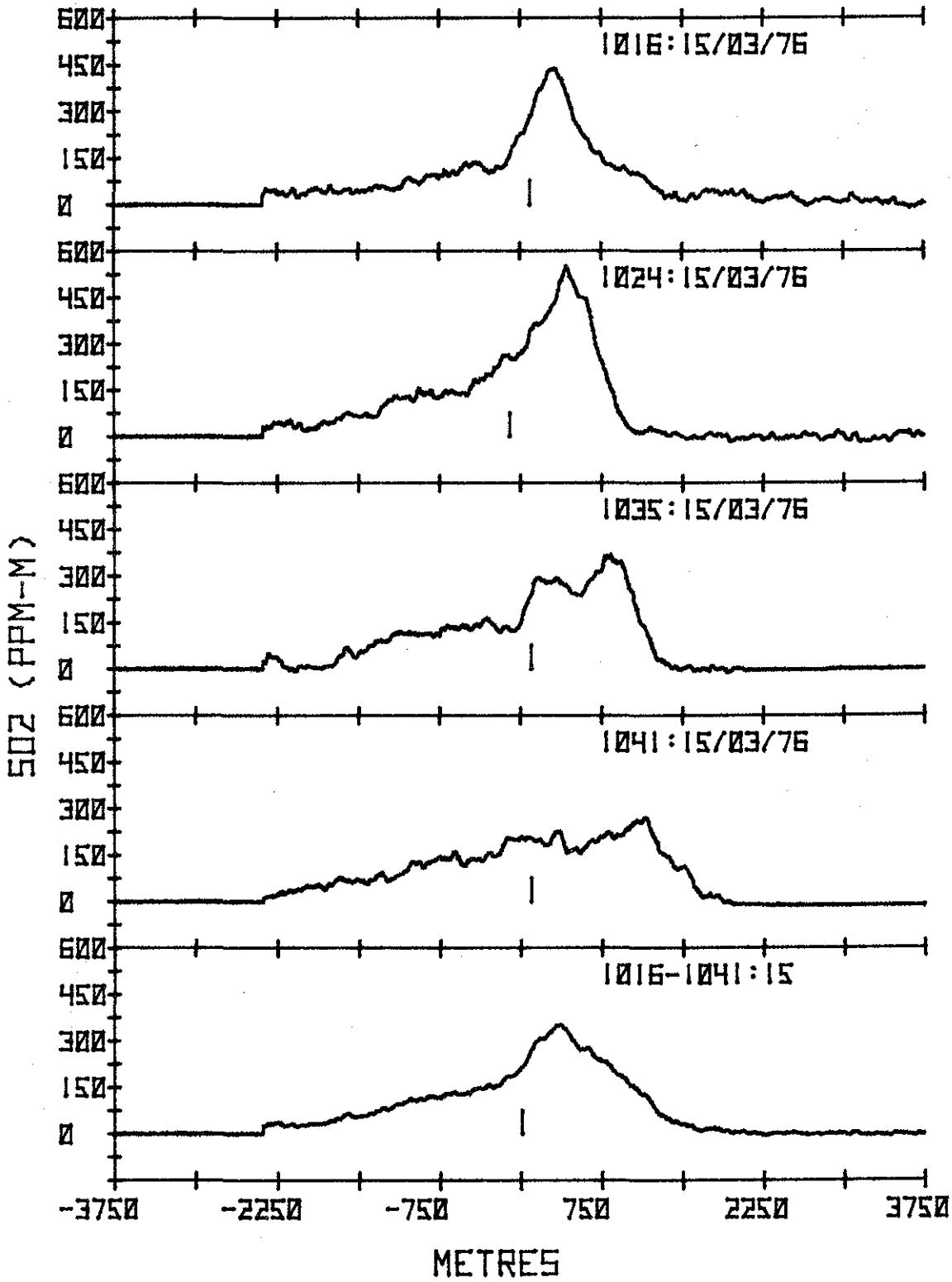

Figure 6.9a. Eulerian Average 1016-1041, 15 March 1976.

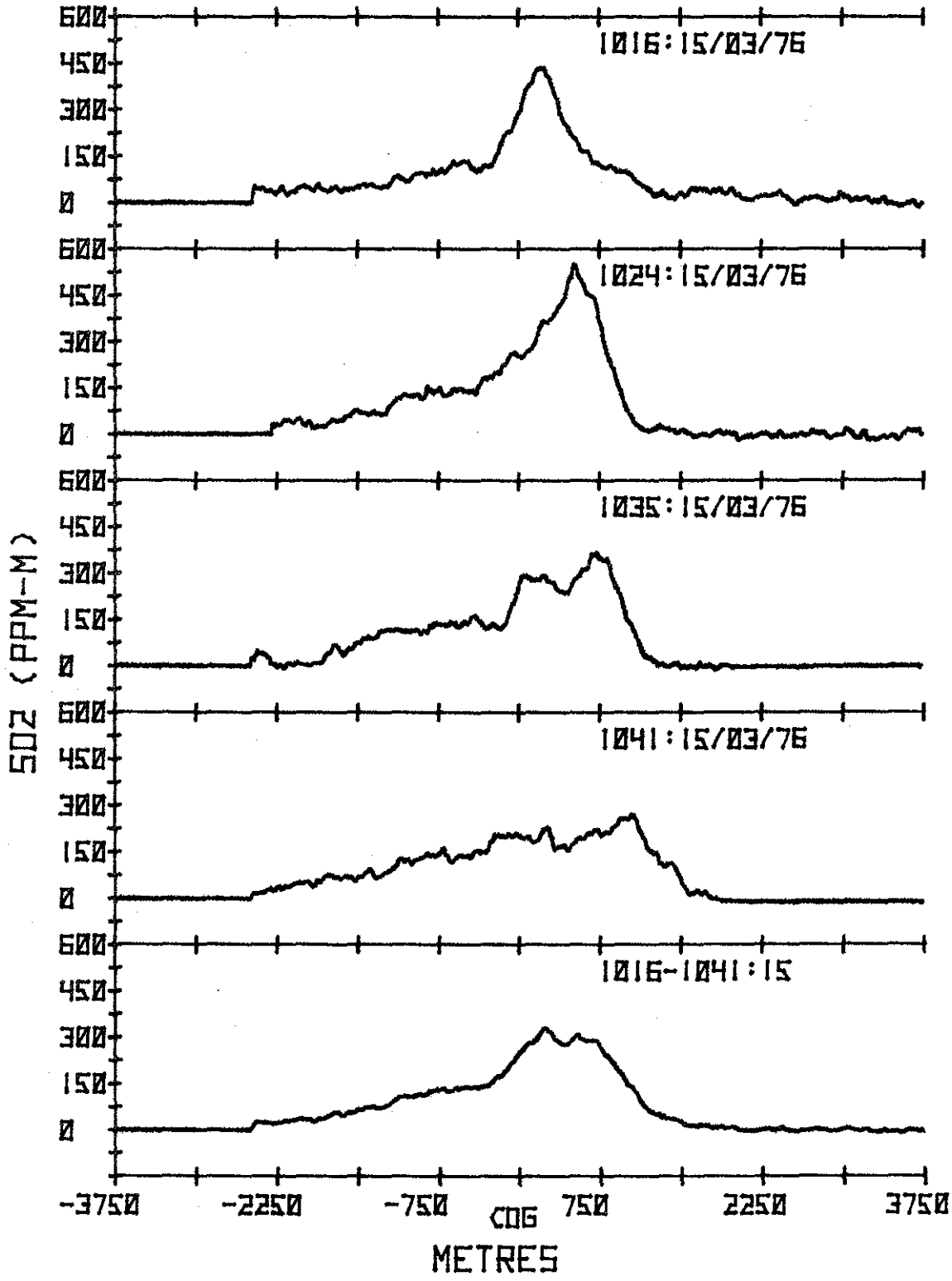

Figure 6.9b. Lagrangian Average 1016-1041, 15 March 1976.

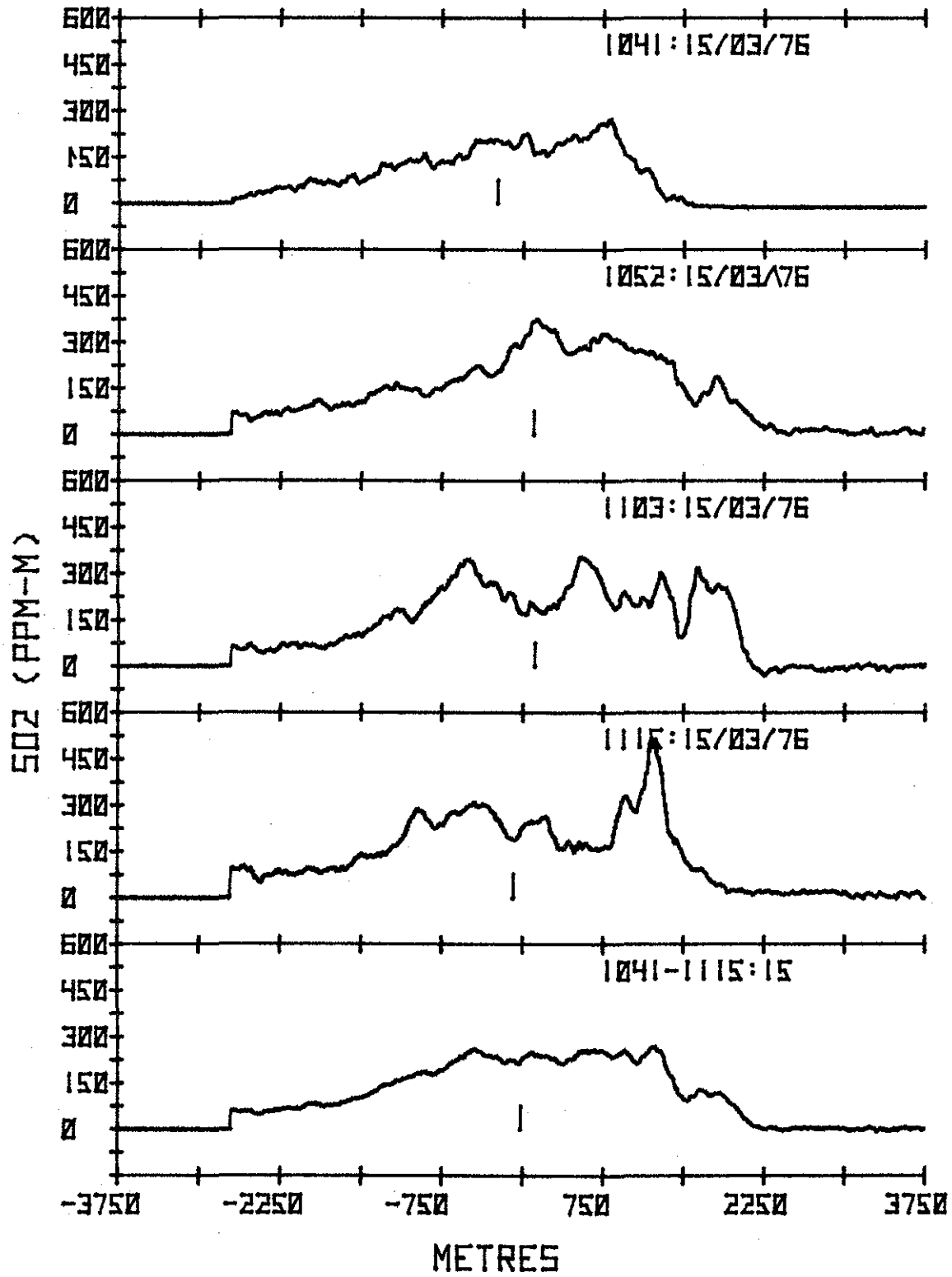

Figure 6.10a. Eulerian Average 1041-1115, 15 March 1976.

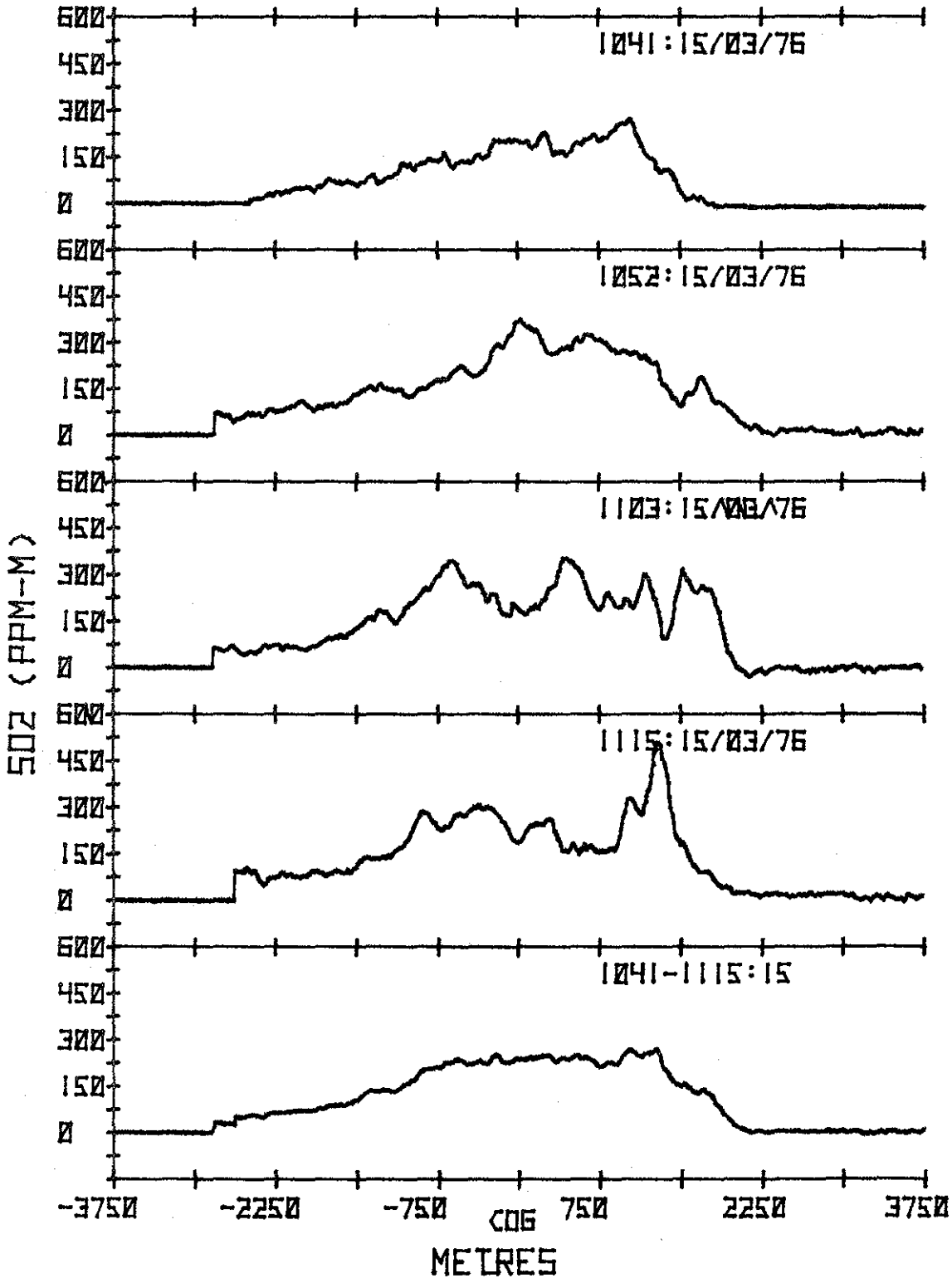

Figure 6.10b. Lagrangian Average 1041-1115, 15 March 1976.

6.5 DISCUSSION

From the bearings in Table 6.2 and the COG's shown on the map of Figure 6.1, the measured plumes on both days seem to be quite stable, varying in bearing by at most 16°. The most noteworthy feature of the two days is that the horizontal dispersion coefficient σ_y is susbstantially larger on 15 March when an inversion was present. On 13 March, σ_y varied from 240 to 530 m, while on 15 March it ranged from 840 to approximately 1300 m. The predicted dispersion from Gaussian plume models at 3.3-3.7 km for stability classes B, C, or D (slight insolation, various wind speeds) ranges from 210 to 520 m. This is in general agreement with the data from 13 March but not for 15 March, when an inversion was present. In an preliminary evaluation, the authors speculated that the large discrepancy of 15 March might be due to the fact that several sources, the power plant stack, the incinerator stack, and the flare, contributed to the SO_2 in the plume. Thus, an area source around GCOS may broaden the expected horizontal dispersion coefficient. This is still a possible explanation, because the bearing of the plume on 13 March would be nearly in line with the geographical position of the three stacks (Figure 6.1), subtending a smaller source angle than it did on 15 March. A more obvious explanation, however, is that the inversion on 15 March has a strong bearing on the horizontal dispersion of the plume. This is evident in the fanning under the inversion noted visually. This points out vividly the care that must be employed in modelling in winter conditions where inversions are the rule rather than the exception. Even using the corrections applied for cases of inversion (Turner 1970) the dispersion is far larger than would be expected from the Gaussian model.

Another interesting effect on 15 March is the directional shear of the plume with height. This effect is readily seen in comparing the COSPEC vertically integrated SO_2 ground concentration of 0.16 ppm averaged over the 0.5-h period 1026-1102 at point E (Figure 6.1). This point is approximately 1560 m to the southern side of the COSPEC-measured plume center lines if point E is projected into the effective plane of transect. Even though the

widths of the instantaneous plumes given by the σ_y values was increasing over this period, this shear is consistently larger than one standard deviation of the profile aloft.

The availability of a measurement of σ_z on 13 March by F. Fanaki makes it possible to estimate the peak concentration of SO_2 in the plume. With a vertical σ_z of 85 m at 1030, peak concentration aloft ranged from 1.8 to 5.3 ppm of SO_2.

6.6 MASS FLUXES

Measurements of mass fluxes of SO_2 can be made from the data taken, but the results of such calculations are highly dependent on support data. The mass of SO_2 in tonnes per hour crossing the effective plane is given by:

$$M = A \cdot K \cdot V_w \cdot 3600 \ s \cdot h^{-1}$$

where A = area under the profile in $ppm \cdot m^2$

K = conversion from ppm to kg or t (tonnes)

$= 2.64 \times 10^9 \ \frac{t}{m^3}$; and

V_w = mean wind speed in $m \cdot s^{-1}$ measured in plume height.

As one can see, the mass flux calculation is only as accurate as the mean wind seen by the plume over the averaging period. This can be a significant source of error, especially in cases of low or calm wind speeds. Preliminary calculations using raw minisonde data gave considerable disagreement with measured in-stack SO_2 emissions obtained from W.L. Cary of GCOS. In an attempt to reach an "average wind", the wind speed at plume height was obtained from three sources: the minisonde site at the GCOS southwest boundary, the Lower Syncrude minisonde, and the tethersonde package. The height of the plume was fixed at 1.6 km downwind on 13 March to be at approximately 475 m of above stack top by the plume photography of F. Fanaki. Assuming negligible plume rise (evident from 1.0 to 1.6 km), this places the plume at 838 m MSL with an apparent vertical full width of 180 m.

The plume height for 15 March was estimated from the minisonde and tethersonde data to be the height at which the wind direction corresponds to the plume bearing of $\approx 220^{\circ}$N. This height was approximately 550 m MST for most of the morning. This uncertainty in measuring the plume height causes a direct uncertainty in the average wind speed obtained. An estimate of this error in the wind speed is chosen to be the largest difference between the average speed obtained and the adjacent soundings at lower and higher heights. On 13 March, the thickness of the plume itself obtained from the plume photography gives the uncertainty in the mean wind, as there was a wind speed gradient across the plume in the vertical. By choosing the largest wind speed difference, the authors have placed a very conservative limit on the obtainable accuracy of the mass flux measurements. The estimated percentage errors in the average wind speed (roughly 20-50%) are squared, added to the squared errors of the signal and temperature at plume height, and the square root of the result is displayed as an absolute error in the mass fluxes calculated in tonnes per hour in Table 6.3. Except for the data of 13 March, the measured values seem to overlap fairly well when the probable error is considered. The GCOS minisonde of 13 March obtained a wind speed at plume height of 16 $m \cdot s^{-1}$, which is far larger than the general 9-11 $m \cdot s^{-1}$ obtained from both minisonde at plume height for the rest of the morning.

A conclusion that can be drawn, then, is that SO_2 mass flux measurements can be made using a single COSPEC, provided that reliable 0·5-h or hourly average wind speed information at plume height is available. Neither the minisonde nor the tethersonde is expected to give such an average except under ideal circumstances. One can envisage a slave tethered balloon obtaining this average at plume height near the COSPEC traverses, but this is generally infeasible and is, in fact, at variance with some of the advantages of a remote measurement itself. These problems in making accurate mass flux measurements with the COSPEC have been treated in an earlier paper (Millan et al. 1976), and the methodology of the process, while admittedly far less reliable than the measurement of dispersion parameters, continues to be improved.

Table 6.3. Mass fluxes from COSPEC data.

TIME	AREA (10^5 ppm-m^2)	GCOS EMISSIONS (t/h) (1)	MASS FLUXES USING WIND SPEED FROM		
			GCOS MINISONDE	LOWER SYNCRUDE MINISONDE	TETHERSONDE
0909 - 0938: 13/03	2.01 ± 10%	8.6 ± 10%	33.8 ± 9.0	19.3 ± 3.8	N/A
0951 - 1015: 13/03	2.08 ± 10%	8.6 ± 10%	35.0 ± 9.4	20.0 ± 3.9	N/A
0825 - 0857: 15/03	5.61 ± 10%	11.7 ± 10%	N/A	18.9 ± 7.0	9.4 ± 3.3
0857 - 0927:15/03	4.81 ± 10%	12.6 ± 10%	18.0 ± 8.2	22.0 ± 10.4	9.0 ± 3.0
1016 - 1041:15/03	5.35 ± 10%	13.1 ± 10%	6.5 ± 2.9	9.7 ± 3.1	6.7 ± 3.1
1041 - 1115:15/03	7.84 ± 10%	13.1 ± 10%	9.5 + 4.2	14.2 ± 4.4	5.5 ± 4.2

(1) Data obtained from W.L. Cary, GCOS, Ltd. Note that the conversion of 1 metric tonne (t) = 0.98 long ton has been used and that the emission figures include the contribution from both stacks. The error is that estimated by CGOS.

Reliable single-day dispersion parameters have been obtained from COSPEC ground traversing in the Tar Island area. It was noted in the preliminary report that, by nature of the road network, the results are biased towards those days with a wind direction out of the eastern quadrants. For this reason, futher COSPEC work on the GCOS emissions could be made more representative if the instrument were flown in a helicopter. For the Lower Syncrude site, however, the availability of a nearly complete perimeter road (assuming accessibility) makes ground traversing with the COSPEC an effective way of obtaining dispersion statistics when the plant comes on stream.

6.7 REFERENCES CITED

Csanady, G. 1973. Turbulent diffusion in the environment. D. Reidel Publ. Co. Dordrecht, Holland. 248 pp.

Millan, M.M. 1976. A note on the geometry of plume diffusion measurements. Atmospheric Environment 10: 655-657.

Millan, M.M., A.J. Gallant and H.E. Turner. 1976. The application of correlation spectroscopy to the study of dispersion from tall stacks. Atmospheric Environment. 10: 499-511.

Turner, D.B. 1970. Workbook of atmospheric dispersion estimates. NAPCA. 84 pp.

6.8 ACKNOWLEDGEMENTS

We would like to thank Mr. Robert Quinney and Mr. Thomas Sainsbury of AES, Western Region, and Dr. John Walmsley and Dr. Leonard Barrie of AES Headquarters for their help in driving the vehicles and taking COSPEC data. We would also like to thank the AOSERP staff who made our stay at Mildred Lake comfortable and kept the vehicles rolling, especially the efforts of Av Mann and John Mulloch. One of the authors (R.M.H.) acknowledges the National Research Council of Canada for his Postdoctoral fellowship.

7. BACKGROUND AIR AND PRECIPITATION CHEMISTRY

by L.A. Barrie and D.M. Whelpdale

7.1 AIR CHEMISTRY STUDY

Ever since vast oil reserves were discovered in the oil sands of the Athabasca region, the environmental consequences of exploiting such a resource have been of great concern. One of the many problems facing us is determining the effect of large quantities of gaseous and particulate substances that are released into the atmosphere during the extraction and refining of bitumen from the oil sands. Heavy metals in the form of suspended particulate and sulphur compounds are of particular importance. Some metals are highly toxic even at very low concentrations and must be carefully monitored. Sulphur is a rather abundant by-product of the refining operation (the sulphur content of bitumen is about 5%). Even though some of it is extracted as elemental sulphur, a great deal of it enters the atmosphere as sulphur dioxide or sulphate aerosol (100 or more tonnes per day from GCOS in winter 1975/76).

In order to assess the impact of present and future industrial emissions in the oil sands area, the concentration of these trace substances in both unpolluted and polluted air must be known. As a first step, an aerosol sampling program was conducted in March 1976 to measure the following:

1. the background concentration of 16 elements (including heavy metals) in unpolluted air of the oil sands area; and
2. the concentration of gaseous and particulate sulphur in air near the GCOS mining and extraction plant.

7.1.1 Experimental procedure

The aerosol sampling sites were located at a forestry station on Birch Mountain approximately 80 km north-northwest of the GCOS plant and at Mildred Lake Research Facility 10 km north-northwest of the plant (see Figure 1.2).

Gaseous and particulate sulphur sampling was conducted at the Mildred Lake site with the apparatus shown in Figure 7.1. Air was sucked, at a rate of about 50 L/min, through two filters in series in a sampling head. The front filter, for particulate sulphur, was untreated Whatman 40 paper and the backup filter, for SO_2 collection, consisted of Whatman 41 paper treated with potassium bicarbonate and an organic wetting agent, triethanolamine. Sampling was carried out for 4-h periods during the day and for 12-h at night. The average concentration of sulphur in air during a sampling period was determined by using a sensitive isotope dillution technique (Klockow et al. 1974) to measure the amount of sulphur on the filters and then dividing by the volume of air sampled. Under the above sampling conditions the lower limit of detection was about 0.1 μg $S \cdot m^{-3}$ for SO_2. The accuracy of measurement of particulate and gaseous sulphur concentrations was 20 and 50%, respectively.

At the Birch Mountain site, an apparatus similar to that in Figure 7.1 was used to sample background air for later heavy metal analysis using neutron activation techniques. The flowmeter was replaced by a dry gas meter that measured the total volume of air sampled. The sampling head was an open-faced filter holder containing Whatman 41 cellulose paper. At this remote site, reached only by aircraft, 100-200 m^3 of air were filtered over a period of time ranging from 4 to 6 days. Atmospheric elemental concentration could be determined with an accuracy of ±25%. Simultaneous wind direction and temperature measurements were made by an automatic meteorological station located approximately 80 m from the samplers.

7.1.2 Results and discussion

7.1.2.1 Background aerosol. At Birch Mountain, three aerosol samples were collected between 3 and 17 March. The average atmospheric concentration of 16 elements for each of the sampling periods is listed in Table 7.1 along with the prevailing meteorological conditions. In each case, the winds were such that only unpolluted continental arctic air was sampled.

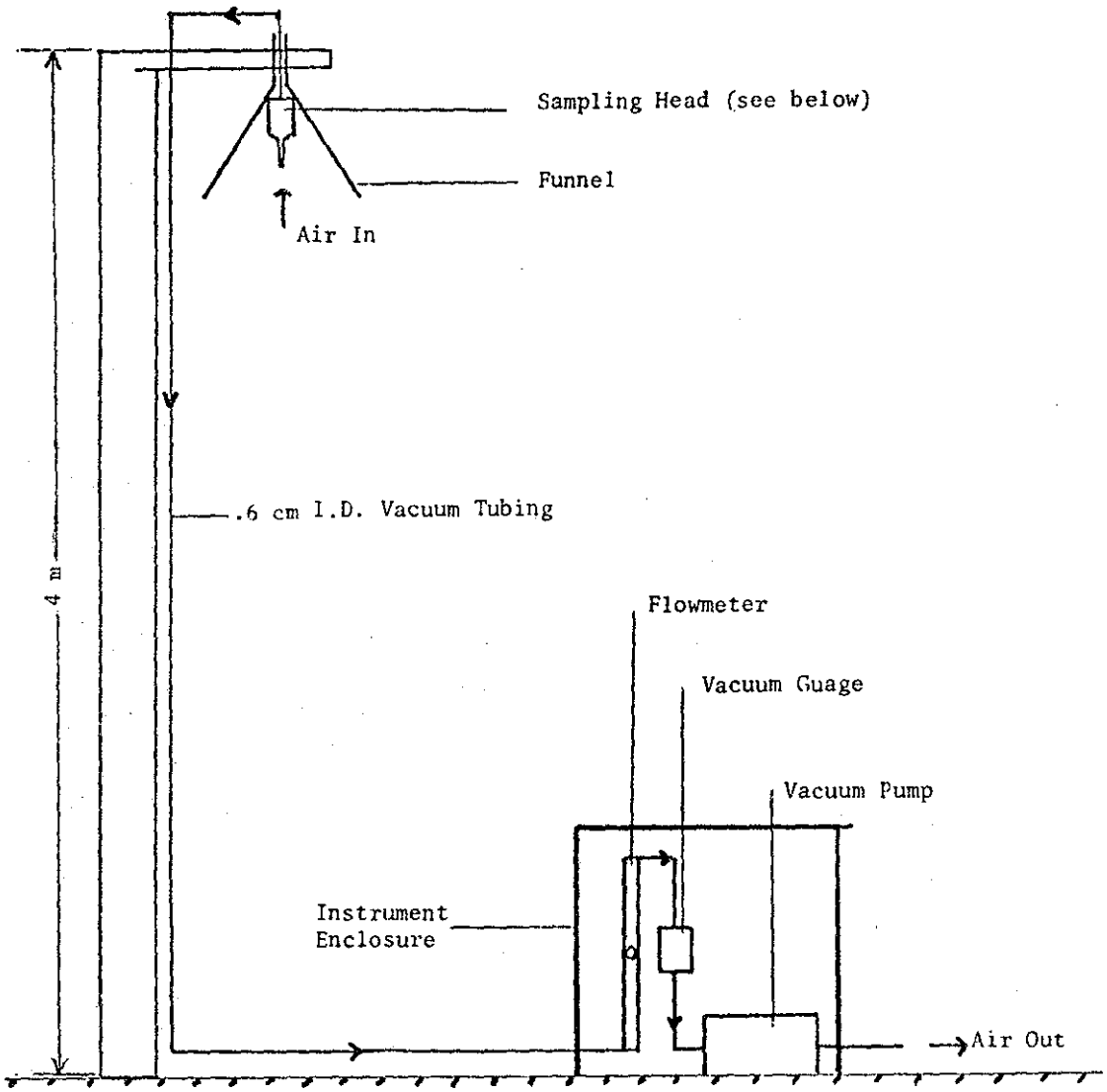

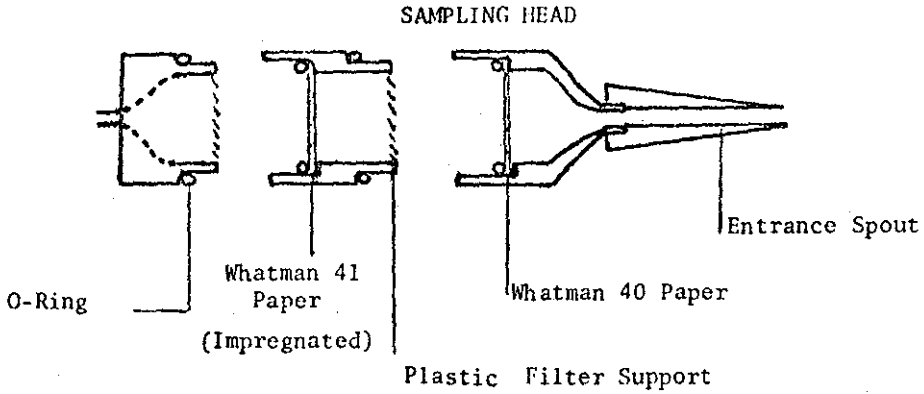

Figure 7.1. SO_2 - $SO_4^=$ sampling apparatus.

Table 7.1. Concentration of various elements in particulate at Birch Mountain during March 1976 ($ng \cdot m^{-3}$).

Element	Sample 1 3-7 March	Sample 2 7-13 March	Sample 3 13-17 March
Al	41.	56.	70.
As	0.37	1.1	0.44
Br	4.7	2.1	1.8
Ca	19.	41.	40.
Cl	185.	54.	60.
Cu	<1.0	<1.3	<1.5
I	.52	.47	.54
K	32.	25.	35.
Mg	31.	23.	26.
Mn	.66	.93	1.0
Na	130.0	76.	67.
Sb	< .11	.17	<.08
Sc	< .013	.011 - .017	.012 - .021
Ti	<4.9	6.7	7.9
V	.52	4.5	4.7
Zn	-	4.1 - 7.7	<5.64
Mean Temperature (^{o}C)	-16	-14	-10
Wind Direction ($km \cdot h^{-1}$)	N to SE	NW-N-NE	SW-W-N
Maximum Wind Speed	20	-	-

Some elements could not be detected due to the insensitivity of neutron activation analysis. They include iron (Fe), cobalt (Co), nickel (Ni), and silicon (Si). Of those detected the most abundant elements were sodium (Na), chlorine (Cl), aluminum (Al), calcium (Ca), potassium (K), and magnesium (Mg) all with concentrations greater than 10 $ng \cdot m^{-3}$. With the exception of Al all are present, in abundance, in sea salt. Following the procedure of Peirson et al. (1974), one can calculate an enrichment factor F defined as:

$$F = \frac{\text{Air concentration of element}}{\text{Air concentration of Sc}} \Big/ \frac{\text{Average soil concentration of element}}{\text{Average soil concentration of Sc}}$$

where Sc is Scandium. Nonmaritime elements of anthropogenic origin can be distinguished from those of soil origin since F values near 1 correspond to a soil source while values much greater than 1 indicate an anthropogenic source. The reference material used to calculate the denominator of F above was Bowen's average soil (Bowen 1966).

In Figure 7.2, enrichment factors of nonmaritime elements calculated from concentrations in Table 7.1 are compared with those determined in background air of the United Kingdom by Peirson et al. (1974). The results from two widely separated background air masses agree well. The good agreement shows that even in winter the results of other investigations in remote localities can be applied to the background aerosol of the oil sands region. Since the enrichment factor of aluminum and manganese (Mn) are close to one, it may be concluded that they are soil-derived. On the other hand, arsenic (As), antimony (Sb), vandium (V), and zinc (Zn), which have enrichment factors much greater than one, probably originate from anthropogenic sources. Thus, even the cleanest air contains man-made trace constituents. The concentration and composition of particulates that are emitted into this air from the oil sands region remains to be determined. This will be done by sampling aerosol in polluted air downwind of the sources. In the future, the enrichment factor approach can be used to detect the influence of anthropogenic sources at any location in the oil sands area.

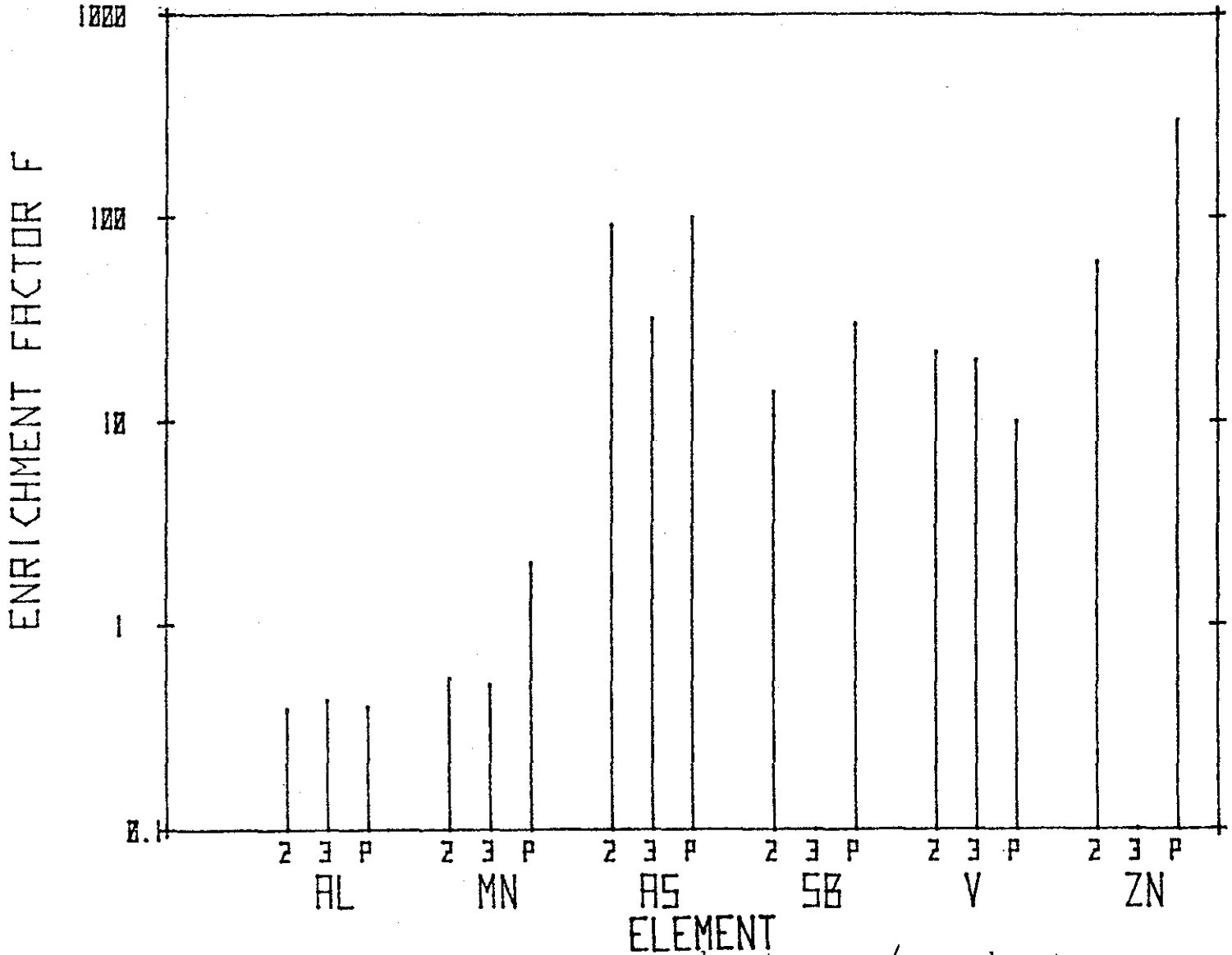

Figure **7.2.** Enrichment factor F = $\left(\frac{\text{conc. element}}{\text{conc. Sc}}\right)$ aersol $/ \left(\frac{\text{conc.element}}{\text{conc. Sc}}\right)$ soil for various elements in background air in the oil sands area (samples 2 and 3) compared to background air measured by Pierson et al, 1974 (P).

7.1.2.2 Atmospheric sulphur. At Mildred Lake, sampling for particulate and gaseous sulphur ran smoothly from 3 to 17 March except for some interruptions due to digging activities near the camp between 5 and 13 March. In particular, sampling was stopped during the day on 10, 11, and 12 March. Nevertheless, 37 samples were enough to determine the range of concentrations expected in polluted and unpolluted air.

Four-hour average particulate-sulphur concentrations (Figure 7.3) ranged from 0.1 to 0.5 μg $S \cdot m^{-3}$ in unpolluted background air, while during pollution episodes they varied from 0.5 to 4.5 μg $S \cdot m^{-3}$. The gaseous sulphur concentration averaged over 4 h (Figure 7.4) was less than 1 μg $S \cdot m^{-3}$ in background air. However, in two cases on 8 and 15 March, when the GCOS plumes were carried to the ground by daytime convection, levels rose to between 30 and 50 μg $S \cdot m^{-3}$. At the same site, Fanaki et al. (Section 5) measured instantaneous peak SO_2 concentrations of 290 and 860 μg $S \cdot m^{-3}$ on 8 and 15 March respectively. On these days when pollution from the GCOS plant prevailed, the ratio of gaseous to particulate sulphur ranged between 5 and 20. Not only does such an excess of gaseous sulphur reflect the fact that a major part of GCOS sulphur emissions are SO_2 gas but also it indicates that the transformation of SO_2 to particulate is relatively slow. In background air, the ratio of gaseous to particulate sulphur was close to one.

It was also noticed that in pollution originating from slash burning operations no detectable gaseous sulphur (SO_2, H_2S) was present. At night on 3 March west winds carried smoke from the burning brush piles at the Lower Syncrude complex to the monitoring site. The smell of smoke was clearly evident. A concentration of 4.5 μg $S \cdot m^{-3}$ in suspended particulate was measured; no gaseous-sulphur could be detected.

7.1.3 Conclusions

Methods for measuring the concentration of trace elements in background and polluted air have proven reliable under extremely cold winter conditions. The background air concentration of 16

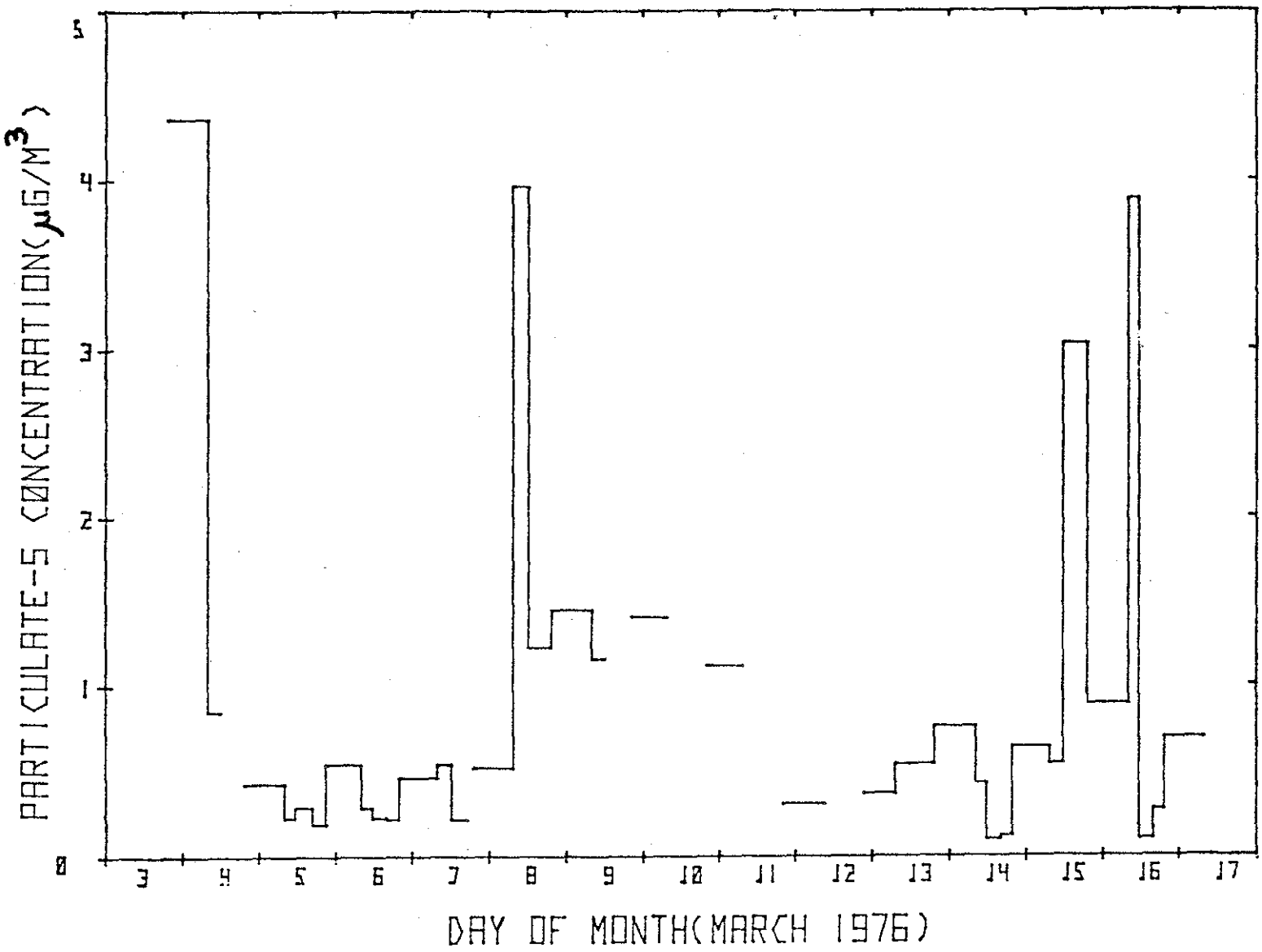

Figure 7.3. Particulate sulphur concentration at Mildred Lake during the winter field study.

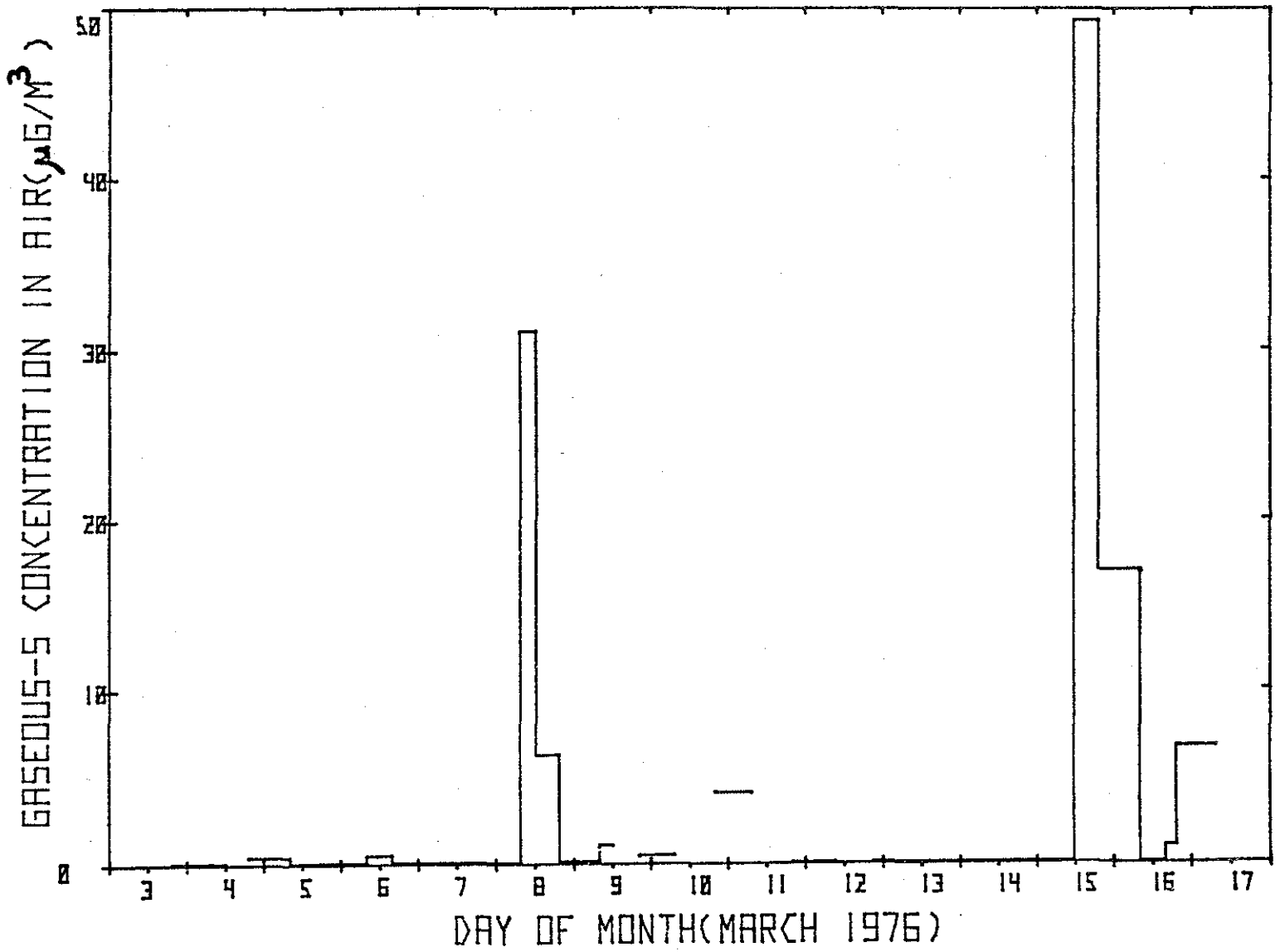

Figure 7.4. Gaseous sulphur concentration at Mildred Lake Research Facility during the winter field study.

different elements, including many metals, was determined. Now that a baseline has been established, the next step will be to collect and analyze aerosol in polluted as well as unpolluted air. Another result of the field study is a 2-week record of gaseous and particulate sulphur concentration for the Mildred Lake area. During the 15-day period two major pollution events occurred. In the future, such a record will be compared with ones obtained under the same conditions but with more plants operating in the area in order to estimate their effect on the levels of sulphur in the air.

7.2 PRECIPITATION CHEMISTRY STUDY

The eventual disposition of pollutants emitted in the oil sands area is a central question to AOSERP. The fate of sulphur compounds is of particular concern, since they are characteristically associated with acidity. During the winter months, sulphur is deposited in the snowpack both as a result of scavenging during precipitation events and also, during dry periods, by particulate deposition and direct gaseous transfer. During the March field study, a snowpack sampling program was conducted to determine the deposition patterns of sulphur emitted during the winter months. The ultimate aim was to ascertain how much sulphur emitted by the GCOS plant remains in the area.

7.2.1 Experimental procedure

During the winter before the field study, snow samples were collected from plastic sheets at about 11 sites at distances up to approximately 100 km from the GCOS plant. Chemical analysis was later carried out for sulphur and pH.

During the field study snow was sampled at 56 sites between 3 and 9 March (Figures 7.5 and 7.6). All sites lay within a 25-km radius of GCOS, primarily in six radial directions, several being with 5 km of GCOS. They were reached by helicopter and snowmobile. Each location was chosen, where possible, in forest clearings away from sources of blowing dust and organic material from trees.

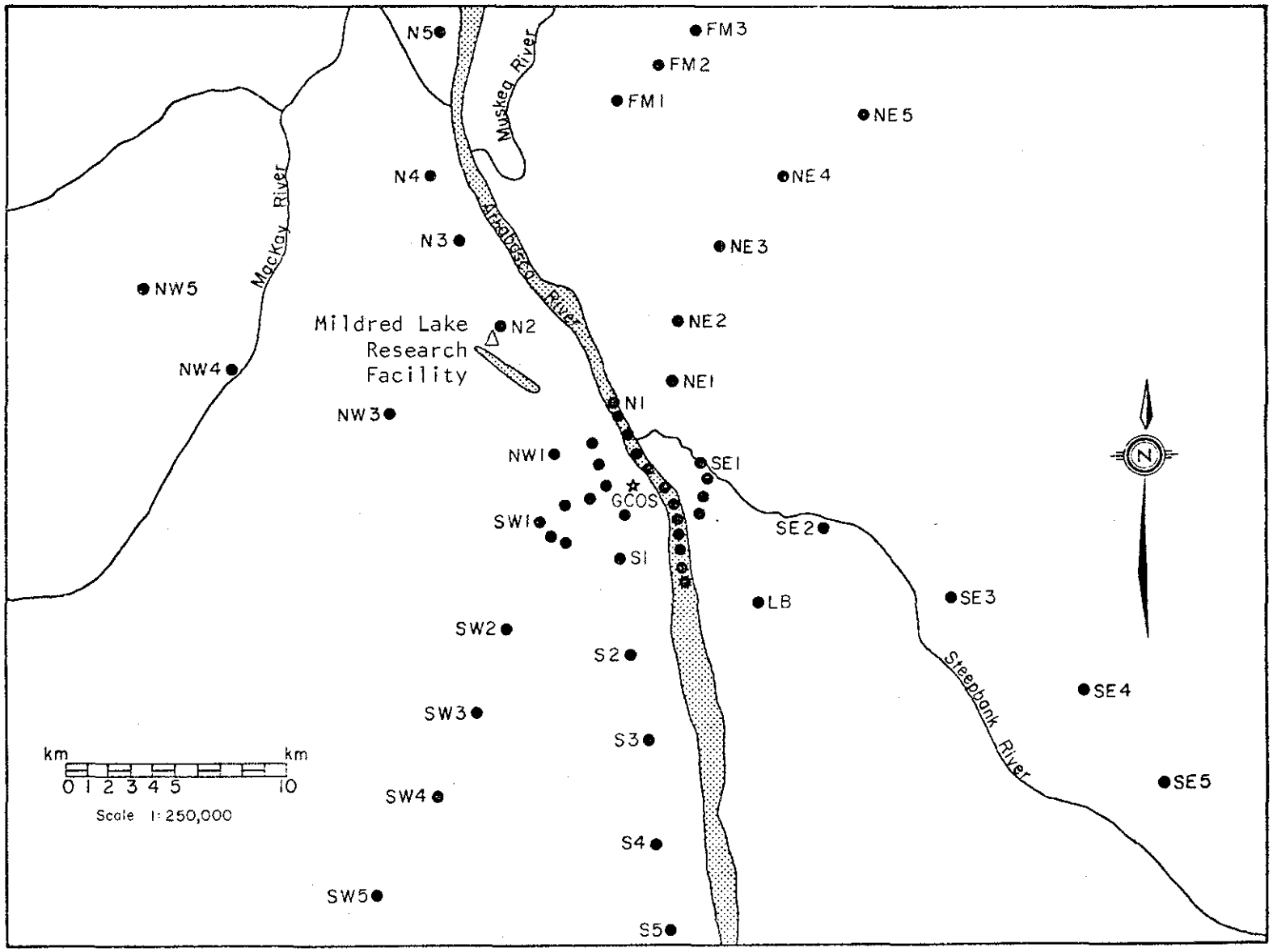

Figure 7.5. Snowpack sampling sites for the March 1976 Field Study.

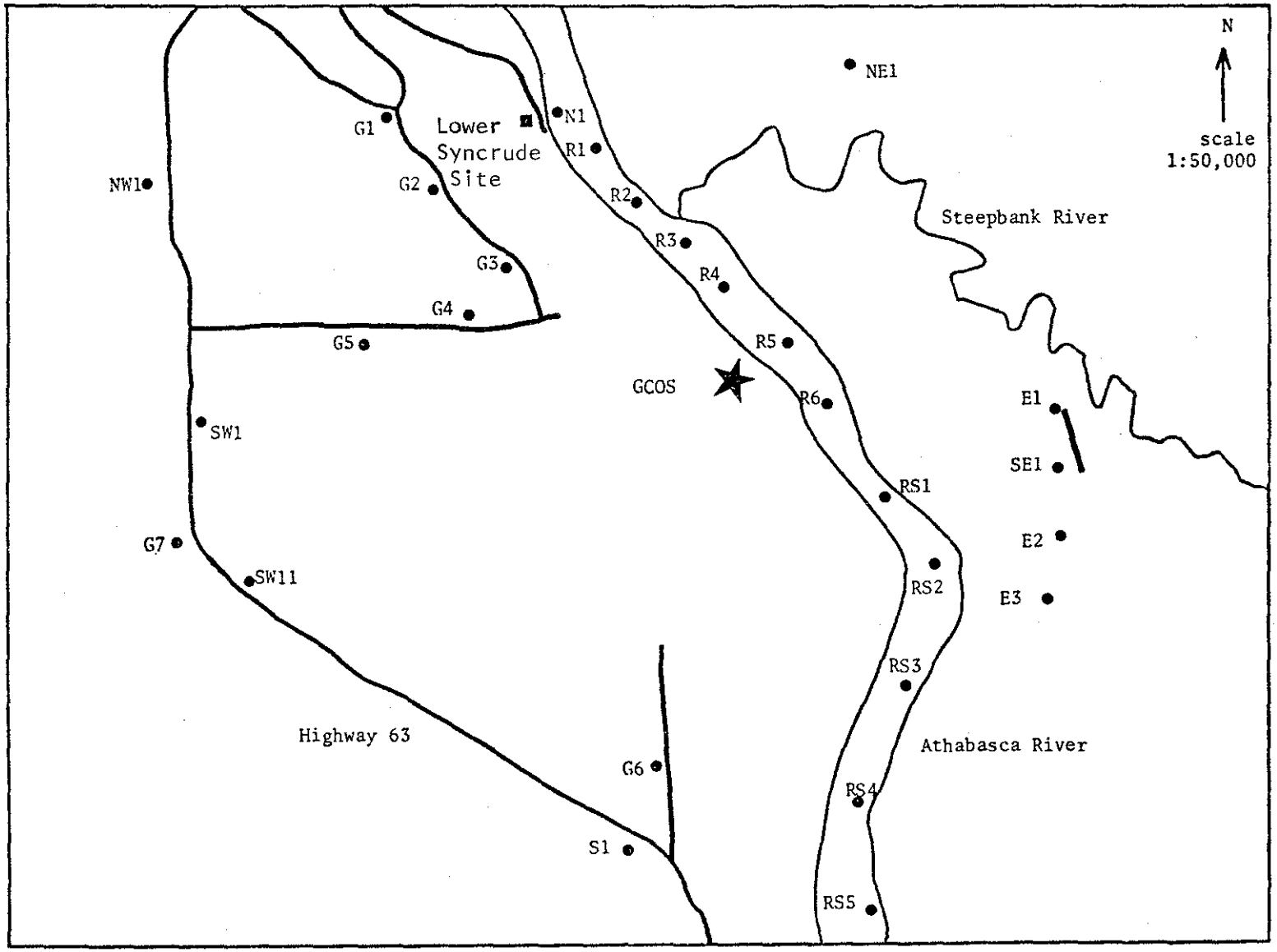

Figure 7.6. Snowpack sampling sites close to GCOS.

Samples were taken with a specially designed sampler that consisted of a half-cylinder, aluminum tube 8.1 cm in radius and 121 cm in length. The plane side was removable to permit vertical snowpack sections to be taken.

At each sampling site the sampling procedure was as follows:

1. measure snow depth,
2. insert sampler vertically to bottom of snowpack,
3. clear snow from plane face of sampler to surface
4. insert clean scoop under lower end of sampler and tilt sampler until horizontal on snow,
5. slide plane surface out to expose "core",
6. measure core length and crust positions,
7. use scoop to separate core at desired levels and slide into plastic bags, and
8. repeat twice to provide three cores at each location.

The samples were kept frozen in plastic bags until immediately before initial analyses. Immediately prior to analysis, samples were allowed to melt and reach room temperature. Preliminary analyses included volume, electrical conductivity, and pH. Conductivity was measured using a Radiometer Conductivity meter, type CDM 2f, with a 5-ml capacity cell, and pH with a Fisher Accumet 320 Research pH meter, which was carefully calibrated before use. Sample aliquots were preserved and taken to AES at Downsview, Ontario for analysis for sulphur. Samples were filtered prior to analysis. The isotope dilution technique (Klockow et al. 1974) used for analysis has a lower detection limit of 0.01 $mg \cdot S \cdot L^{-1}$.

The accuracy of measurement of the various parameters determined in snowmelt was:

pH	±0.3 units
conductivity	±10%
sulphur concentration	±20%
sulphur deposition	±25%

7.2.2 Results and discussion

Table 7.2 lists the pH, conductivity, and sulphur concentrations of background snow samples taken in December and January at forestry sites. Sulphur concentrations ranged from .07 to .40 mg-S/L, while pH varied from 4.9 to 6.6.

During the field study, it was found that snowpack conditions were surprisingly uniform throughout the sampled area, except at highly exposed locations where wind packing had occurred. The snow depth was typically 40 cm at the beginning of the study period and about 50 cm near the end as a result of fresh snowfall.

The typical structure of the snowpack was as follows:

earth surface up to 25 cm: large grains, loose flowing;

next 5-10 cm up: two or three distinct crusts, the lowest being 0.5 cm of ice, the next a 1-cm crust of porous, icy snow grains, and the last a thin icy porous crust;

up to snowpack top: light fluffy snow, progressively less dense toward top.

The snow structure is a result of the meteorological conditions shown in Figure 7.7. Daily temperature maxima and minima are depicted as well as accumulated "fresh" snow depth. Periods of thaw during which crusts form are cross hatched.

Each snow core was divided into two sections. The upper one was a relatively fresh layer of snow (3-4 days old) about 8-10 cm deep. Its depth increased to 15 cm due to snow flurries during the sampling week. Since no thaws had occurred since its formation, the upper layer was unmodified by leaching.

Results of physical measurements and chemical analysis are listed in Table 7.3. Typical standard deviations of the conductivity and sulphur measurements from a given site were approximately 15 and 20%, respectively.

Table 7.2. Snowpack sample analysis results from remote sites.

Sampling Location	Sampling date	Electrical Conductivity (S)	pH	Sulphate Concentration[1] (mg $S \cdot l^{-1}$)
Birch Mountain	29/11/75	3.8	5.36	0.14
Firebag River	29/11/75	4.0	5.19	0.19
Richardson	1/12/75	3.9	5.21	0.19
Robert River	29/11/75	7.2	5.45	0.33
Stoney Mountain	30/11/75	6.5	6.59	0.23
Stoney Plain (distilled H_2O)	2/12/75	6.0	6.07	b.d[2]
Birch Mountain	12/1/76	3.3	5.01	0.067
Birch Mountain (AAPS Sampler)	12/1/76	-[3]	-	0.12
Ells	14/1/76	5.1	5.15	0.083
Firebag River	14/1/76	6.3	4.89	0.13
Muskeg	12/1/76	3.3	4.95	0.10
Richardson	12/1/76	4.7	4.90	0.12
Robert River	14/1/76	6.2	4.96	0.18
Steepbank	13/1/76	6.8	5.74	0.33
Stoney Mountain	13/1/76	5.2	5.12	0.12
Thickwood	13/1/76	4.7	5.15	0.16

(1) Turbidimetric method used to measure SO_4

(2) b.d. ≡ below detection limit

(3) - ≡ insufficient sample

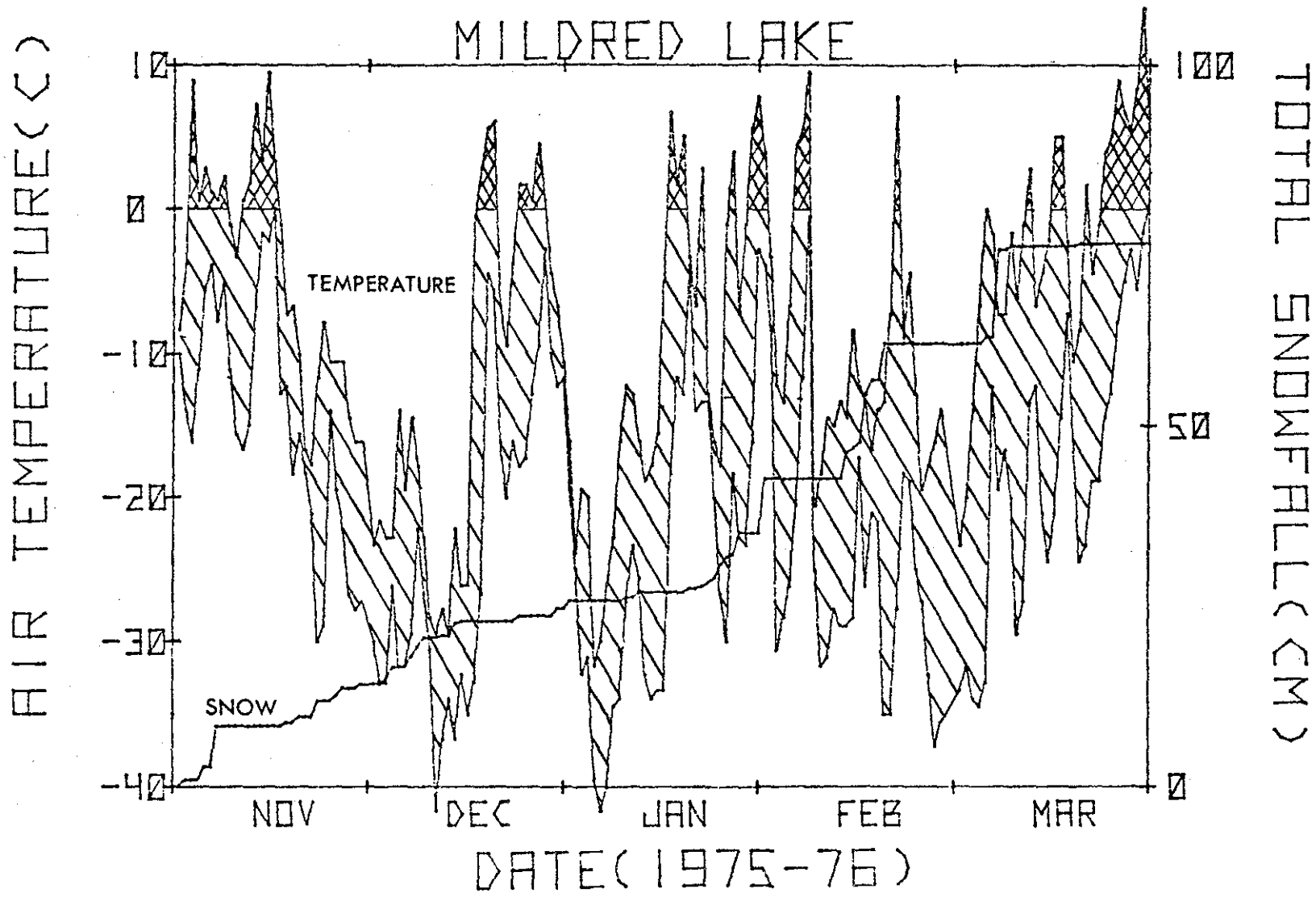

Figure 7.7. Snowfall and temperature (max. and min.) at Mildred Lake for the winter of 1976-77.

Table 7.3. Snowpack sample analysis from AOSERP field study, March 1976.

sample location		sample date	snow depth (cm)[1]	crust depth (cm)[2]	conductivity at 20°C (μS)[3]	pH at 20°C	S concentration (mg S·l^{-1})
NE1	t[4]	5/3	42	11	6.6	4.9	0.26
	b[5]				5.2	5.0	0.25
NE2	t	5/3	52	13	6.4	4.8	0.18
	b				5.1	4.9	0.17
NE3	t	5/3	40	10	7.6	4.8	0.21
	b				5.9	4.8	0.17
NE4	t	5/3	43	13	5.7	4.9	0.15
	b				5.2	4.9	0.12
NE5	t	5/3	42	14	5.2	4.9	0.18
	b				5.5	4.9	0.18
SE1	t	5/3	31	9	9.6	4.8	0.32
	b				5.6	5.1	0.18
SE2	t	5/3	39	11	7.0	4.8	0.21
	b				5.1	5.0	0.16
SE3	t	5/3	52	11	6.3	4.8	0.14
	b				4.5	5.0	0.13
SE4	t	5/3	27	11	6.1	4.8	0.08
	b				6.0	6.3	0.12
SE5	t	5/3	23	7	6.8	-	0.16
	b				4.0	5.4	0.14
S1	t	4/3	45	12	10.8	5.8	0.87
	b				8.9	5.7	0.52
S2	t	4/3	36	11	11.5	5.9	0.70
	b				8.3	5.9	0.50
S3	t	4/3	38	11	36.5	7.2	0.72
	b				8.7	6.3	0.38
S4	t	4/3	39	10	31.0	7.1	0.76
	b				9.8	6.5	0.39
S5	t	4/3	37	9	42.1	7.4	0.89
	b				13.7	6.2	0.30

continued .....

Table 7.3. Continued.

sample location		sample date	snow depth (cm)	crust depth (cm)	conductivity at 20°C (μS)	pH at 20°C	S concentration (mg S·l^{-1})
SW1	t	7/3	40	12	18.7	7.2	0.38
	b				12.2	6.8	0.41
SW2	t	6/3	39	13	4.9	5.4	0.26
	b				4.1	5.3	0.38
SW3	t	6/3	44	12	5.5	5.0	0.23
	b				3.9	5.4	0.22
SW4	t	6/3	38	8	7.0	4.8	0.28
	b				4.7	5.1	0.18
SW5	t	6/3	23	7	6.6	4.7	0.21
	b				5.6	5.1	0.26
NW1	t	4/3			10.0	6.5	0.28
	b				13.6	6.9	0.18
NW2	t						
	b						
NW3	t	6/3	36	11	6.6	5.1	0.19
	b				4.0	5.6	0.14
NW4	t	6/3	28	11	5.9	5.4	0.26
	b				14.9	6.6	1.03
NW5	t	6/3	36	12	6.4	-	0.18
	b				5.7	6.0	0.13
N1	t	4/3	28	11	9.4	4.9	0.27
	b				10.8	6.0	0.77
N2	t	4/3	46	12	6.6	5.1	0.29
	b				5.3	6.0	0.22
N3	t	4/3	47	14	4.5	5.6	0.20
	b				5.3	5.6	0.23
N4	t	4/3	47	12	5.6	5.0	0.23
	b				4.8	5.3	0.24
N5	t	4/3	47	12	5.1	5.1	0.13
	b				6.5	5.5	0.23

continued .....

Table 7.3. Continued.

sample location		sample date	snow depth (cm)	crust depth (cm)	conductivity at 20°C (μS)	pH at 20°C	S concentration
FM1	t	6/3	23	12	5.5	4.9	0.14
	b				5.9	6.3	0.15
FM2	t	6/3	19	12	5.8	4.9	0.11
	b				22.0	7.1	0.11
FM3	t	6/3	22	9	6.3	4.8	0.21
	b				5.1	5.3	0.18
LB	t	6/3	39	12	8.3	4.7	0.26
	b				6.3	4.9	0.21
N2	t	3/3					0.28
	b						0.26
N2	t	5/3	40	14	6.8	5.6	0.33
	b				12.3	6.3	0.29
N2	t	6/3	41	14	5.6	5.4	-
	b				5.3	6.1	0.32
N2	t	7/3	34	13	7.0	5.2	-
	b				5.2	6.1	-
N2	t	8/3	52	28	4.5	5.4	0.25
	b				6.2	6.5	0.32
N2	t	9/3	48	24	5.7	5.2	0.23
	b				5.6	6.2	0.30
N2	t	10/3	46	24	7.6	5.4	0.35
	b				6.1	6.0	0.32
BM	t	7/3	53	12	6.8	4.8	0.17
	b				3.7	5.1	0.12
RN1	t	5/3	20	8	8.2	5.3	0.30
	b				21.5	7.0	0.46
RN2	t	5/3	28	9	8.1	5.1	0.43
	b				14.8	6.4	0.57
RN3	t	5/3	26	6	12.0	5.2	0.50
	b				11.6	5.6	0.59

continued .....

Table 7.3. Continued.

sample location		sample date	snow depth (cm)	crust depth (cm)	conductivity at 20°C (μS)	pH at 20°C	S concentration (mg S·l^{-1})
RN4	t	5/3	24	7	12.4	5.0	0.84
	b				6.6	5.1	0.34
RN5	t	5/3	23	7	9.1	4.8	0.31
	b				10.7	5.2	0.62
RN6	t	5/3	23	6	9.9	4.8	0.47
	b				12.9	5.3	0.68
RS1	t	9/3	32	16	7.0	5.0	0.41
	b				7.1	5.2	0.41
RS2	t	9/3	32	13	8.3	5.0	0.29
	b				8.0	5.3	0.37
RS3	t	9/3	37	16	8.7	5.2	0.51
	b				7.8	5.1	0.44
RS4	t	9/3	32	15	12.1	5.1	0.71
	b				8.5	4.9	0.50
RS5	t	9/3	30	16	10.0	5.0	0.58
	b				8.0	5.0	0.42
E1	t	9/3	43	17	7.0	4.9	0.17
	b				6.3	5.0	0.34
E2	t	9/3	39	15	7.1	4.9	0.27
	b				6.2	5.0	0.17
E3	t	9/3	50	18	6.7	4.9	0.26
	b				5.2	5.2	0.19
G1	t	8/3	50	22	7.4	5.4	0.45
	b				6.2	6.0	0.48
G2	t	8/3	49	20	13.4	6.8	0.63
	b				8.5	6.4	0.57
G3	t	8/3	38	17	23.2	7.0	0.68
	b				26.5	7.5	0.45
G4	t	8/3	38	16	26.9	7.2	0.96
	b				8.6	6.6	0.38

continued .....

Table 7.3. Concluded.

sample location		sample date	snow depth (cm)	crust depth (cm)	conductivity at 20°C (μS)	pH at 20°C	S concentration (mg S·l^{-1})
G5	t	8/3	48	17	42.0	8.5	0.68
	b				14.8	6.9	0.30
G6	t	8/3	41	19	12.0	5.2	0.78
	b				9.7	5.2	0.65
G7	t	8/3	37	17	10.3	6.5	0.32
	b				9.3	6.9	0.32
SW11	t	7/3	29	10	13.4	7.3	0.50
	b				29.5	7.2	0.65

[1]Average of three measurements

[2]Average of three measurements of new fluffy snow

[3]Average value

[4]Top of snow core

[5]Bottom of snow core

7.2.2.1 Geographical distribution of snowpack chemistry. The geological distribution of pH, conductivity, sulphur concentration, and sulphur loading are shown in Figures 7.8-7.11, respectively. A north-south strip running parallel to the Athabasca River receives most of the anthropogenic sulphur deposited in the area (Figure 7.11 a, b, c). Within the 25-km circle (dashed line), the quality of snow at sites outside the main strip of deposition was indistinguishable from that of snow collected at the remote forestry sites (Table 7.2).

Regions of maximum sulphur deposition are located southwest of the GCOS operation and along the river valley between the plant and Fort McMurray. Strong deposition along the river as well as in the areas bordering on the river suggest that air currents that transport pollutants to the snow surface follow the Athabasca River valley. Wind roses calculated from wind measurements made by Syncrude from November 1975 to February 1976 demonstrate clearly that there is a predominant north-south wind in the vicinity of GCOS (Murray and Kurtz 1976).

Areas of high sulphur deposition generally coincide with regions having high snowpack pH and conductivity (cf. Figures 7.8, 7.9, 7.11). If all the sulphur were present as sulphuric acid, and if it were the only substance influencing the snowpack's ion balance, snow having sulphur concentrations of 0.16 and 0.5 mg $S \cdot L^{-1}$ would have pH values of 5 and 4.5 respectively. However, this is not the case. The pH in such snow is well above 5. Thus sulphur is either deposited as a neutral compound or deposited as SO_2 or sulphuric acid, which are then neutralized by alkaline pollutants in the snowpack. The alkaline pollutants may be windblown dust raised by operations at GCOS, products of slash burning, or alkaline metal oxides that are emitted from the powerhouse or incinerator stacks. They are, however, definitely of anthropogenic origin, since the pH of snow in remote areas is 4.9 to 5.5 (Table 7.2).

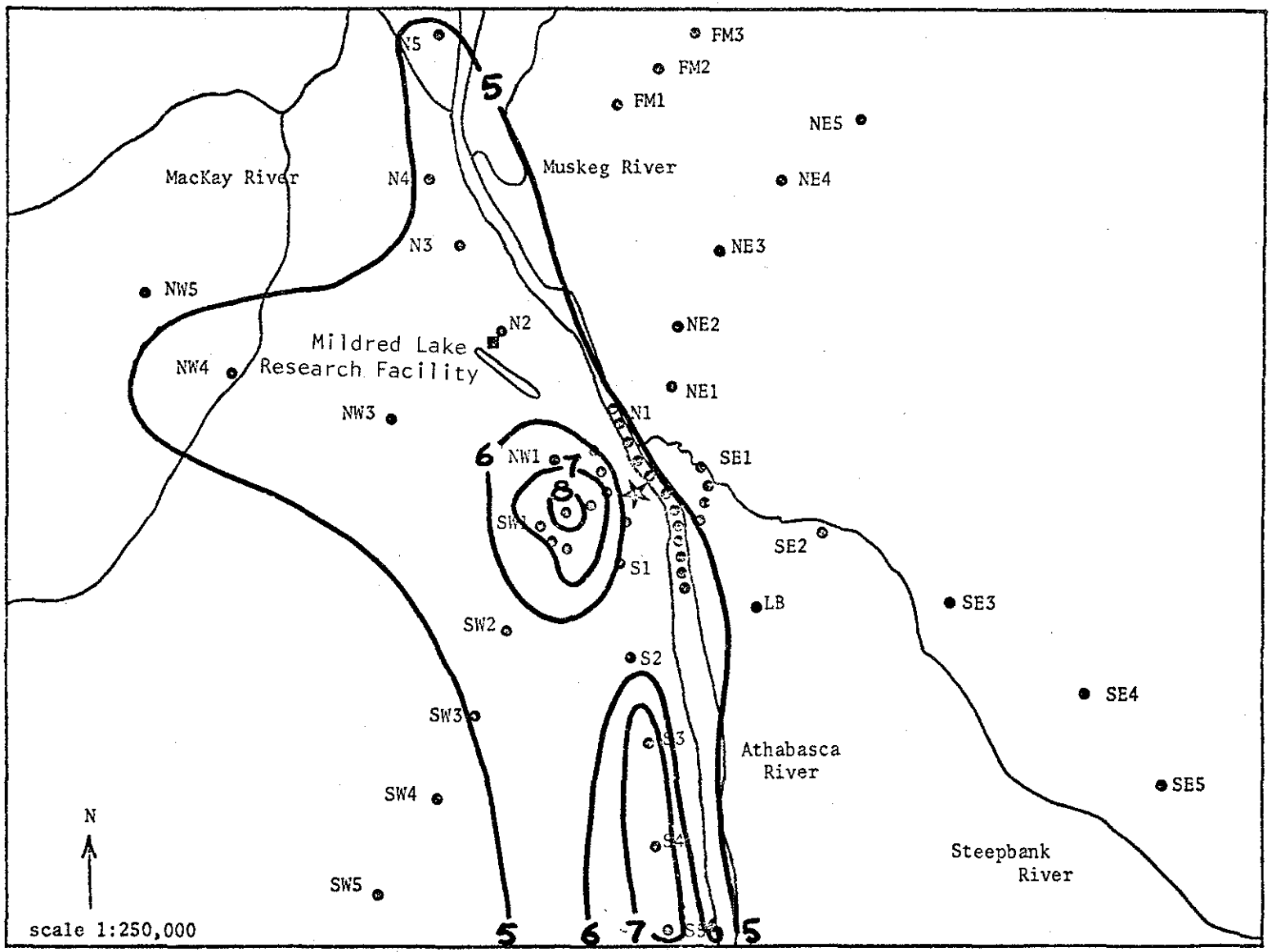

Figure 7.8(a). The geographical distribution of pH for the "top" snow layer.

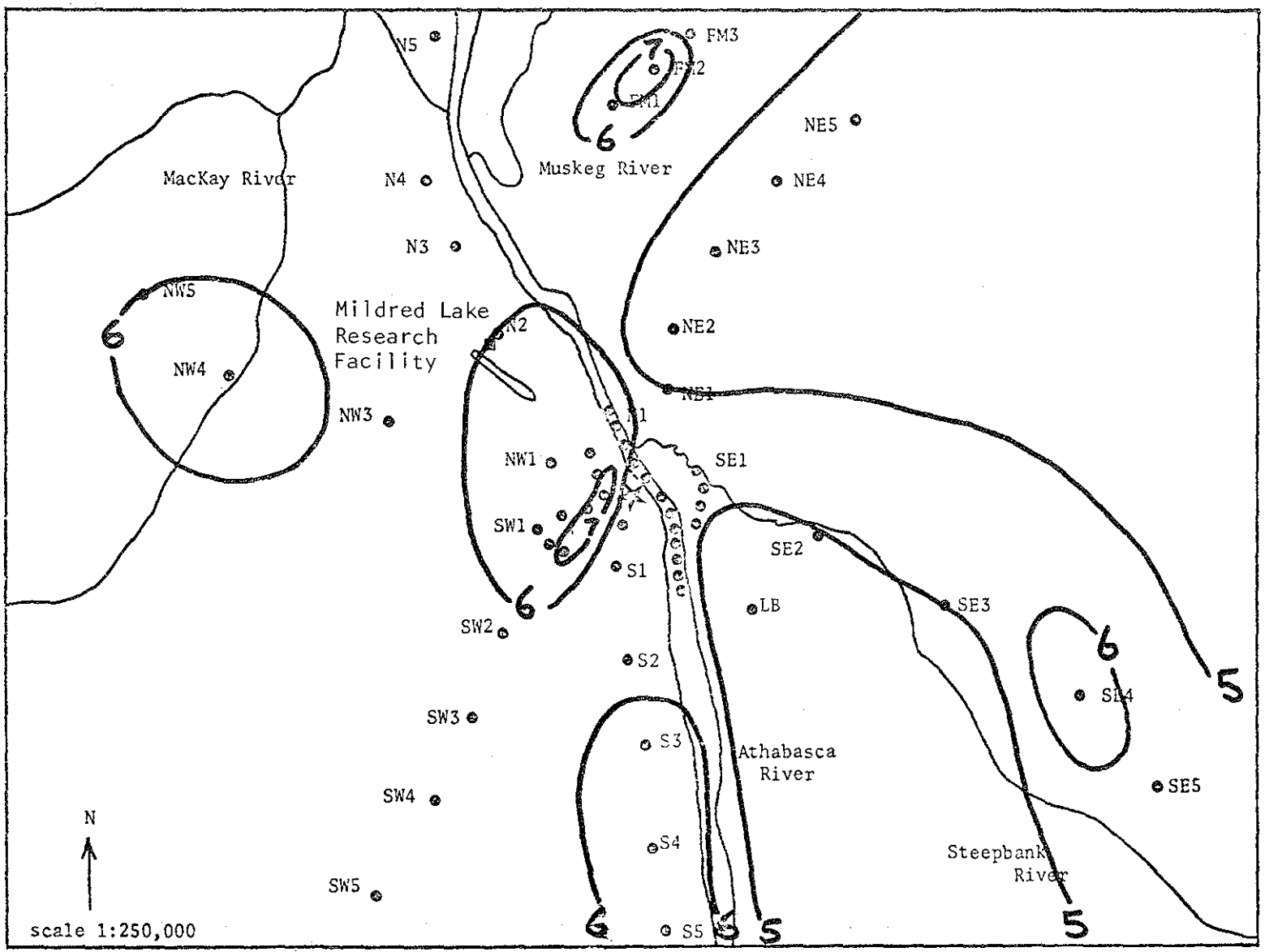

Figure 7.8(b). The geographical distribution of pH for the "bottom" snow layer.

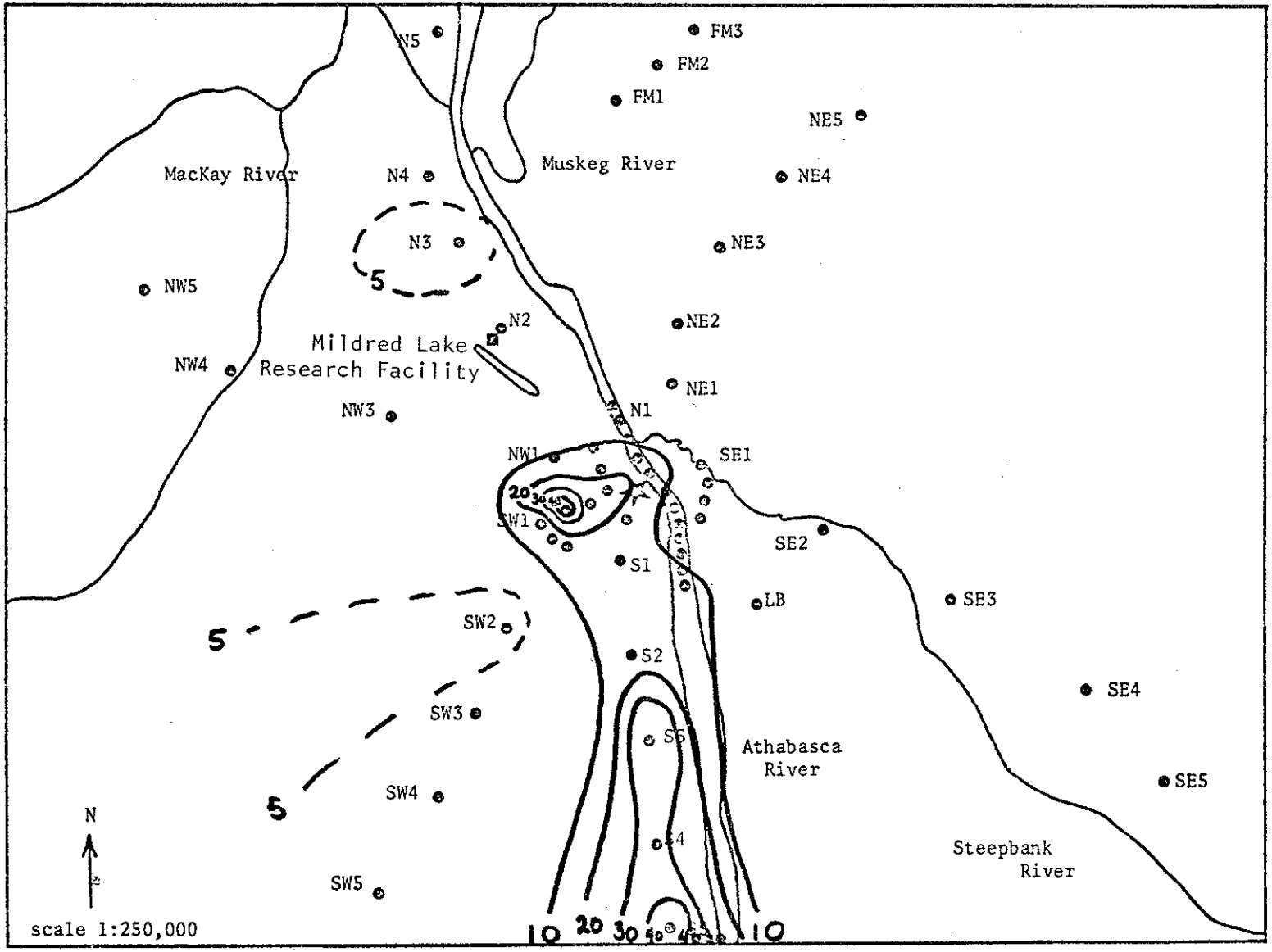

Figure 7.9(a). The geographical distribution of conductivity (μS) for the "top" snow layer.

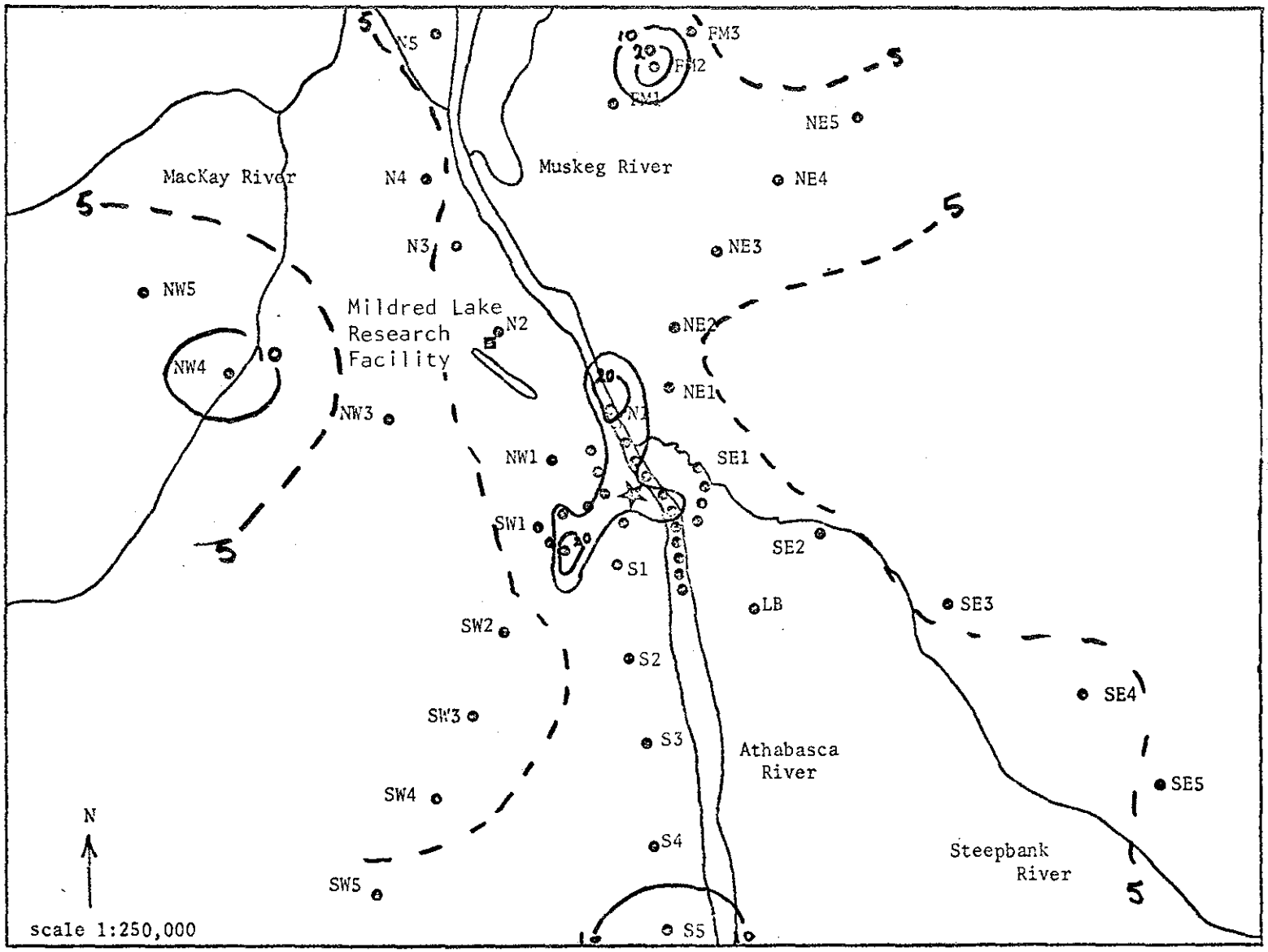

Figure 7.9(b). The geographical distribution of conductivity (μS) for the "bottom" snow layer.

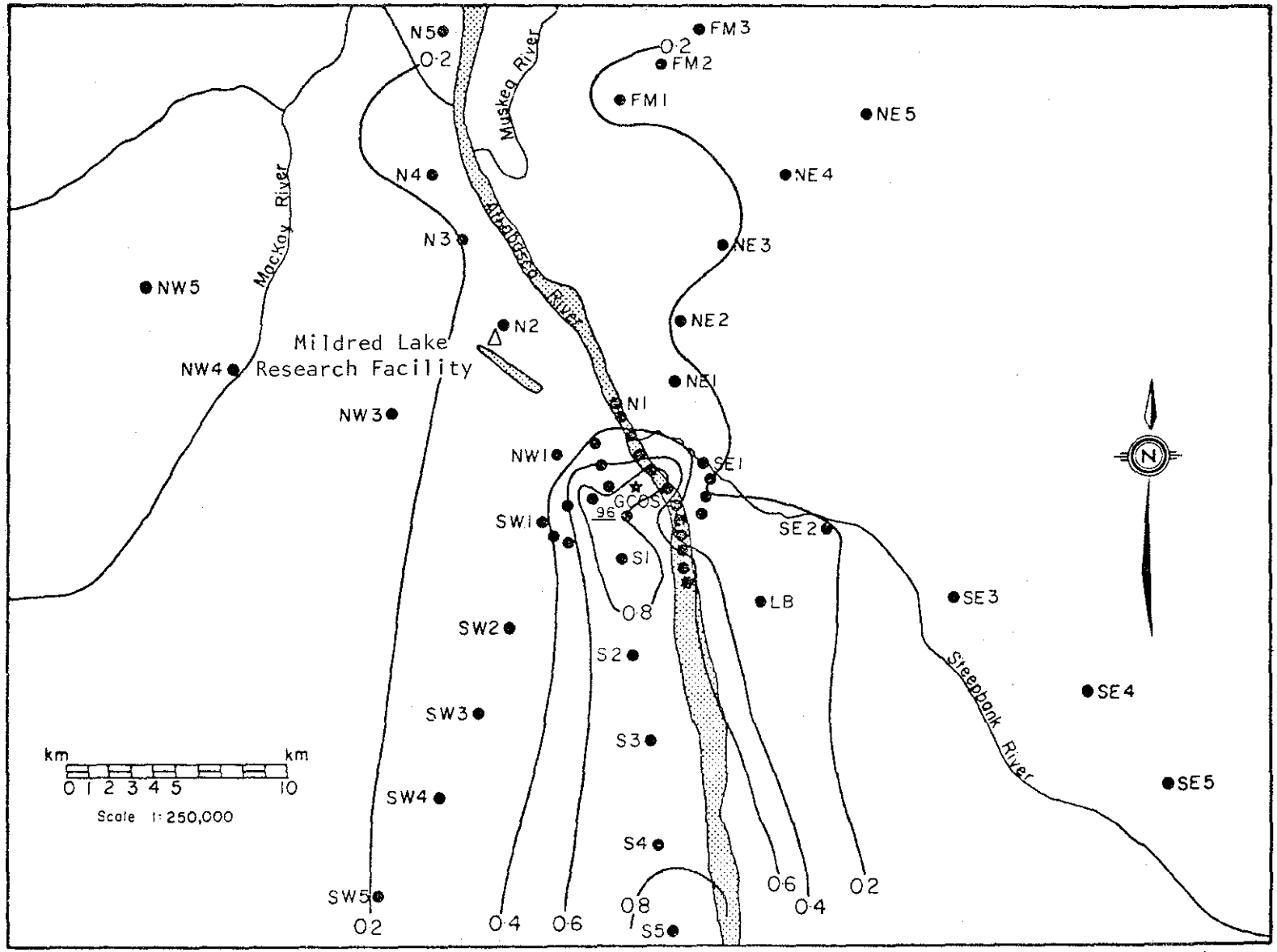

Figure 7.10(a). The geographical distribution of sulphur concentration (mg $S \cdot l^{-1}$) for the "top" snow layer.

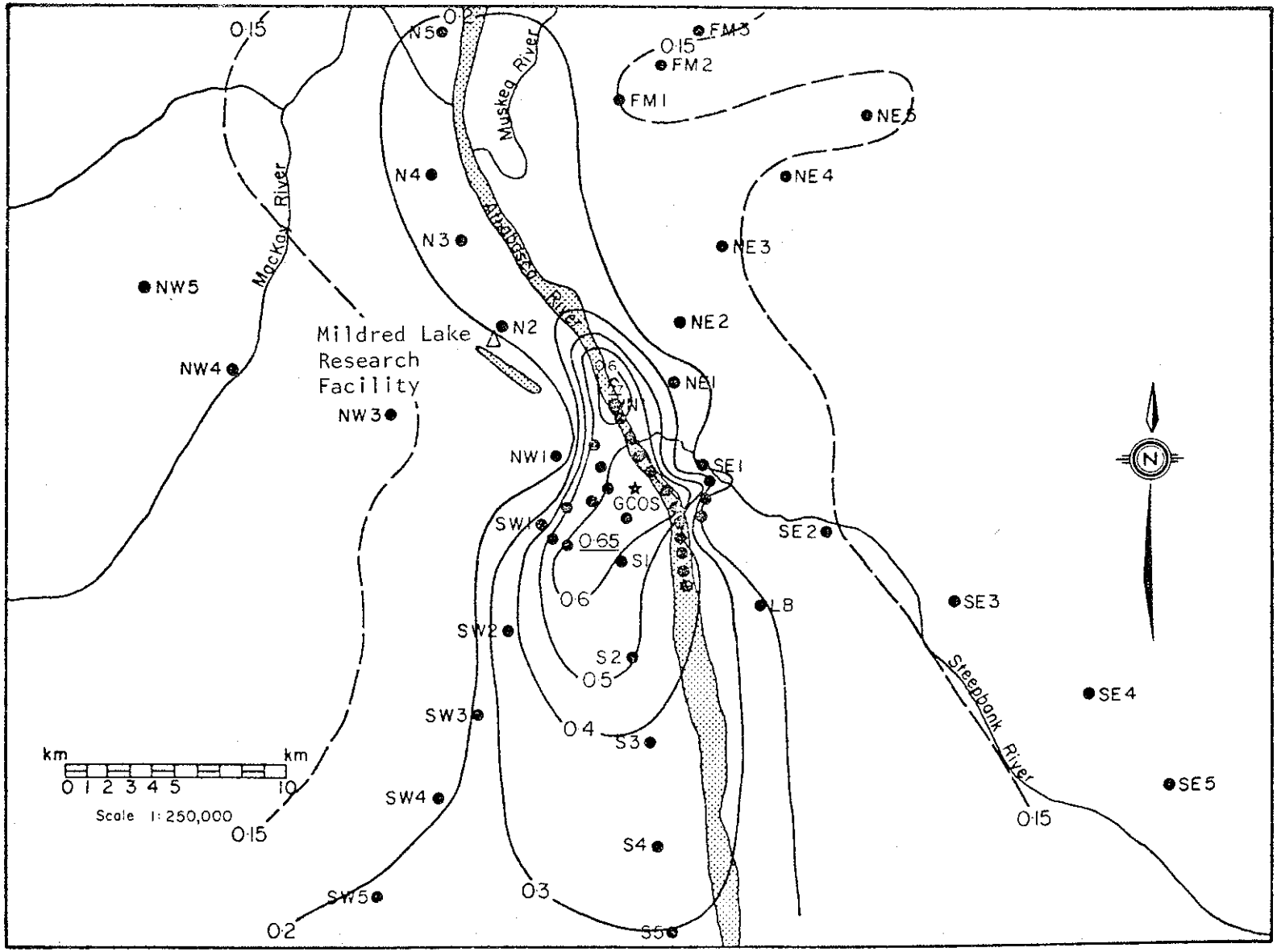

Figure 7.10(b). The geographical distribution of sulphur concentration (Mg $S \cdot l^{-1}$) for the "bottom" snow layer.

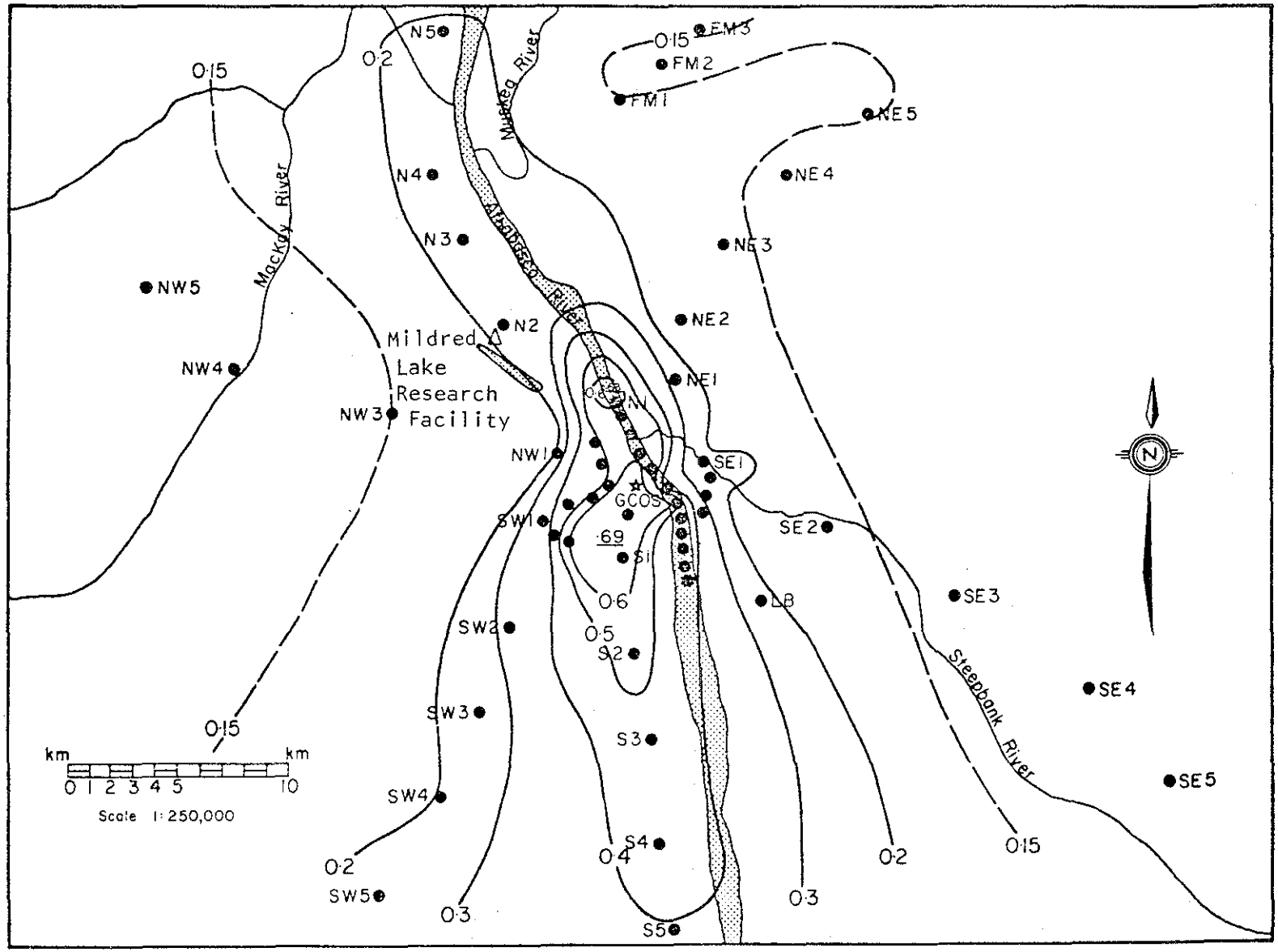

Figure 7.10(c). The geographical distribution of sulphur concentration (mg $S \cdot l^{-1}$) for the total snowpack.

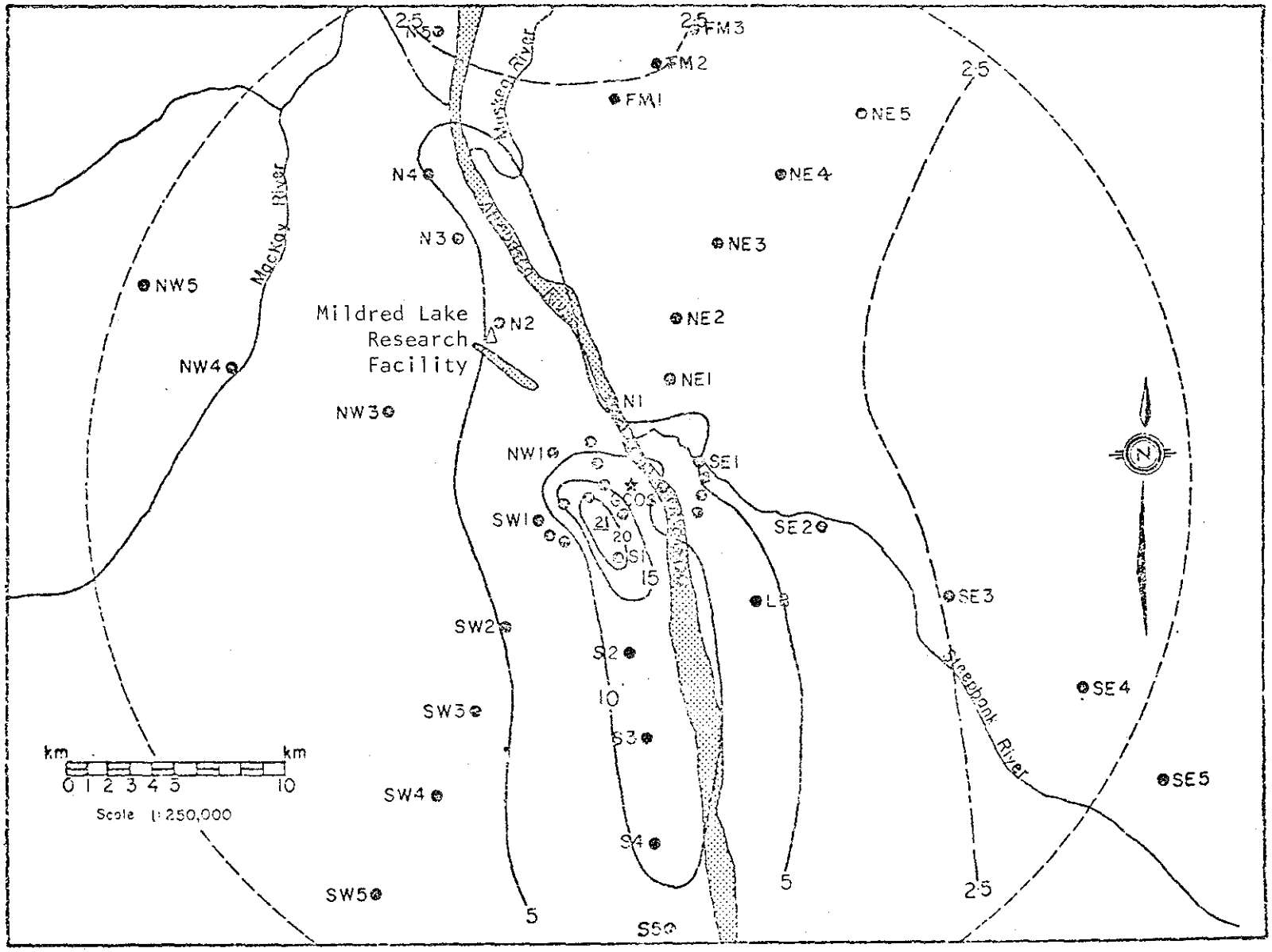

Figure 7.11(a). The geographical distribution of sulphur loading (mg $S \cdot m^{-2}$) for the "top" snow layer. The dashed line marks the 25-km circle.

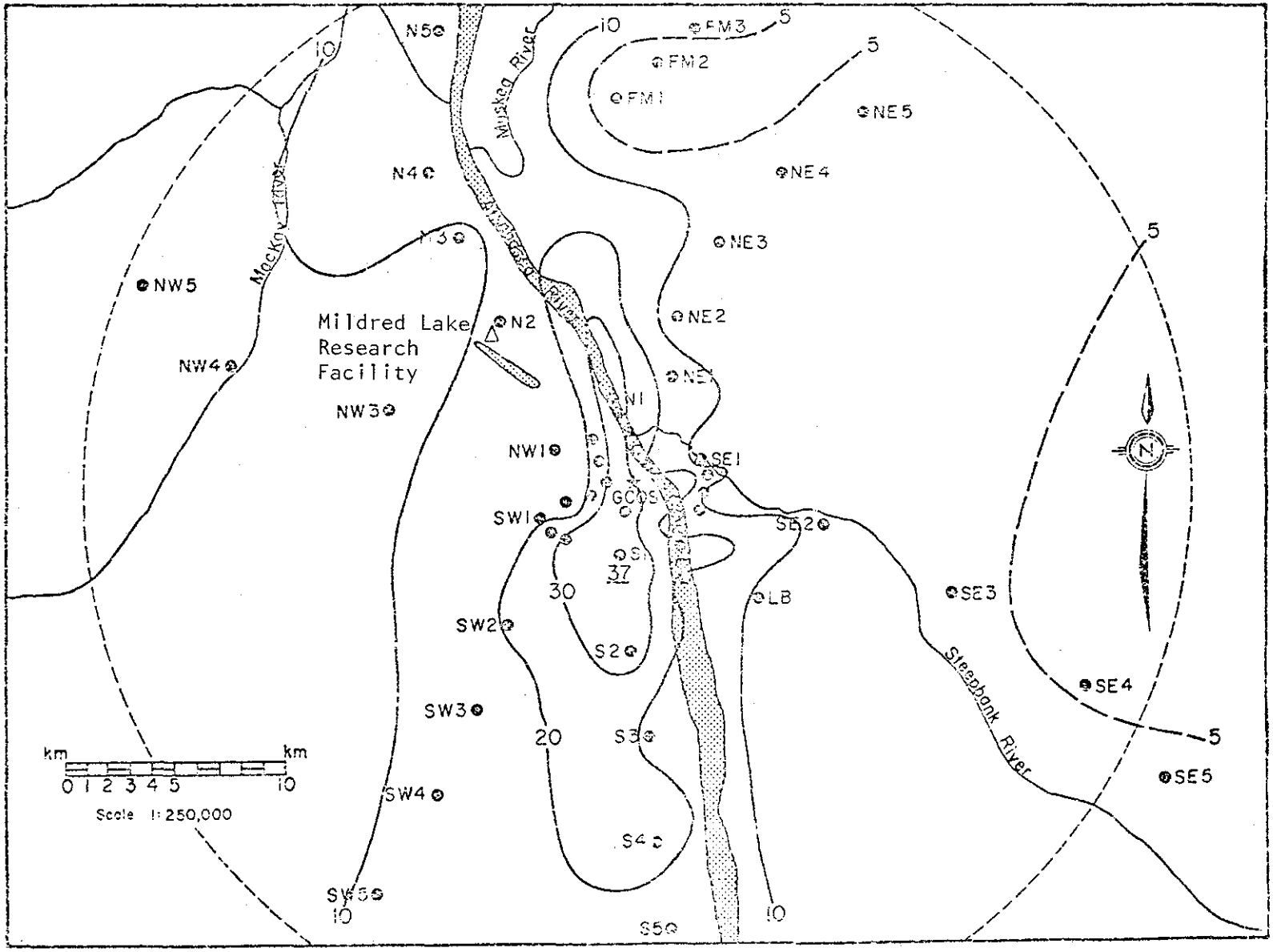

Figure 7.11(b). The geographical distribution of sulphur loading (mg $S \cdot m^{-2}$) for the "bottom" snow layer. The dashed line marks the 25-km circle.

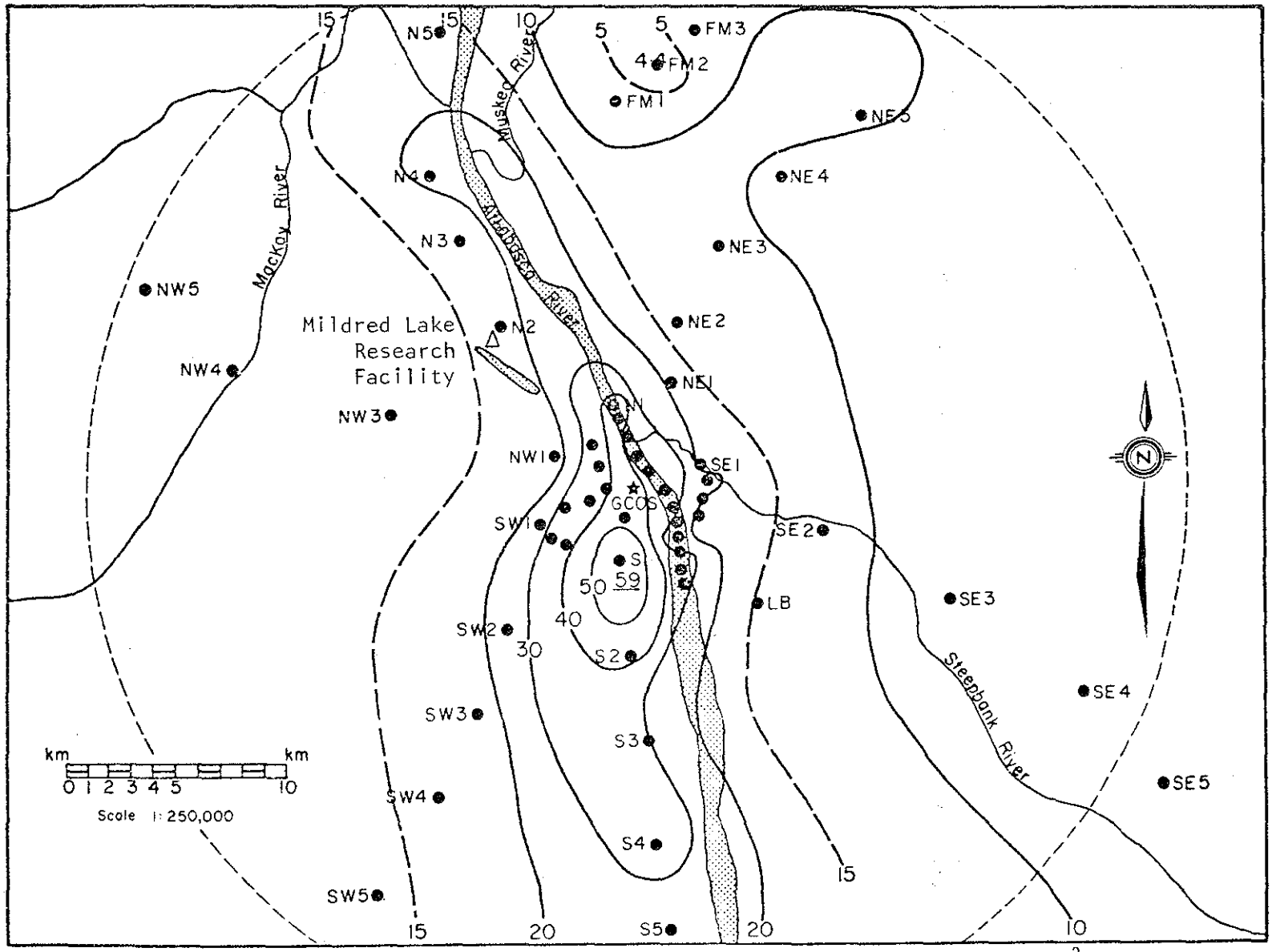

Figure 7.11(c). The geographical distribution of sulphur loading (mg $S \cdot m^{-2}$) for the total snowpack. The dashed line marks the 25-km circle.

7.2.2.2 Sulphur collection efficiency of snowpack. The amount of sulphur in the top and bottom snow layer within 25 km of GCOS was calculated using geographical distributions of sulphur loading (Figure 7.11 a, b, c). These total amounts were corrected for a background sulphur component to yield the amount of anthropogenic sulphur in each layer; 2 and 5 mg $S \cdot m^{-2}$ were assumed as the background loading for top and bottom layers, respectively. In Table 7.4, the amount of anthropogenic sulphur in the snow is compared with the total amount released by GCOS during each layer's lifetime. Of the sulphur emitted by GCOS, 0.14% was trapped in the top snow layer, while the bottom layer contained only 0.062%.

Due to problems of site representativeness, the estimated amount of sulphur in each layer (Table 7.4) has an uncertainty associated with it. The estimates are accurate within a factor of two.

Leaching of the lower snow layer during several periods of thaw (Figure 7.7, cross-hatched areas) probably accounts for the lower sulphur retention of that layer. Indeed, leaching experiments carried out during the field study showed that the first melt water reaching the bottom of a snow core heated from above had sulphur concentrations 5 to 10 times higher than the sulphur concentration of the initial core when melted. Thus, only a small amount of water trickling through the snowpack during a warm period would remove a considerable amount of sulphur. The 0.14% trapping efficiency of the top layer is probably close to the true collection efficiency of the snowpack in the region within 25 km of GCOS since no leaching occurred before the layer was sampled. This result is consistent with the results of Summers and Hitchon (1973), who found that less than 2% of the sulphur released from a sour gas plant in central Alberta was deposited in snow within 40 km of the plant.

Even though the amount of sulphur deposited in snow is small compared to emissions, it may not be small from an environmental point of view. This is especially true in springtime when, as a result of snowpack leaching, pollutants are concentrated in the first runoff water. Sensitive elements in aquatic ecosystems can be adversely affected by unusually high ion concentrations. A case in point is the

Table 7.4. Comparision of the amount of sulphur within 25 km of GCOS in top and bottom snow layers with sulphur released by GCOS during each layer's lifetime.

	Anthropogenic Sulphur Retained by Snow (m Tonnes)	Sulphur Released[1] by GCOS (m Tonnes)	Fraction Retained in Snow
Top Layer (unleached)	3.8	2690	0.14%
Bottom Layer (leached)	10.2	16617	0.062%

[1] Calculated from emission data supplied to Alberta Environment by GCOS

salmon kill in a Norwegian river when the pH dropped drastically at the beginning of spring thaw (Leivestad and Muniz 1976) due to snowpack leaching.

The results of this field study show that acid runoff is not likely to occur since the polluted snowpack is alkaline. However, other pollutants such as heavy metals may cause problems. More leaching experiments are planned for the next field trip. In addition, a complete chemical analysis of collected samples will be carried out in order to determine the spatial distribution patterns of major ions and trace metals.

7.2.3 Conclusions

1. The pattern of sulphur deposition suggests that the river valley, particularly to the south of GCOS, is the area most heavily affected by the atmospheric loading of pollutants.
2. Within 25 km of the source, an unleached snow layer on the top contained approximately 0.14% of the sulphur emitted by GCOS during the layer's lifetime. The underlying snow that had been exposed to emissions for the whole winter contained only 0.06% of the sulphur emitted during its lifetime. It is likely that sulphur had been removed from the layer by leaching associated with thaws occurring several times during the winter and that the real fraction of sulphur deposited in the area was greater than 0.06%.
3. Areas of greatest sulphur deposition do not have acidic snow, as might be expected because sulphur dioxide and its oxidation product, sulphuric acid, are acidic. Thus, we conclude that acid-neutralizing agents are present in the snowpack. Although these substances are of anthropogenic origin, their composition was not determined in this study.

4. As a result of experience gained during this field study, there is reason to expect that this technique may be improved to the stage where it could make continuous precipitation sampling during winter months unnecessary. Snowpack samples may provide an adequate integrated record.

The present field study results have laid the groundwork for a follow-up field study in the winter of 1976-1977. The next program will include a more extensive chemical survey of the snowpack as well as more experimental investigations of leaching. It is felt that the leaching process may be very important from an aquatic environmental point of view.

7.3 REFERENCES CITED

Bowen, H.J. 1966. Trace elements in biochemistry. Academic Press.

Klockow, D., H. Denzinger, and G. Rönicke. 1974. Chemie Ingenieur Technik, 46: 831.

Leivestad, H., and I.P. Muniz. 1976. Fish kill at low pH in a Norwegian river. Nature 359:391.

Murray, W., and J. Kurtz. 1976. A predictive study of the dispersion of emissions from the Syncrude Mildred Lake Plant. Prep. for Syncrude Canada Ltd. by the MEP Company. Environmental Research Monograph 1976-1. 128 pp.

Peirson, D.H., P.A. Cawse and R.S. Cambray. 1974. Chemical uniformity of airborne particulate material, and a maritime effect. Nature 251: 675-679.

Summers, P.W. and B. Hitchson. 1973. Source and budget of sulphate in precipitation from central Alberta, Canada. J. Air Poll. Cont. Assoc. 23: 194-199.

7.4 ACKNOWLEDGEMENTS

The authors would like to thank Mr. J. Godin for his valuable technical assistance during the field study, as well as Messrs. R. Angle and M. Strosher, Alberta Environment for providing GCOS emission data.

8. APPENDICES

8.1 WEATHER AND ACTIVITIES SUMMARY

Explanation

WEATHER

Clouds and Weather

Clear	○
Scattered Cloud	◐
Broken cloud	◍
Overcast	⊕
Snow or snow flurries	S

Surface wind - mean speed and direction in the first 30 seconds (approximately 60 m) of the minisonde flights from the Lower Syncrude site.

Upper wind - mean speed and direction at a height above the inversion, if present (otherwise approximately 500 m above ground) from the Lower Syncrude minisonde flights.

Surface temperature - from the Lower Syncrude minisonde.

Surface stability - from the vertical gradient of potential temperature in the surface layer (the mixed layer below the inversion, if present; otherwise the surface-based inversion layer) from the Lower Syncrude minisonde flights.

S	Stable ($\frac{\partial\Theta}{\partial z} > +2$ K/km)
N	Neutral ($-1 \leq \frac{\partial\Theta}{\partial z} \leq +2$ K/km)
U	Unstable ($\frac{\partial\Theta}{\partial z} < -1$ K/km)
o	Surface-based inversion
i	Capping inversion
T	Trapping
F	Fanning

C Coning
L Lofting
S Looping
U Fumigating

ACTIVITIES

The hours of data gathering operation are indicated for each experiment (minisondes by a dot; other experiments by a bar graph).

Minisondes: Four locations. The Lower Syncrude and GCOS sites are shown on the topographic map which appears elsewhere in this report. The Beaver Creek site was near the intersection of Highway 63 and Beaver Creek (approximately 4.5 km to the northwest of the AOSERP Camp. The Fort MacKay site was on the Athabasca River ice at Fort MacKay.

Tethersonde and Delta-T sonde:

Located at the Lower Syncrude site.

P Profile mode
FL Fixed level

Acoustic sounder:

Located at the Lower Syncrude site.

OSPEC: Traverses under the GCOS plumes at several locations.

Sign-X: Sulphur dioxide ground-level concentration measurements in the vicinity of GCOS.

AOSERP Field Study - March 1976
Weather and Activity Summary

Date: 4 March

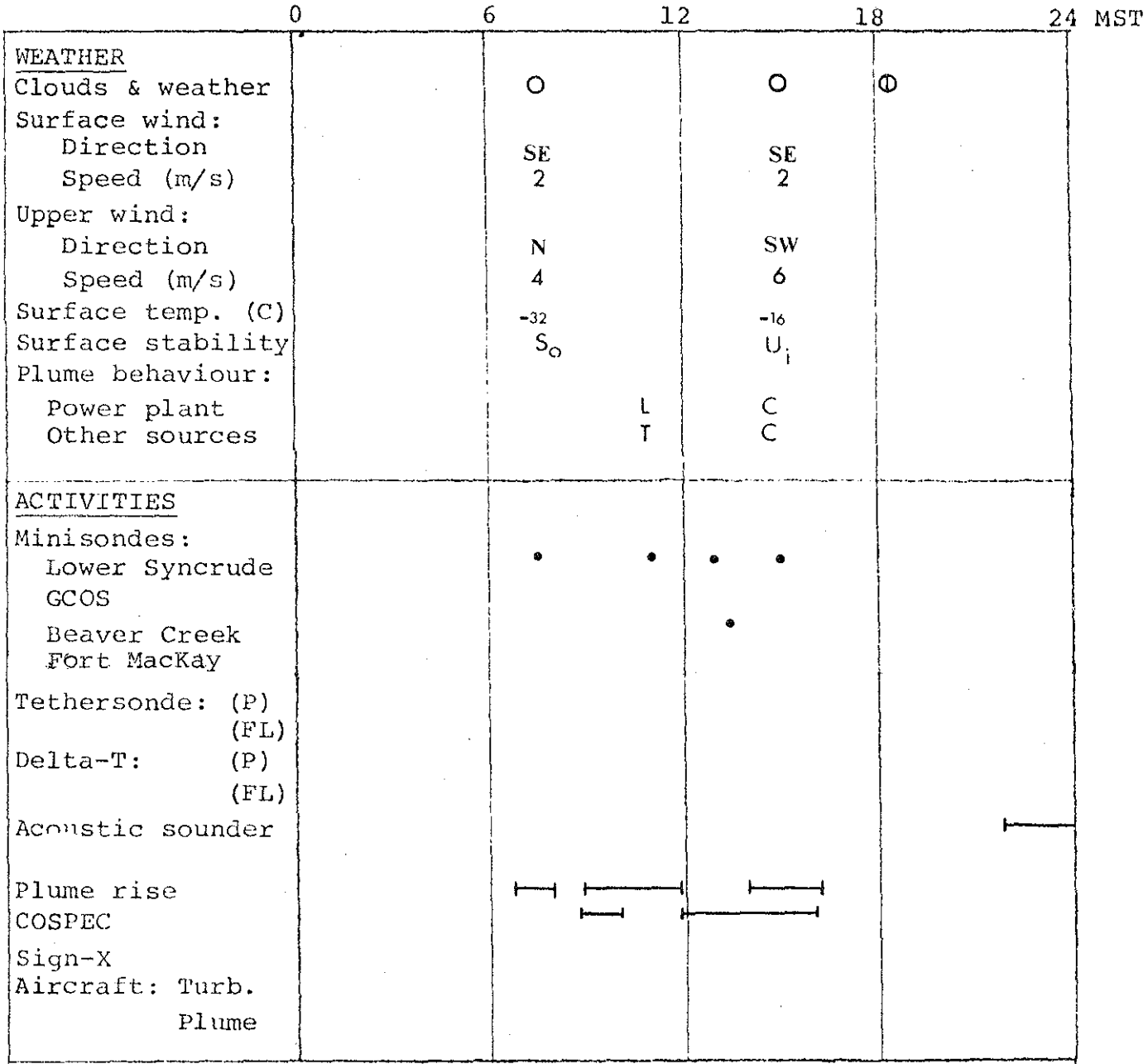

REMARKS * 0700 Plume blowing towards ENE. Ice crystals observed.
1400 Plume spreading over the valley.

* The Remarks section on this and following pages are primarily visual observations of Mr. A.J. Gallant who also contributed the "Clouds and weather" observations.
The visual observations of plume behaviour recorded in the "Weather" section were made by Dr. F.H. Fanaki.
Mr. G.G. Vickers did the computations of surface stability.

AOSERP Field Study - March 1976
Weather and Activity Summary

Date: 5 March

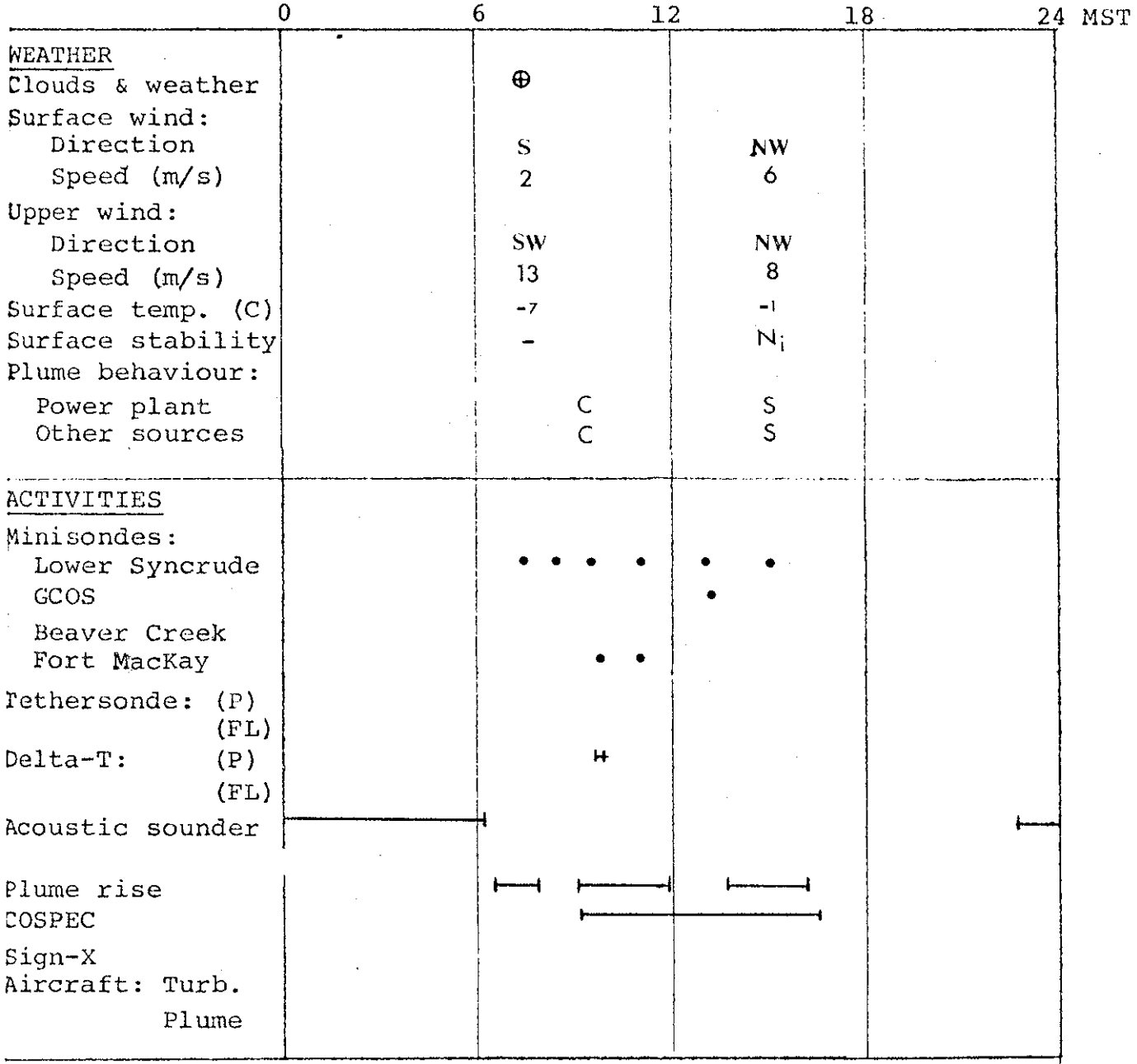

REMARKS 0630-0700 Snow grains.

AOSERP Field Study - March 1976
Weather and Activity Summary

Date: 6 March

	0	6	12	18	24 MST
WEATHER					
Clouds & weather					
Surface wind:					
Direction		N		W	
Speed (m/s)		2		5	
Upper wind:					
Direction		N		NW	
Speed (m/s)		10		6	
Surface temp. (C)		-12		-3	
Surface stability		S_o		U	
Plume behaviour:					
Power plant		C T		C	
Other sources		C T		C	
ACTIVITIES					
Minisondes:					
Lower Syncrude		• • • •		• •	
GCOS		• •		•	
Beaver Creek					
Fort MacKay					
Tethersonde: (P)		⊢⊣ ⊢⊣		⊢⊣ ⊢⊣	
(FL)					
Delta-T: (P)		⊣		⊢⊣	
(FL)					
Acoustic sounder	———	⊢———	———	———	⊢
Plume rise		⊢⊣ ⊢——⊣		⊢⊣	
COSPEC		⊢——⊣			
Sign-X				⊢⊣	
Aircraft: Turb.					
Plume					

REMARKS 0600 Snow overnight.

AOSERP Field Study - March 1976
Weather and Activity Summary

Date: 7 March

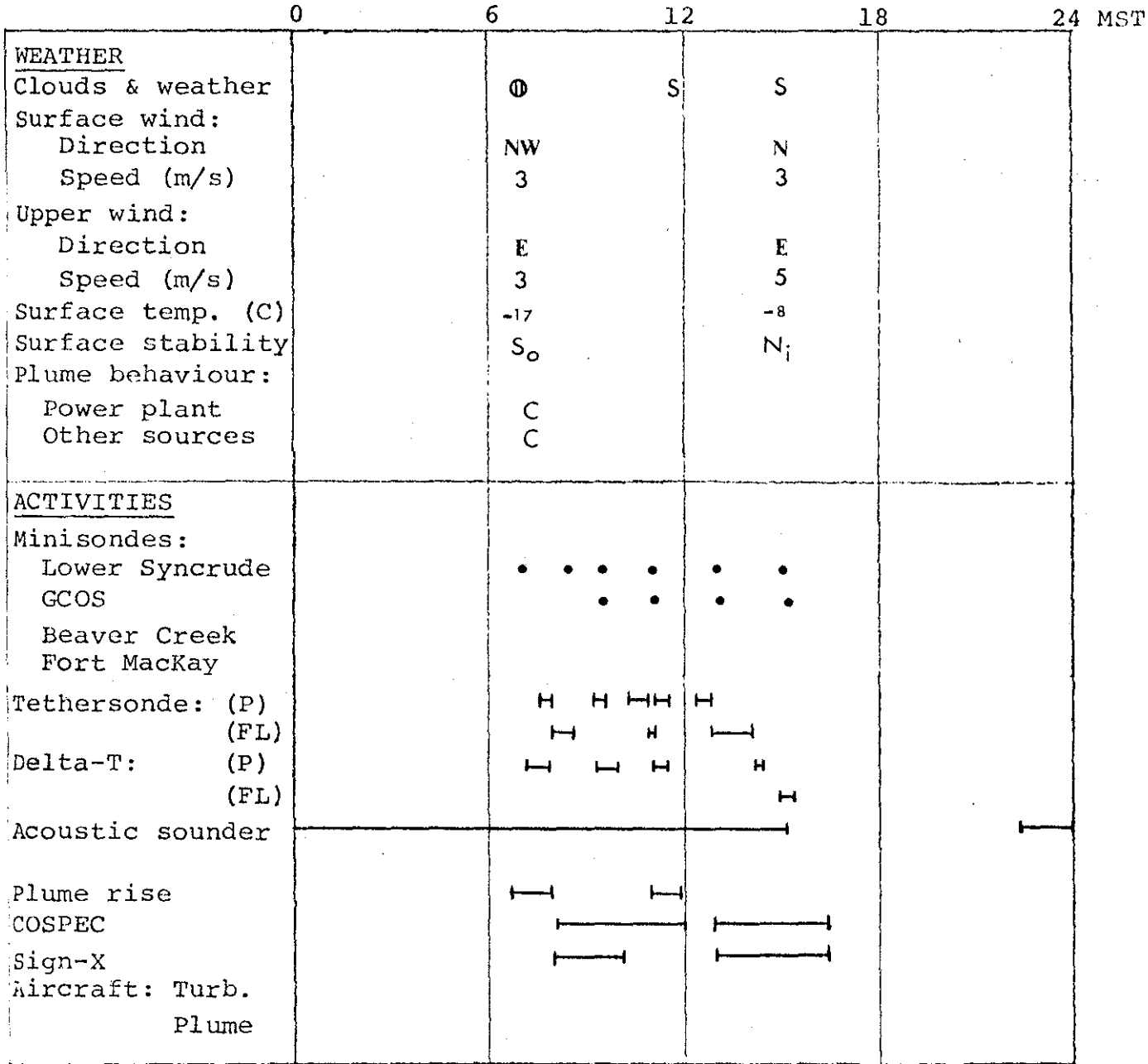

REMARKS
0600 Ice crystals. Easterly wind at plume level.
0710 Snow started.
1500 Snow decreasing.

AOSERP Field Study - March 1976
Weather and Activity Summary

Date: 8 March

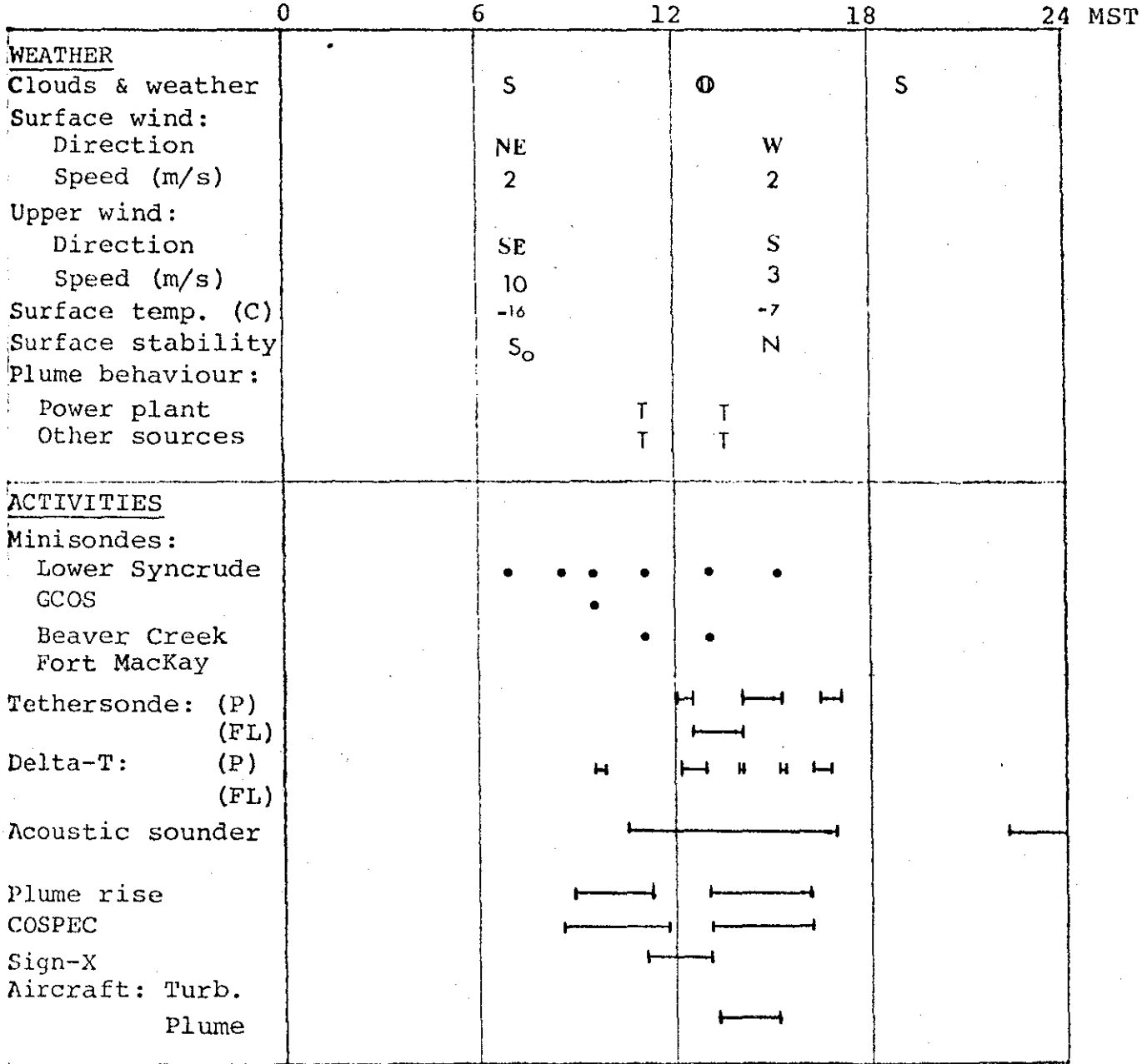

REMARKS 0645 Snow still falling. Accumulation so far, 12 cm.
0730 Snow stopped. Ice crystals. Plume moving over the Lower Syncrude site and towards the north.
1300 Ice crystals. Plume meandering over the Lower Syncrude site and towards the north.
1530 Snow started. Stopped by 1900.
2000 Fog forming.
1400-1430 SO_2 concentration readings at Alberta Environment Air Pollution trailer at Fort McKay.

AOSERP Field Study - March 1976
Weather and Activity Summary

Date: 9 March

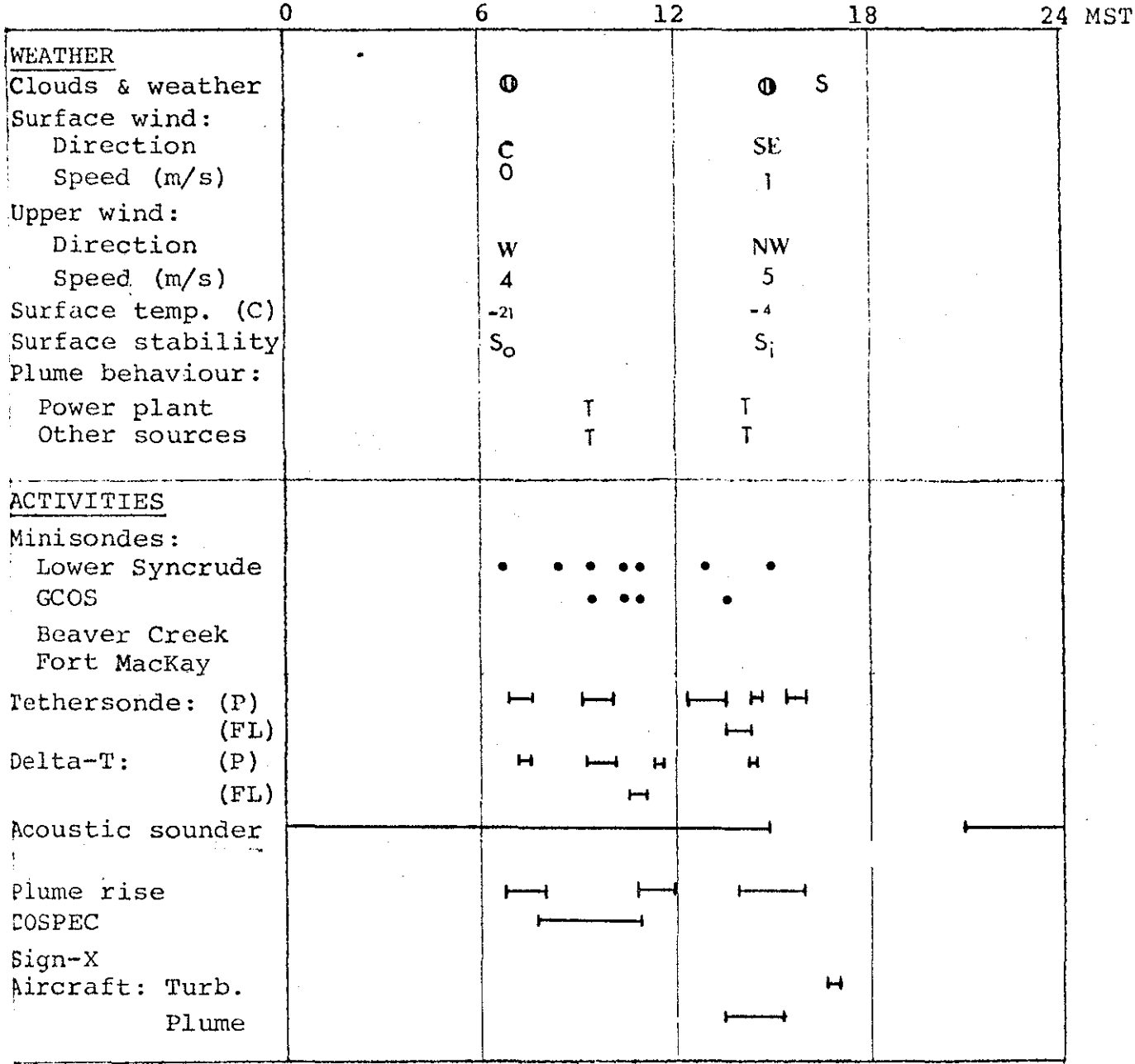

REMARKS 0700 Snow and fog overnight.
1500 Wind WSW at plume level. Plume impinging on east bank of the Athabasca River.
1640 Snow started.

AOSERP Field Study - March 1976
Weather and Activity Summary

Date: 10 March

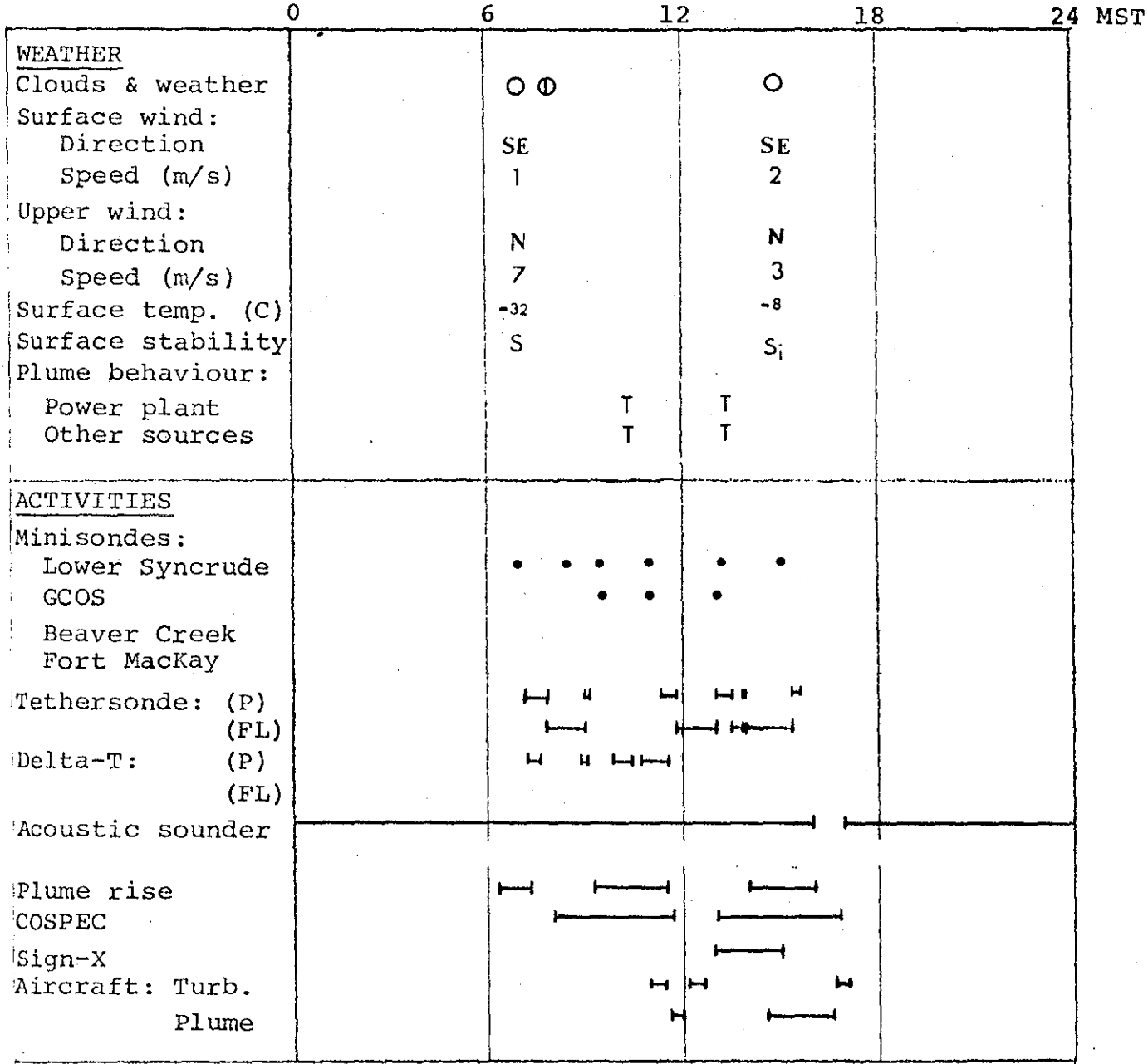

REMARKS 0700 Snow stopped overnight. Accumulation 1 cm.
0800 Fog in patches over Athabasca River and moving along top of hill to the west of the Lower Syncrude site. Plume moving towards the north; wind westerly aloft.
1500 Plume moving toward the SSW.

AOSERP Field Study - March 1976
Weather and Activity Summary

Date: 11 March

	0	6	12	18	24 MST
WEATHER					
Clouds & weather		○	◑	◑	
Surface wind:					
Direction		SE	E	SW	
Speed (m/s)		2	1	6	
Upper wind:					
Direction		NW	W	W	
Speed (m/s)		10	3	11	
Surface temp. (C)		-20	-6	-4	
Surface stability		S_o	S	S_o	
Plume behaviour:					
Power plant		T	T		
Other sources		T	T		
ACTIVITIES					
Minisondes:					
Lower Syncrude		• • • •	•		
GCOS		• • •	•		
Beaver Creek		•			
Fort MacKay					
Tethersonde: (P)		⊢ ⊢⊢ ⊢	⊢ ⊢		
(FL)		⊢⊢⊢	⊢		
Delta-T: (P)		⊢ ⊢⊢ ⊢			
(FL)		⊢⊢⊢			
Acoustic sounder	⊢———	⊢———	⊢———	⊢———	
Plume rise		⊢—— ⊢——	⊢——		
COSPEC					
Sign-X					
Aircraft: Turb.		⊢—	⊢— ⊢—		
Plume		⊢—	⊢—		

REMARKS 0600 Plume moving towards the east. Cloud cover moving off towards the south.
1300 Plume moving towards the east.
2000 Plume moving towards the east.

AOSERP Field Study - March 1976
Weather and Activity Summary

Date: 12 March

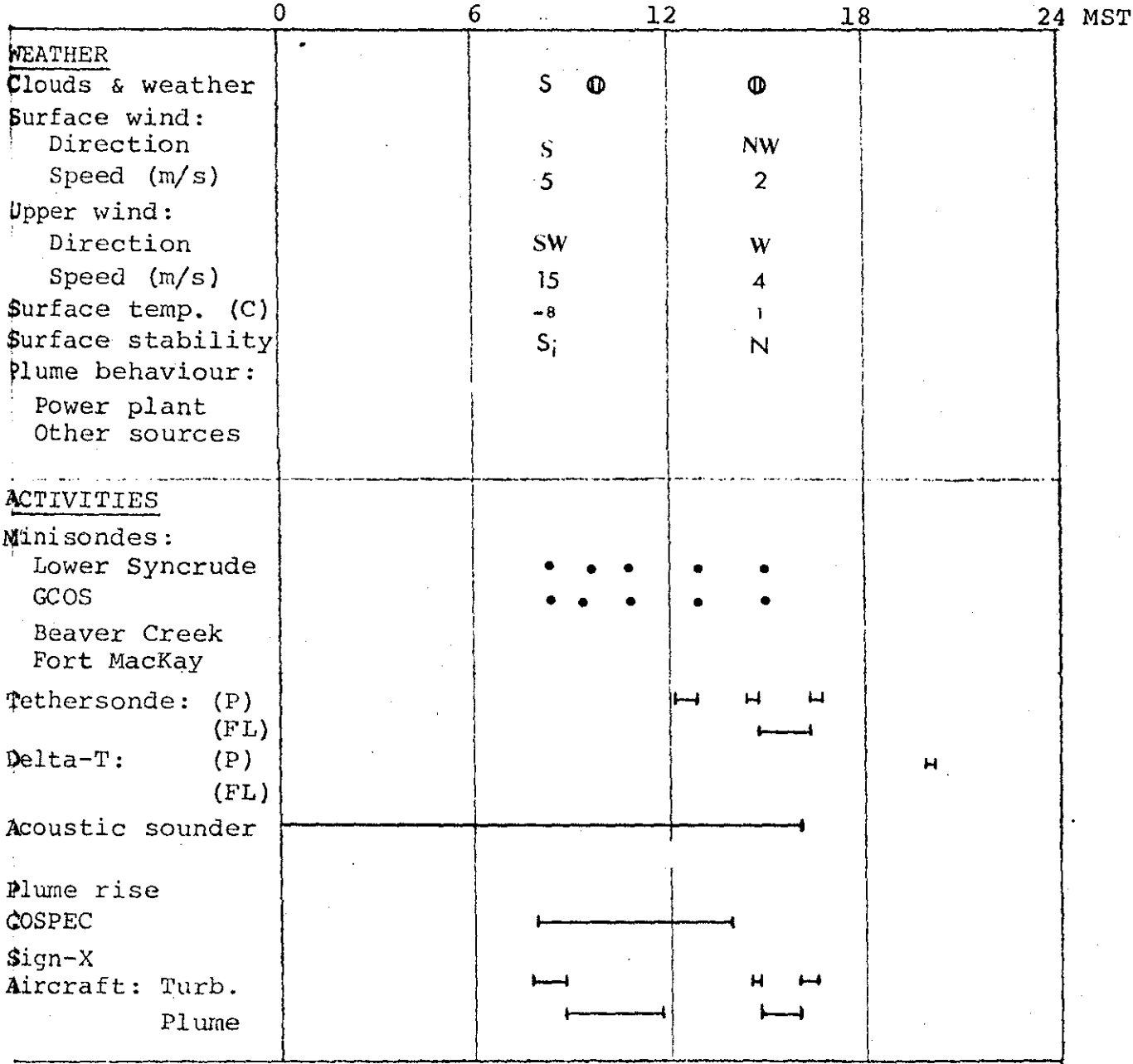

REMARKS
0800 Snow started overnight.
0950 Snow stopped. Plume moving towards the NE.
1500 Plume moving towards the NE.

Micrometeorological tower - wind only.

AOSERP Field Study - March 1976
Weather and Activity Summary

Date: 13 March

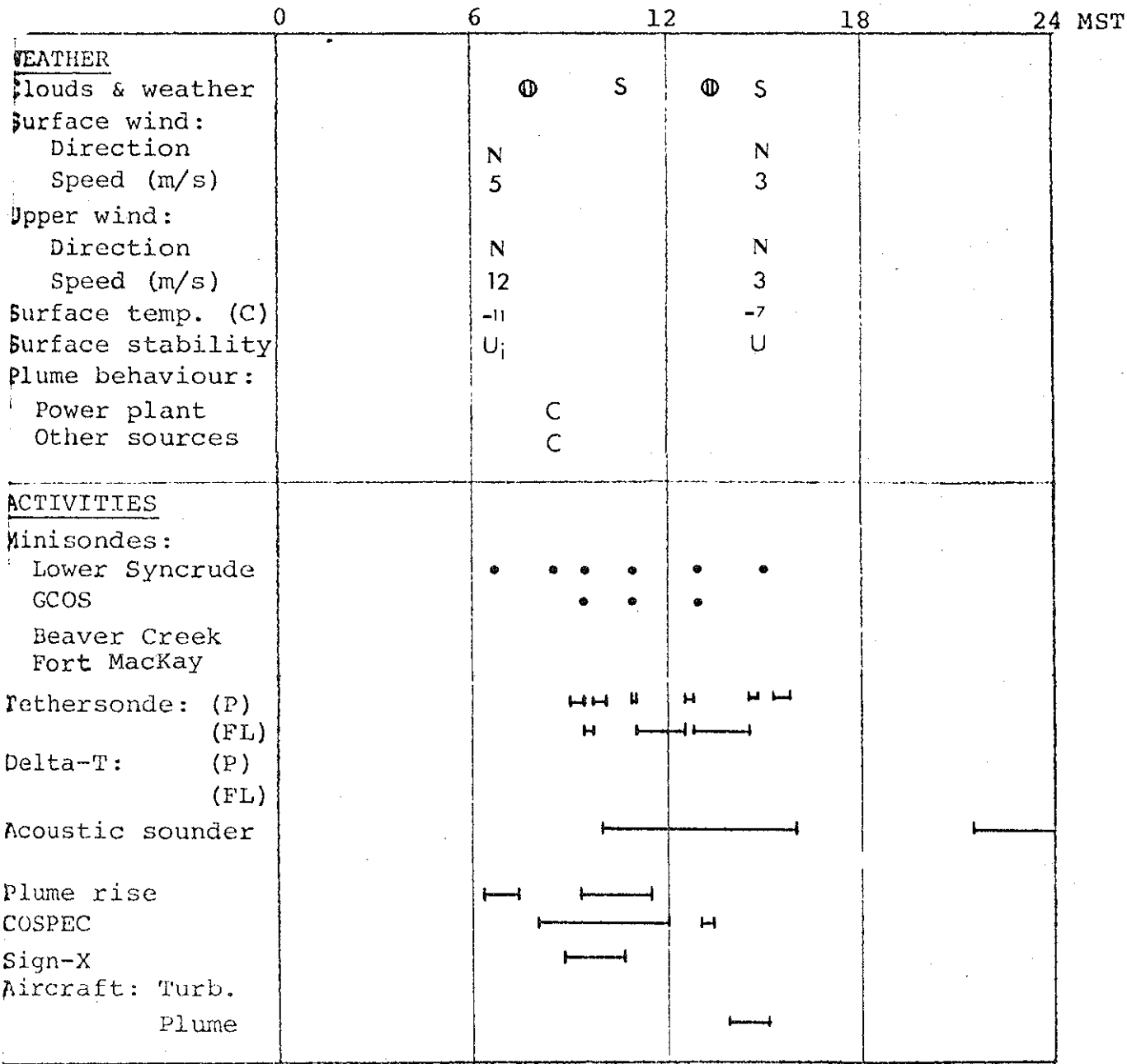

REMARKS
0730 Ice crystals begin.
0800 Ice crystals. Plume moving towards the SSW.
1045 Snow started. Plume moving towards the SSW over Highway 63.
1330 Snow stopped.
1500 Snow flurries. Towering cumulus. Plumes invisible.
1930 Snow flurries ended.

AOSERP Field Study - March 1976

Weather and Activity Summary

Date: 14 March

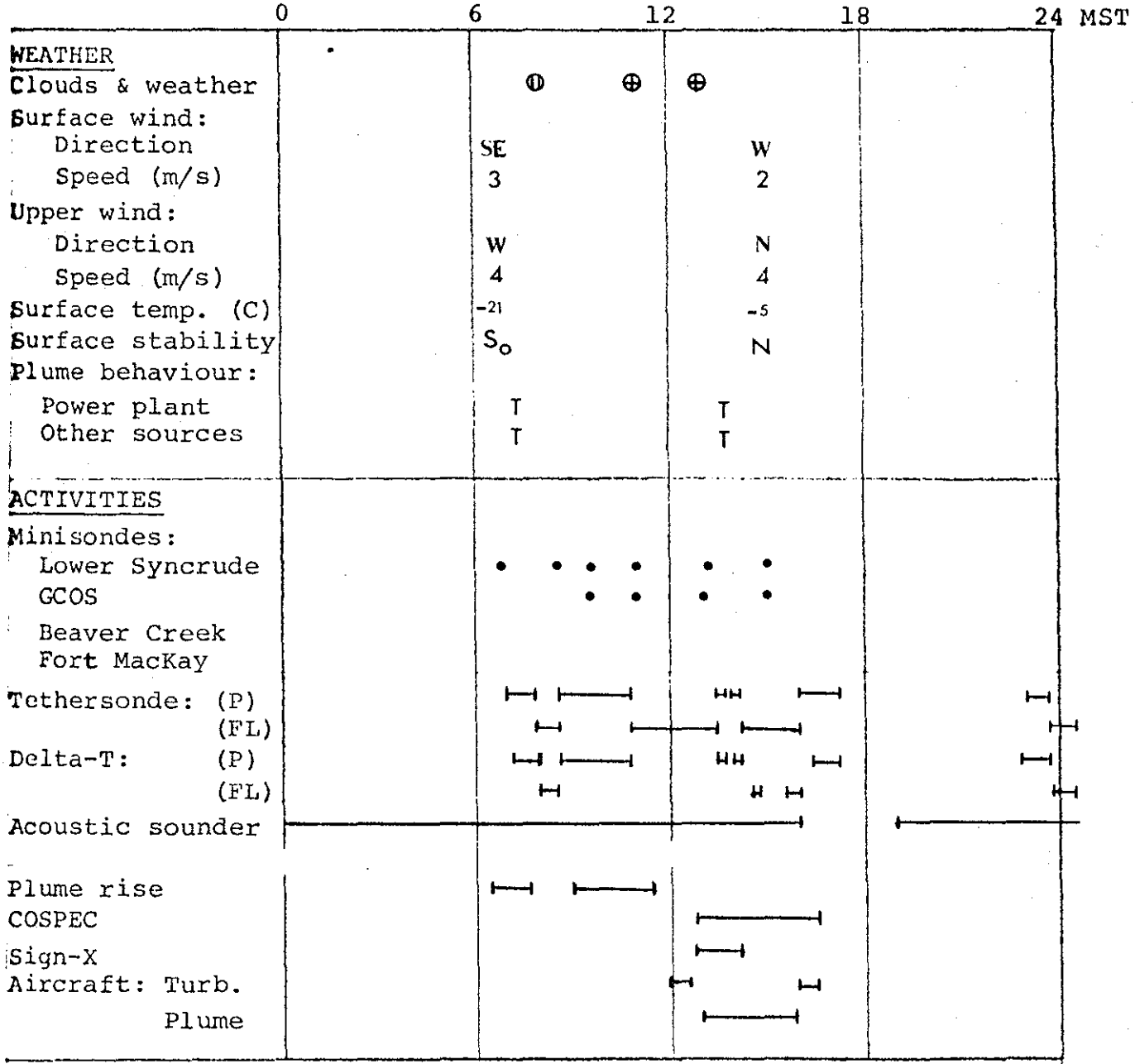

REMARKS 0800 Fog in patches on the river near GCOS. Plume moving towards the east.

1100 Plume moving towards the SW.

1300 Plume rising straight up, then moving towards SW.

AOSERP Field Study - March 1976
Weather and Activity Summary

Date: 15 March

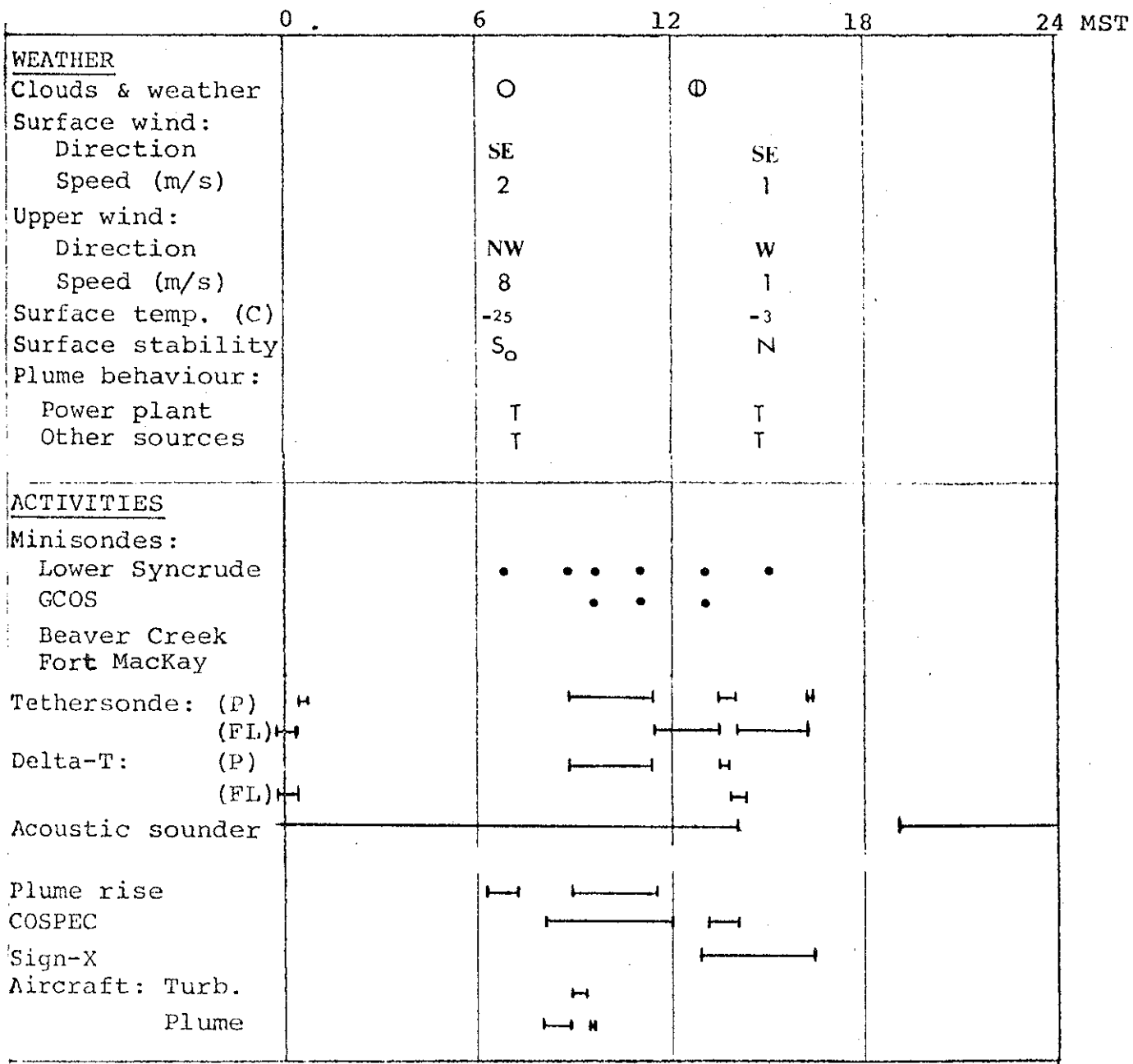

REMARKS 0700 Fog over the river near GCOS. Plume moving towards the SE, then curving eastward.

1300 Plume moving towards the south in late morning, towards SE in early afternoon.

AOSERP Field Study - March 1976
Weather and Activity Summary

Date: 16 March

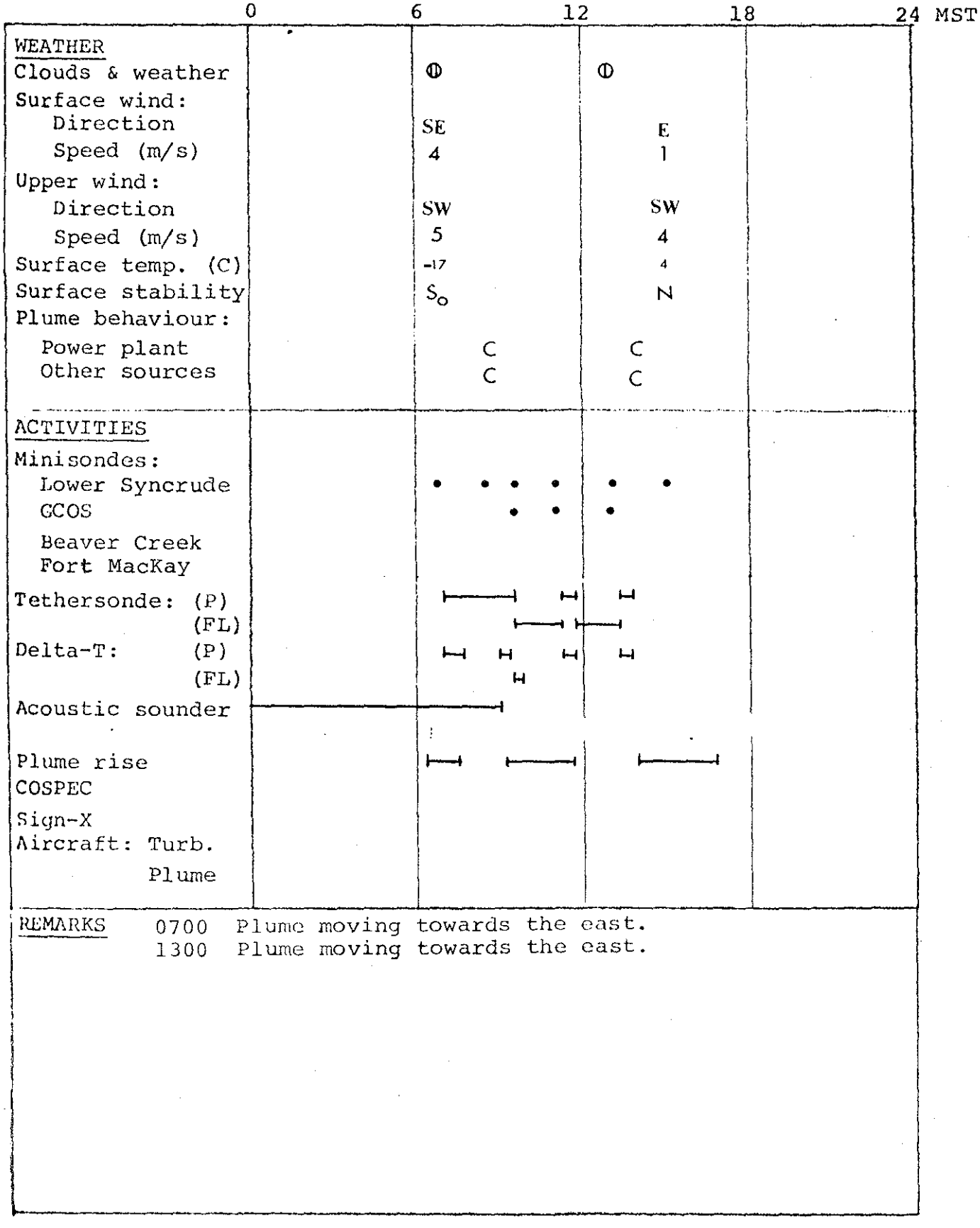

REMARKS
0700 Plume moving towards the east.
1300 Plume moving towards the east.

AOSERP Field Study - March 1976
Weather and Activity Summary

Date: 17 March

	0	6	12	18	24 MST
WEATHER					
Clouds & weather		⊕			
Surface wind:					
Direction		C	W		
Speed (m/s)		0	1		
Upper wind:					
Direction		N	E		
Speed (m/s)		7	2		
Surface temp. (C)		-3	5		
Surface stability		S_o	N_i		
Plume behaviour:					
Power plant					
Other sources					
ACTIVITIES					
Minisondes:					
Lower Syncrude		• • • •	•		
GCOS		• •	•		
Beaver Creek					
Fort MacKay					
Tethersonde: (P)					
(FL)					
Delta-T: (P)					
(FL)					
Acoustic sounder					
Plume rise					
COSPEC					
Sign-X					
Aircraft: Turb.					
Plume					

REMARKS 0700 Plume moving towards the east.

8.2 LIST OF PARTICIPANTS

The following is a list of the experiments comprising the field study together with the names of the participants.

Minisonde:	Team 'A'	Team 'B'
	S. Melnichuk	J. Kovalick
	J.A. Arnold	A.J. Gallant
	V.E. Nespliak	J.E. Mullock
	T.A. Sainsbury	R.C. Quinney
Tethersonde:	Dr. R.E. Mickle	
	W. Kobelka	
	L. Guise-Bagley	
Delta-T sonde:	Dr. H.E. Turner	
	J. Markes	
Acoustic sounder:		
	Dr. B.R. Kerman	
	K. Wu	
Plume Photography:		
	Dr. F. Fanaki	
	F. Froude	
COSPEC:	Dr. R. Hoff	
	Dr. M. Millan	
Precipitation and Air Chemistry:	Dr. L.A. Barrie	
	Dr. D.M. Whelpdale	
Project Management:		
	Dr. J.L. Walmsley	
	A.S. Mann	
	D.B. Hadler	

8.3 TETHERSONDE PROFILES

Legend

Measurement	Units	Symbol
Temperature	^{o}C	T •
Potential Temperature	^{o}C	VPT ⊙
Relative Humidity	%	RH ◇
Wind Speed	$m.s^{-1}$	U ⊡
Wind Direction	radians-reference magnetic North	DIR *
Height	m	

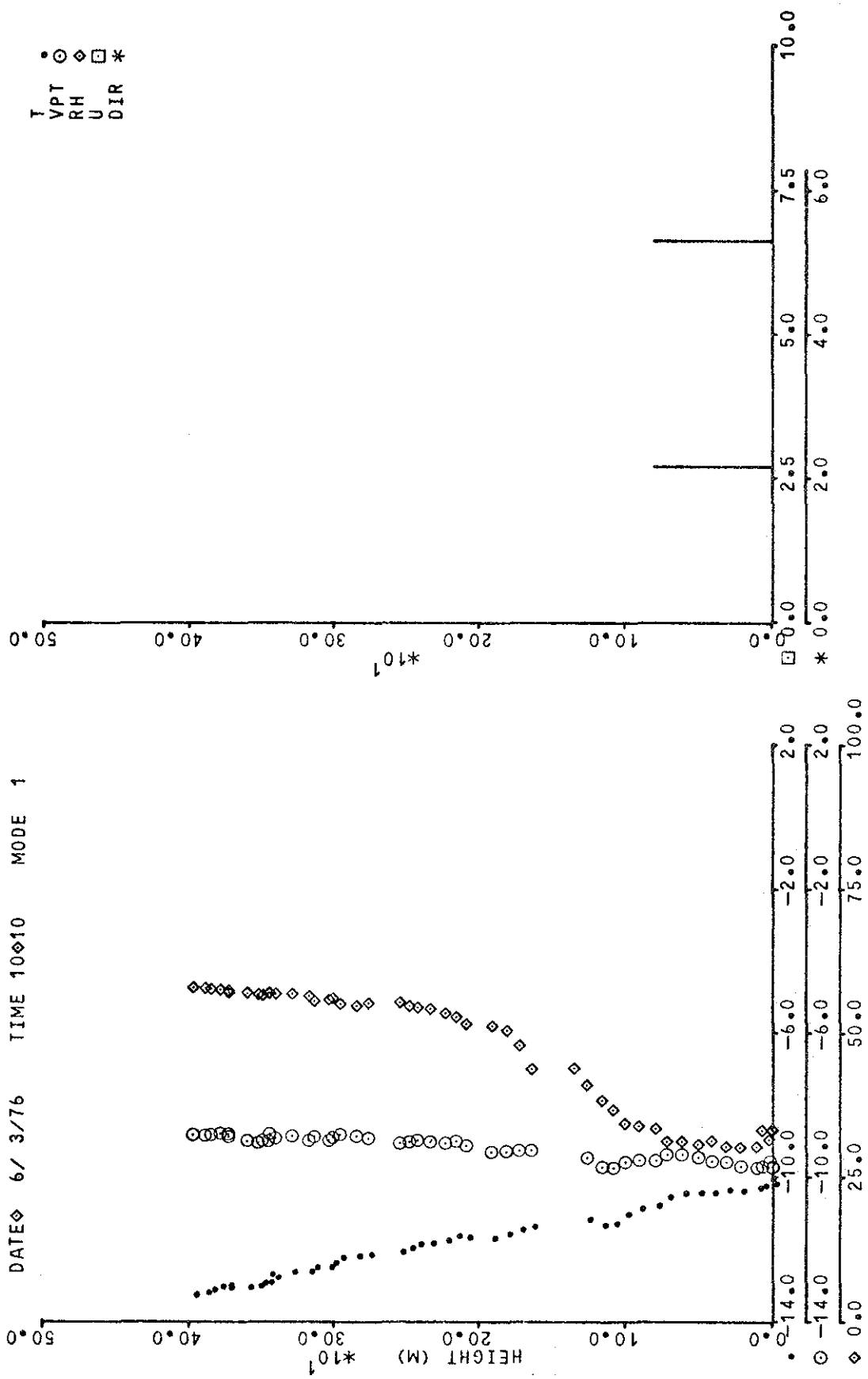
DATE◇ 6/ 3/76 TIME 10◇10 MODE 1
T •
VPT ⊙
RH ◇
U □
DIR *
HEIGHT (M) *10¹
*10¹
0.0
10.0
20.0
30.0
40.0
50.0
-14.0
-10.0
-6.0
-2.0
2.0
0.0
25.0
50.0
75.0
100.0
2.5
5.0
7.5

DATE◇ 6/ 3/76 TIME 11◇18 MODE 1
T
VPT
RH
U
DIR
HEIGHT (M) *10¹
*10¹
0.0
10.0
20.0
30.0
40.0
50.0
-12.0
-8.0
-4.0
0.0
4.0
25.0
50.0
75.0
100.0
2.5
5.0
7.5
10.0
6.0

T
VPT
RH
U
DIR
DATE◇ 6/ 3/76 TIME 14◇15 MODE 1
HEIGHT (M) *10¹
*10¹
0.0
10.0
20.0
30.0
40.0
50.0
10.0
7.5
5.0
2.5
0.0
6.0
4.0
2.0
0.0
8.0
4.0
0.0
-4.0
-8.0
100.0
75.0
50.0
25.0
0.0

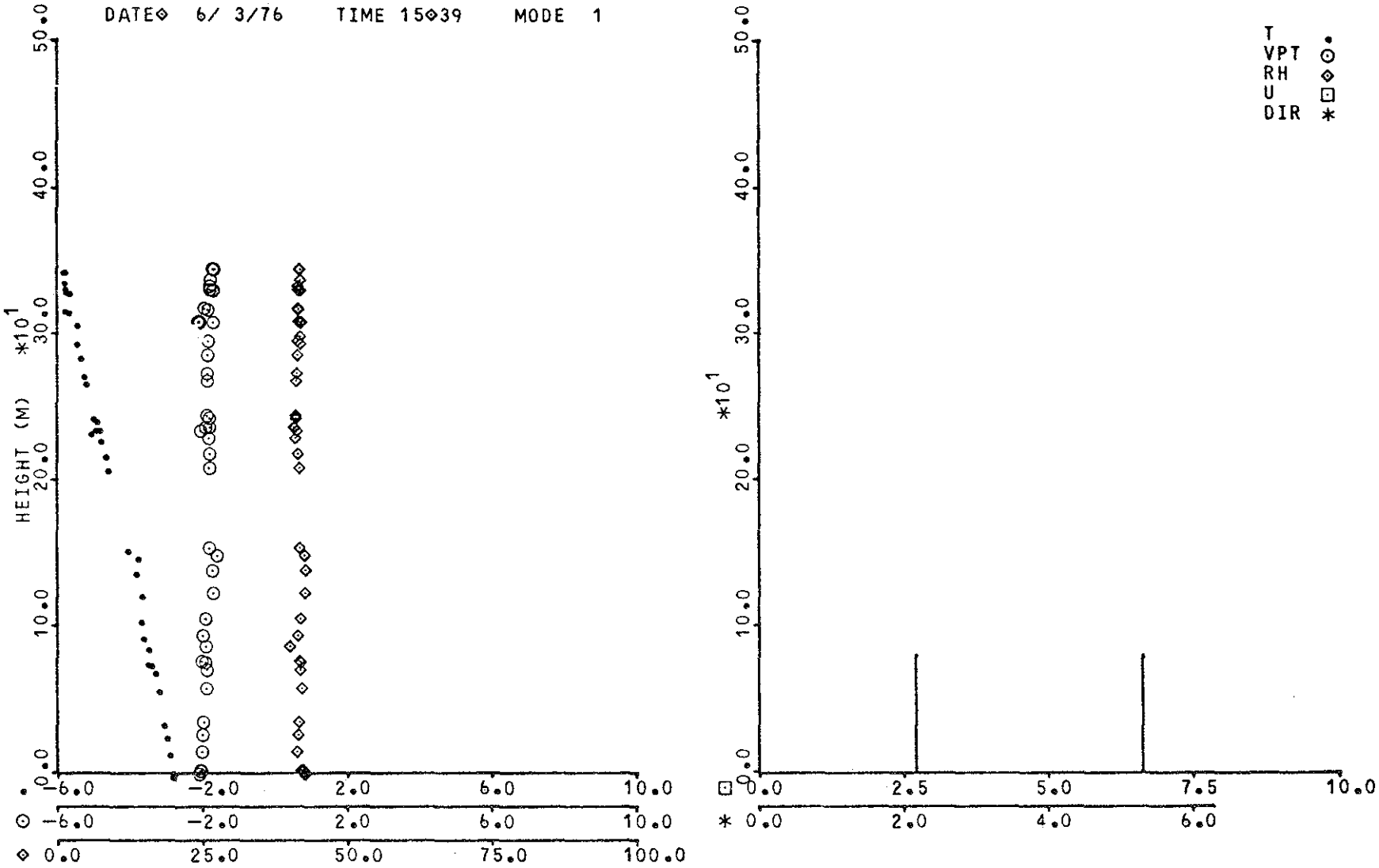
DATE◇ 6/ 3/76 TIME 15◇39 MODE 1
HEIGHT (M) *10^1
50.0
40.0
30.0
20.0
10.0
0.0
−6.0 −2.0 2.0 6.0 10.0
−6.0 −2.0 2.0 6.0 10.0
0.0 25.0 50.0 75.0 100.0
T
VPT
RH
U
DIR
*10^1
0.0 2.5 5.0 7.5 10.0
0.0 2.0 4.0 6.0

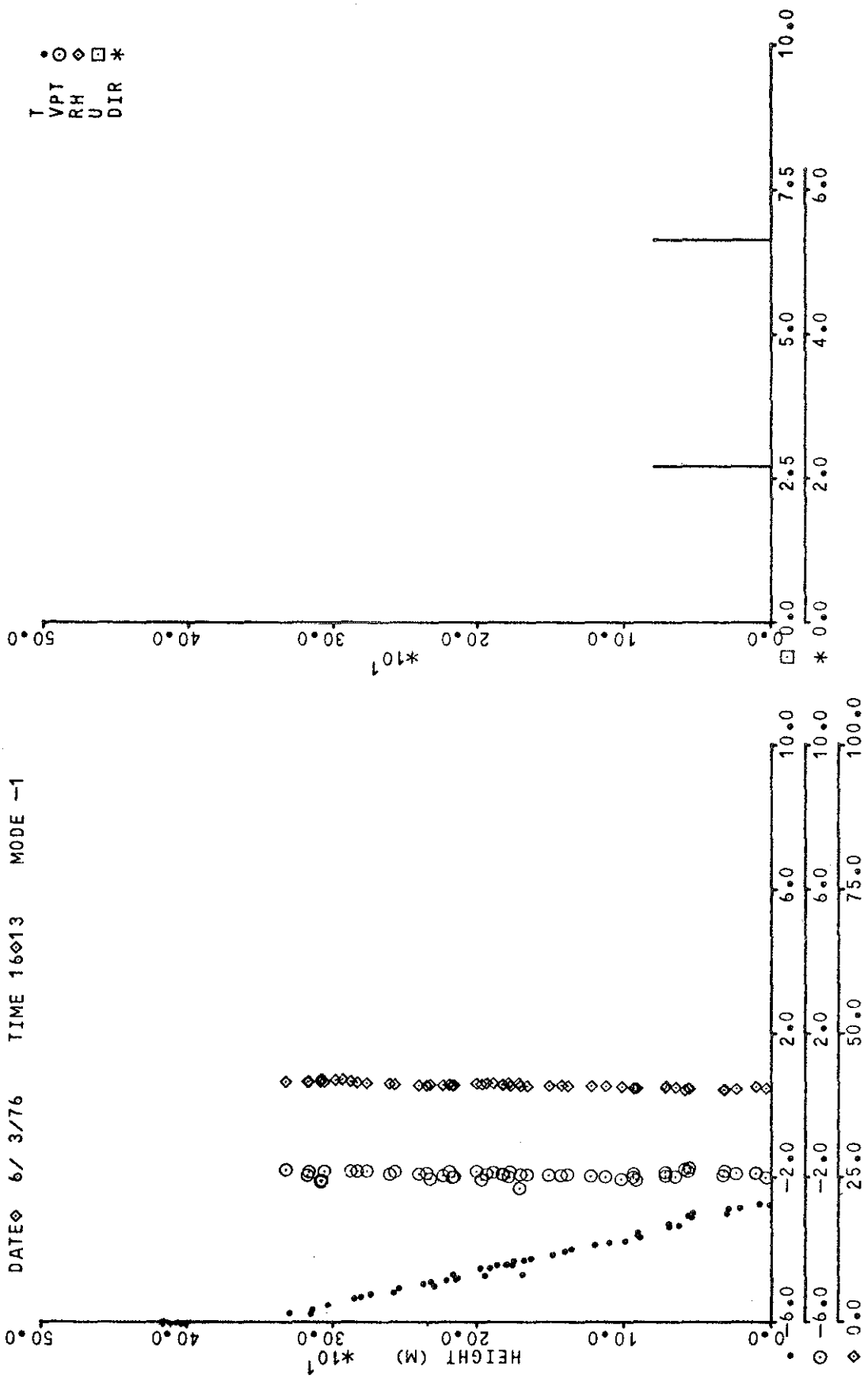
DATE◇ 6/ 3/76 TIME 16◇13 MODE -1
HEIGHT (M) *10¹
T
VPT
RH
U
DIR
*10¹

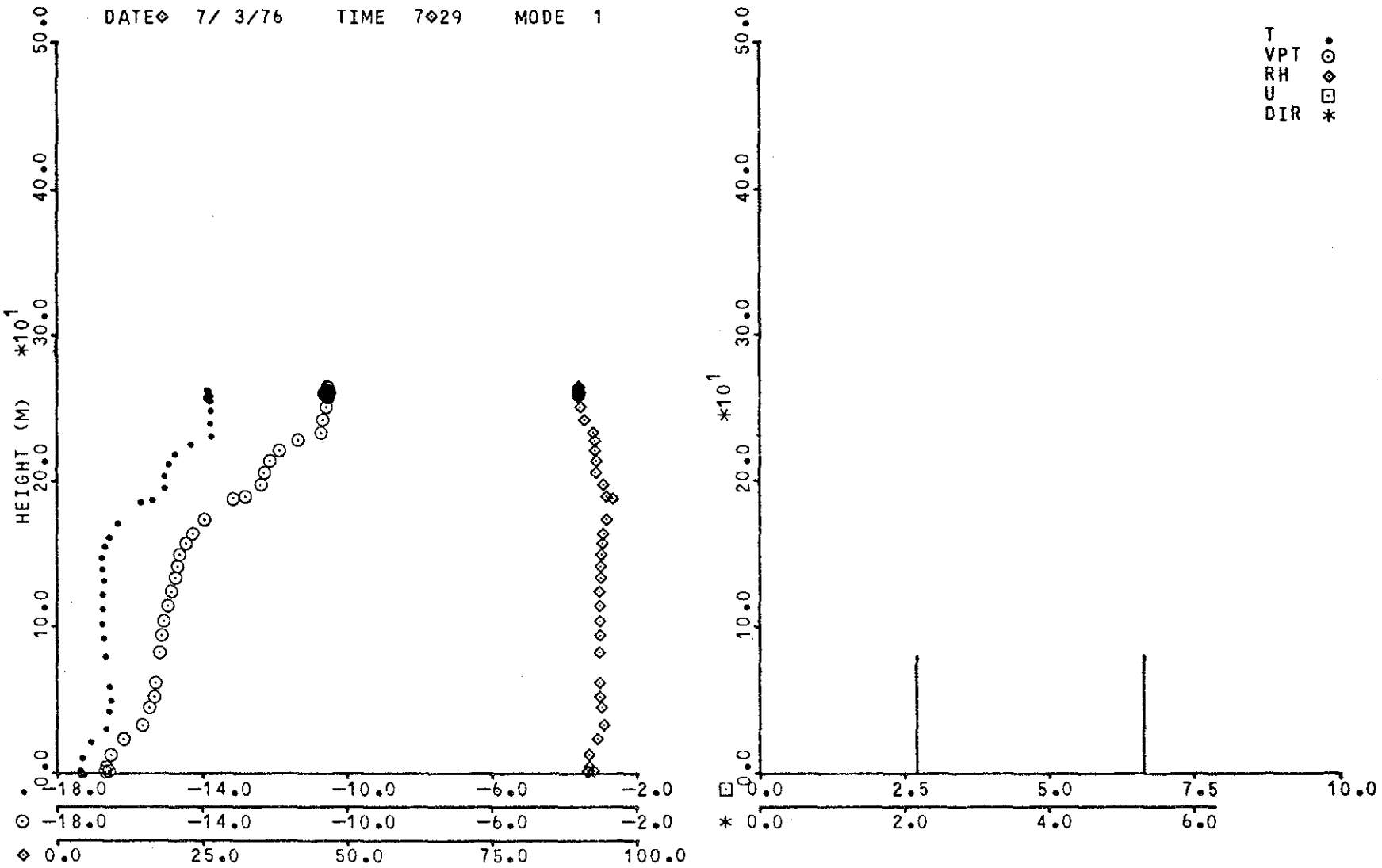
DATE◇ 7/ 3/76 TIME 7◇29 MODE 1
HEIGHT (M) *10^1
50.0
40.0
30.0
20.0
10.0
0.0
-18.0
-14.0
-10.0
-6.0
-2.0
0.0
25.0
50.0
75.0
100.0
T
VPT
RH
U
DIR
2.5
5.0
7.5
10.0
2.0
4.0
6.0

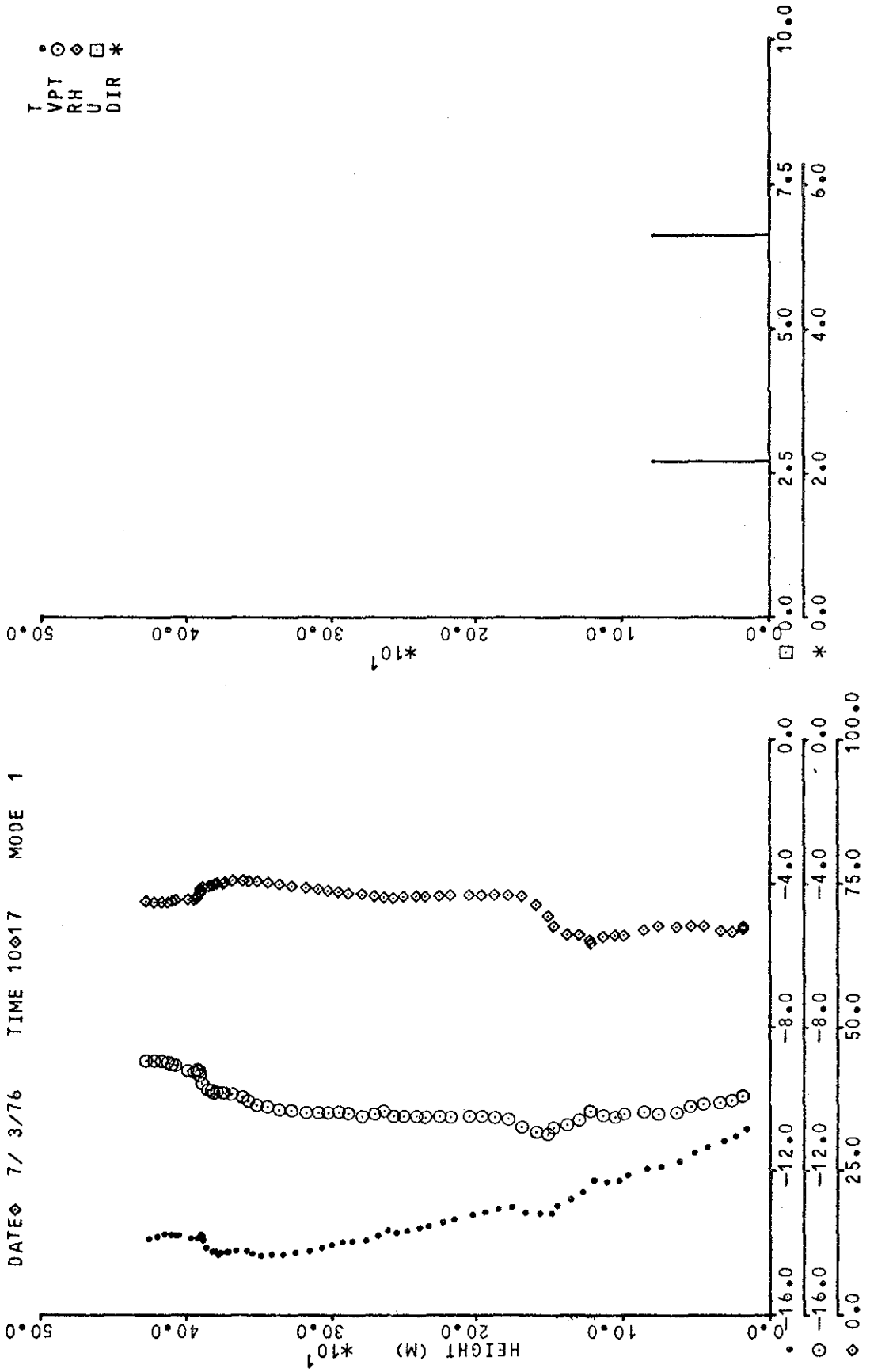
T
VPT
RH
U
DIR
DATE◇ 7/ 3/76 TIME 10◇17 MODE 1
HEIGHT (M) *10¹
*10¹
0.0
10.0
20.0
30.0
40.0
50.0
2.5
5.0
7.5
-4.0
-8.0
-12.0
-16.0
25.0
50.0
75.0
100.0

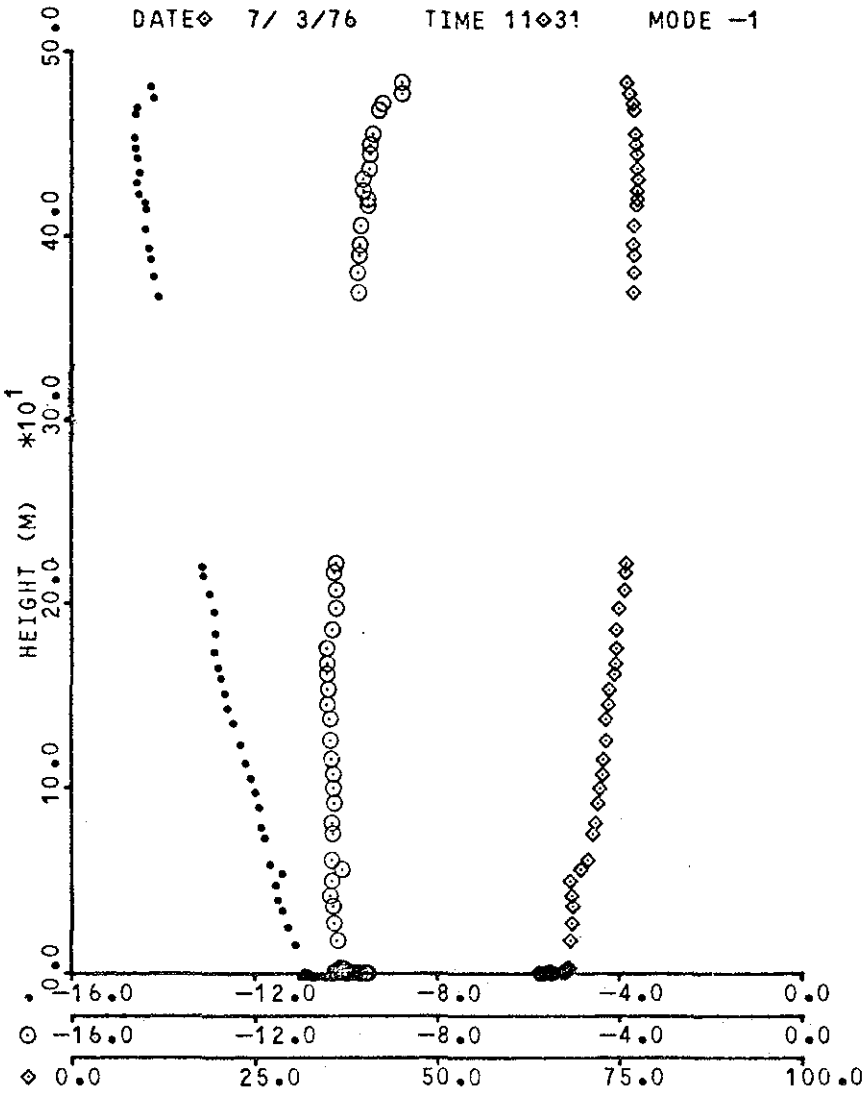
DATE◇ 7/ 3/76 TIME 11◇31 MODE -1
HEIGHT (M) *10^1
50.0
40.0
30.0
20.0
10.0
0.0
-16.0
-12.0
-8.0
-4.0
0.0
25.0
50.0
75.0
100.0

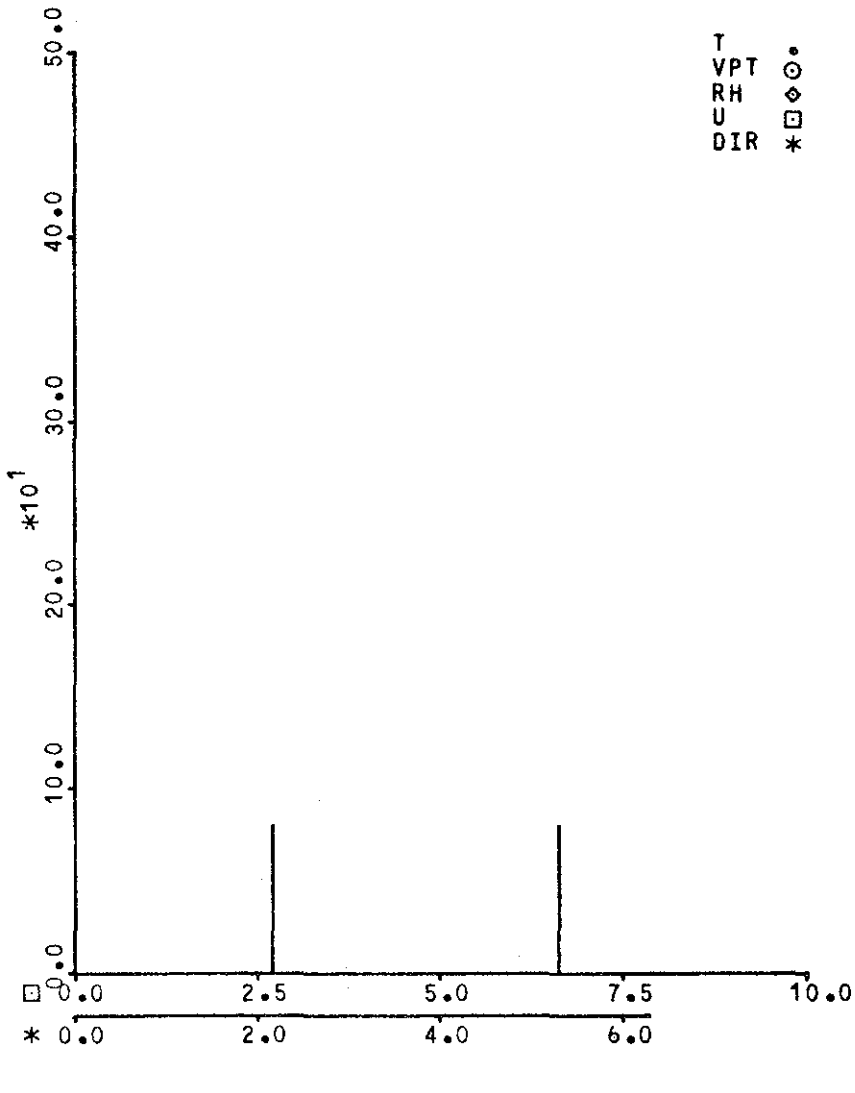
T
VPT
RH
U
DIR
*10^1
50.0
40.0
30.0
20.0
10.0
0.0
2.5
5.0
7.5
10.0
2.0
4.0
6.0

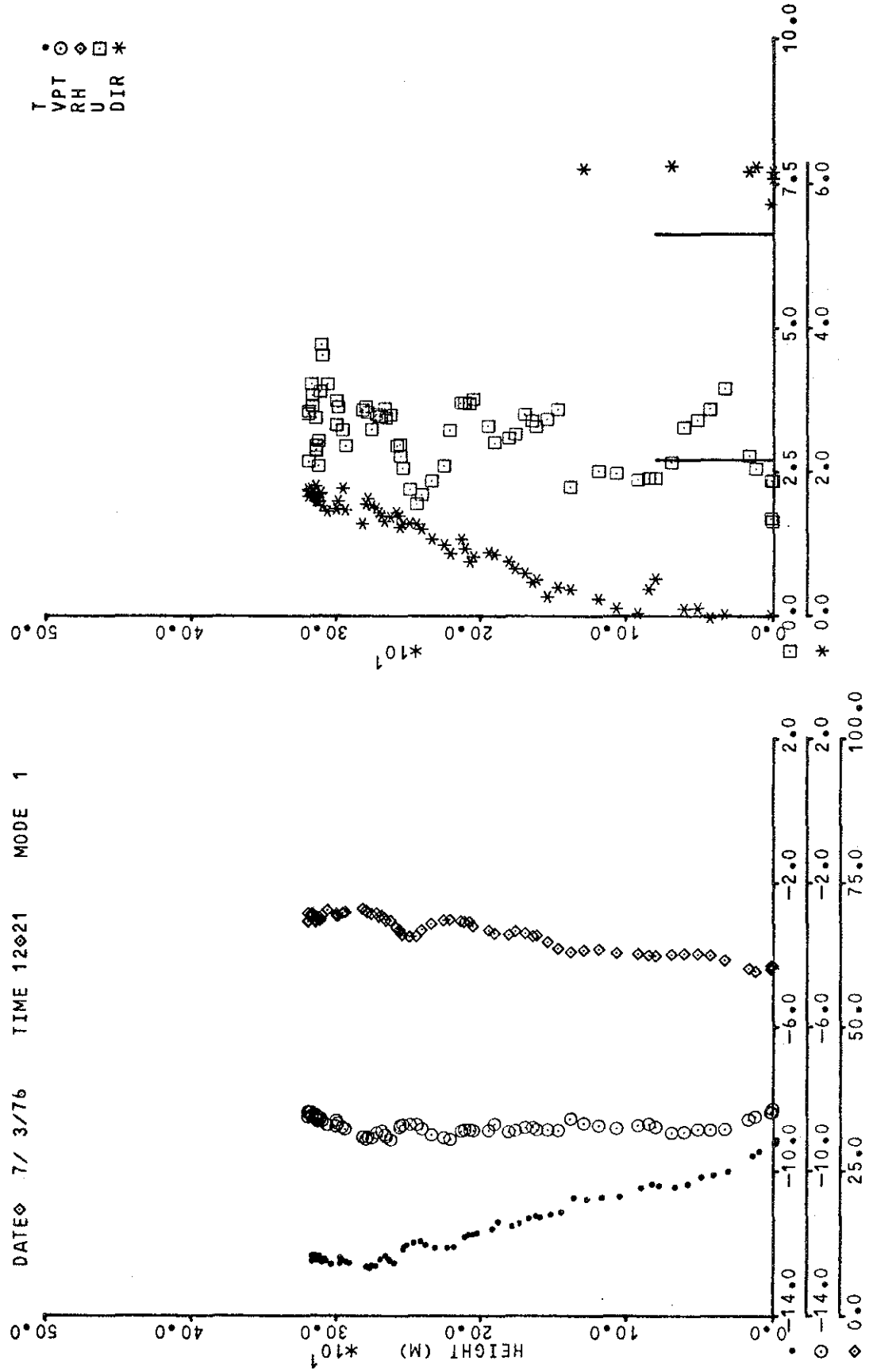
T
VPT
RH
U
DIR
DATE◇ 7/ 3/76 TIME 12◇21 MODE 1
HEIGHT (M) *10¹
*10¹

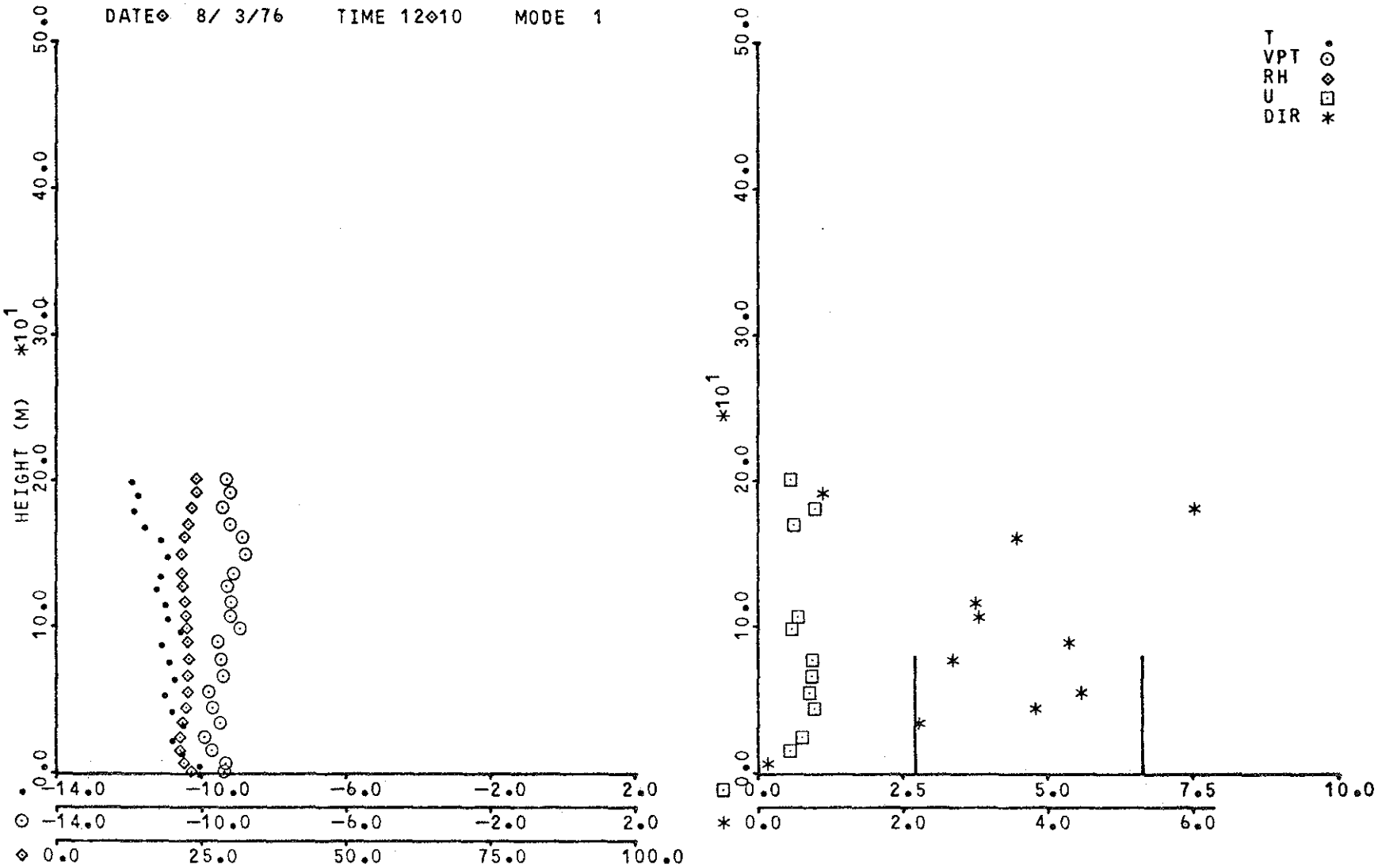
DATE◇ 8/ 3/76 TIME 12◇10 MODE 1
HEIGHT (M) *10^1
50.0
40.0
30.0
20.0
10.0
0.0
-14.0
-10.0
-6.0
-2.0
2.0
0.0
25.0
50.0
75.0
100.0
T
VPT
RH
U
DIR
2.5
5.0
7.5
10.0
4.0
6.0

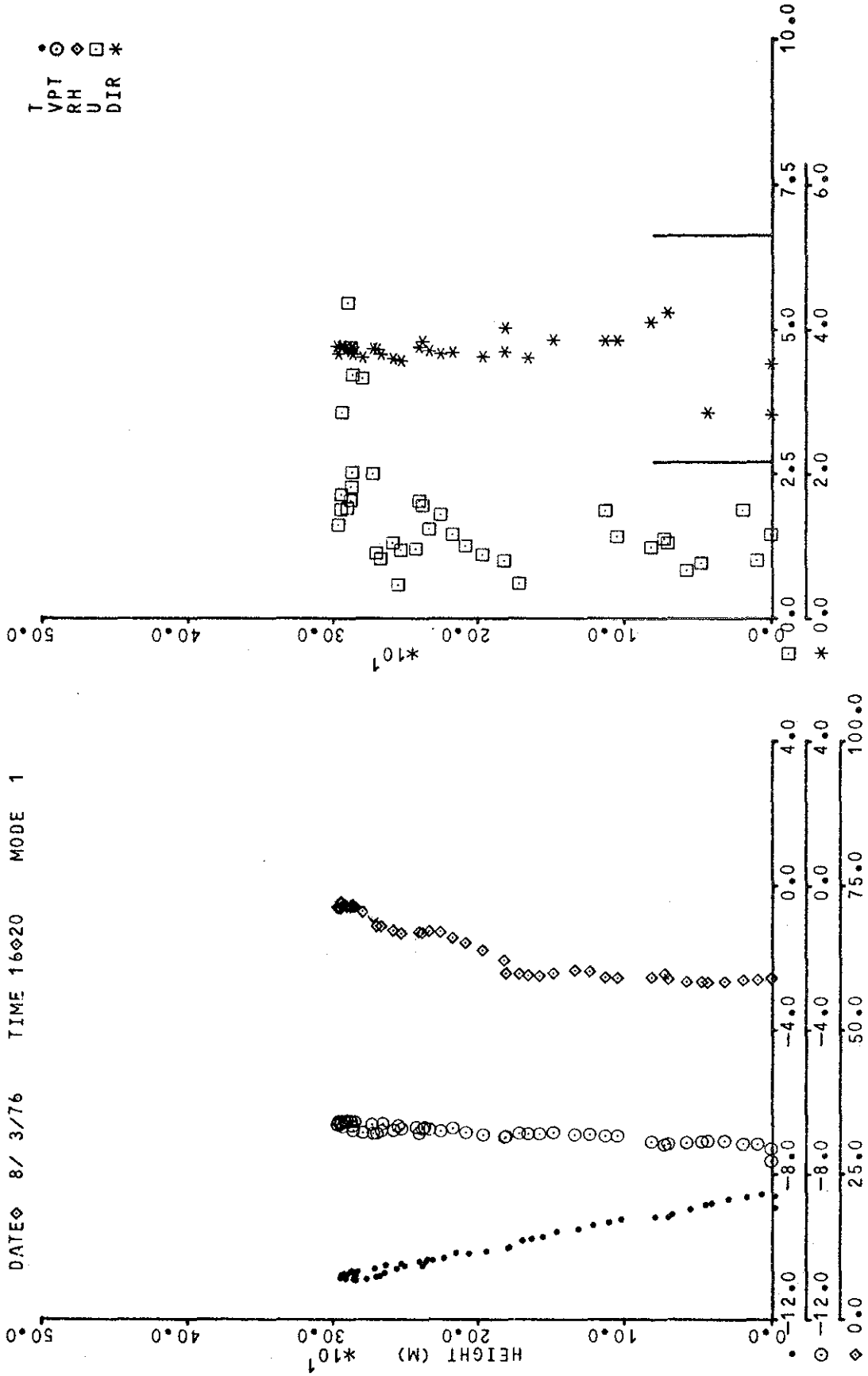
T
VPT
RH
U
DIR
DATE◇ 8/ 3/76 TIME 16◇20 MODE 1
HEIGHT (M) *10¹
*10¹

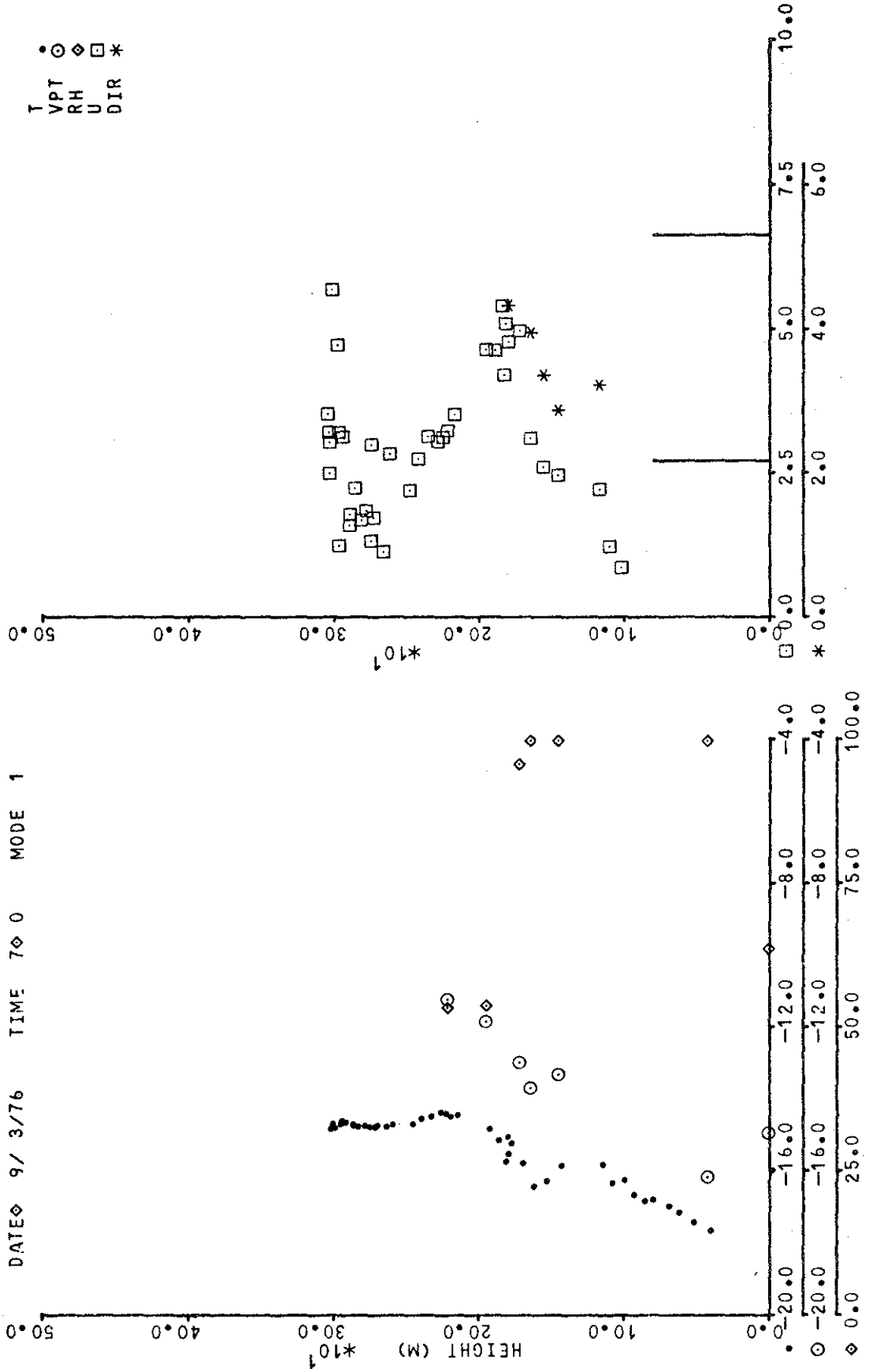
T
VPT
RH
U
DIR
DATE 9/ 3/76 TIME 7 0 0 MODE 1
HEIGHT (M) *10¹
*10¹

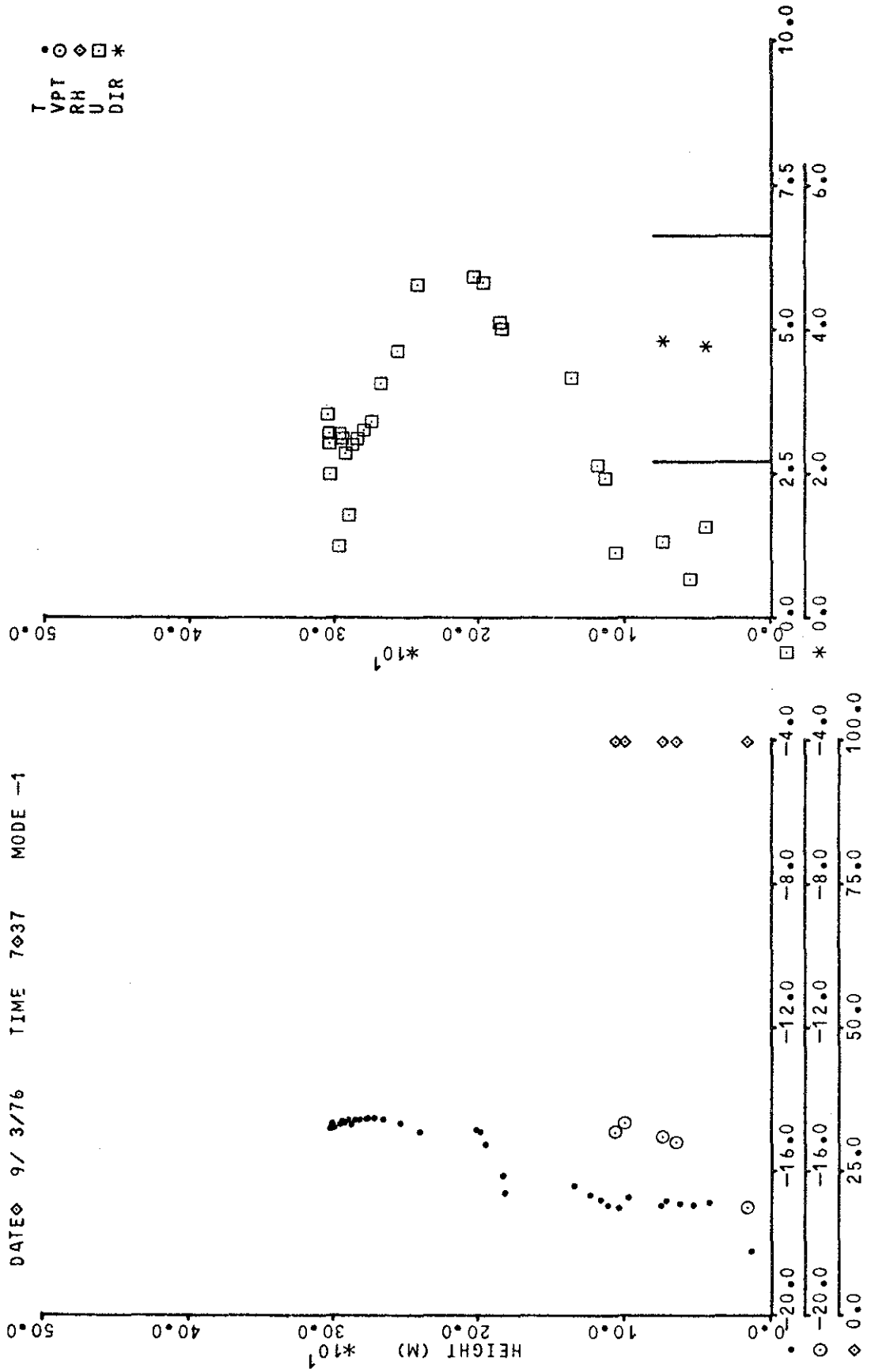
T
VPT
RH
U
DIR
DATE◇ 9/ 3/76 TIME 7◇37 MODE -1
HEIGHT (M) *10¹
*10¹
0.0
10.0
20.0
30.0
40.0
50.0
-4.0
-8.0
-12.0
-16.0
-20.0
100.0
75.0
50.0
25.0
0.0
2.5
5.0
7.5
10.0
4.0
6.0

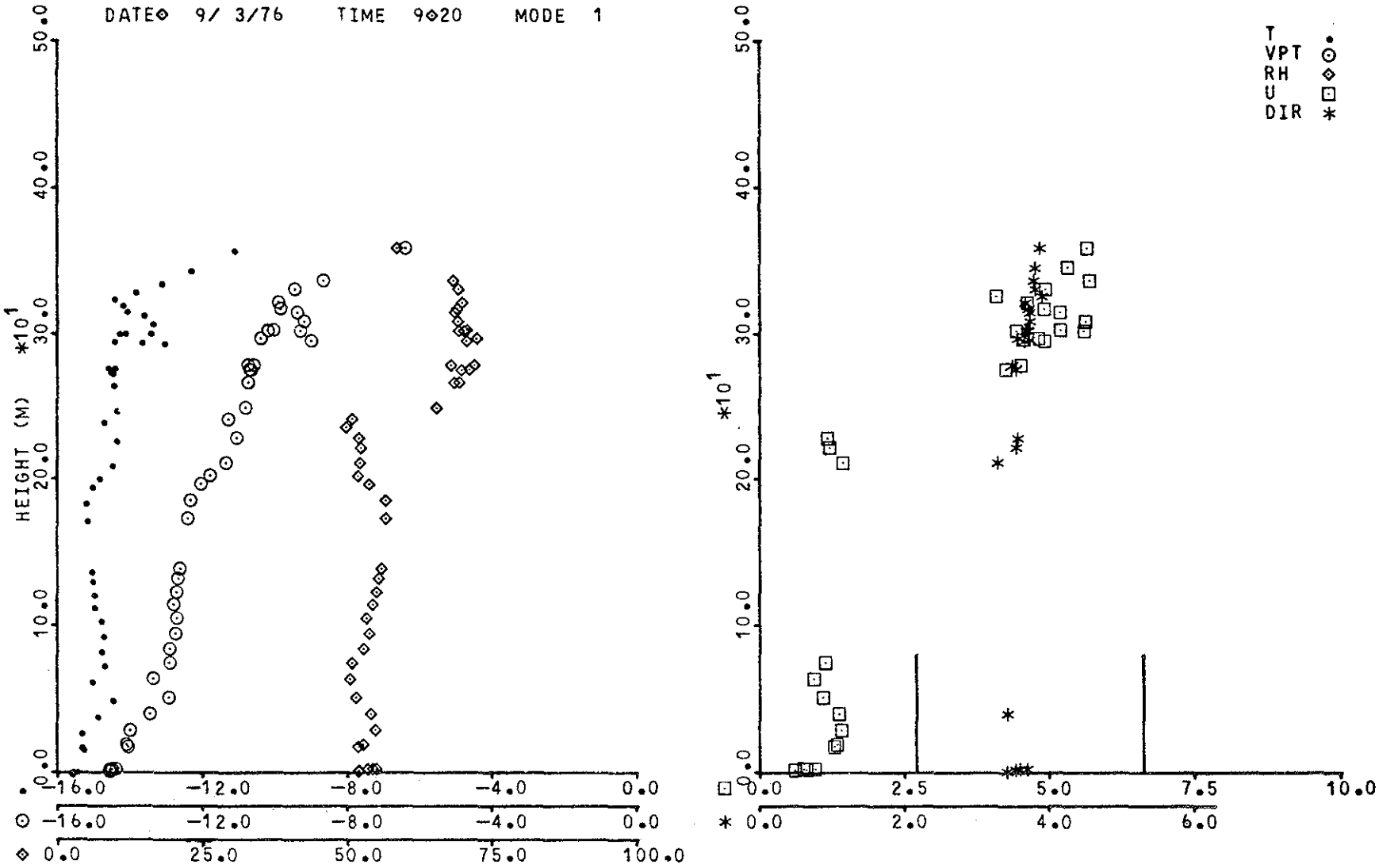
DATE⊙ 9/ 3/76 TIME 9⊙20 MODE 1
HEIGHT (M) *10^1
50.0
40.0
30.0
20.0
10.0
0.0
−16.0
−12.0
−8.0
−4.0
0.0
25.0
50.0
75.0
100.0
T
VPT
RH
U
DIR
2.5
5.0
7.5
10.0
2.0
4.0
6.0

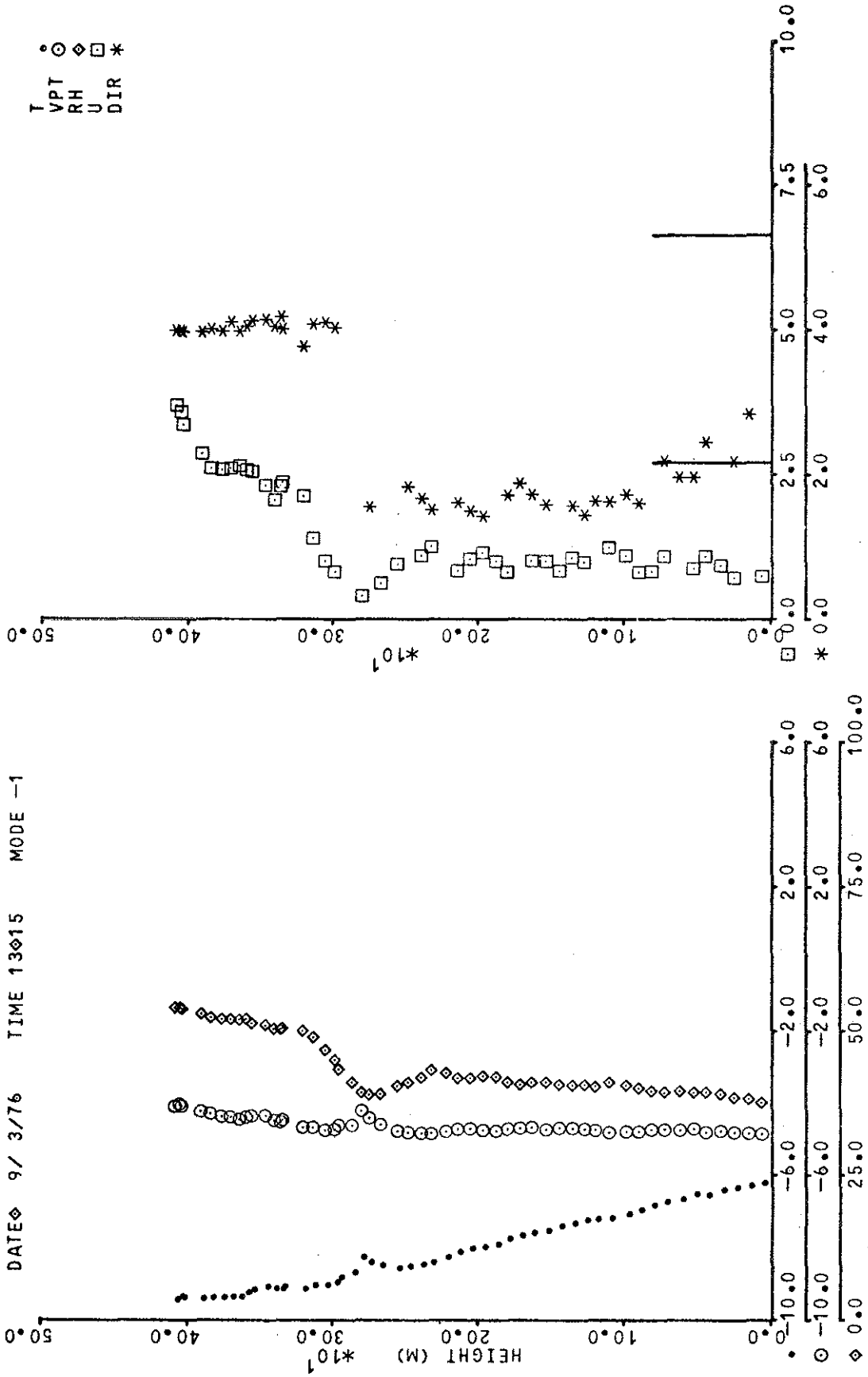
T
VPT
RH
U
DIR
*10¹
HEIGHT (M) *10¹
DATE◇ 9/ 3/76 TIME 13◇15 MODE -1

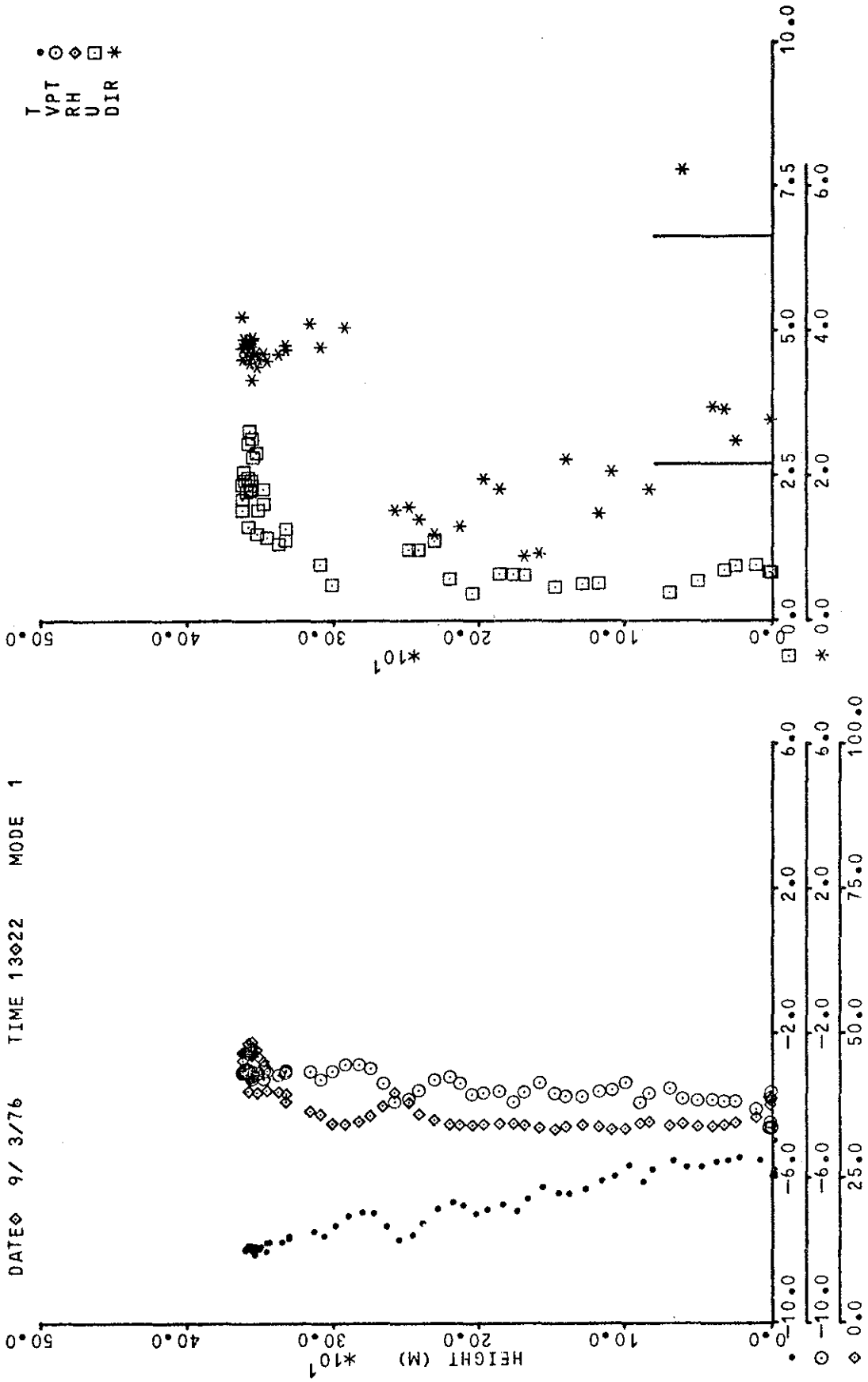
T
VPT
RH
U
DIR
DATE◇ 9/ 3/76 TIME 13◇22 MODE 1
HEIGHT (M) *10¹
*10¹

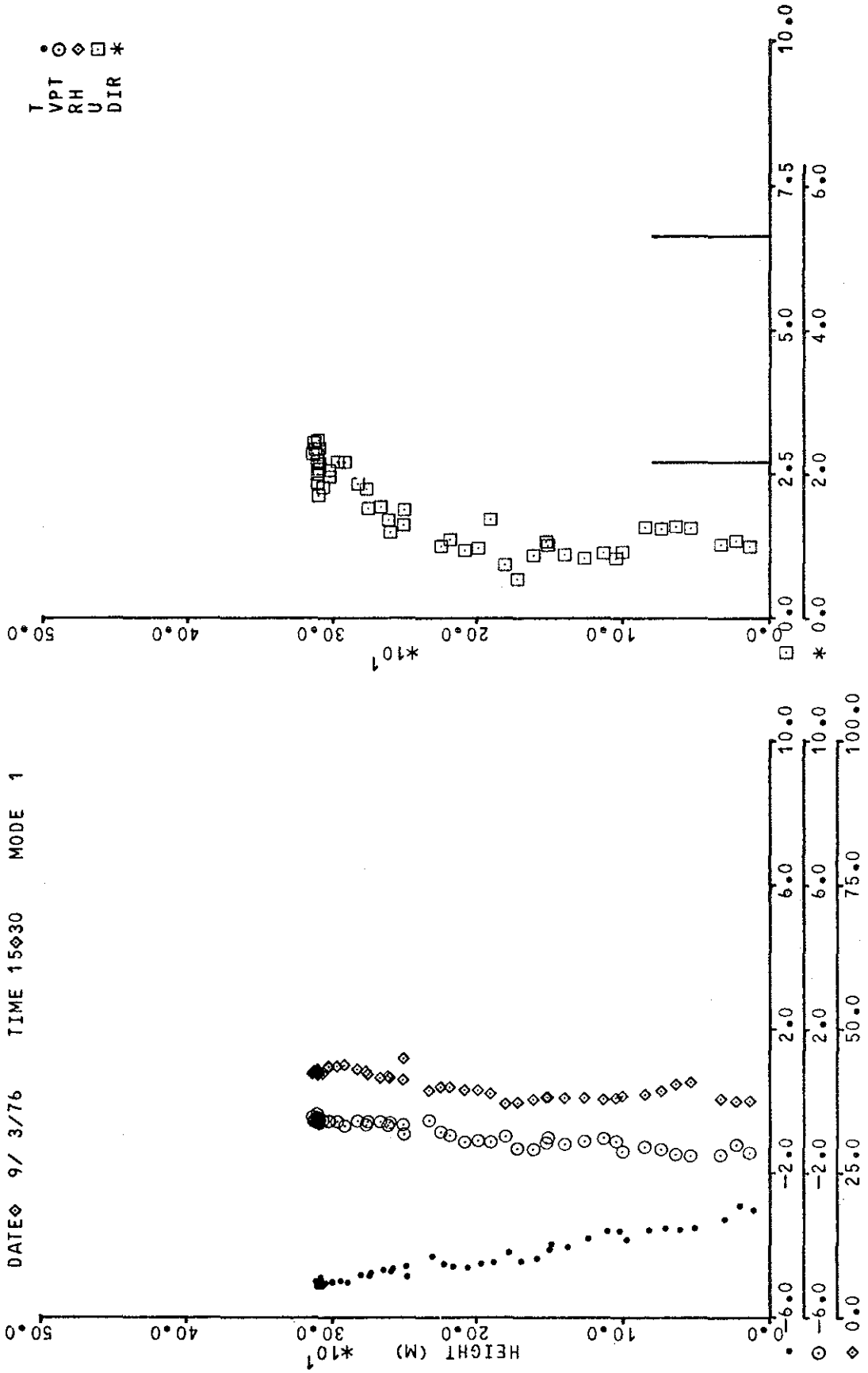
T
VPT
RH
U
DIR
*10¹
HEIGHT (M) *10¹
DATE◇ 9/ 3/76 TIME 15◇30 MODE 1

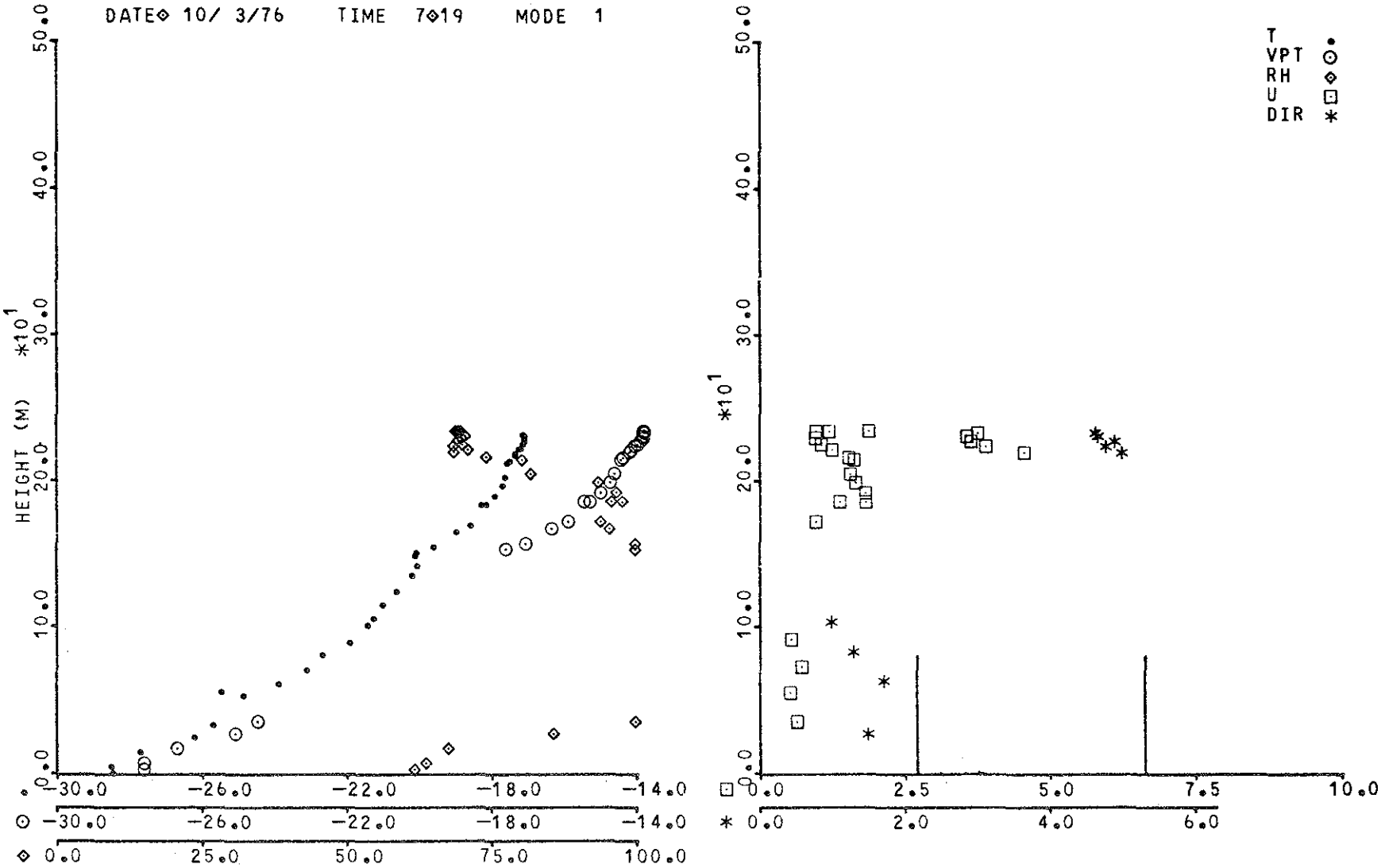
DATE◇ 10/ 3/76 TIME 7◇19 MODE 1
HEIGHT (M) *10^1
50.0
40.0
30.0
20.0
10.0
0.0
−30.0 −26.0 −22.0 −18.0 −14.0
−30.0 −26.0 −22.0 −18.0 −14.0
0.0 25.0 50.0 75.0 100.0
*10^1
0.0 2.5 5.0 7.5 10.0
0.0 2.0 4.0 6.0
T •
VPT ⊙
RH ◇
U □
DIR *

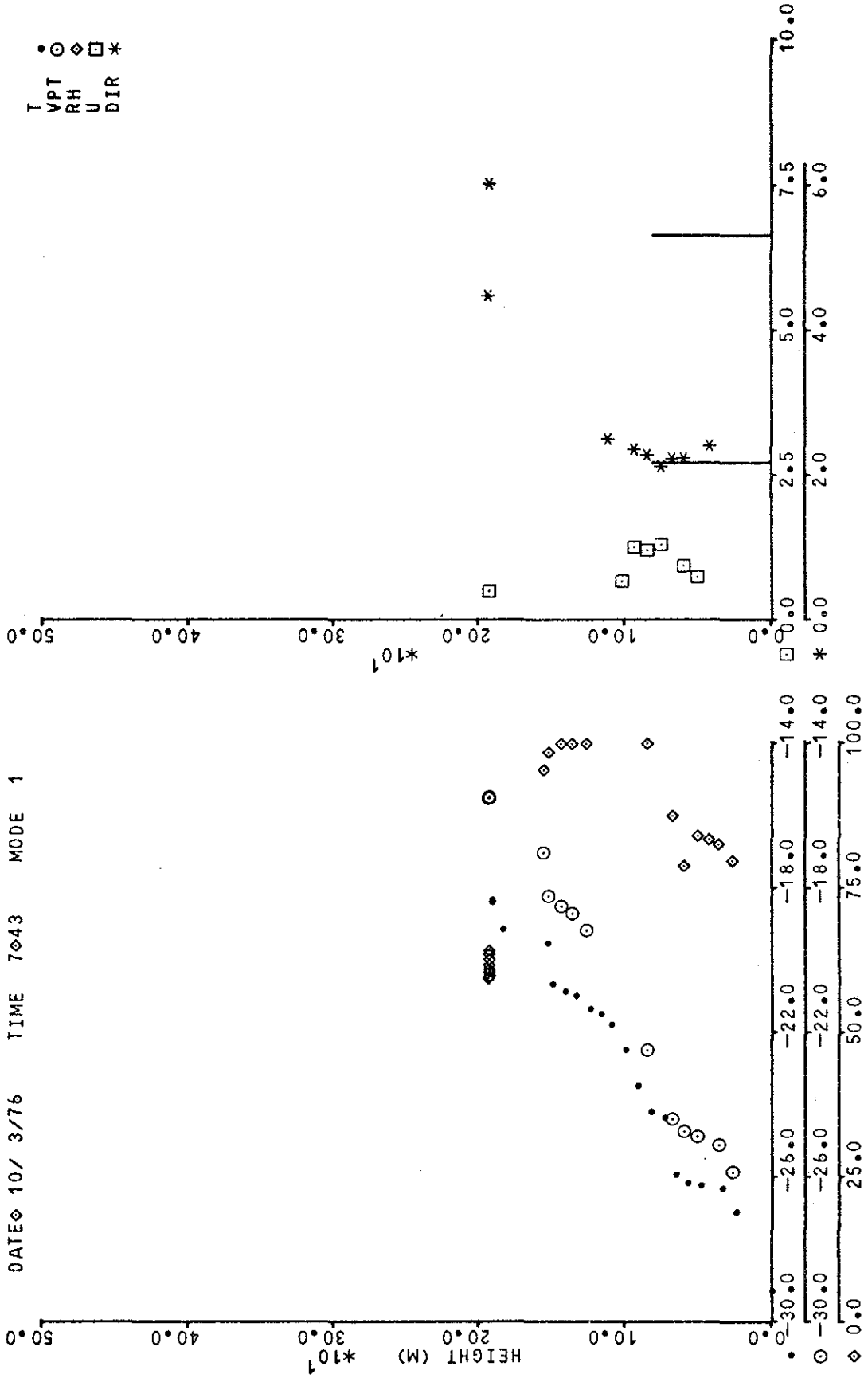
T
VPT
RH
U
DIR
DATE◇ 10/ 3/76 TIME 7◇43 MODE 1
HEIGHT (M) *10¹
*10¹
0.0
10.0
20.0
30.0
40.0
50.0
2.5
5.0
7.5
10.0
4.0
6.0
-14.0
-18.0
-22.0
-26.0
-30.0
100.0
75.0
50.0
25.0

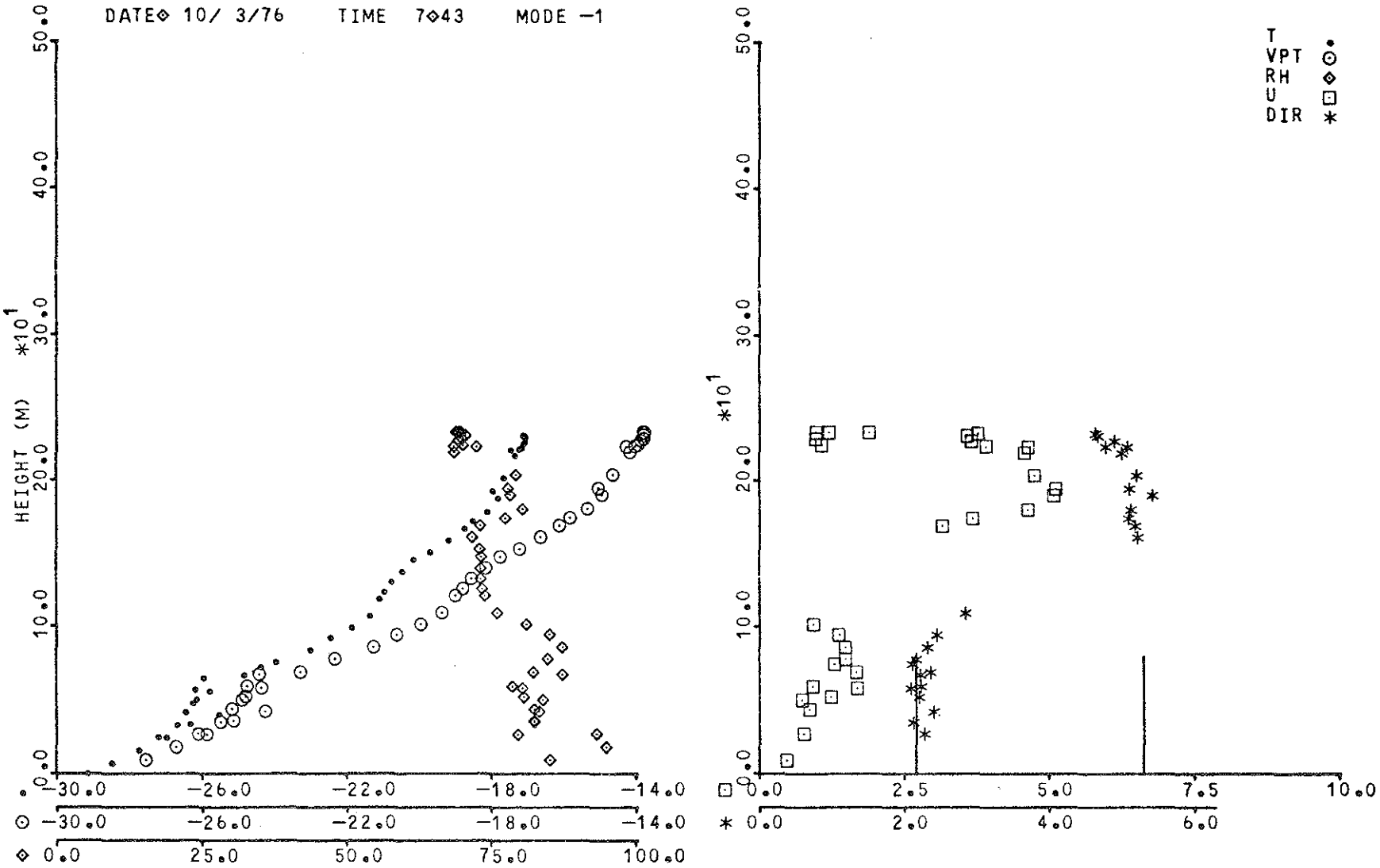
DATE◇ 10/ 3/76 TIME 7◇43 MODE −1
HEIGHT (M) *10^1
50.0
40.0
30.0
20.0
10.0
0.0
−30.0 −26.0 −22.0 −18.0 −14.0
−30.0 −26.0 −22.0 −18.0 −14.0
0.0 25.0 50.0 75.0 100.0
*10^1
0.0 2.5 5.0 7.5 10.0
0.0 2.0 4.0 6.0
T •
VPT ⊙
RH ◇
U □
DIR *

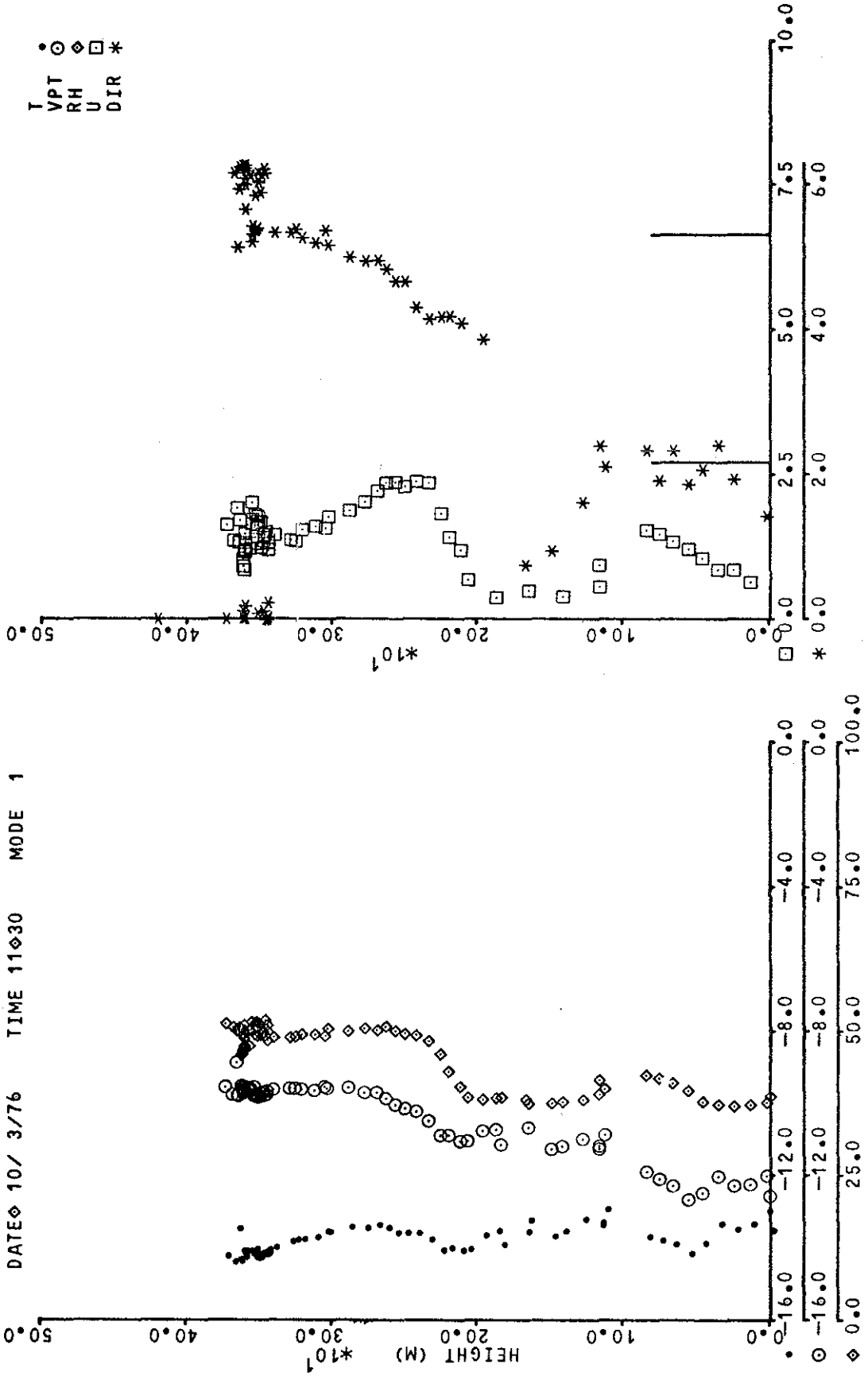
T
VPT
RH
U
DIR
DATE◇ 10/ 3/76 TIME 11◇30 MODE 1
HEIGHT (M) *10¹
*10¹

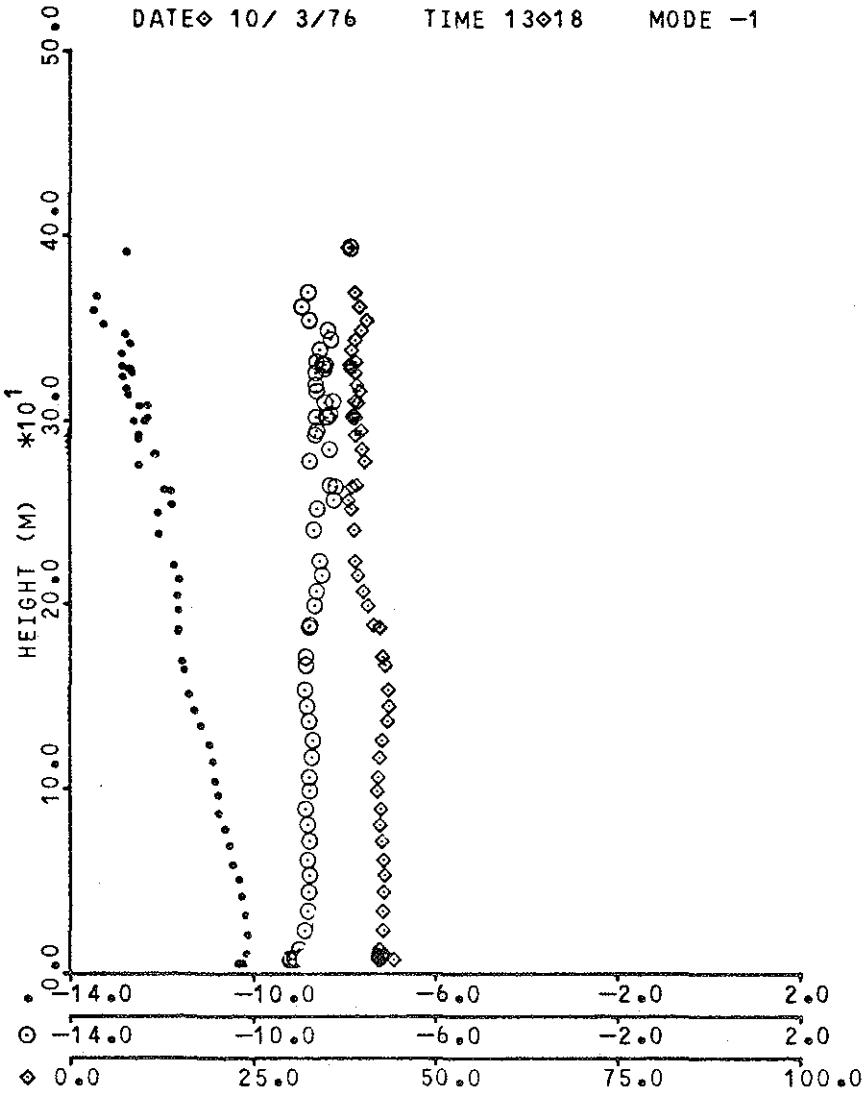
DATE◇ 10/ 3/76 TIME 13◇18 MODE -1
HEIGHT (M) *10^1
50.0
40.0
30.0
20.0
10.0
0.0
-14.0
-10.0
-6.0
-2.0
2.0
0.0
25.0
50.0
75.0
100.0

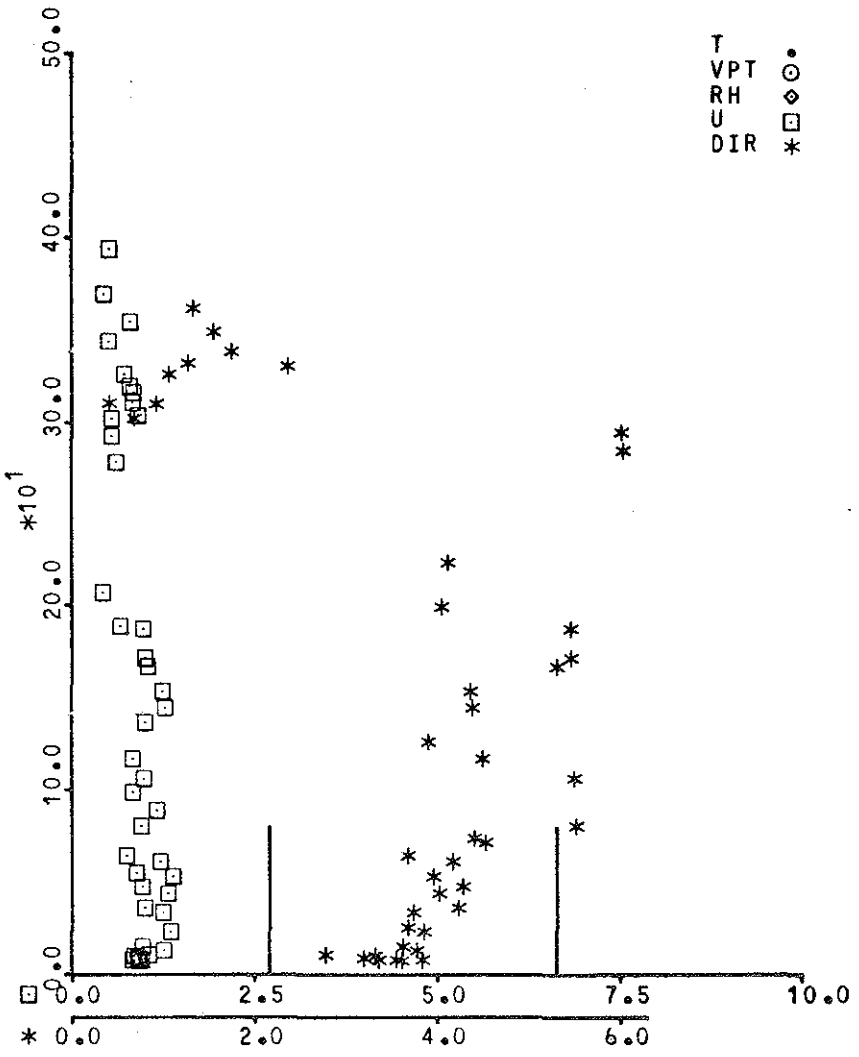
T
VPT
RH
U
DIR
*10^1
50.0
40.0
30.0
20.0
10.0
0.0
2.5
5.0
7.5
10.0
2.0
4.0
6.0

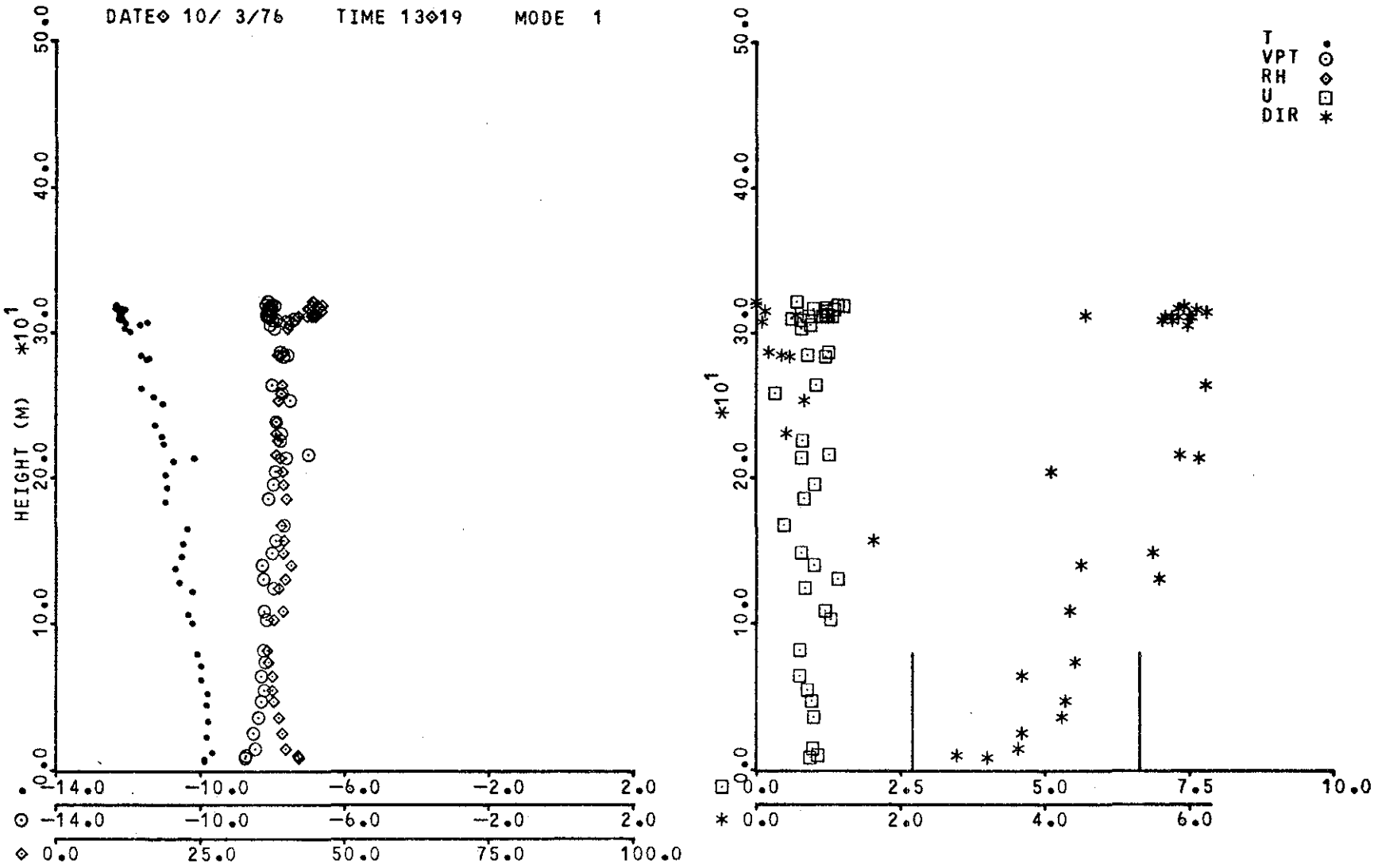
DATE⋄ 10/ 3/76 TIME 13⋄19 MODE 1
HEIGHT (M) *10¹
0.0
10.0
20.0
30.0
40.0
50.0
−14.0
−10.0
−6.0
−2.0
2.0
0.0
25.0
50.0
75.0
100.0
T
VPT
RH
U
DIR
*10¹
2.5
5.0
7.5
10.0
2.0
4.0
6.0

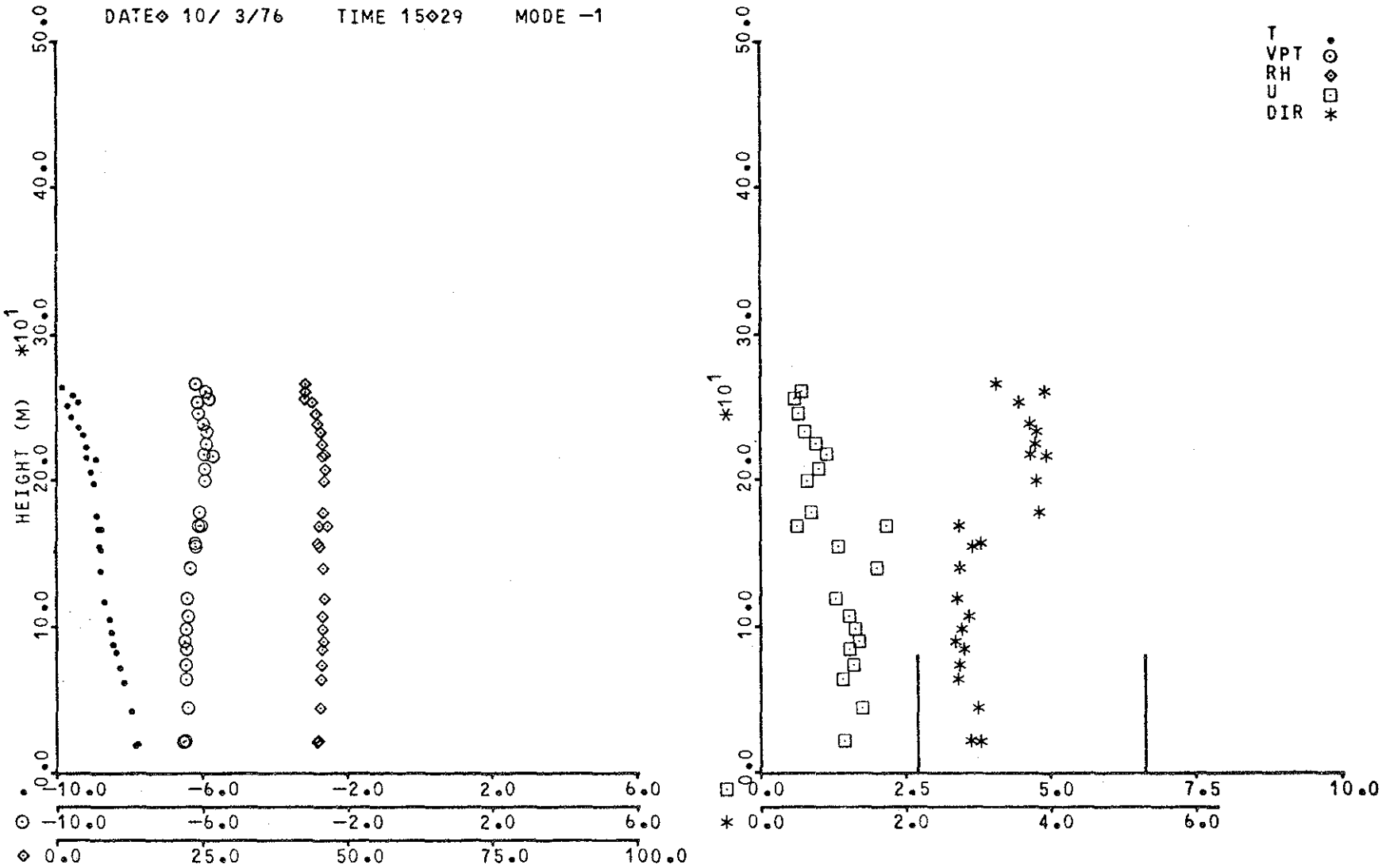
DATE◇ 10/ 3/76 TIME 15◇29 MODE −1
HEIGHT (M) *10^1
50.0
40.0
30.0
20.0
10.0
0.0
−10.0 −6.0 −2.0 2.0 6.0
−10.0 −6.0 −2.0 2.0 6.0
0.0 25.0 50.0 75.0 100.0
*10^1
0.0 2.5 5.0 7.5 10.0
0.0 2.0 4.0 6.0
T
VPT
RH
U
DIR

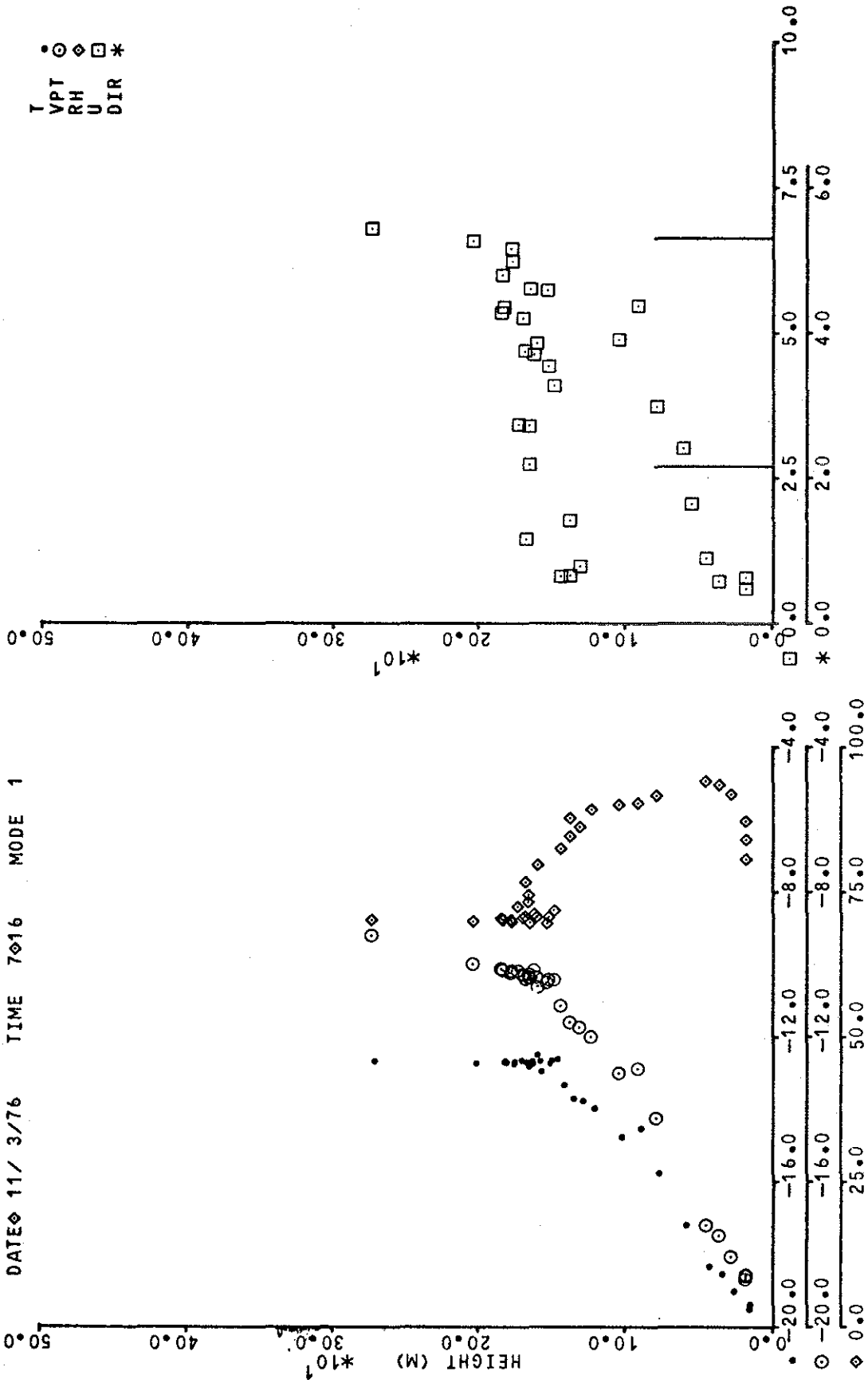
T
VPT
RH
U
DIR
DATE◇ 11/ 3/76 TIME 7◇16 MODE 1
HEIGHT (M) *10¹
*10¹
0.0
10.0
20.0
30.0
40.0
50.0
-20.0
-16.0
-12.0
-8.0
-4.0
0.0
25.0
50.0
75.0
100.0
2.5
5.0
7.5
10.0
2.0
4.0
6.0

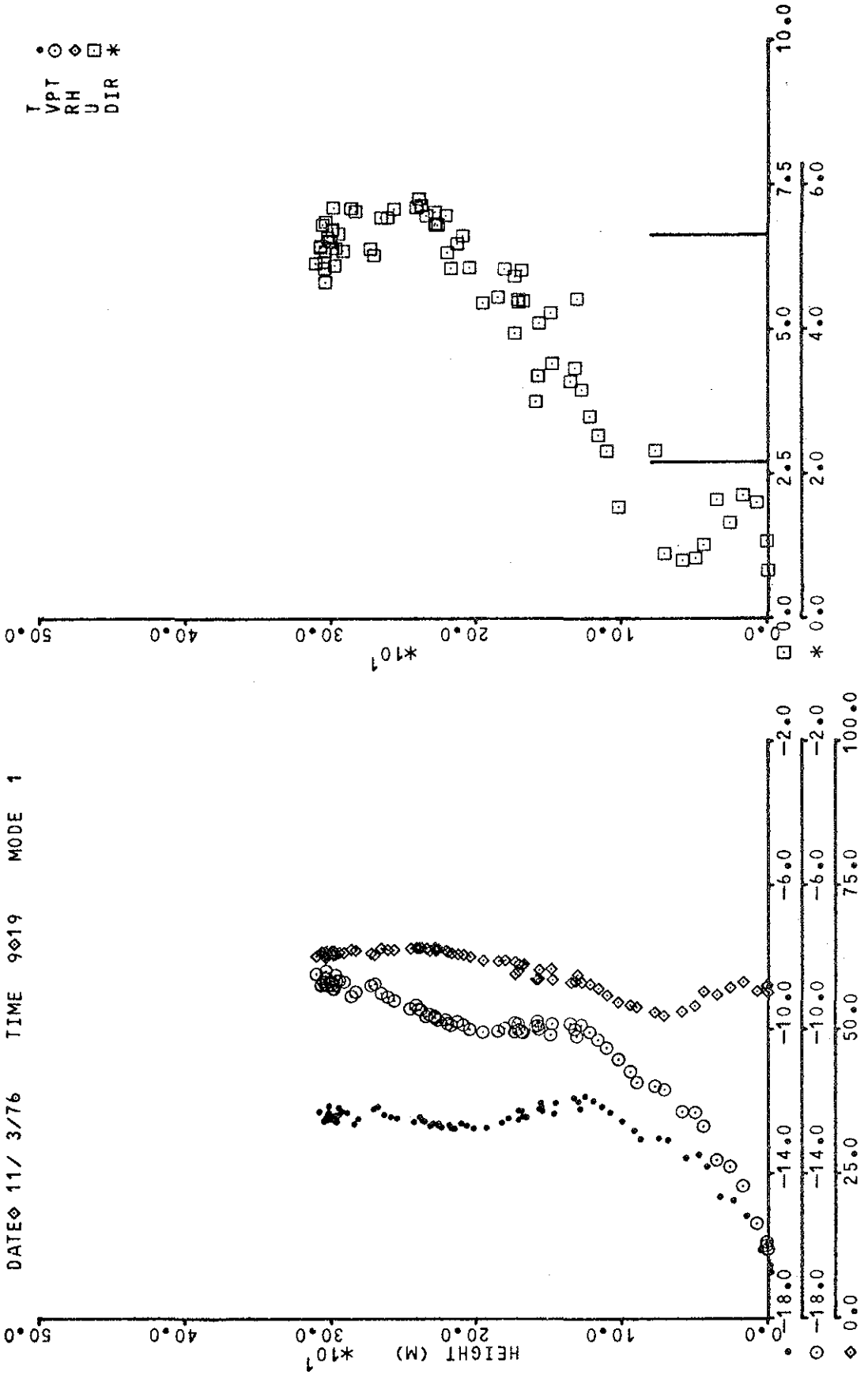
T
VPT
RH
U
DIR
DATE◇ 11/ 3/76 TIME 9◇19 MODE 1
HEIGHT (M) *10¹
*10¹
0.0
10.0
20.0
30.0
40.0
50.0
-2.0
-6.0
-10.0
-14.0
-18.0
100.0
75.0
50.0
25.0
0.0
2.5
5.0
7.5
10.0
4.0
6.0

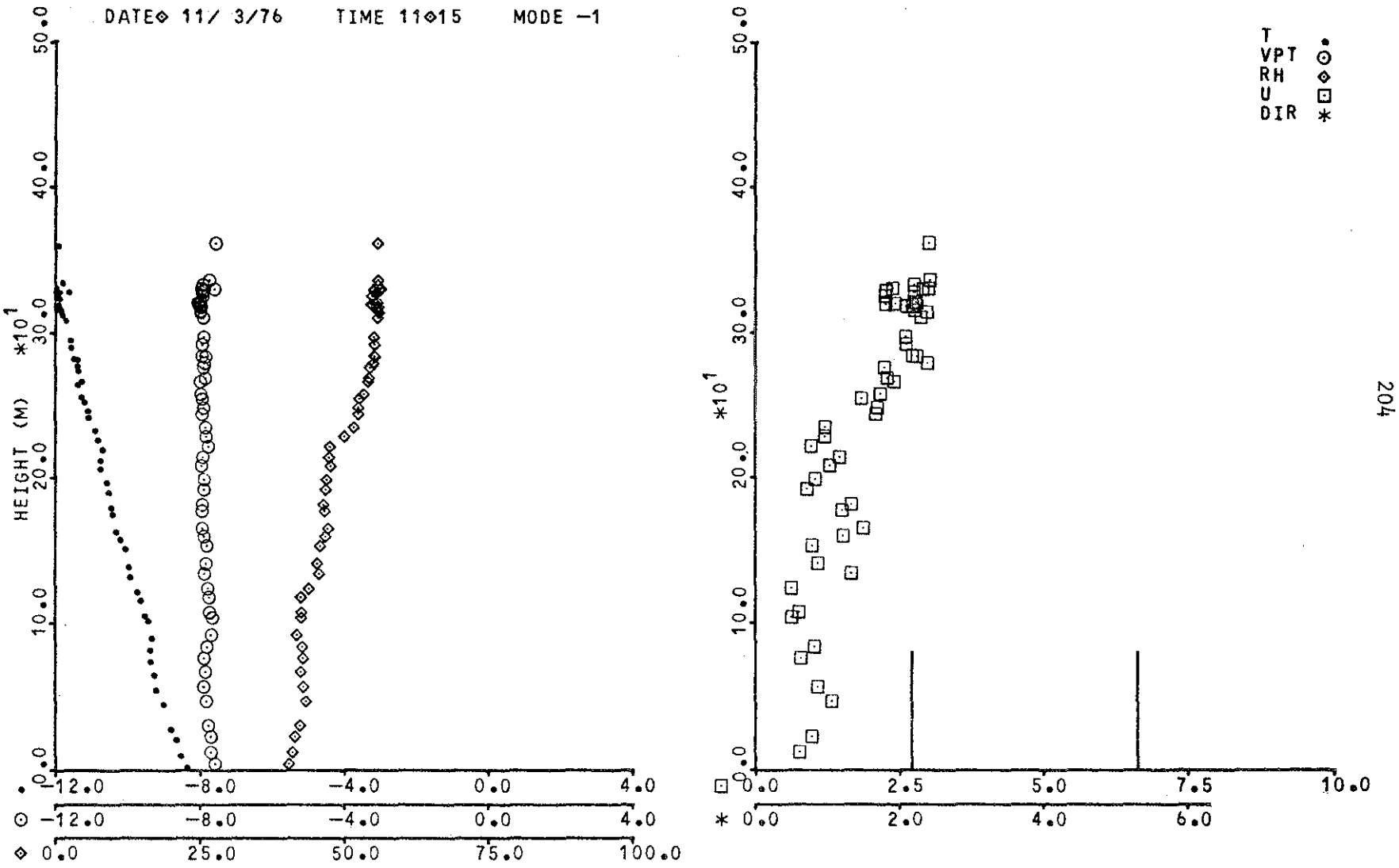
DATE◇ 11/ 3/76 TIME 11◇15 MODE −1
HEIGHT (M) *10^1
50.0
40.0
30.0
20.0
10.0
0.0
−12.0
−8.0
−4.0
0.0
4.0
0.0
25.0
50.0
75.0
100.0
T
VPT
RH
U
DIR
2.5
5.0
7.5
10.0
2.0
4.0
6.0

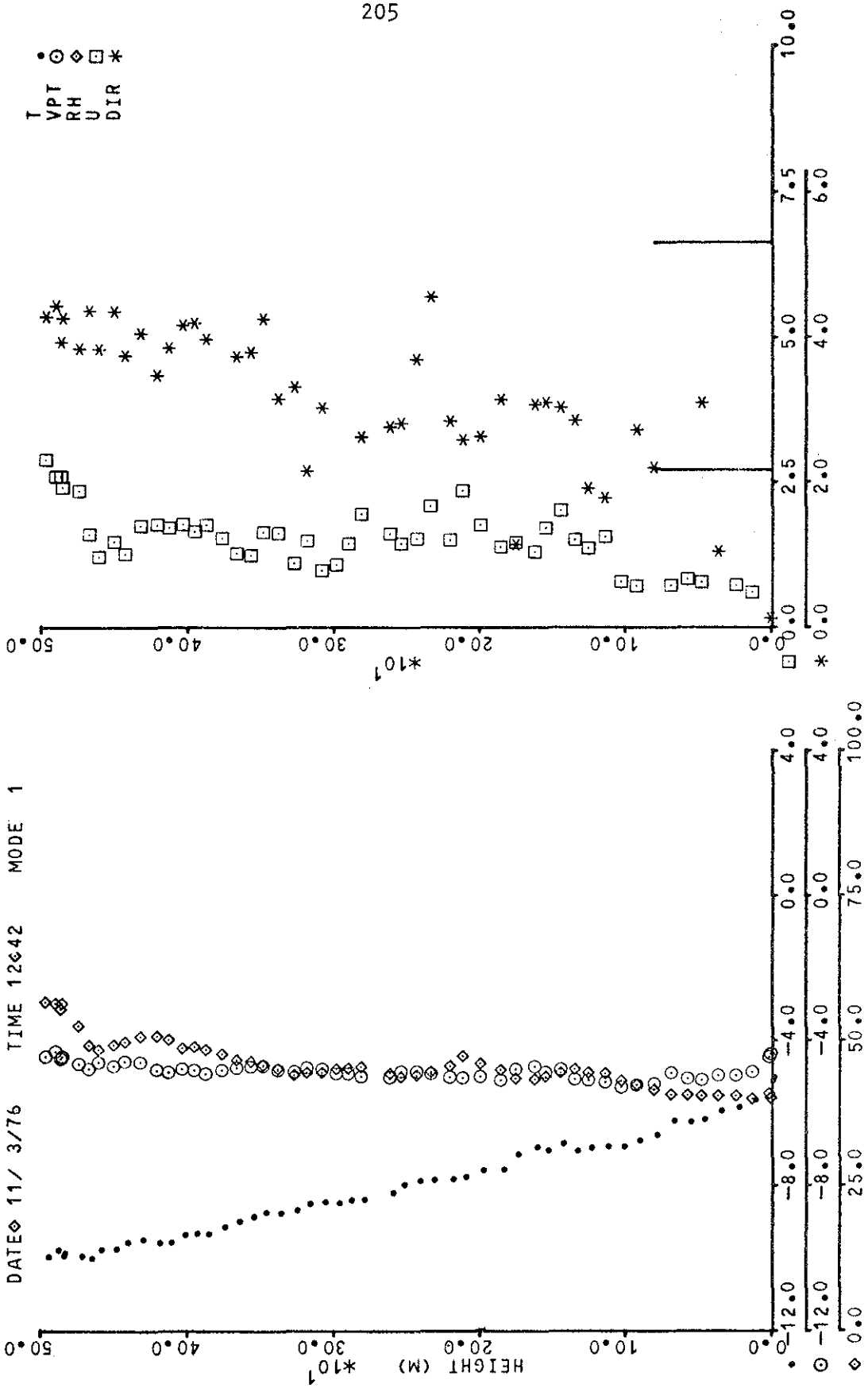
T
VPT
RH
U
DIR
DATE◇ 11/ 3/76
TIME 12◇42
MODE 1
HEIGHT (M)
*10¹
0.0
10.0
20.0
30.0
40.0
50.0
0.0
2.5
5.0
7.5
10.0
0.0
2.0
4.0
6.0
-12.0
-8.0
-4.0
0.0
4.0
0.0
25.0
50.0
75.0
100.0

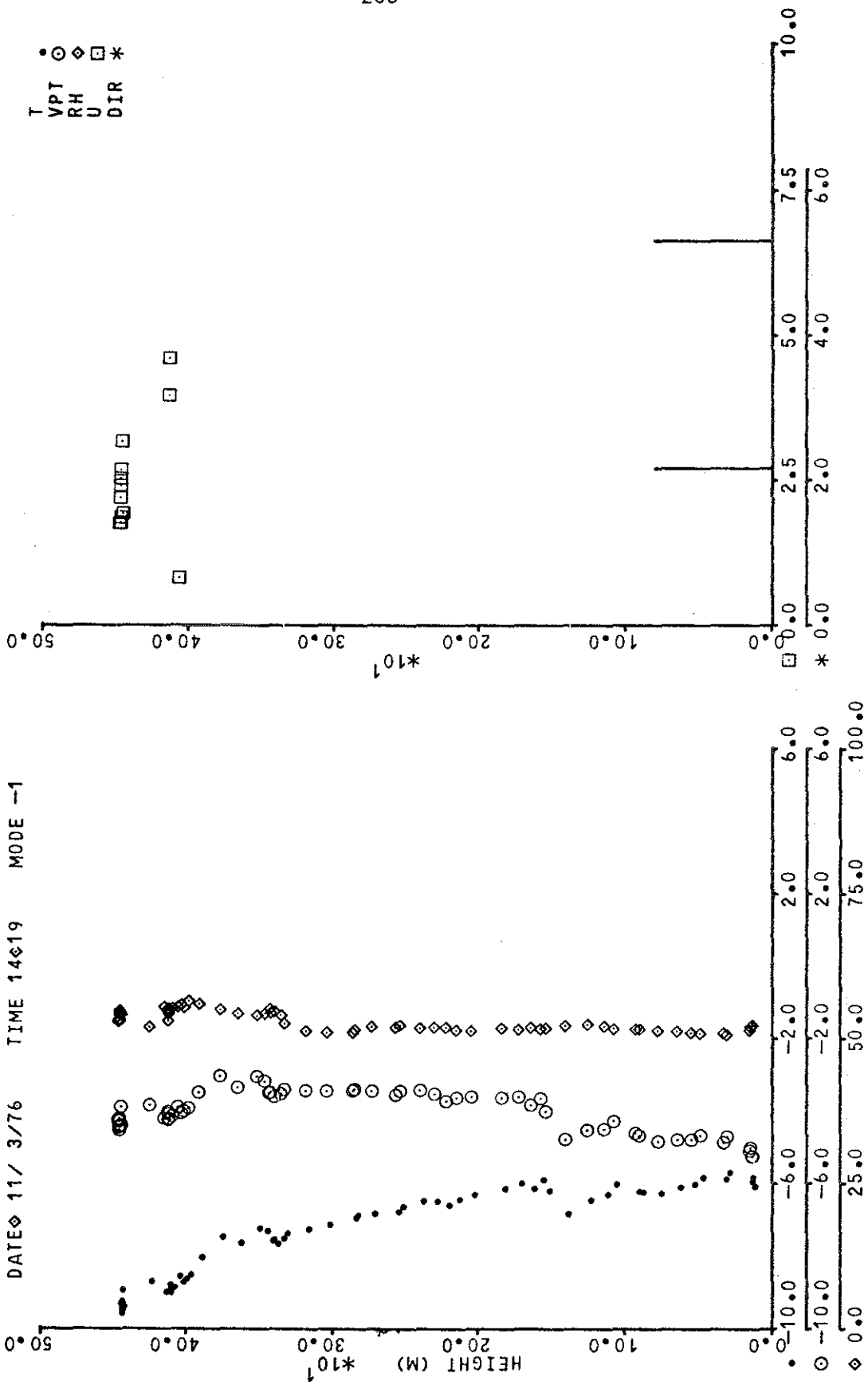
T
VPT
RH
U
DIR
DATE◇ 11/ 3/76 TIME 14◇19 MODE -1
HEIGHT (M) *10¹
*10¹

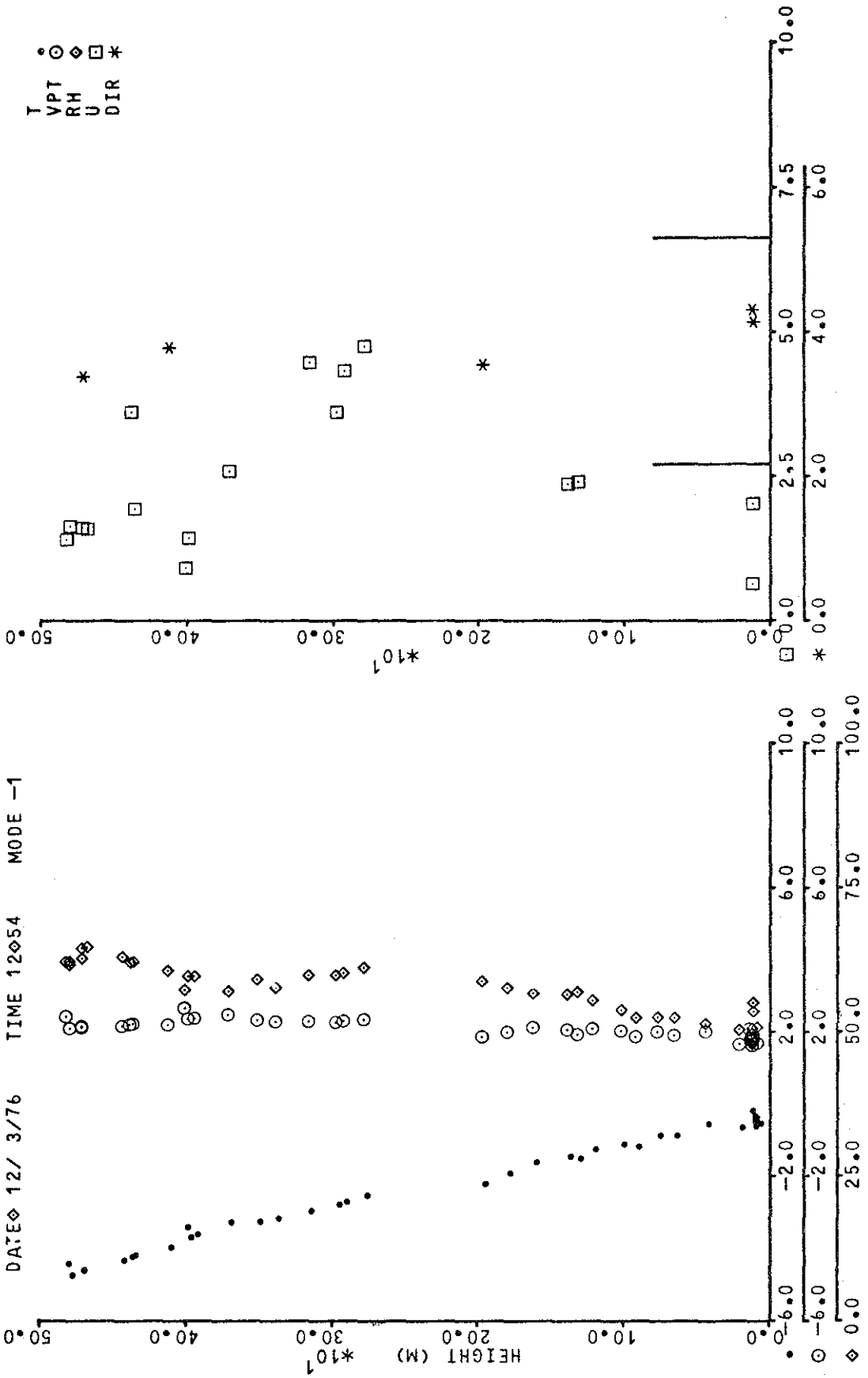
T
VPT
RH
U
DIR
HEIGHT (M) *10^1
DATE 12/ 3/76
TIME 1205
MODE -1

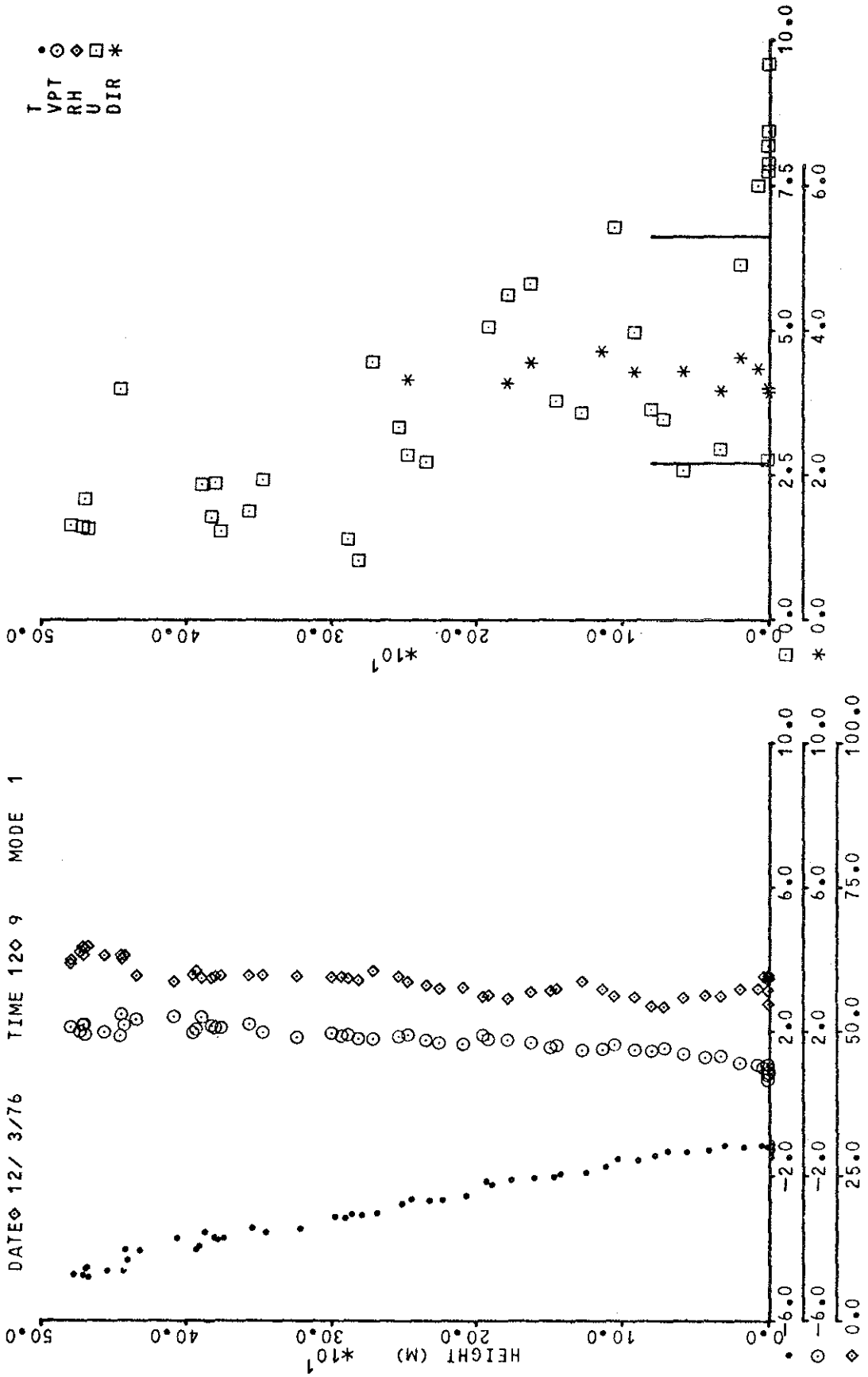
T
VPT
RH
U
DIR
DATE◇ 12/ 3/76 TIME 12◇ 9 MODE 1
HEIGHT (M) *10¹
*10¹

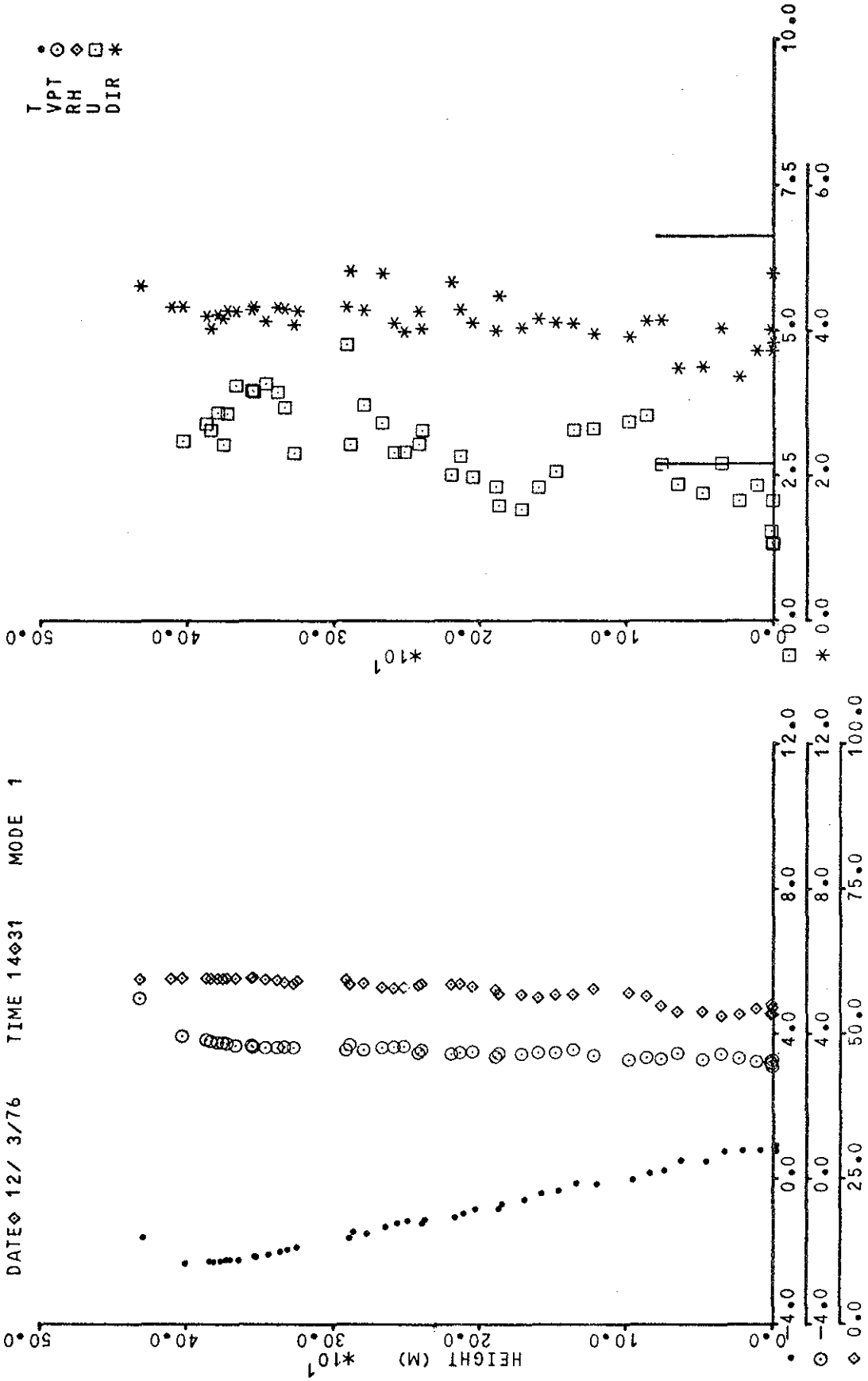
T
VPT
RH
U
DIR
DATE◇ 12/ 3/76 TIME 14◇31 MODE 1
HEIGHT (M) *10¹
*10¹
0.0
10.0
20.0
30.0
40.0
50.0
2.5
5.0
7.5
10.0
4.0
6.0
8.0
12.0
75.0
100.0
25.0
-4.0

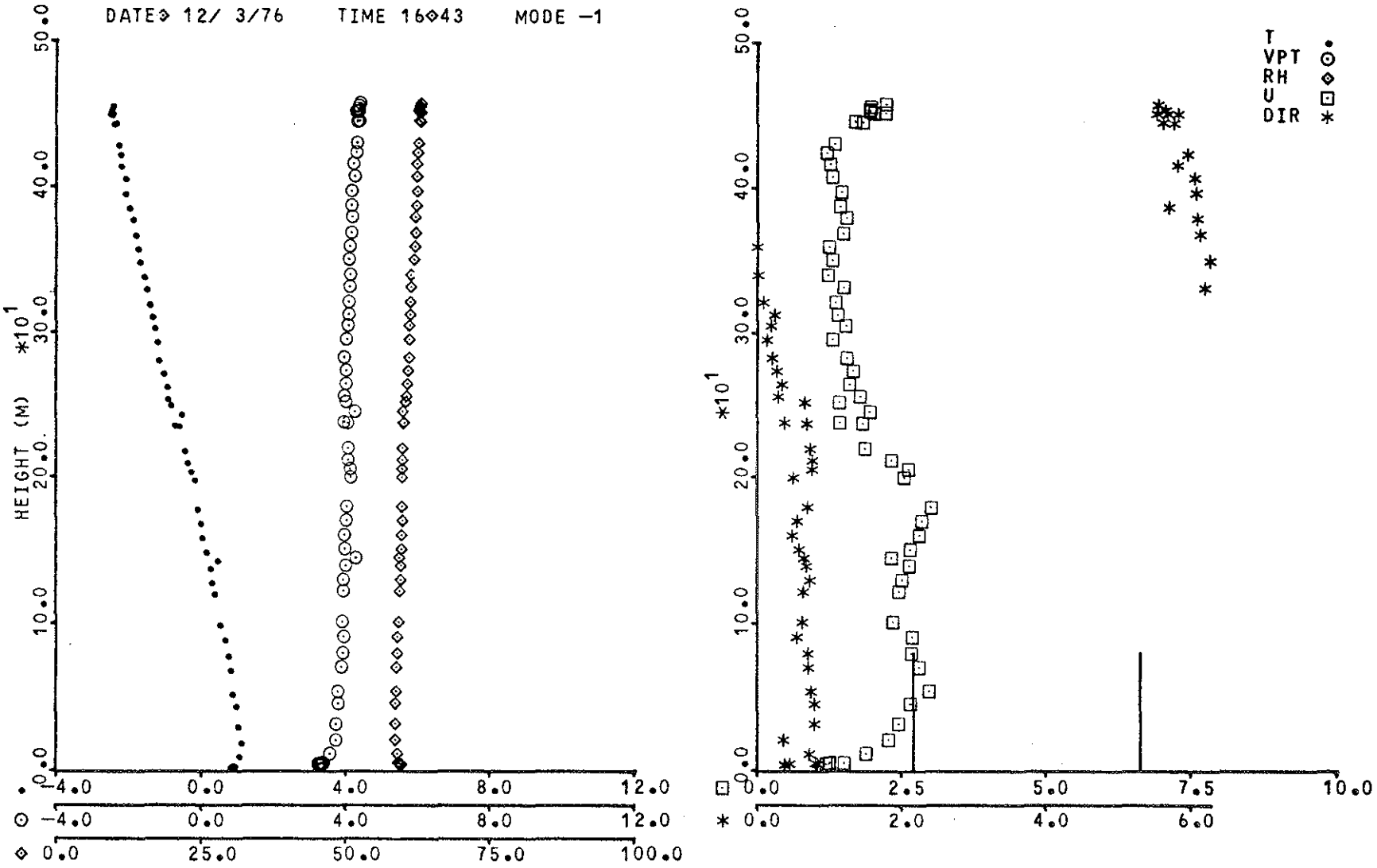
DATE⇒ 12/ 3/76
TIME 16◇43
MODE −1
HEIGHT (M)
*10^1
50.0
40.0
30.0
20.0
10.0
0.0
−4.0
0.0
4.0
8.0
12.0
25.0
50.0
75.0
100.0
T
VPT
RH
U
DIR
2.5
5.0
7.5
10.0
2.0
4.0
6.0

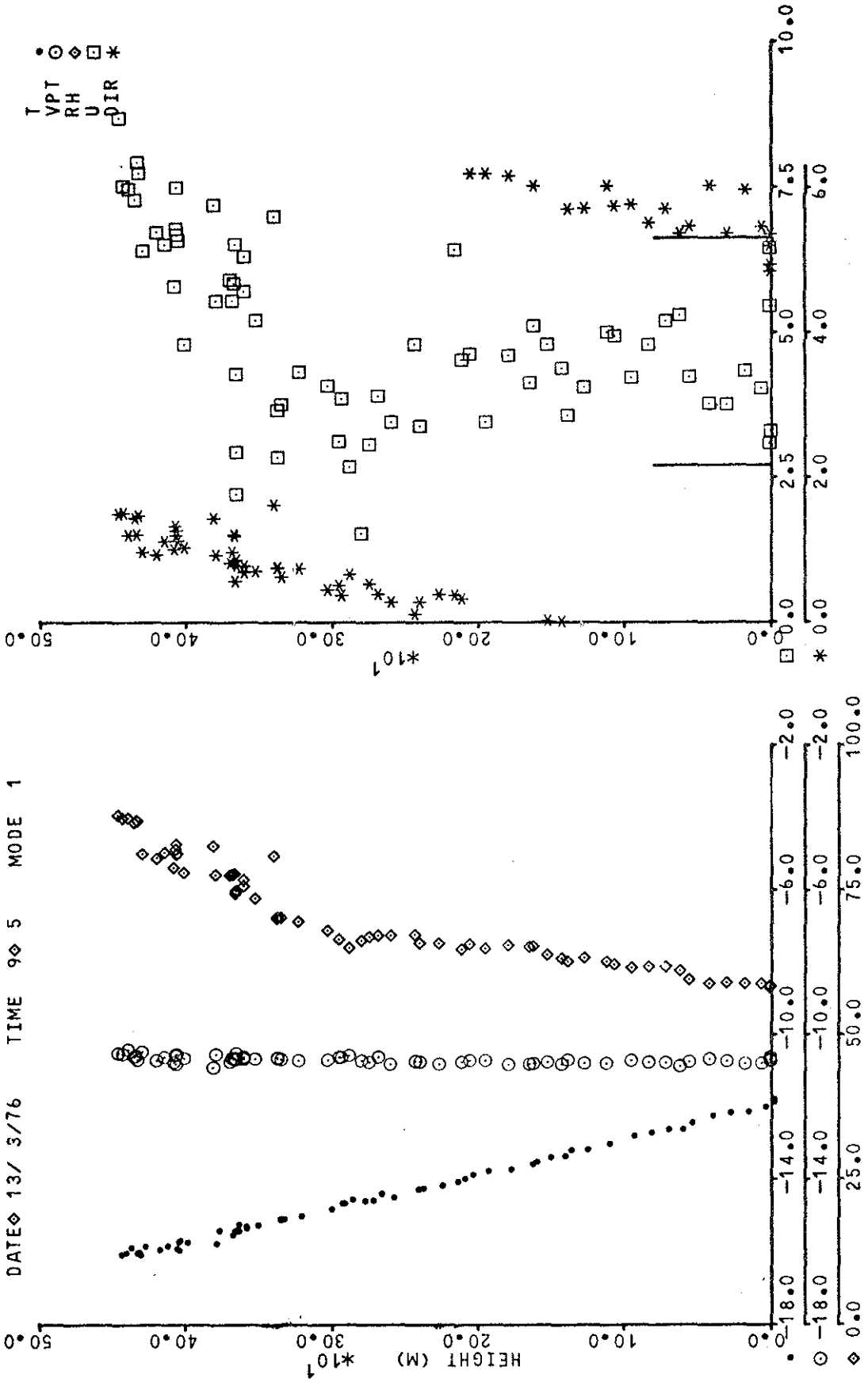
T
VPT
RH
U
DIR
HEIGHT (M) *10¹
DATE◇ 13/ 3/76 TIME 9◇ 5 MODE 1

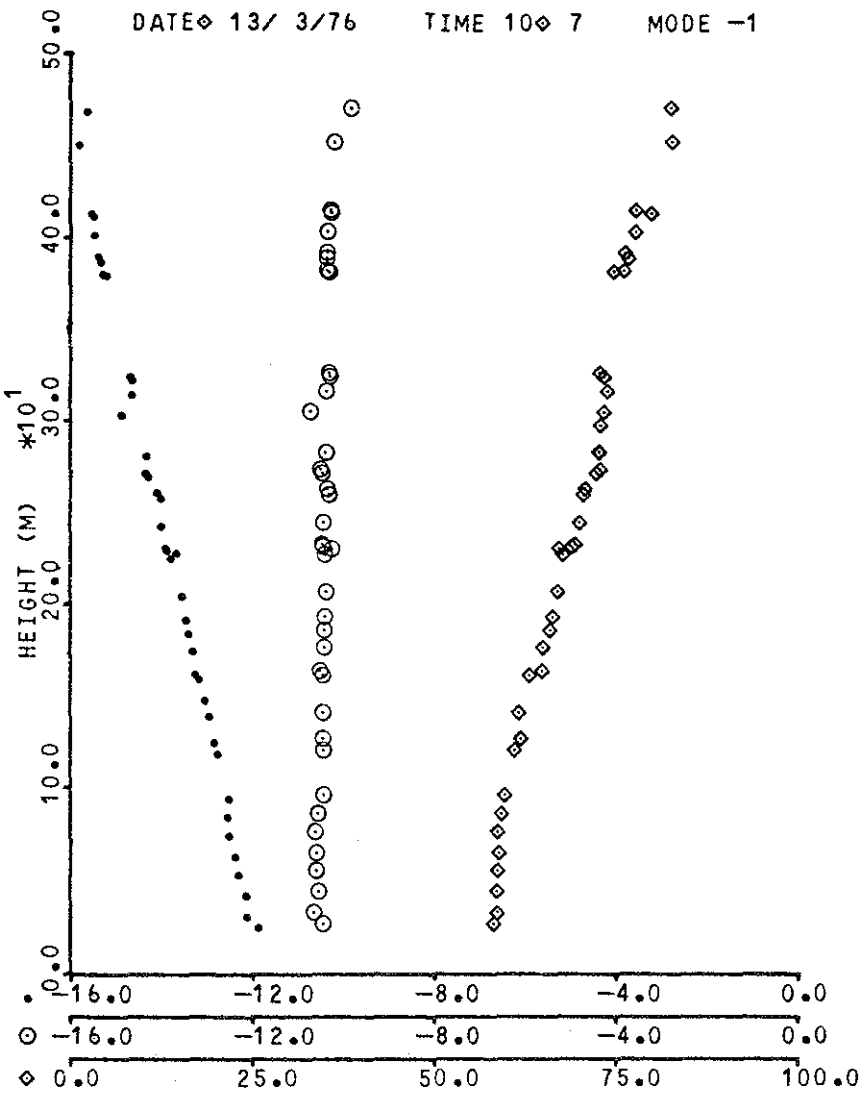
DATE◇ 13/ 3/76 TIME 10◇ 7 MODE -1
HEIGHT (M) *10^1
50.0
40.0
30.0
20.0
10.0
0.0
-16.0 -12.0 -8.0 -4.0 0.0
-16.0 -12.0 -8.0 -4.0 0.0
0.0 25.0 50.0 75.0 100.0

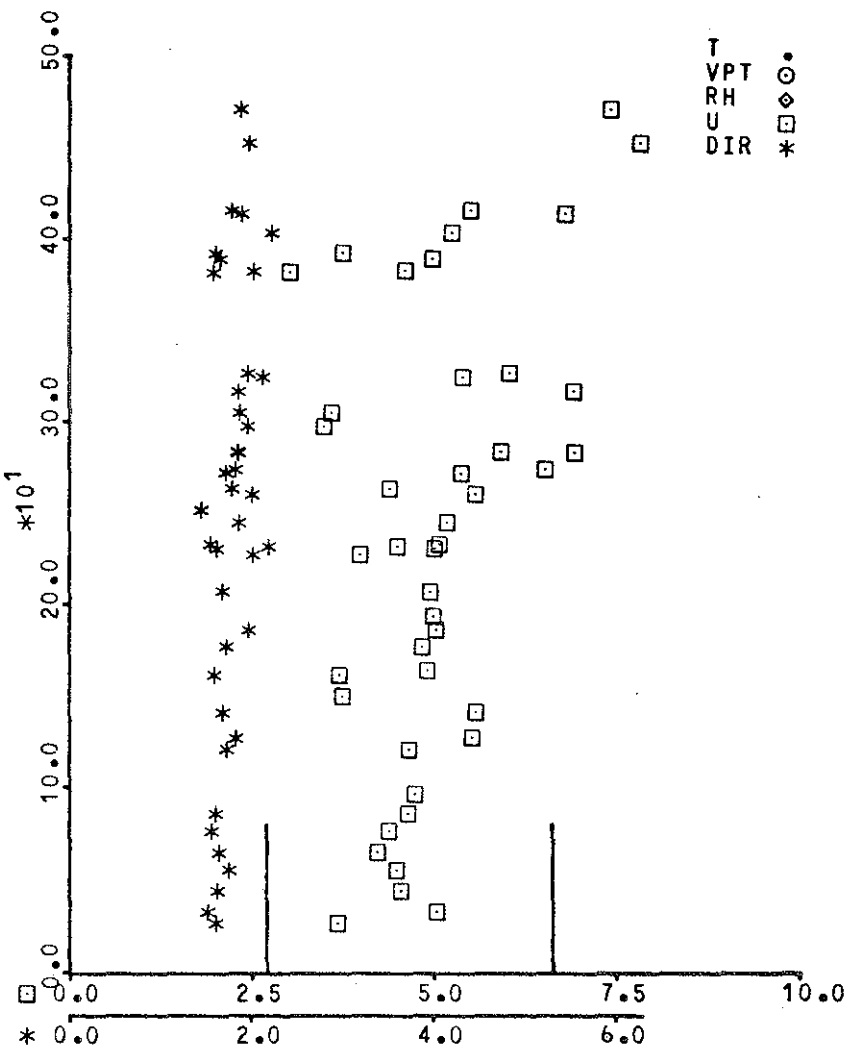
T •
VPT ⊙
RH ◇
U □
DIR *
*10^1
50.0
40.0
30.0
20.0
10.0
0.0
0.0 2.5 5.0 7.5 10.0
0.0 2.0 4.0 6.0

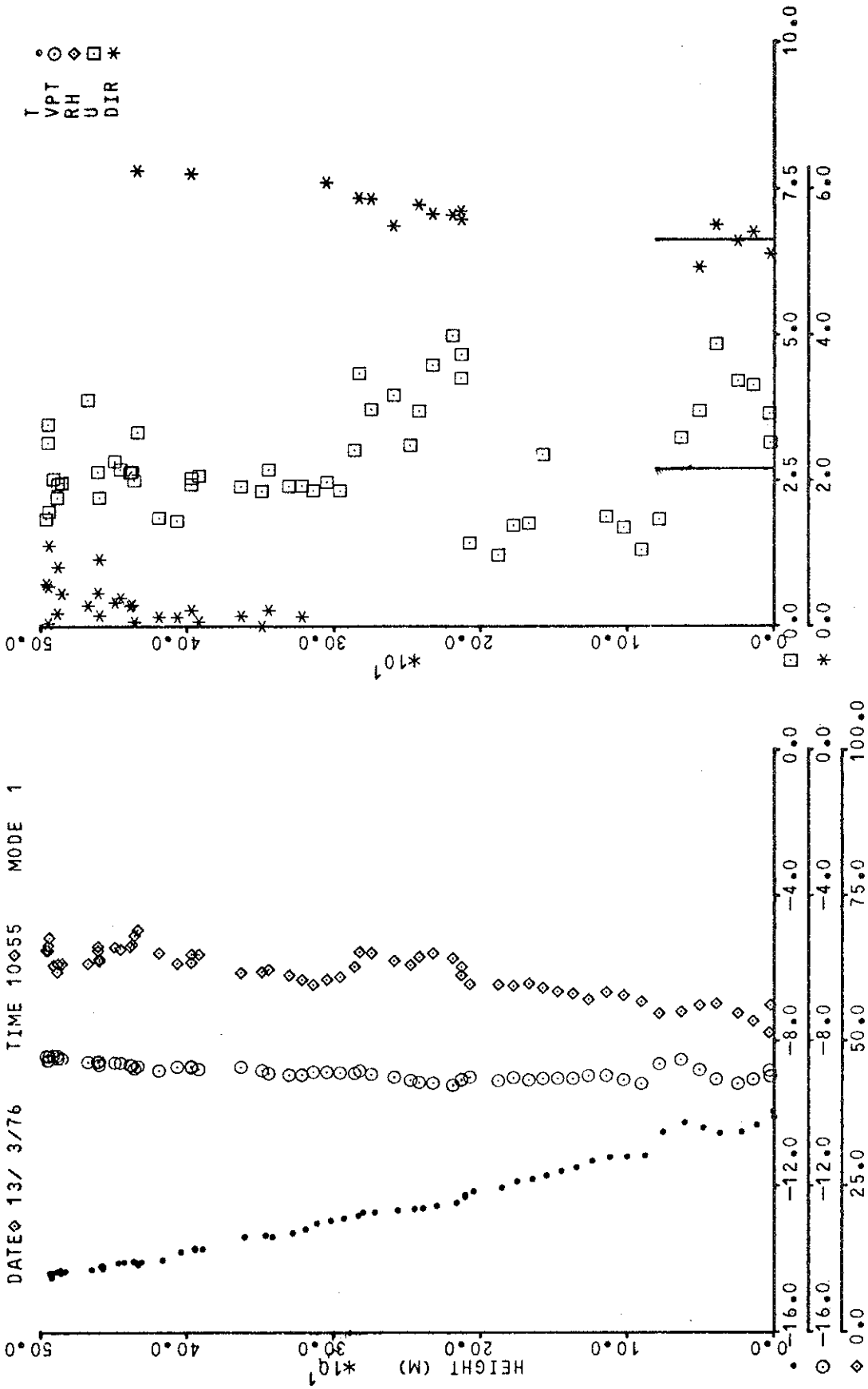
T
VPT
RH
U
DIR
*10¹
DATE◇ 13/ 3/76
TIME 10◇55
MODE 1
HEIGHT (M)
*10¹

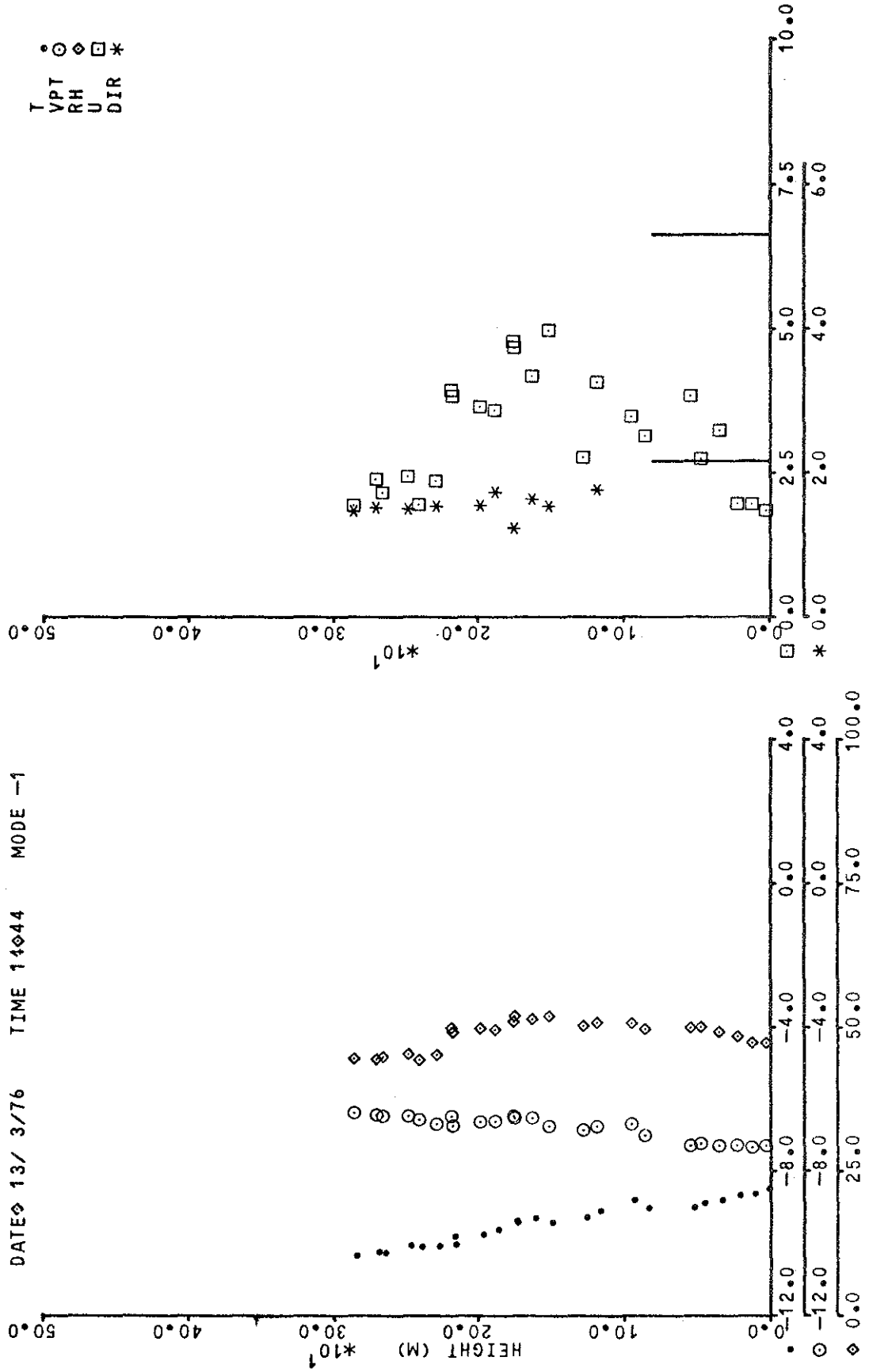
T
VPT
RH
U
DIR
DATE⋄ 13/ 3/76 TIME 14⋄44 MODE −1
HEIGHT (M) *10¹
*10¹

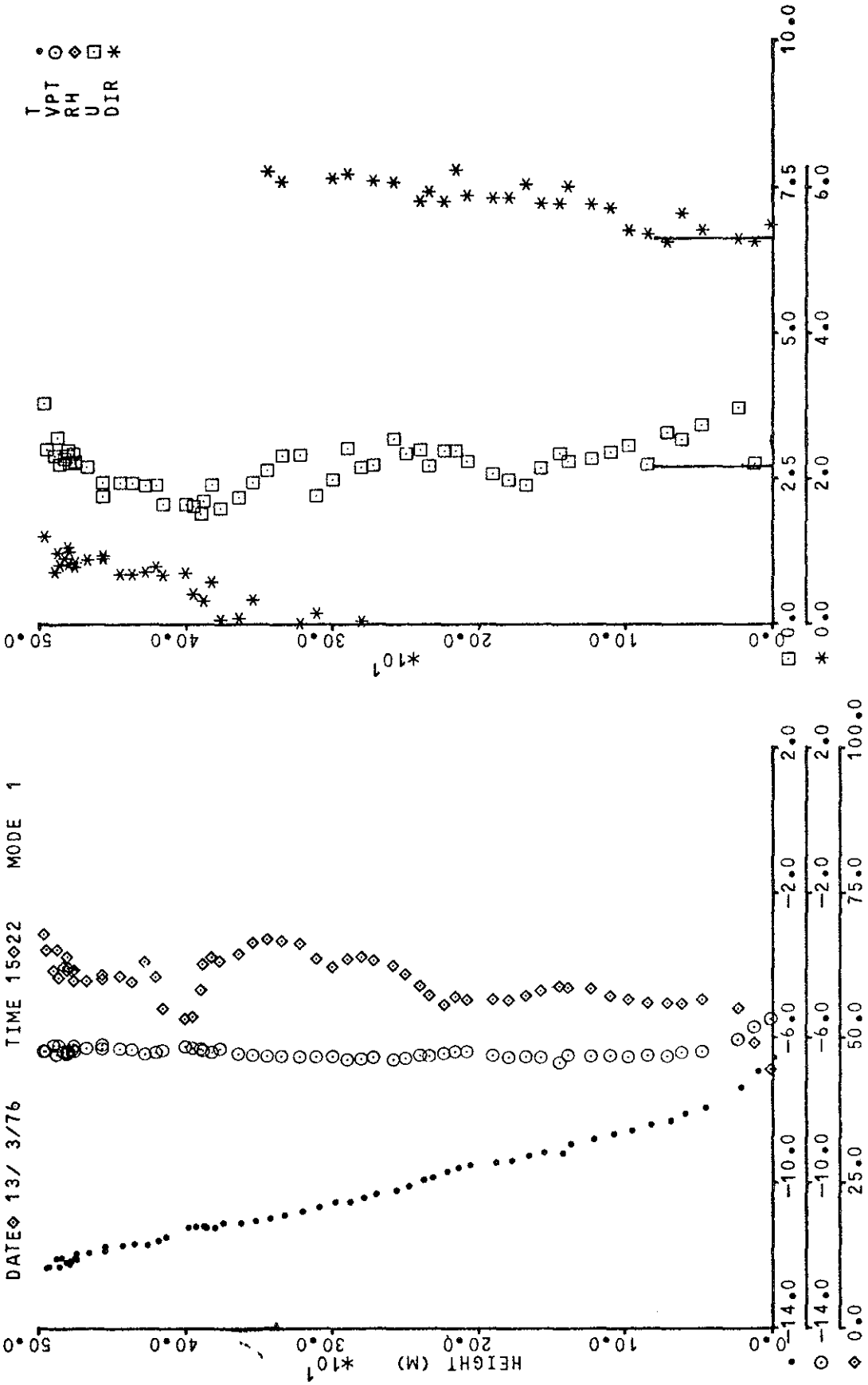
T
VPT
RH
U
DIR
*10¹
HEIGHT (M) *10¹
DATE◇ 13/ 3/76 TIME 15◇22 MODE 1

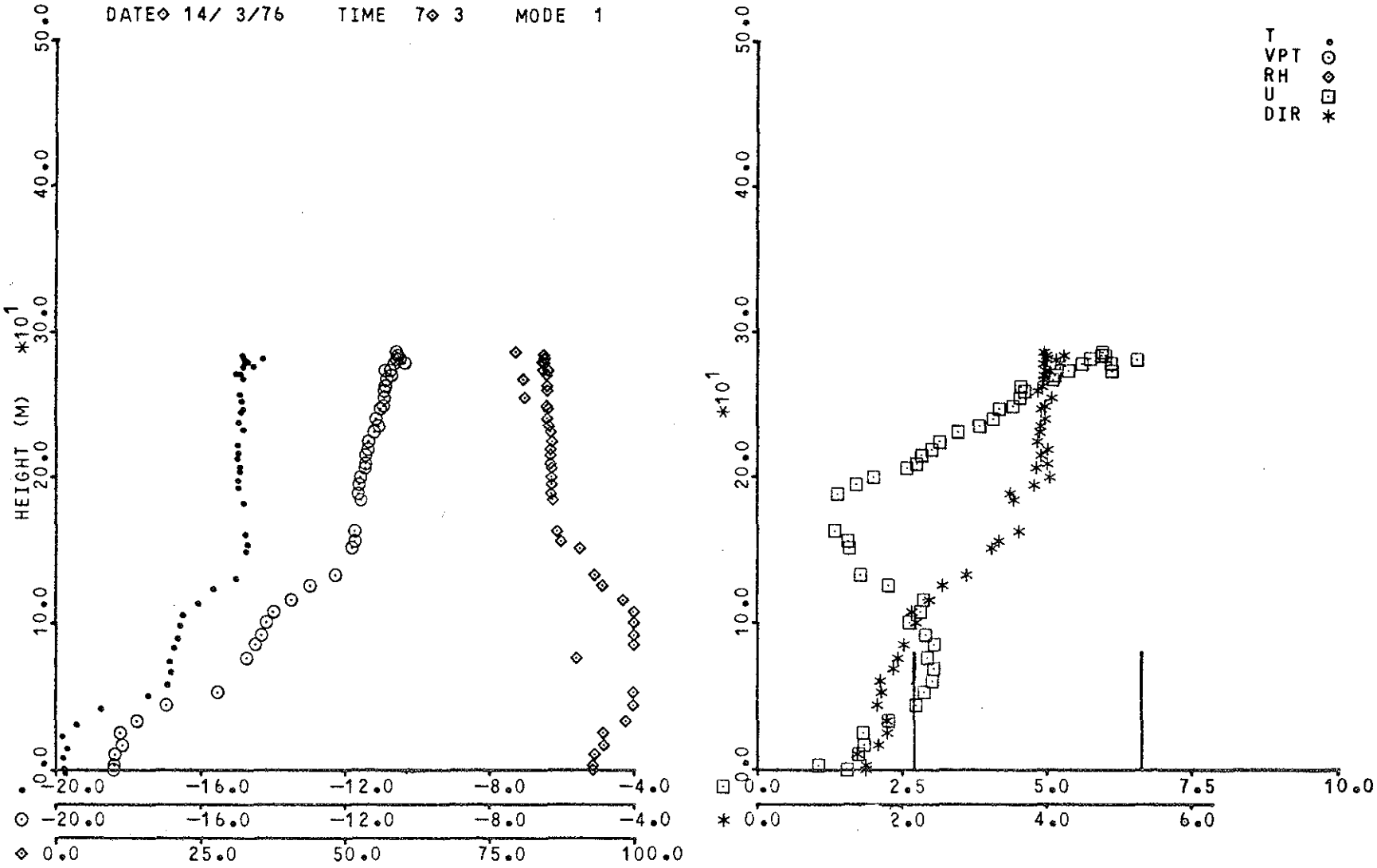
DATE◇ 14/ 3/76 TIME 7◇ 3 MODE 1
HEIGHT (M) *10^1
50.0
40.0
30.0
20.0
10.0
0.0
• −20.0 −16.0 −12.0 −8.0 −4.0
⊙ −20.0 −16.0 −12.0 −8.0 −4.0
◇ 0.0 25.0 50.0 75.0 100.0
T •
VPT ⊙
RH ◇
U ⊡
DIR *
*10^1
⊡ 0.0 2.5 5.0 7.5 10.0
* 0.0 2.0 4.0 6.0

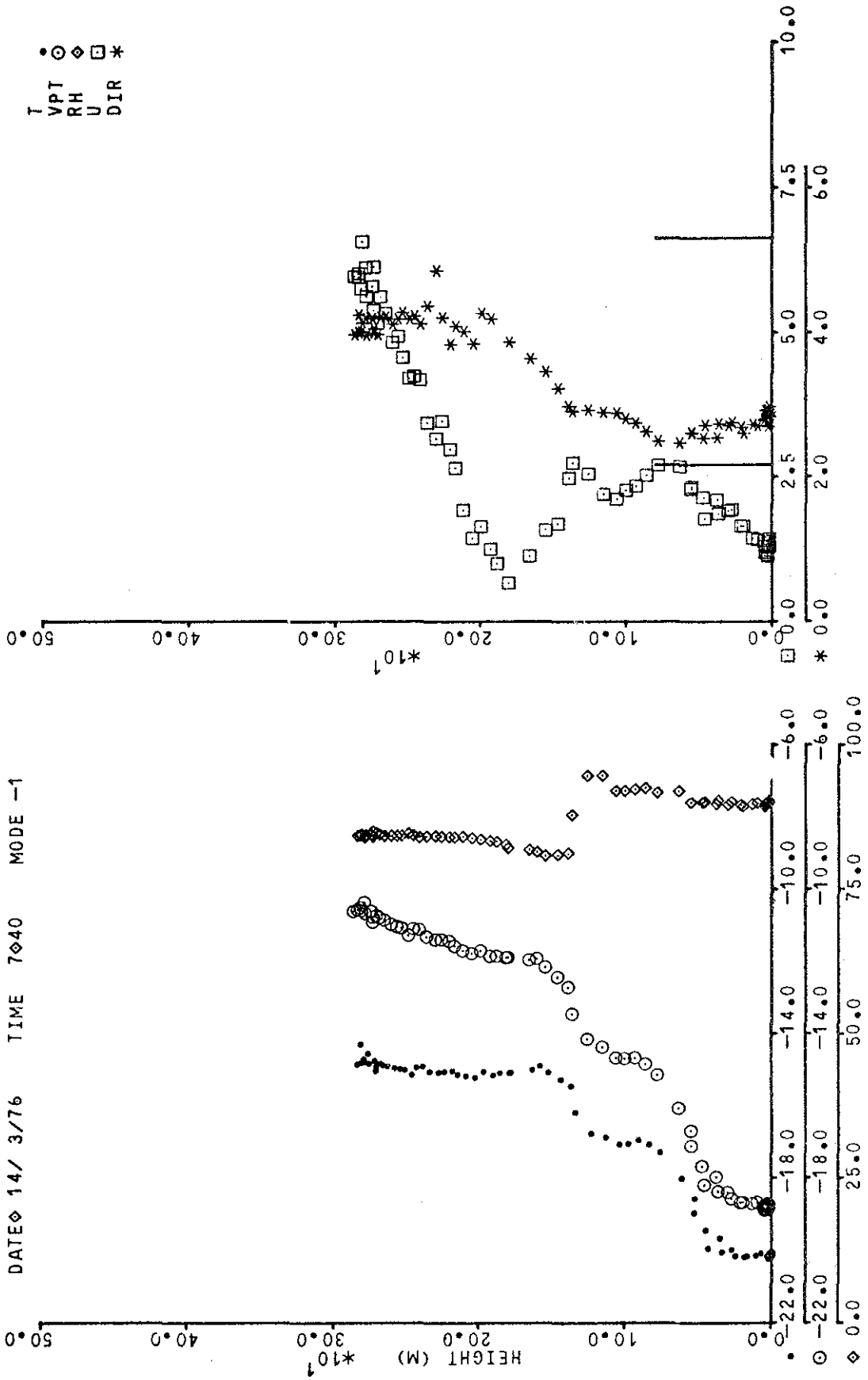
T
VPT
RH
U
DIR
DATE◇ 14/ 3/76 TIME 7◇40 MODE −1
HEIGHT (M) *10¹
*10¹

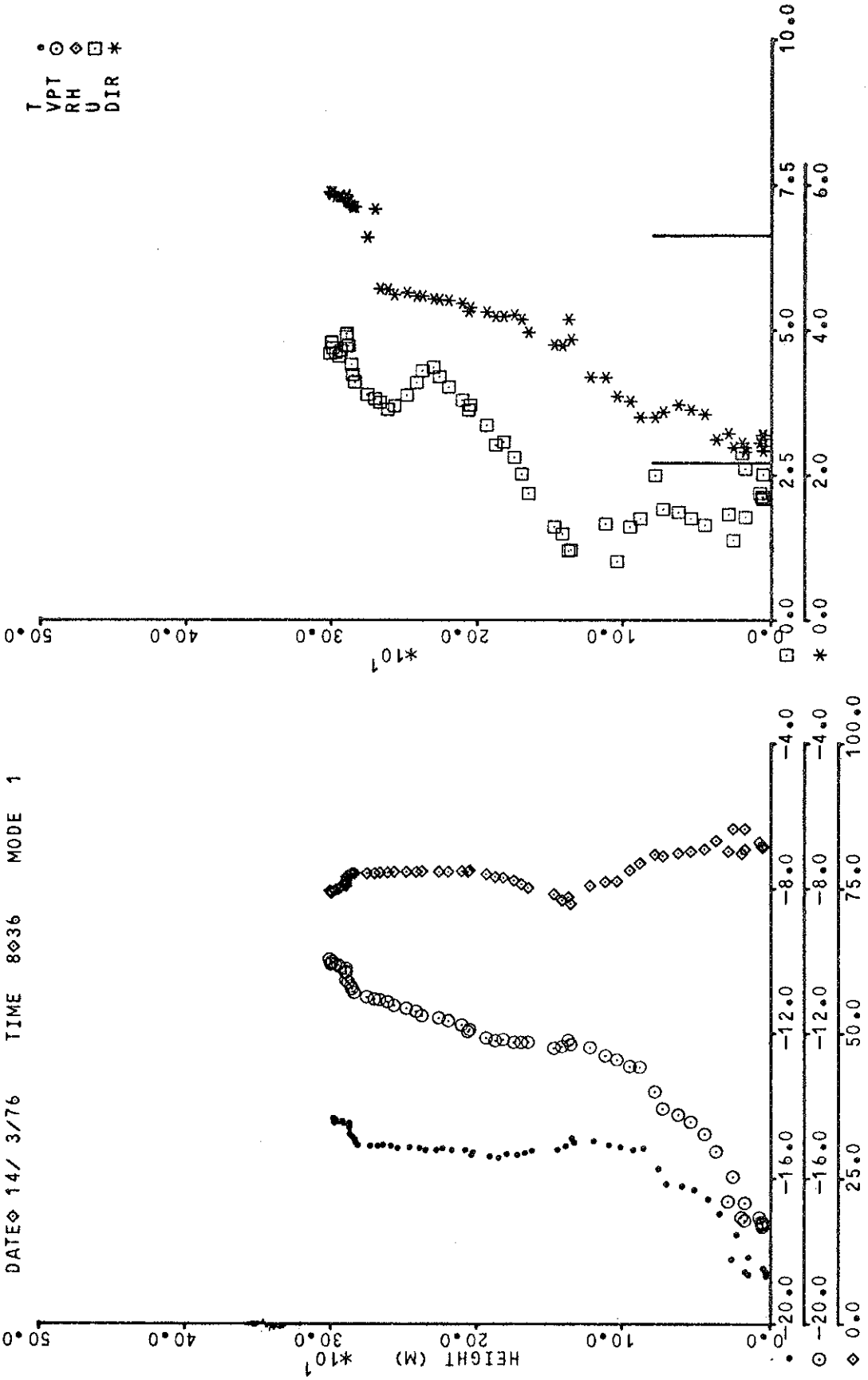
T
VPT
RH
U
DIR
HEIGHT (M) *10¹
DATE◇ 14/ 3/76 TIME 8◇36 MODE 1

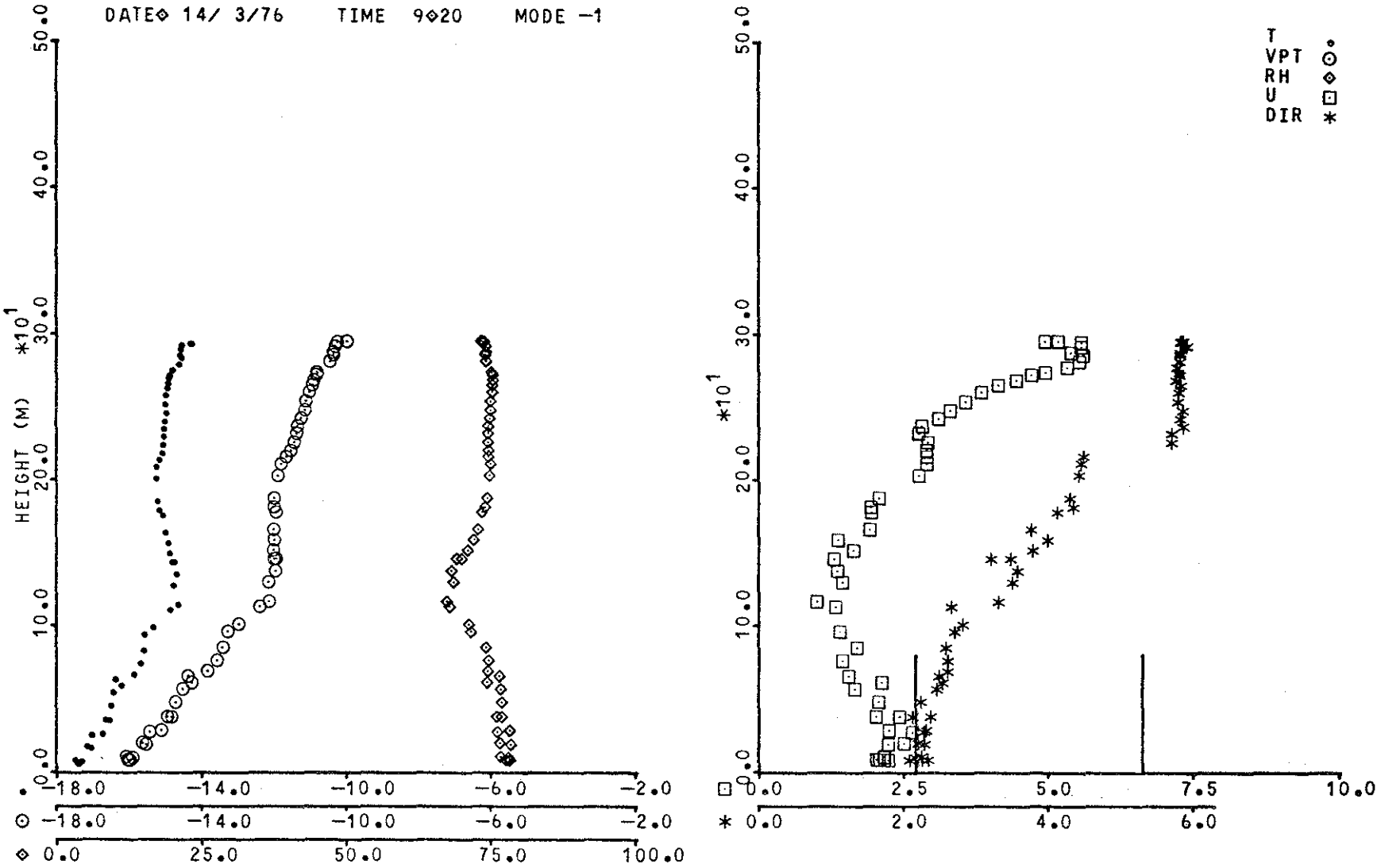
DATE◇ 14/ 3/76 TIME 9◇20 MODE -1
HEIGHT (M) *10^1
50.0
40.0
30.0
20.0
10.0
0.0
-18.0
-14.0
-10.0
-6.0
-2.0
0.0
25.0
50.0
75.0
100.0
T
VPT
RH
U
DIR
2.5
5.0
7.5
10.0
2.0
4.0
6.0

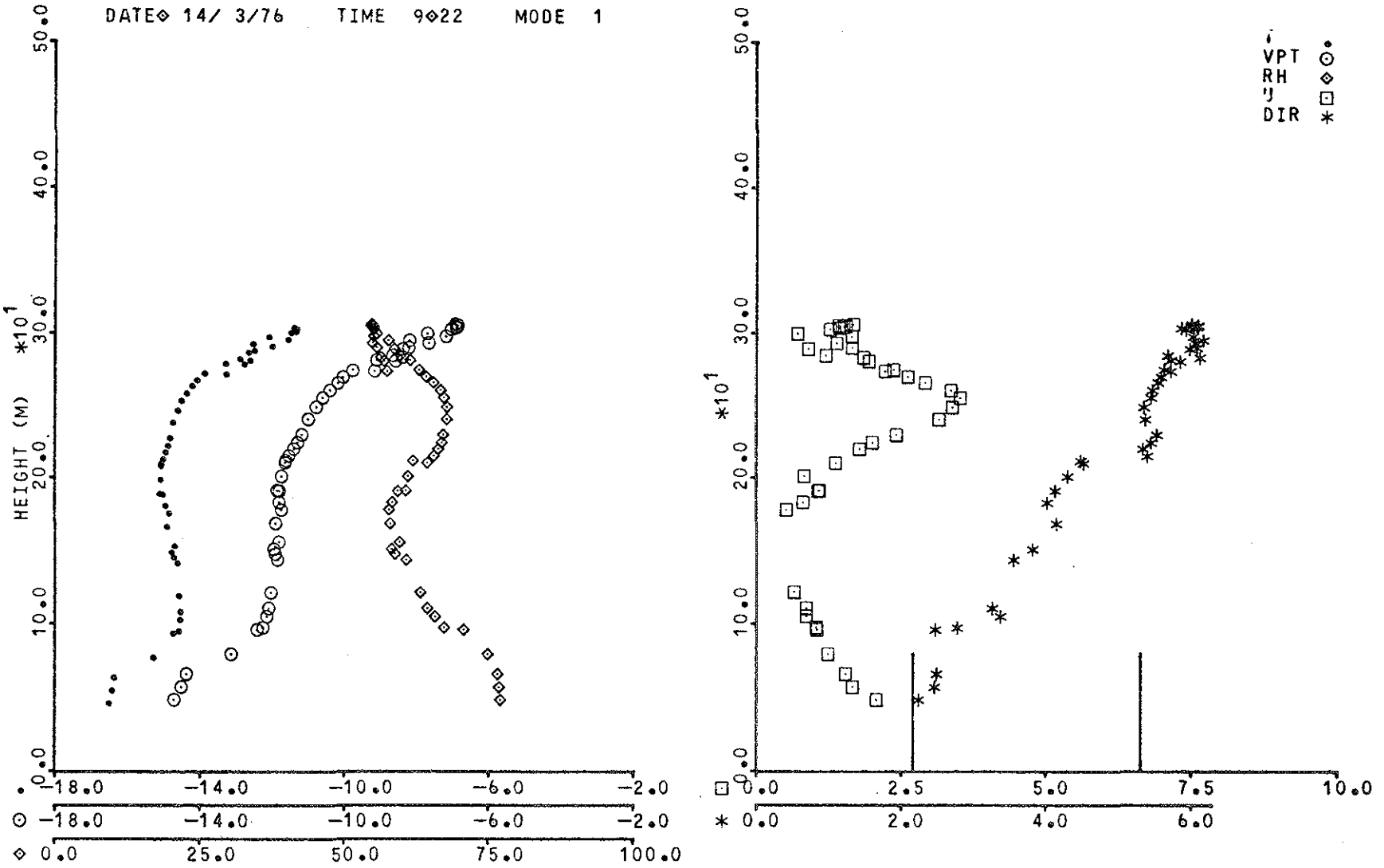
DATE◇ 14/ 3/76 TIME 9◇22 MODE 1
HEIGHT (M) *10^1
50.0
40.0
30.0
20.0
10.0
0.0
−18.0
−14.0
−10.0
−6.0
−2.0
0.0
25.0
50.0
75.0
100.0
VPT
RH
DIR
*10^1
2.5
5.0
7.5
10.0
2.0
4.0
6.0

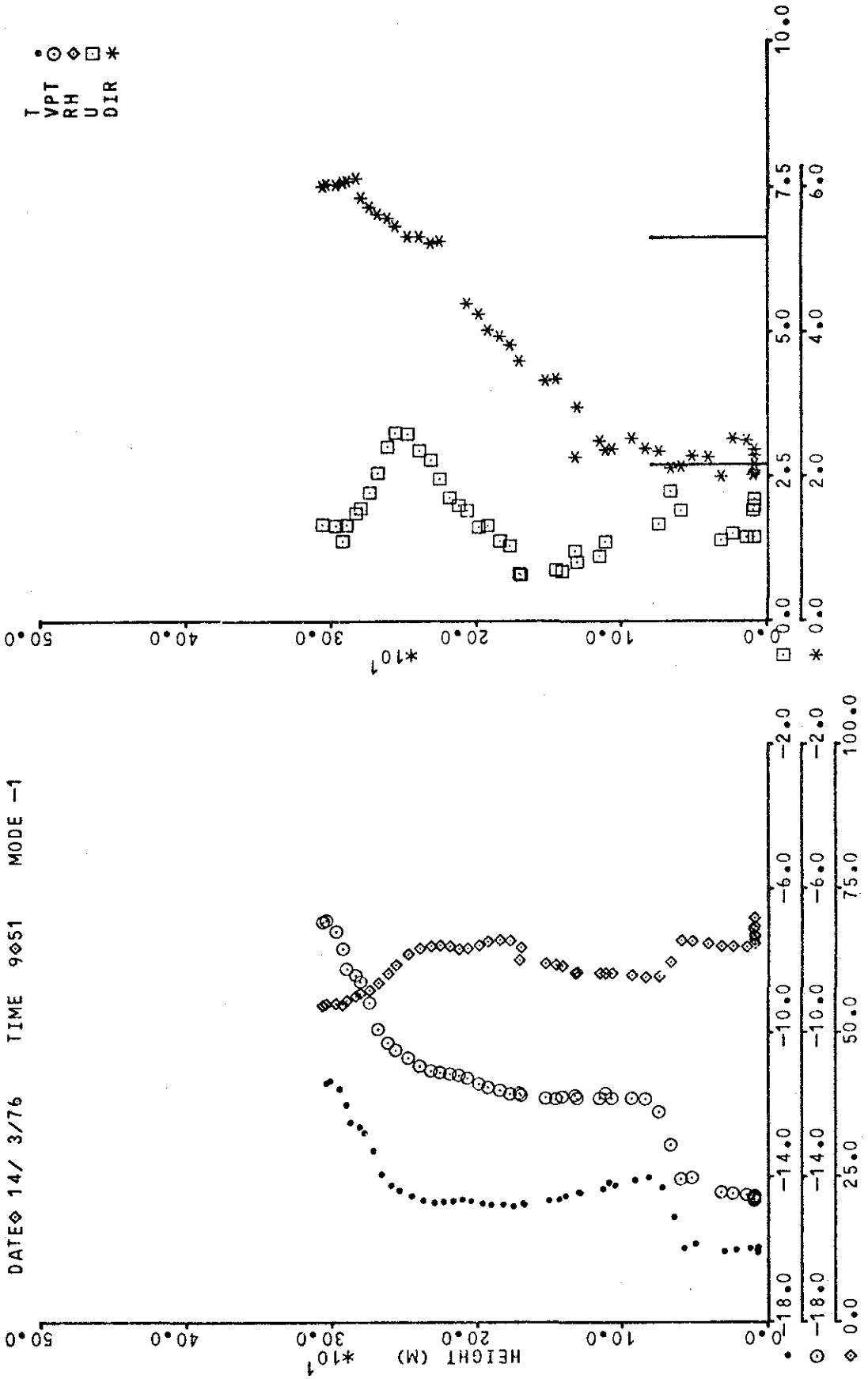
DATE◇ 14/ 3/76 TIME 9◇51 MODE −1
T
VPT
RH
U
DIR
HEIGHT (M) *10¹
*10¹
0.0
10.0
20.0
30.0
40.0
50.0
−18.0
−14.0
−10.0
−6.0
−2.0
0.0
25.0
50.0
75.0
100.0
2.5
5.0
7.5
10.0
2.0
4.0
6.0

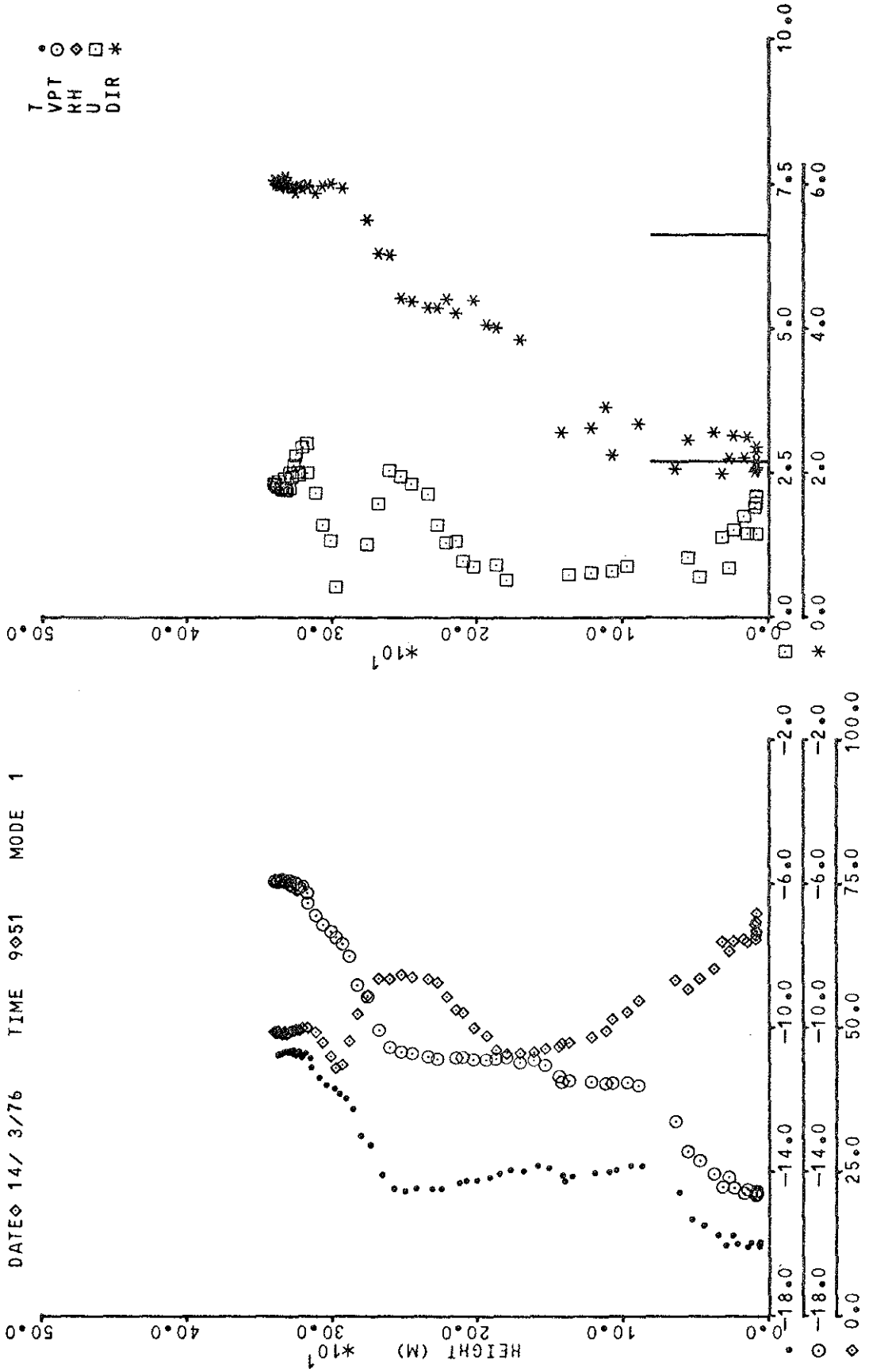
T
VPT
RH
U
DIR
DATE◇ 14/ 3/76 TIME 9◇51 MODE 1
HEIGHT (M) *10¹
*10¹

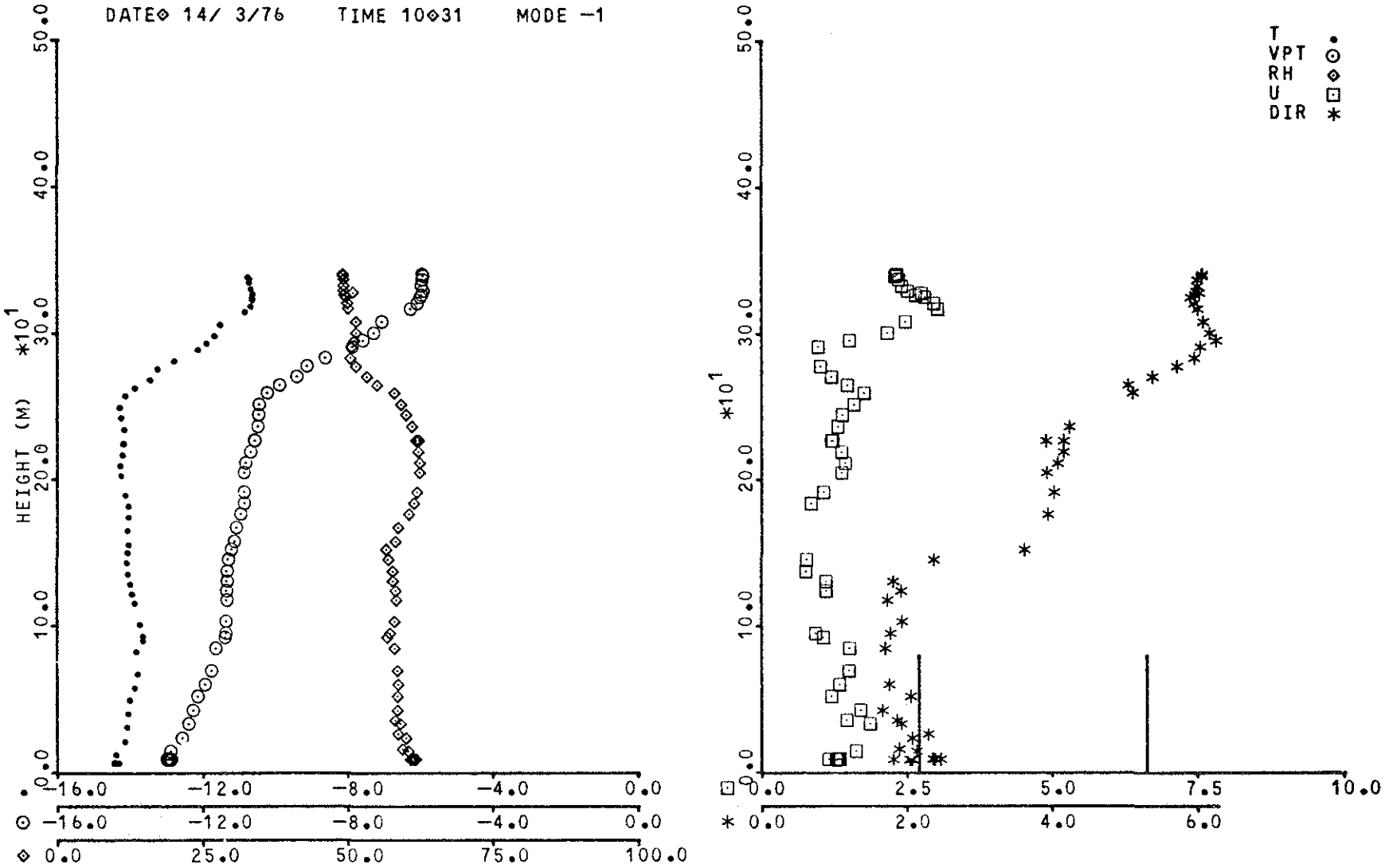
DATE⋄ 14/ 3/76
TIME 10⋄31
MODE −1
HEIGHT (M) *10^1
0.0
10.0
20.0
30.0
40.0
50.0
−16.0
−12.0
−8.0
−4.0
0.0
25.0
50.0
75.0
100.0
T
VPT
RH
U
DIR
2.5
5.0
7.5
10.0
2.0
4.0
6.0

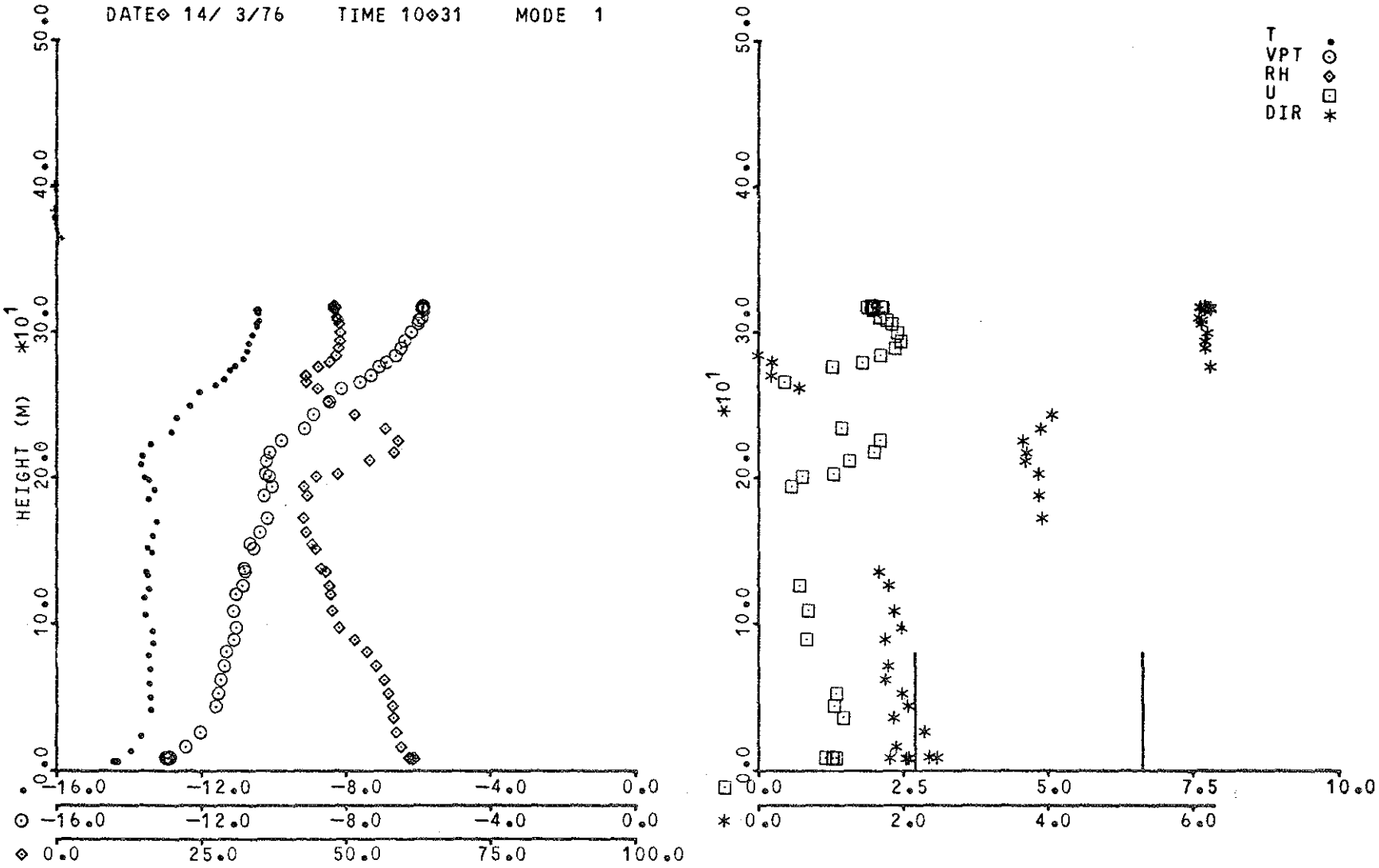
DATE◇ 14/ 3/76 TIME 10◇31 MODE 1
HEIGHT (M) *10^1
50.0
40.0
30.0
20.0
10.0
0.0
−16.0 −12.0 −8.0 −4.0 0.0
−16.0 −12.0 −8.0 −4.0 0.0
0.0 25.0 50.0 75.0 100.0
*10^1
0.0 2.5 5.0 7.5 10.0
0.0 2.0 4.0 6.0
T
VPT
RH
U
DIR

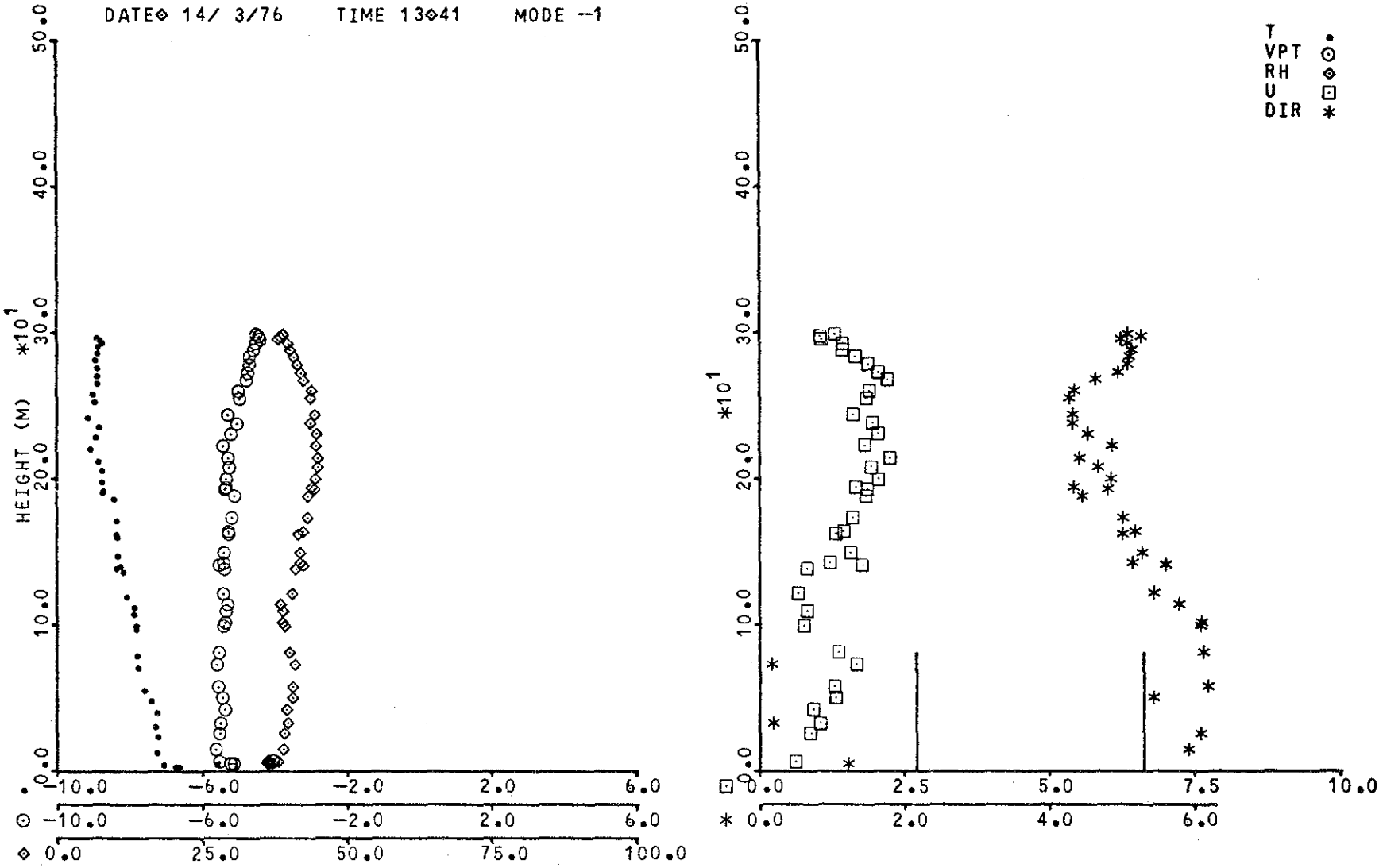
DATE◇ 14/ 3/76 TIME 13◇41 MODE -1
HEIGHT (M) *10^1
50.0
40.0
30.0
20.0
10.0
0.0
-10.0 -6.0 -2.0 2.0 6.0
-10.0 -6.0 -2.0 2.0 6.0
0.0 25.0 50.0 75.0 100.0
*10^1
0.0 2.5 5.0 7.5 10.0
0.0 2.0 4.0 6.0
T •
VPT ⊙
RH ◇
U □
DIR *

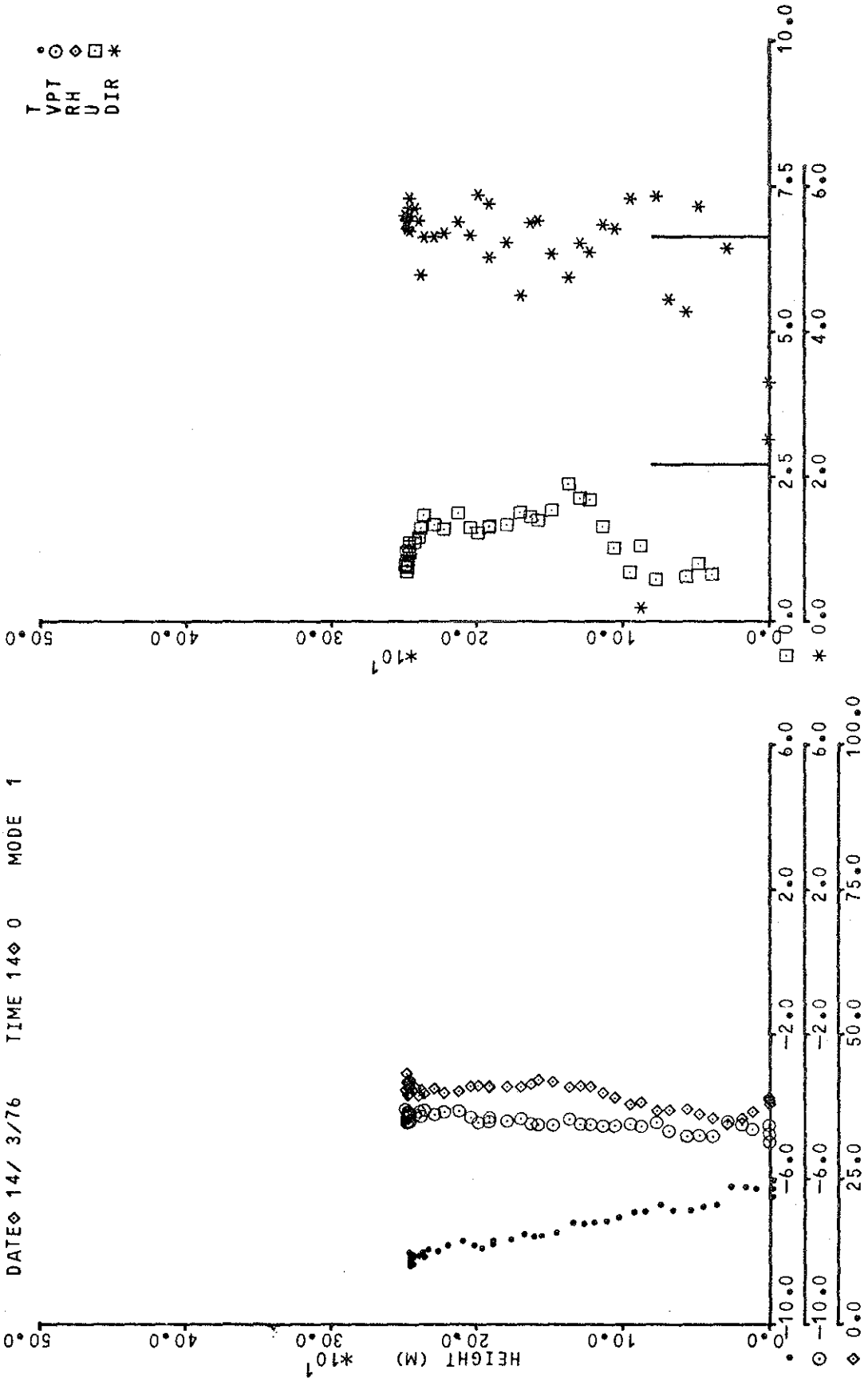
T
VPT
RH
U
DIR
DATE◇ 14/ 3/76 TIME 14◇ 0 MODE 1
HEIGHT (M) *10¹
*10¹

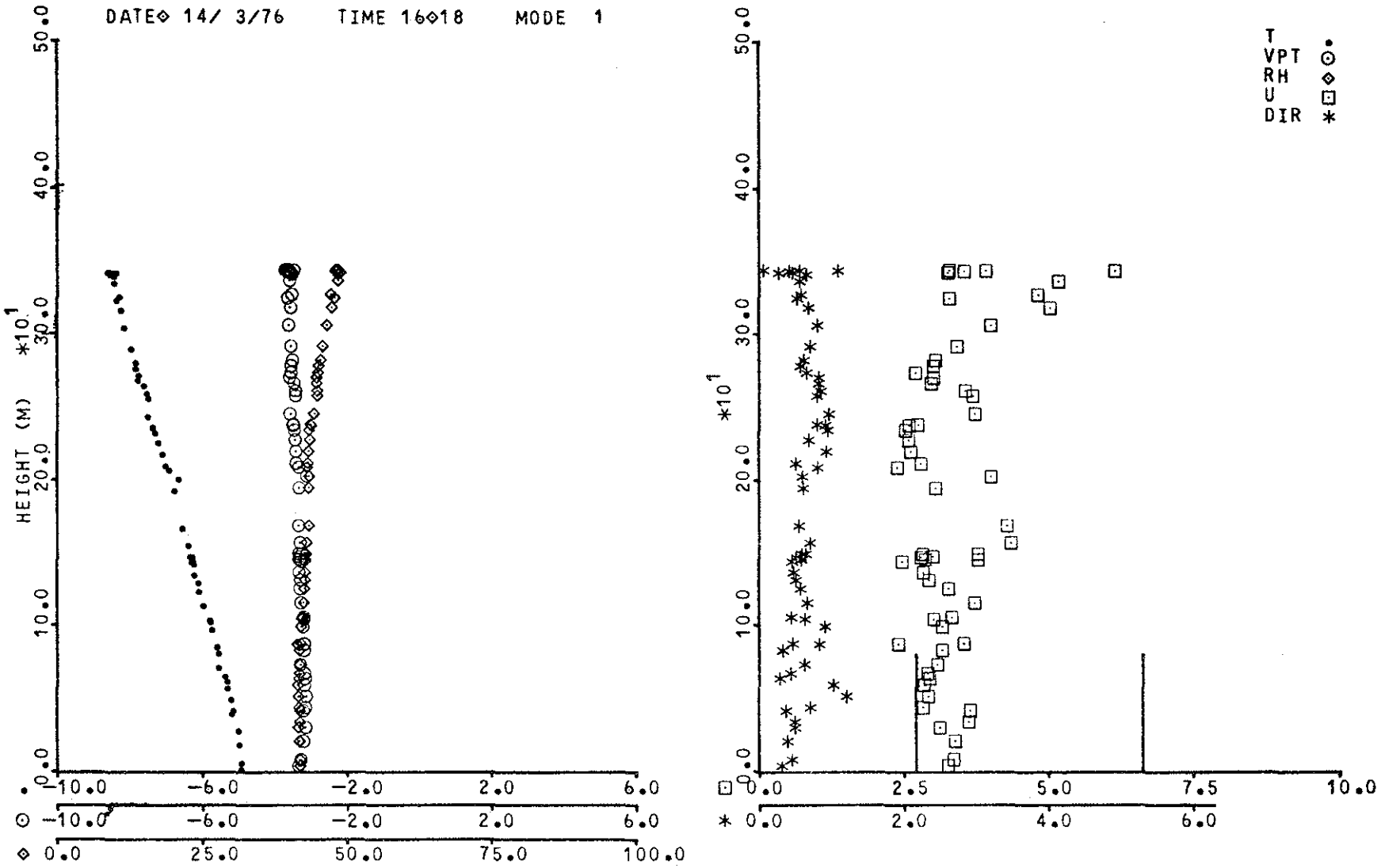
DATE◇ 14/ 3/76 TIME 16◇18 MODE 1
HEIGHT (M) *10^1
50.0
40.0
30.0
20.0
10.0
0.0
-10.0
-6.0
-2.0
2.0
6.0
0.0
25.0
50.0
75.0
100.0
T
VPT
RH
U
DIR
2.5
5.0
7.5
10.0
4.0

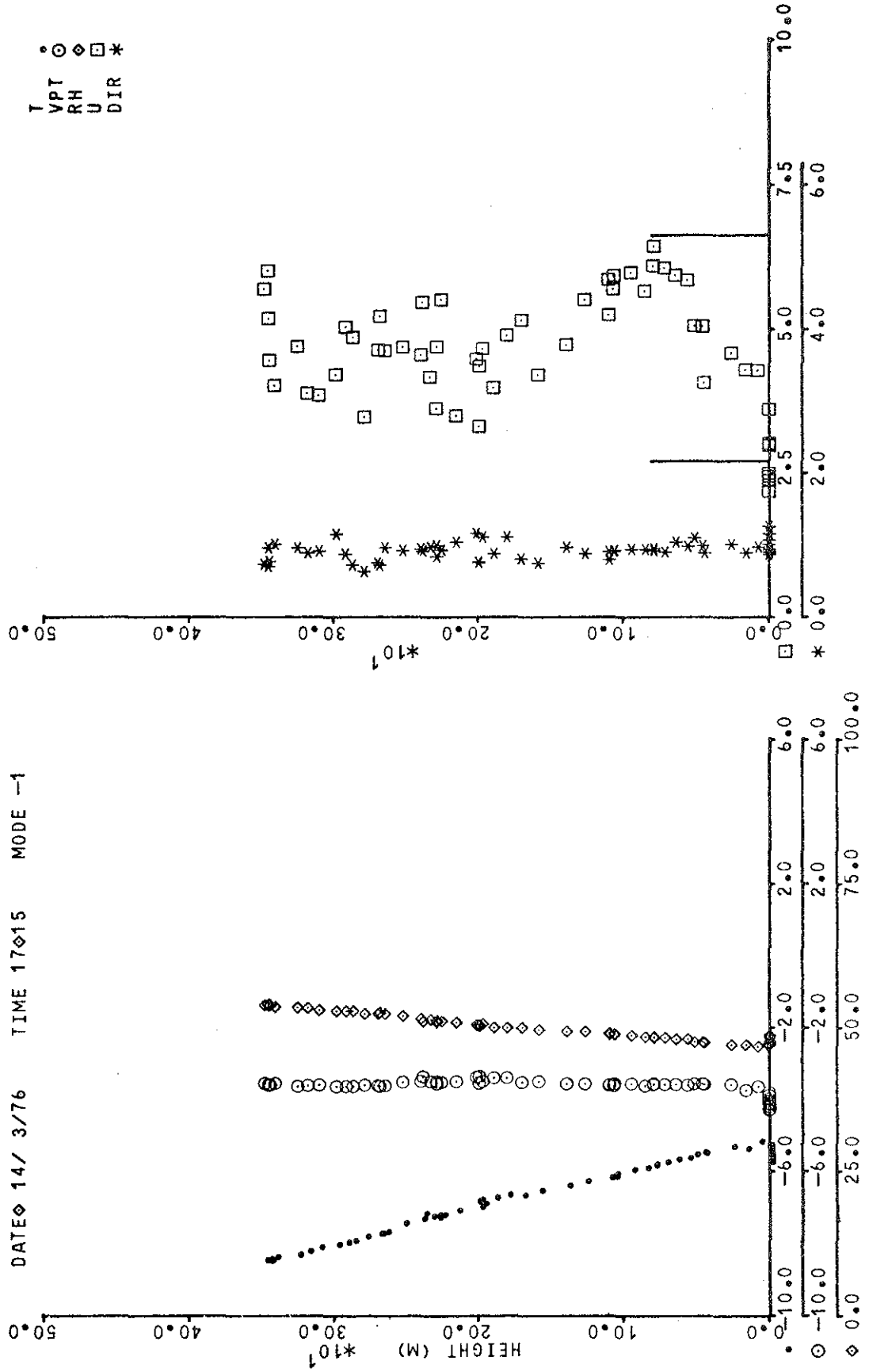
T
VPT
RH
U
DIR
DATE◇ 14/ 3/76 TIME 17◇15 MODE −1
HEIGHT (M) *10¹
*10¹

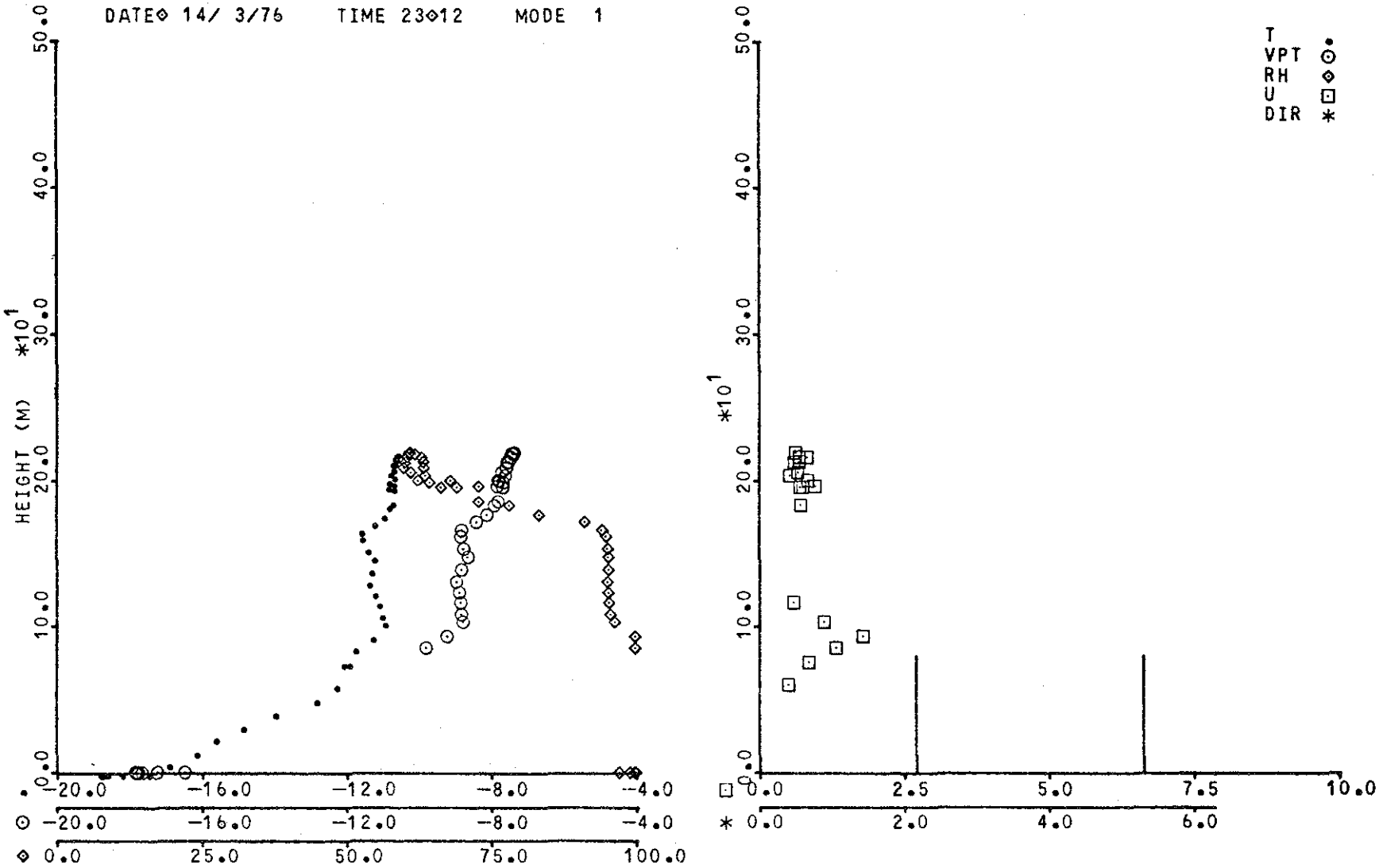
DATE◇ 14/ 3/76 TIME 23◇12 MODE 1
HEIGHT (M) *10^1
50.0
40.0
30.0
20.0
10.0
0.0
−20.0 −16.0 −12.0 −8.0 −4.0
−20.0 −16.0 −12.0 −8.0 −4.0
0.0 25.0 50.0 75.0 100.0
T
VPT
RH
U
DIR
*10^1
0.0 2.5 5.0 7.5 10.0
0.0 2.0 4.0 6.0

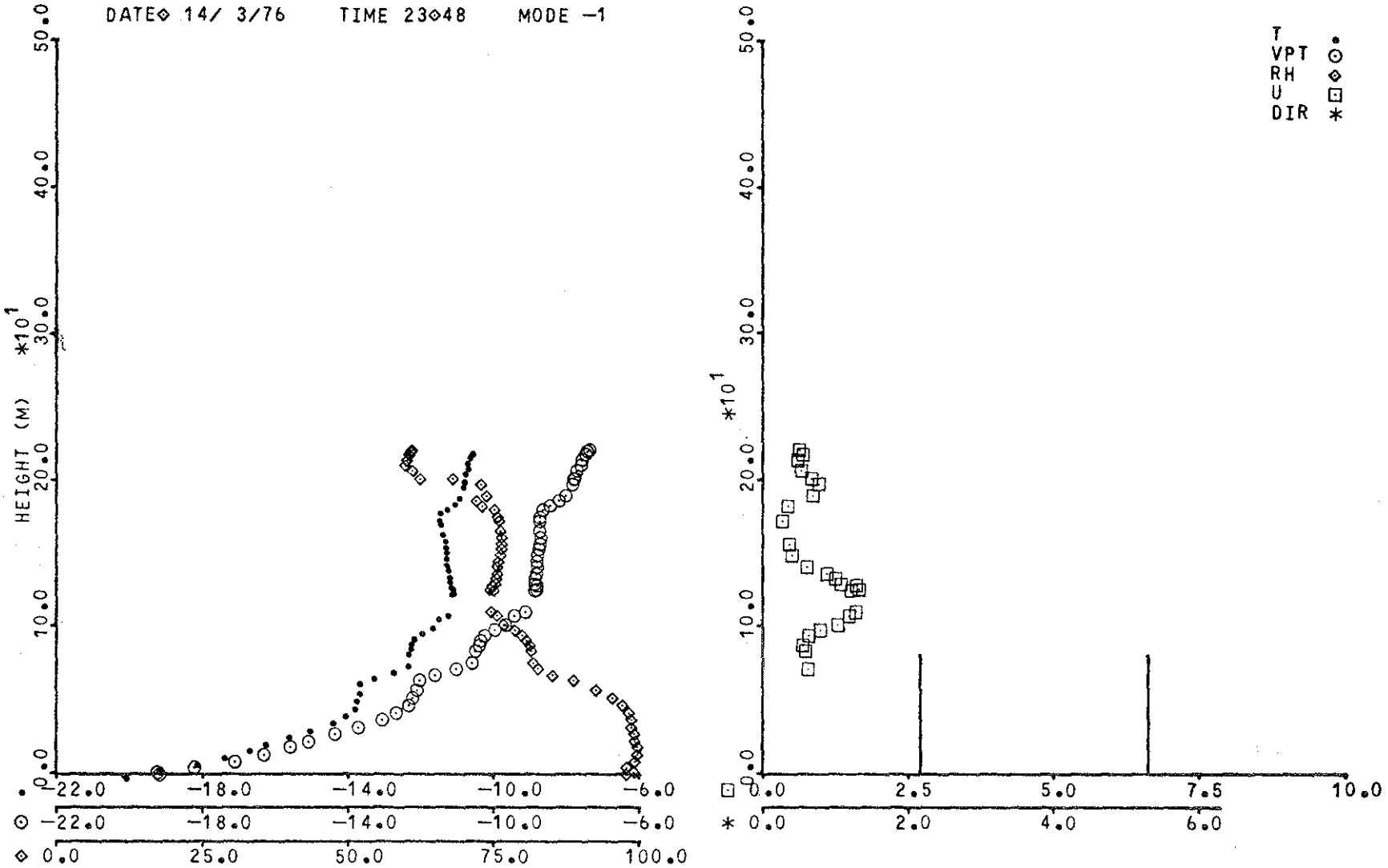
DATE◇ 14/ 3/76 TIME 23◇48 MODE −1
HEIGHT (M) *10^1
50.0
40.0
30.0
20.0
10.0
0.0
−22.0 −18.0 −14.0 −10.0 −6.0
−22.0 −18.0 −14.0 −10.0 −6.0
0.0 25.0 50.0 75.0 100.0
*10^1
0.0 2.5 5.0 7.5 10.0
0.0 2.0 4.0 6.0
T
VPT
RH
U
DIR

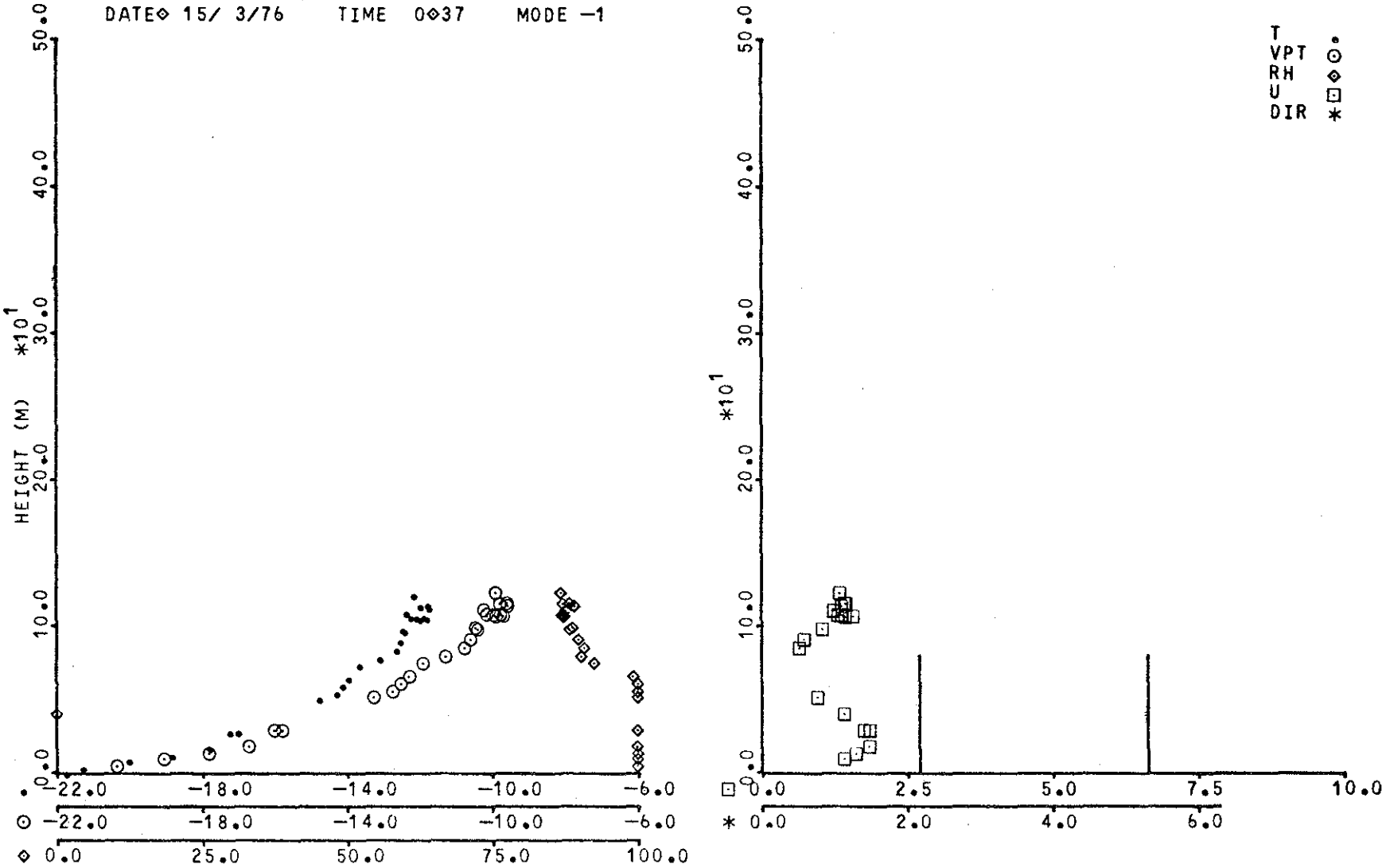
DATE◇ 15/ 3/76 TIME 0◇37 MODE −1
HEIGHT (M) *10^1
50.0
40.0
30.0
20.0
10.0
0.0
−22.0 −18.0 −14.0 −10.0 −6.0
−22.0 −18.0 −14.0 −10.0 −6.0
0.0 25.0 50.0 75.0 100.0
T
VPT
RH
U
DIR
*10^1
0.0 2.5 5.0 7.5 10.0
0.0 2.0 4.0 6.0

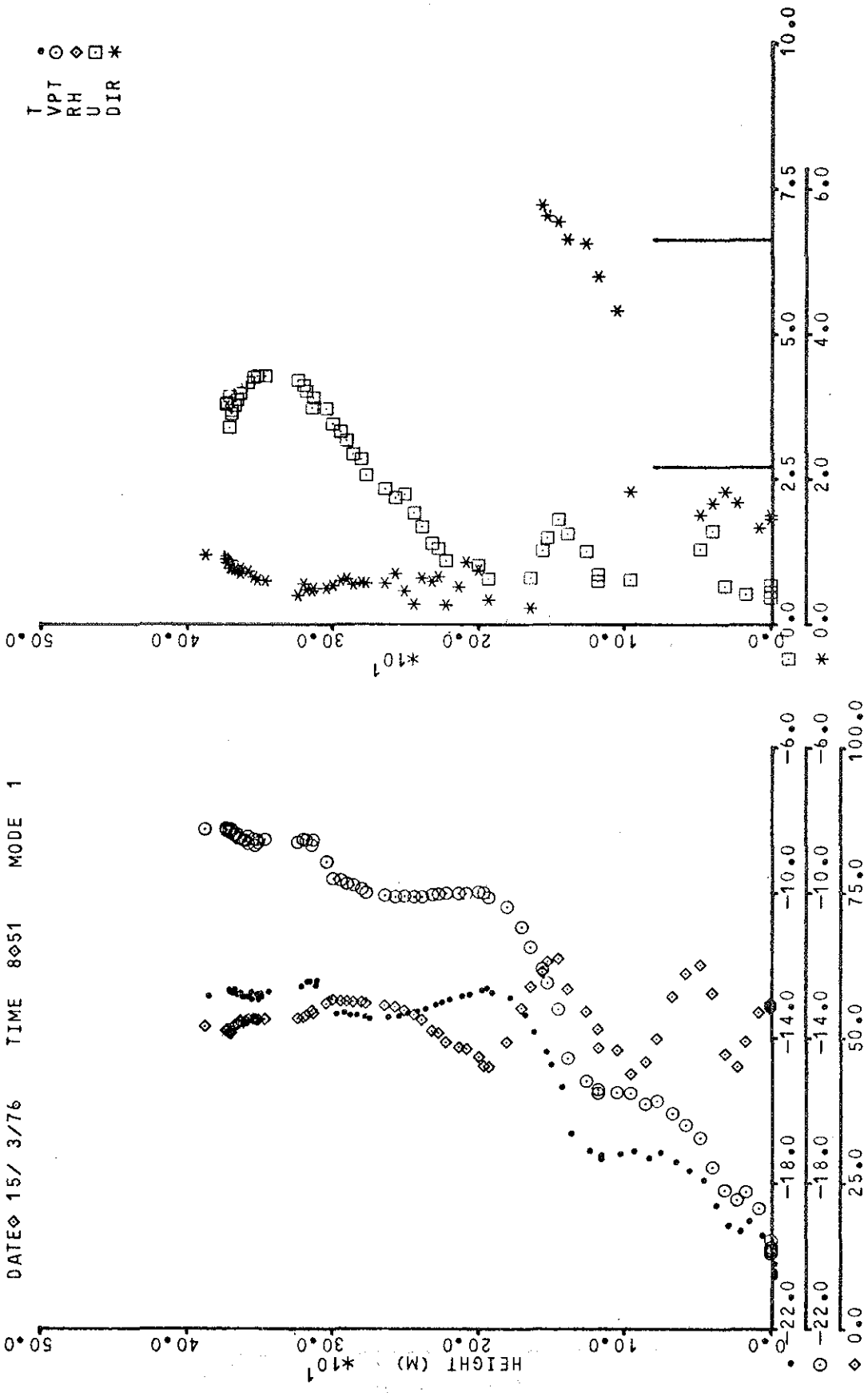
T
VPT
RH
U
DIR
DATE◇ 15/ 3/76 TIME 8◇51 MODE 1
HEIGHT (M) *10^1
*10^1
0.0
10.0
20.0
30.0
40.0
50.0
-6.0
-10.0
-14.0
-18.0
-22.0
0.0
25.0
50.0
75.0
100.0
2.5
5.0
7.5
2.0
4.0
6.0

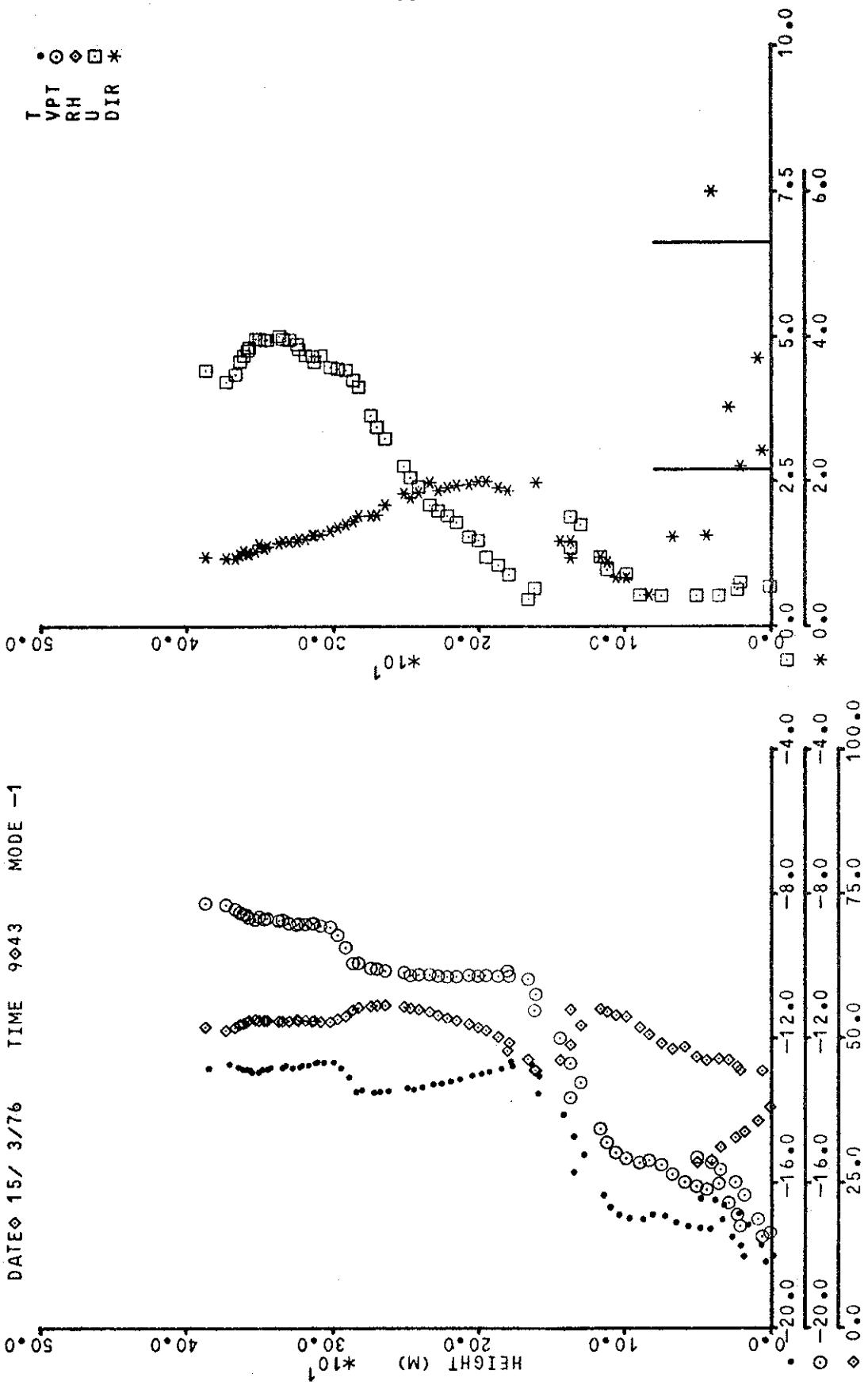
T
VPT
RH
U
DIR
*10¹
HEIGHT (M)
DATE◇ 15/ 3/76
TIME 9◇43
MODE -1

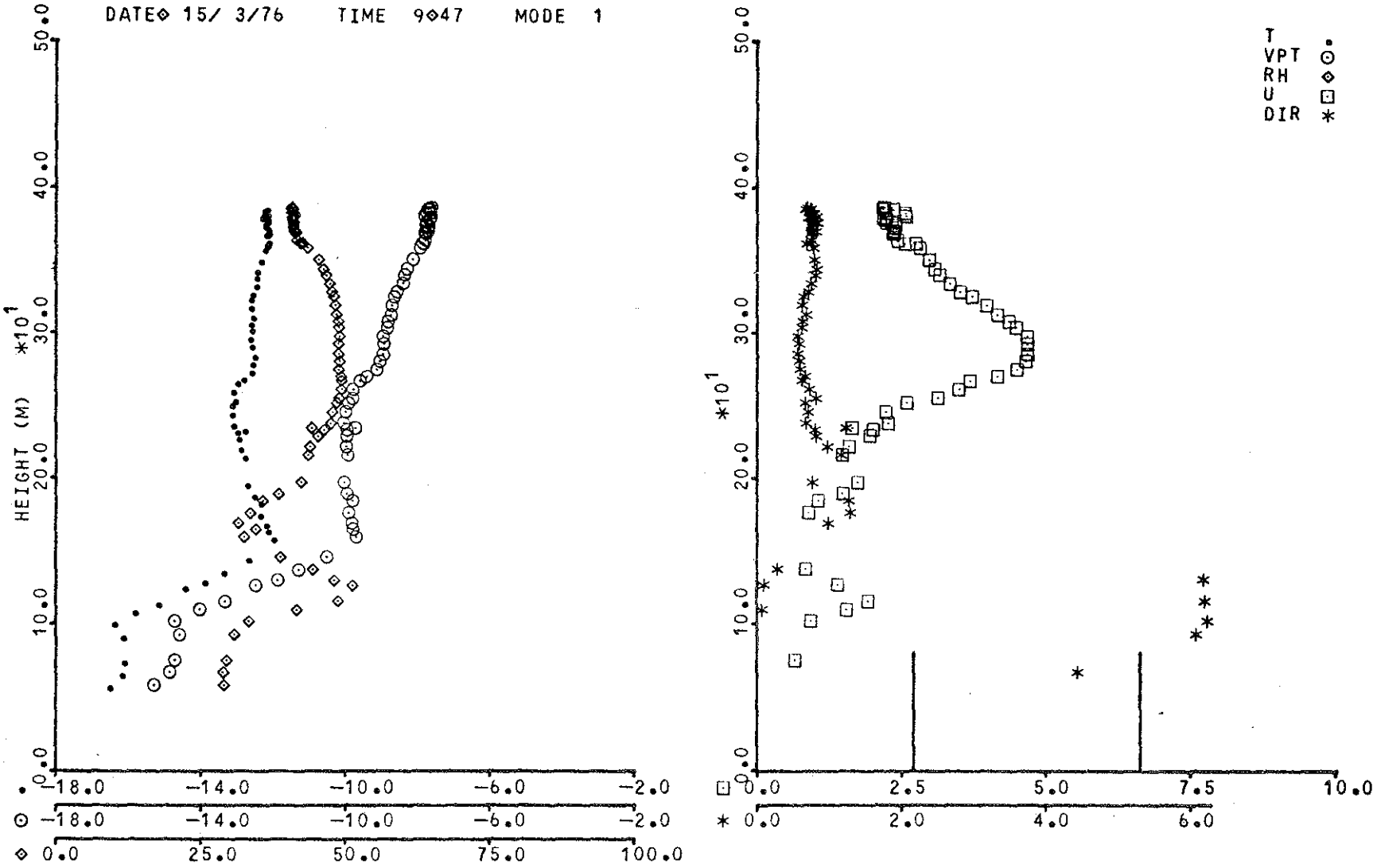
DATE◇ 15/ 3/76 TIME 9◇47 MODE 1
HEIGHT (M) *10^1
50.0
40.0
30.0
20.0
10.0
0.0
−18.0
−14.0
−10.0
−6.0
−2.0
0.0
25.0
50.0
75.0
100.0
2.5
5.0
7.5
10.0
2.0
4.0
6.0
T
VPT
RH
U
DIR

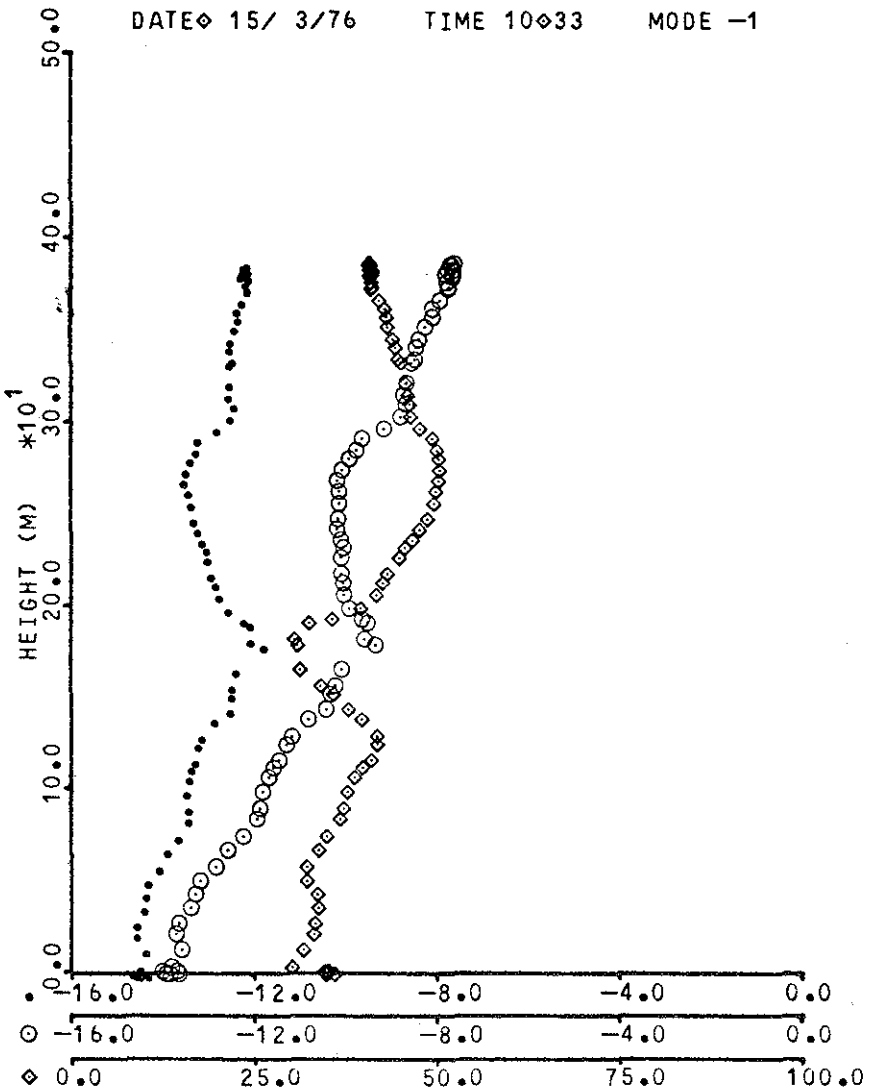
DATE◇ 15/ 3/76
TIME 10◇33
MODE −1
HEIGHT (M)
*10^1
50.0
40.0
30.0
20.0
10.0
0.0
−16.0
−12.0
−8.0
−4.0
0.0
25.0
50.0
75.0
100.0

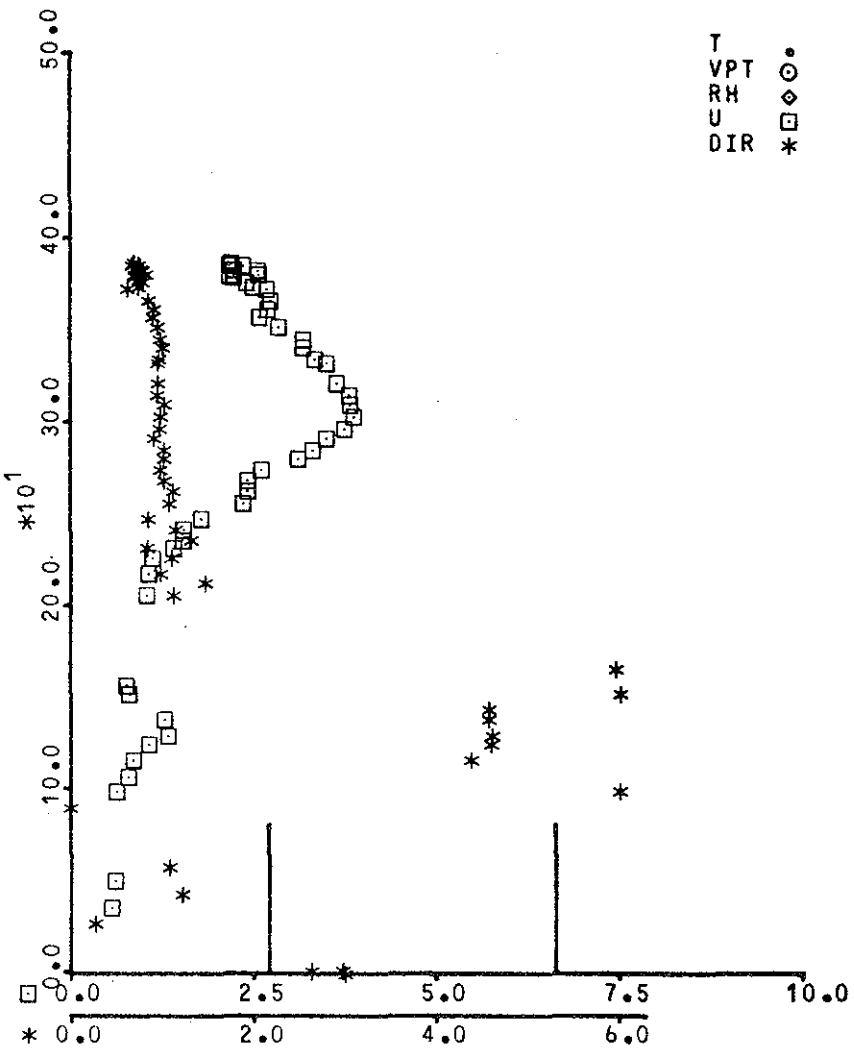
T
VPT
RH
U
DIR
*10^1
50.0
40.0
30.0
20.0
10.0
0.0
2.5
5.0
7.5
10.0
2.0
4.0
6.0

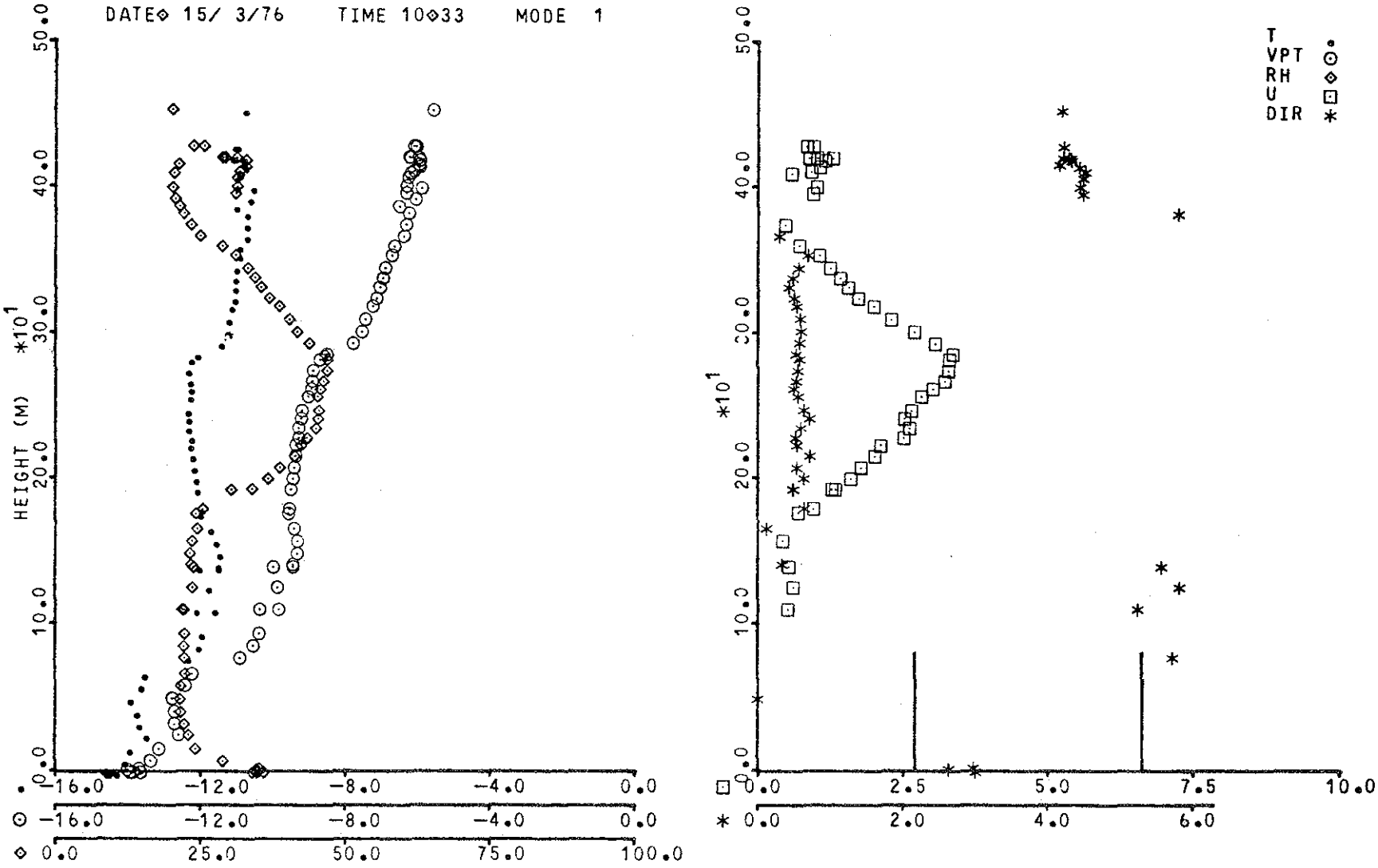
DATE◇ 15/ 3/76 TIME 10◇33 MODE 1
HEIGHT (M) *10^1
50.0
40.0
30.0
20.0
10.0
0.0
−16.0 −12.0 −8.0 −4.0 0.0
−16.0 −12.0 −8.0 −4.0 0.0
0.0 25.0 50.0 75.0 100.0
*10^1
0.0 2.5 5.0 7.5 10.0
0.0 2.0 4.0 6.0
T •
VPT ⊙
RH ◇
U □
DIR *

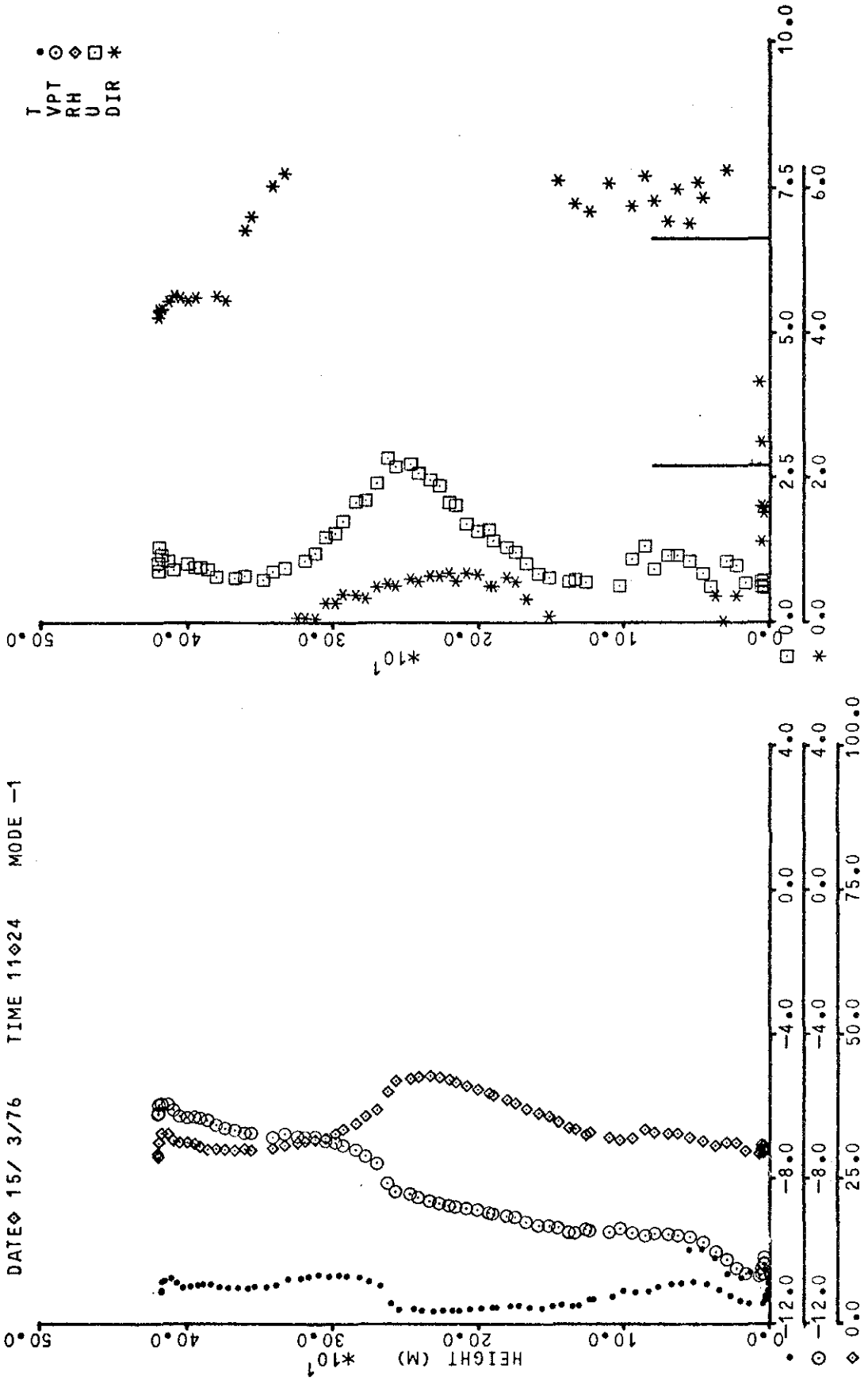
T
VPT
RH
U
DIR
DATE◇ 15/ 3/76 TIME 11◇24 MODE −1
HEIGHT (M) *10¹
*10¹

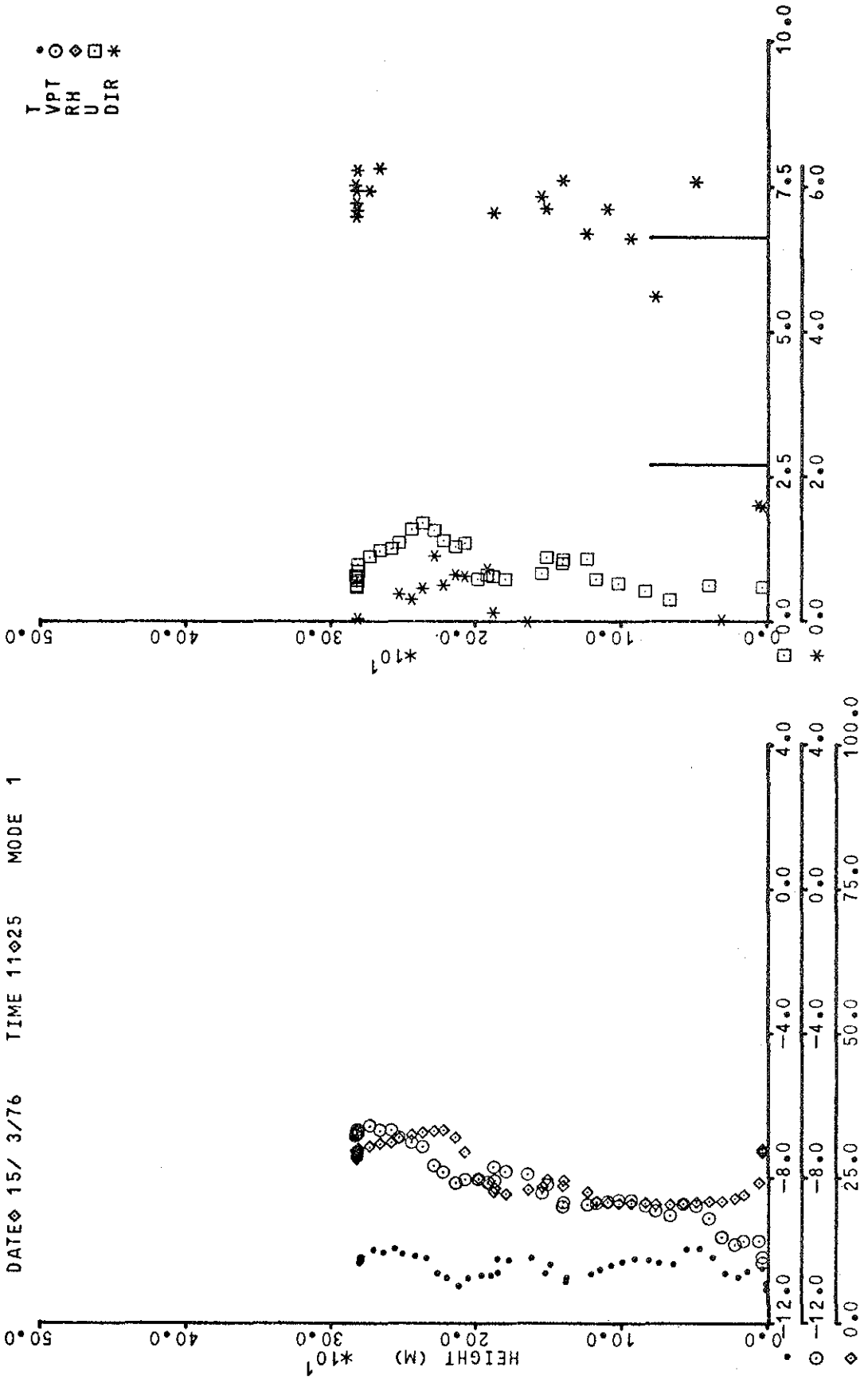
T
VPT
RH
U
DIR
DATE◇ 15/ 3/76 TIME 11◇25 MODE 1
HEIGHT (M) *10¹
*10¹
0.0
10.0
20.0
30.0
40.0
50.0
0.0
2.5
5.0
7.5
10.0
0.0
2.0
4.0
6.0
0.0
4.0
-4.0
-8.0
-12.0
0.0
4.0
-4.0
-8.0
-12.0
0.0
75.0
50.0
25.0
100.0

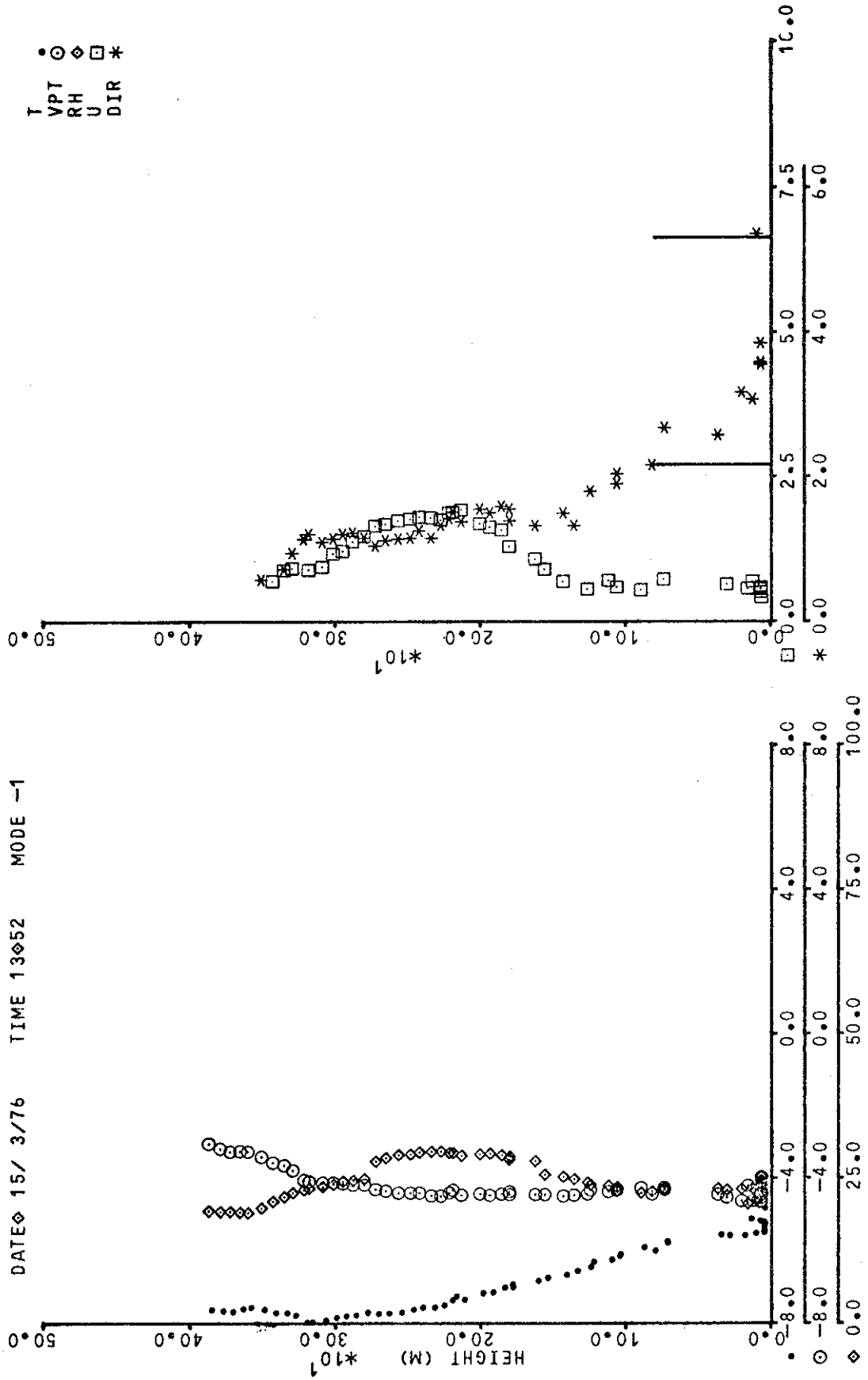
T
VPT
RH
U
DIR
DATE◇ 15/ 3/76 TIME 13◇52 MODE -1
HEIGHT (M) *10¹
*10¹

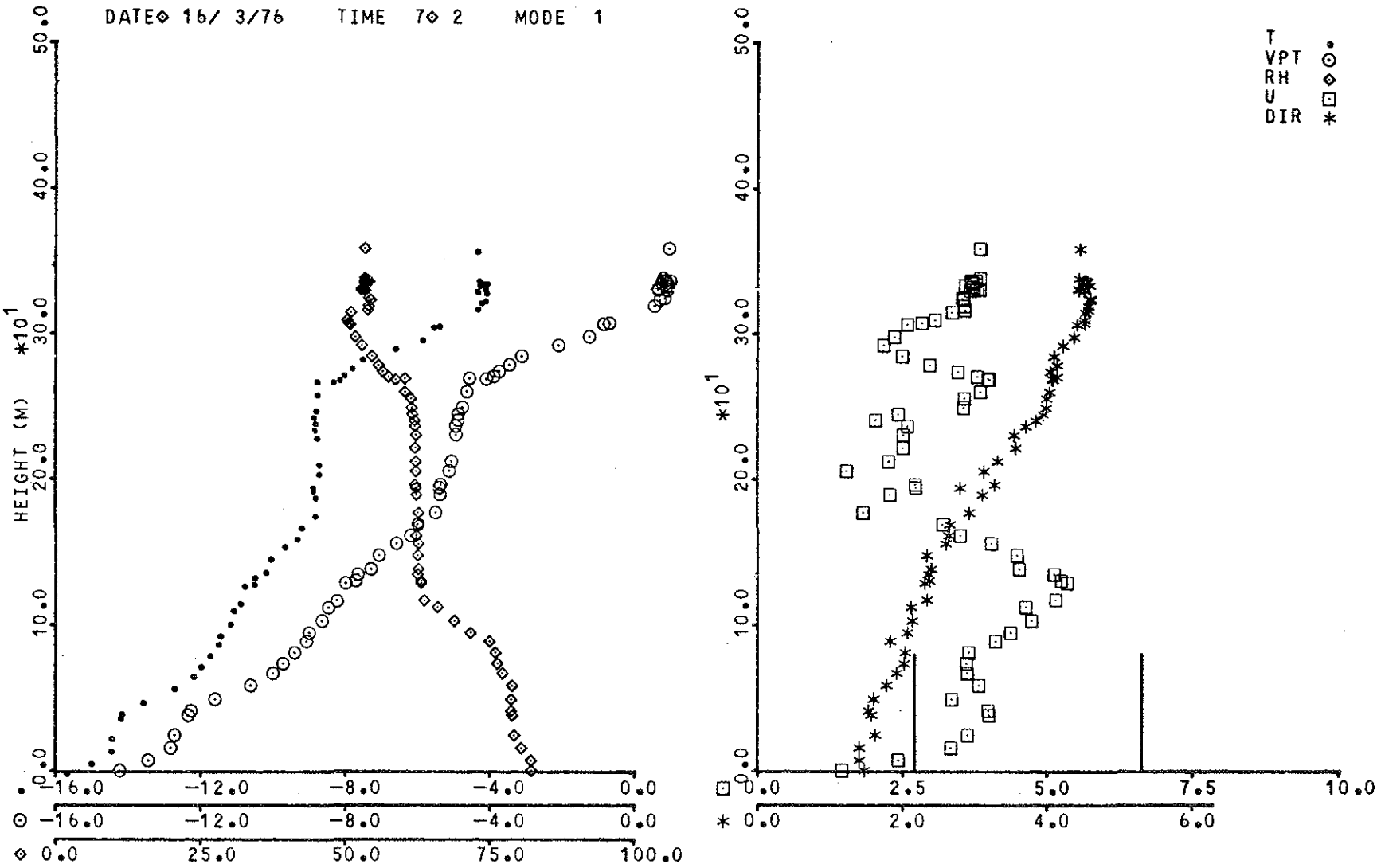
DATE◇ 16/ 3/76 TIME 7◇ 2 MODE 1
HEIGHT (M) *10^1
T
VPT
RH
U
DIR
50.0
40.0
30.0
20.0
10.0
0.0
-16.0
-12.0
-8.0
-4.0
0.0
25.0
50.0
75.0
100.0
2.5
5.0
7.5
10.0
2.0
4.0
6.0

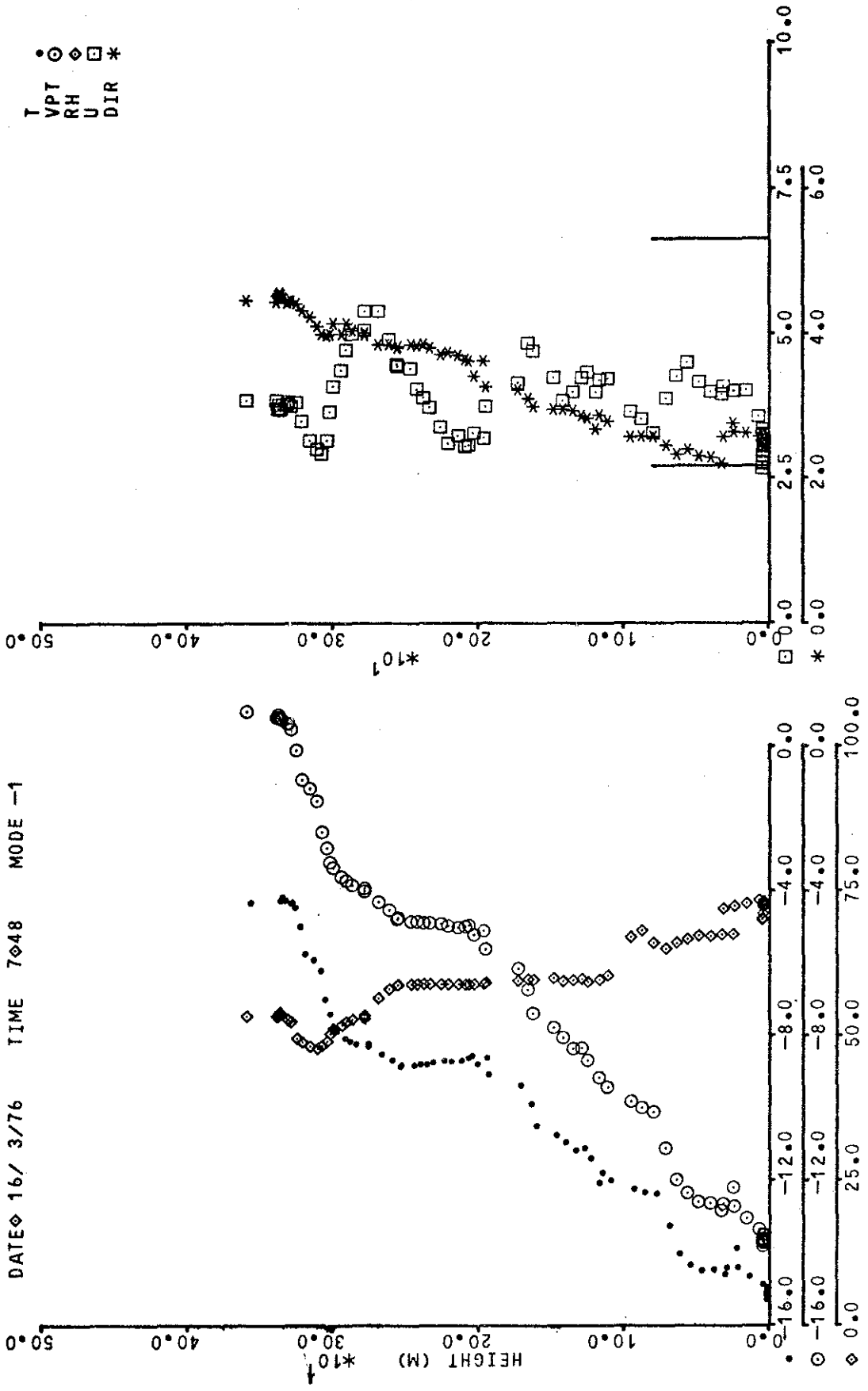
T
VPT
RH
U
DIR
DATE◇ 16/ 3/76 TIME 7◇48 MODE −1
HEIGHT (M)
*10
*10¹
10.0
7.5
6.0
5.0
4.0
2.5
2.0
0.0
−4.0
−8.0
−12.0
−16.0
100.0
75.0
50.0
25.0
0.0
10.0
20.0
30.0
40.0
50.0

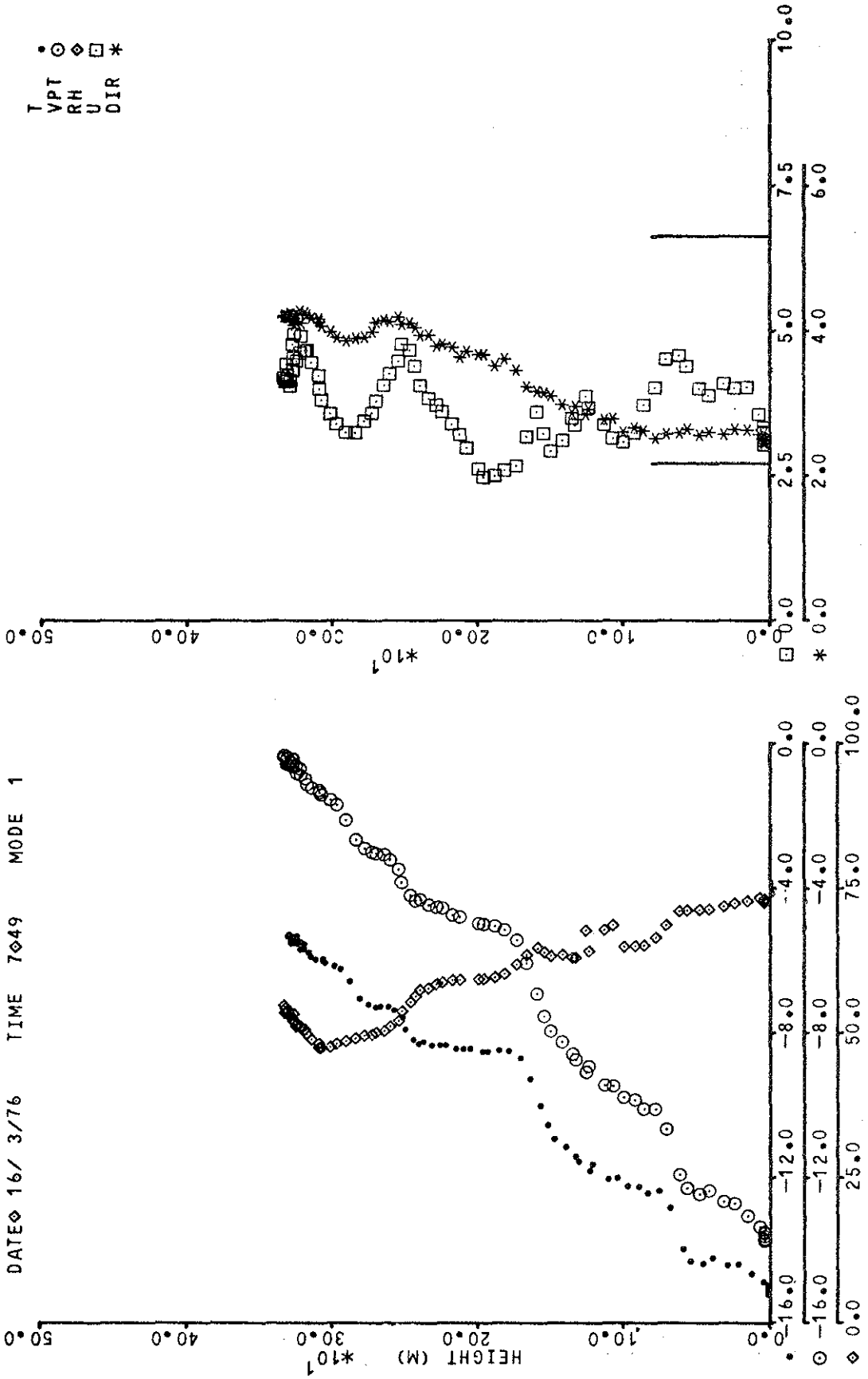
T
VPT
RH
U
DIR
HEIGHT (M) *10¹
DATE◇ 16/ 3/76 TIME 7◇49 MODE 1

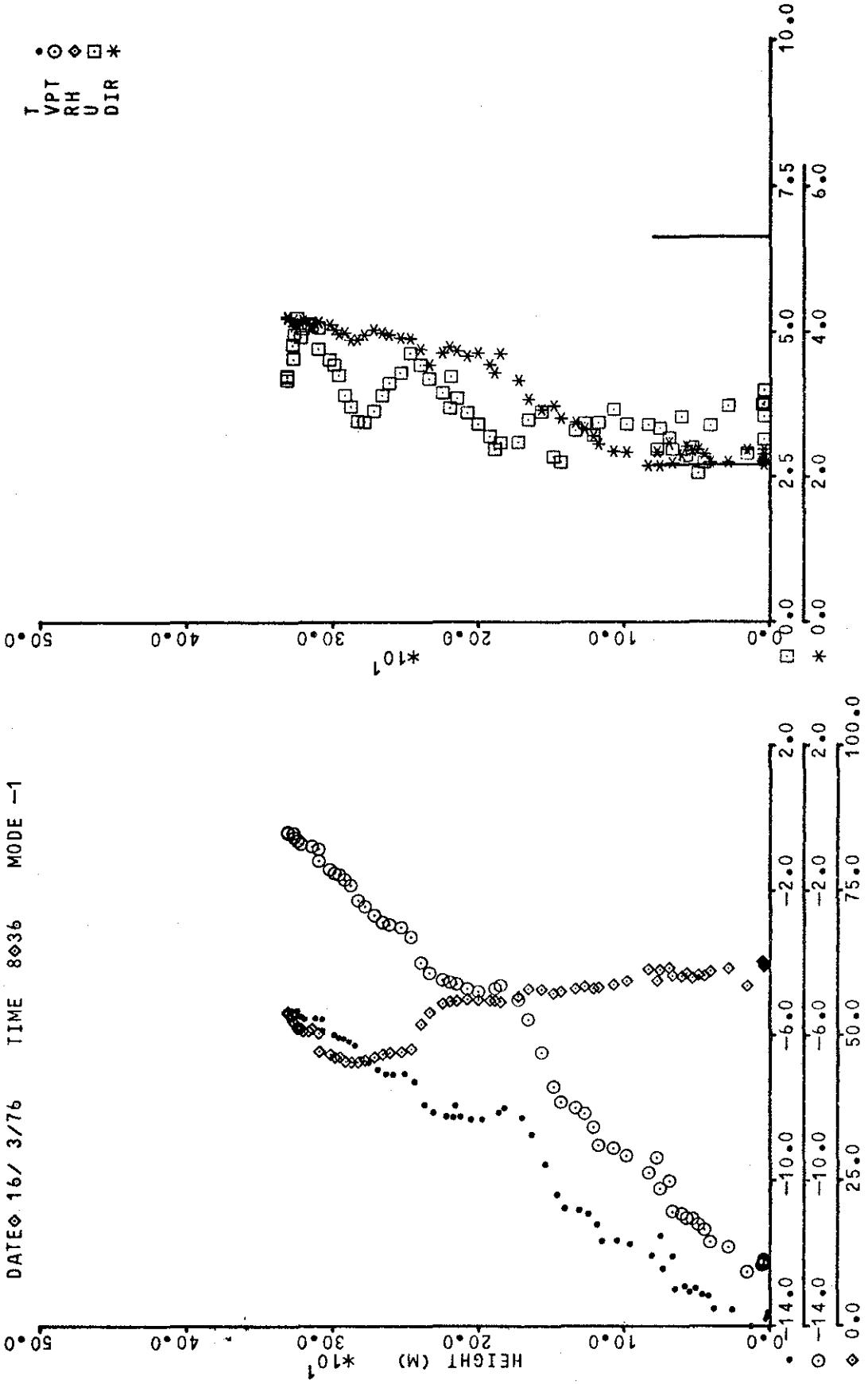
DATE◇ 16/ 3/76 TIME 8◇36 MODE -1
HEIGHT (M) *10¹
*10¹
T
VPT
RH
U
DIR

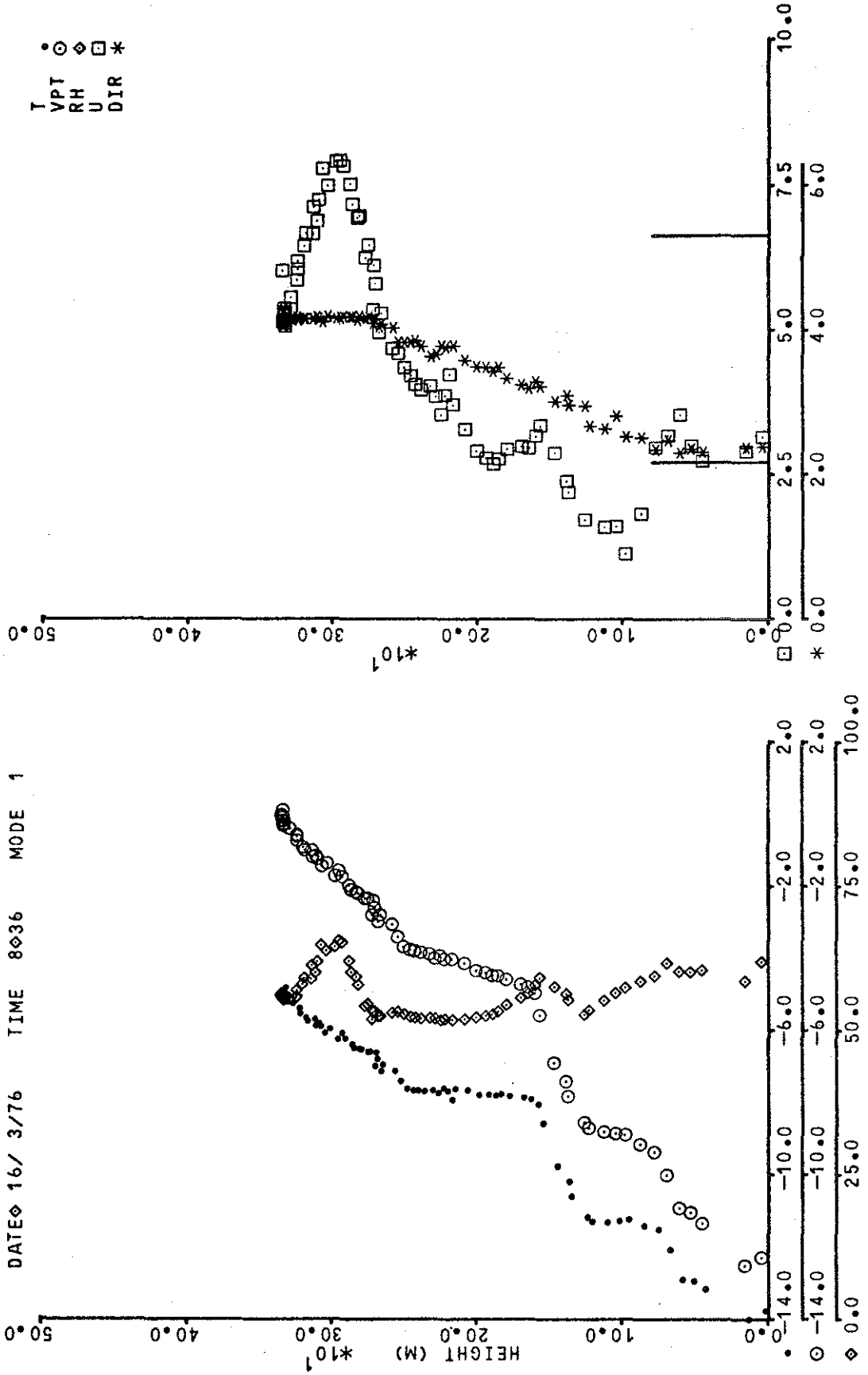
T
VPT
RH
U
DIR
DATE◇ 16/ 3/76 TIME 8◇36 MODE 1
HEIGHT (M) *10¹
*10¹
0.0
10.0
20.0
30.0
40.0
50.0
-14.0
-10.0
-6.0
-2.0
2.0
25.0
50.0
75.0
100.0
2.5
5.0
7.5
4.0
6.0

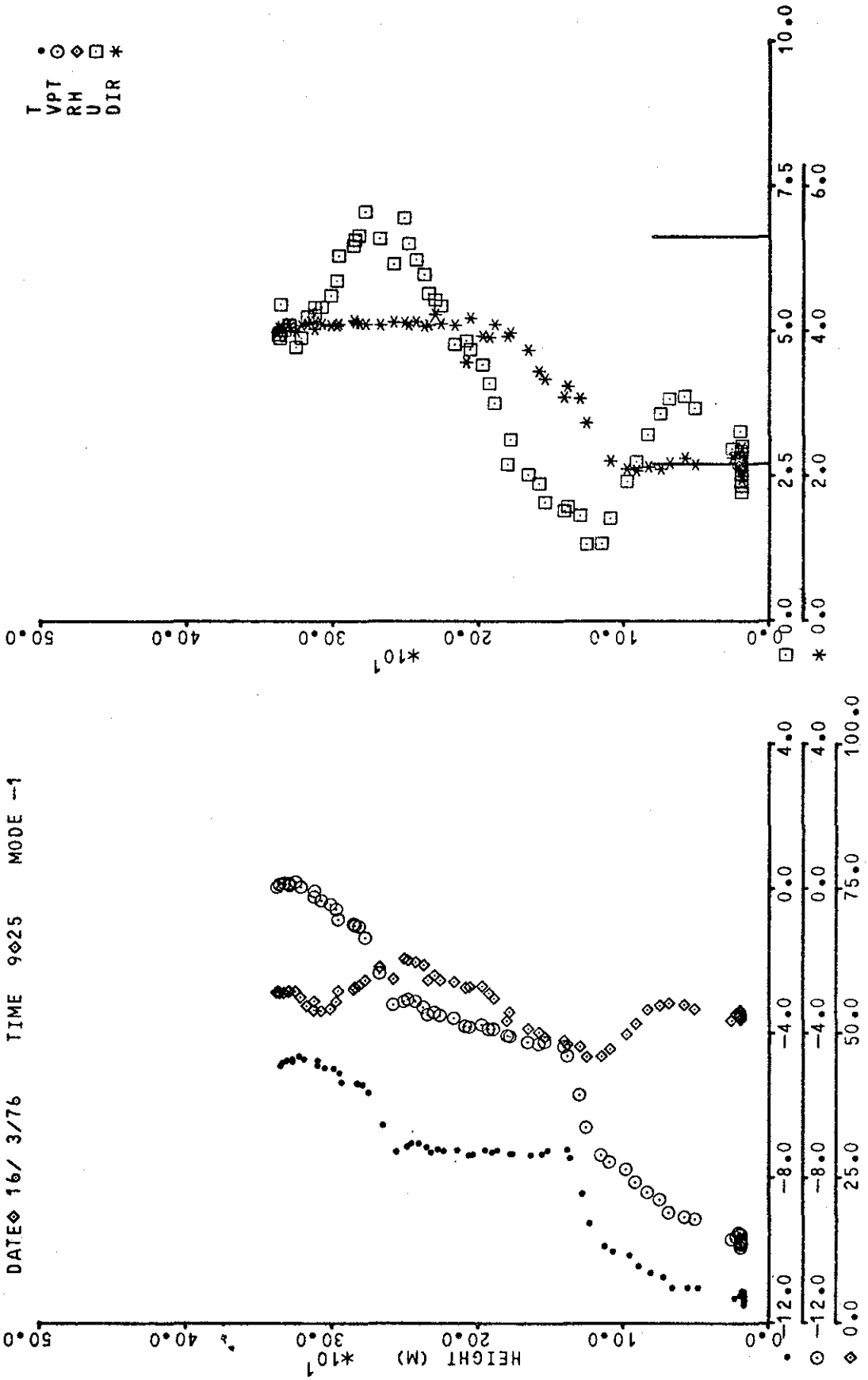
T
VPT
RH
U
DIR
DATE◇ 16/ 3/76 TIME 9◇25 MODE -1
HEIGHT (M) *10¹
*10¹
0.0
10.0
20.0
30.0
40.0
50.0
0.0
2.5
5.0
7.5
10.0
0.0
2.0
4.0
6.0
0.0
4.0
0.0
-4.0
-8.0
-12.0
0.0
25.0
50.0
75.0
100.0

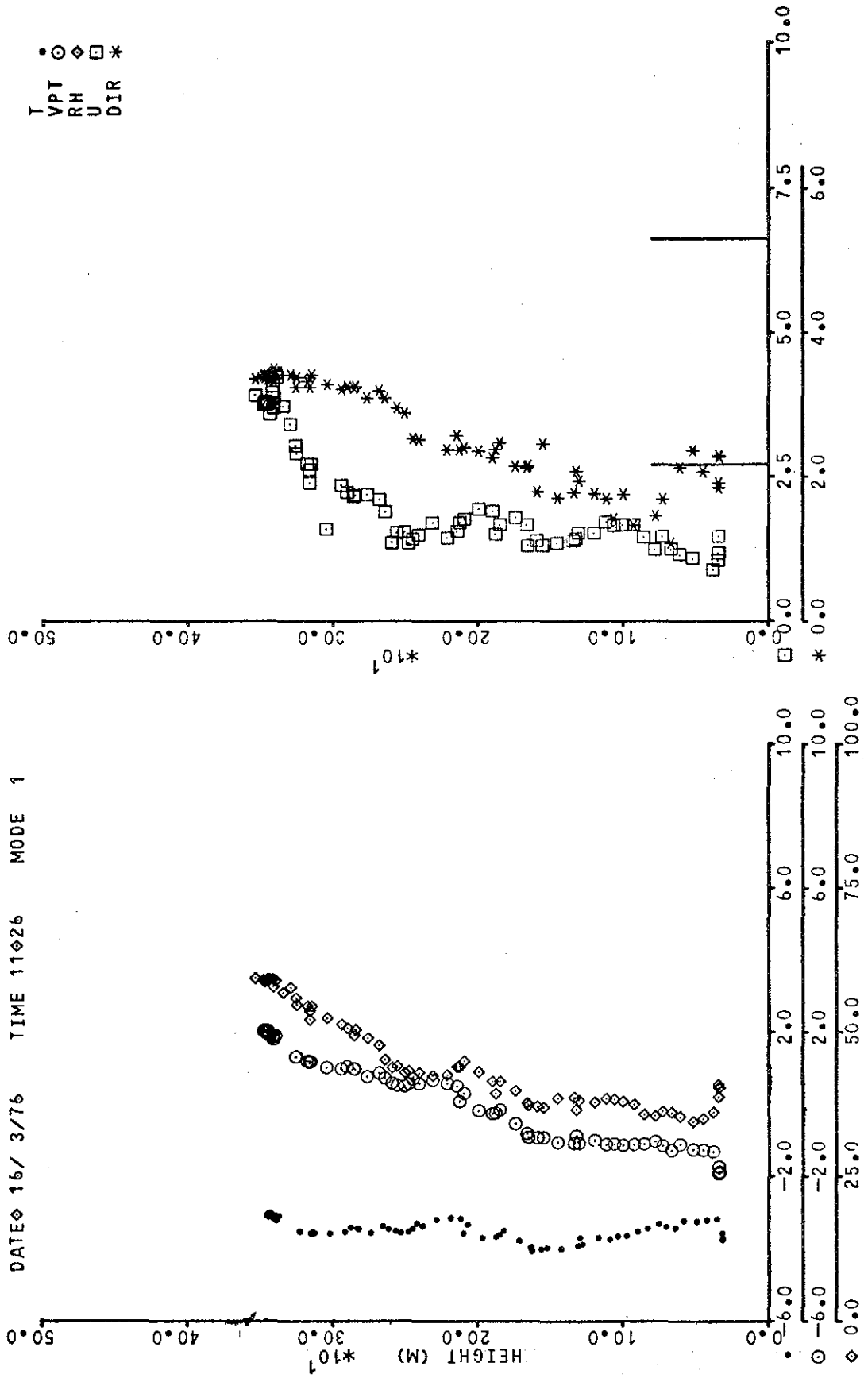
T
VPT
RH
U
DIR
DATE◇ 16/ 3/76 TIME 11◇26 MODE 1
HEIGHT (M) *10¹
*10¹

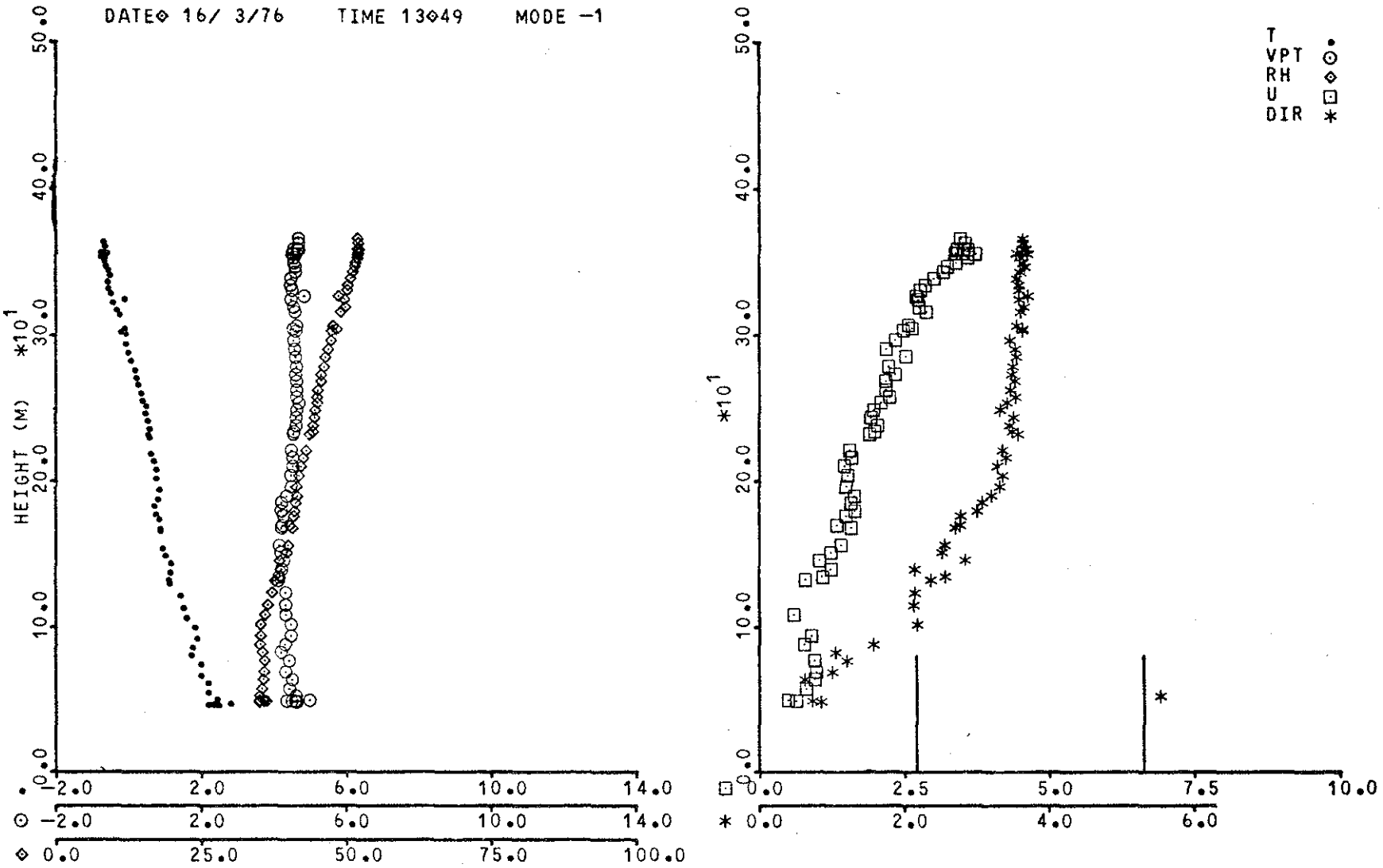
DATE⊙ 16/ 3/76 TIME 13⊙49 MODE -1
HEIGHT (M) *10^1
50.0
40.0
30.0
20.0
10.0
0.0
-2.0 2.0 6.0 10.0 14.0
-2.0 2.0 6.0 10.0 14.0
0.0 25.0 50.0 75.0 100.0
T
VPT
RH
U
DIR
*10^1
0.0 2.5 5.0 7.5 10.0
0.0 2.0 4.0 6.0

9. AOSERP RESEARCH REPORTS

1.		AOSERP First Annual Report, 1975
2.	AF 4.1.1	Walleye and Goldeye Fisheries Investigations in the Peace-Athabasca Delta
3.	HE 1.1.1	Structure of a Traditional Baseline Data System
4.	VE 2.2	A Preliminary Vegetation Survey of the Alberta Oil Sands Environmental Research Program Study Area
5.	HY 3.1	The Evaluation of Wastewaters from an Oil Sand Extraction Plant
6.		Housing for the North--The Stackwall System
7.	AF 3.1.1	A Synopsis of the Physical and Biological Limnology and Fisheries Programs within the Alberta Oil Sands Area
8.	AF 1.2.1	The Impact of Saline Waters Upon Freshwater Biota (A Literature Review and Bibliography)
9.	ME 3.3	Preliminary Investigation into the Magnitude of Fog Occurrence and Associated Problems in the Oil Sands Area
10.	HE 2.1	Development of a Research Design Related to Archaeological Studies in the Athabasca Oil Sands Area
11.	AF 2.2.1	Life Cycles of Some Common Aquatic Insects of the Athabasca River, Alberta
12.	ME 1.7	Very High Resolution Meteorological Satellite Study of Oil Sands Weather, A Feasibility Study
13.	ME 2.3.1	Plume Dispersion Measurements from an Oil Sands Extraction Plant
14.	HE 2.4	Athabasca Oil Sands Historical Research Design (3 Volumes)
15.	ME 3.4	Climatology of Low Level Air Trajectories in the Alberta Oil Sands Area
16.	ME 1.6	The Feasibility of a Weather Radar near Fort McMurray, Alberta
17.	AF 2.1.1	A Survey of Baseline Levels of Contaminants in Aquatic Biota of the AOSERP Study Area

18. HY 1.1 Alberta Oil Sands Region Stream Gauging Data

19. ME 4.1 Calculations of Annual Averaged Sulphur Dioxide Concentrations at Ground Level in the AOSERP Study Area

20. HY 3.1.1 Evaluation of Organic Constituents

21. AOSERP Second Annual Report, 1976-77

22. HE 2.3 Maximization of Technical Training and Involvement of Area Manpower

23. AF 1.1.2 Acute Lethality of Mine Depressurization Water on Trout, Perch and Rainbow Trout

24. ME 4.2.1 Review of Dispersion Models and Possible Applications in the Alberta Oil Sands Area

25. ME 3.5.1 Review of Pollutant Transformation Processes Relevant to the Alberta Oil Sands Area

26. AF 4.5.1 Interim Report on an Intensive Study of the Fish Fauna of the Muskeg River Watershed of Northeastern Alberta

27. ME 1.5.1 Meteorology and Air Quality Winter Field Study, March 1976

28. VE 2.1 Interim Report on a Soils Inventory in the Athabasca Oil Sands Area.